12-2019

Adaptive Boundary Control Using the Natural Switching Surfaces for Flyback Converters

Luciano Andres Garcia Rodriguez
University of Arkansas, Fayetteville

Adaptive Boundary Control Using the Natural Switching Surfaces for Flyback Converters

A dissertation submitted in partial fulfillment
of the requirements for the degree of
Doctor of Philosophy in Electrical Engineering

by

Luciano Andrés Garcia Rodriguez
Universidad Nacional del Sur
Bachelor of Science in Electronics Engineering, 2010

December 2019
University of Arkansas

The dissertation is approved for recommendation to the Graduate Council.

_____
Juan Carlos Balda, Ph.D.
Dissertation Director

_____
Simon Ang, Ph.D.
Committee Member

_____
Roy McCaan, Ph.D.
Committee Member

_____
Alan Mantooth, Ph.D.
Committee Member

_____
Darin Nutter, Ph.D.
Committee Member

ABSTRACT

The derivation and implementation of the natural switching surfaces (NSS) considering certain parametric uncertainties for a flyback converter operating in the boundary conduction mode (BCM) is the main focus of this dissertation. The NSS with nominal parameters presents many benefits for the control of nonlinear systems; for example, fast transient response under load-changing conditions. However, the performance worsens considerably when the converter actual parameters are different from the ones used in the design process. Therefore, a novel control strategy for NSS considering the effects of parameter uncertainties is proposed. This control law can estimate and adapt the control trajectories in a minimum number of switching cycles to obtain excellent performances even under extreme parameter uncertainties. The analytical derivation of the proposed adaptive switching surfaces is presented together with simulations and experimental results showing adequate performance under different tests, including comparisons with a standard PI controller.

ACKNOWLEDGMENTS

I want to thank my advisor Dr. Juan Carlos Balda for allowing me to come to the USA to work in his laboratory, and for providing me with funding for many years. Thanks to Dr. Simon Ang, Dr. Alan Mantooth, Dr. Roy McCaan and Dr. Darin Nutter for accepting being a member of my committee. I also want to thank Mr. Robert Saunders for allowing me to work as a teaching assistant.

I want to specially thank Héctor Gerardo Chiacchiarini, a professor from the Universidad Nacional del Sur in Argentina, who was part of all the papers produced from this dissertation. I want to thank all the undergraduate students that worked under my guidance during my first years as a PhD student. Thanks to Ethan Williams, Vinson Jones, and Brett Schauwecker. You made it possible to write multiple conference papers during my first years at the university.

I want to thank all the masters and PhD students that help me when I was in trouble with a transaction paper revision. Thanks to Vinson Jones and Edgar Escala for their help in the Solid-State Transformer (SST) transaction paper. Thanks to David Carballo Rojas for his help in the Natural Switching Surface transaction paper. Thank you Obaid Aldosari for his help in the Department of Energy (DOE) project simulating the high frequency transformers in Ansys and helping me with the transformer design and reports.

Thanks to Daniel Klein, Jarod Medart, Chris Farnell and Joshua Bishop for helping us solving issues with the computers and equipment in the laboratory.

Thanks to Omar Vitobaldi for hiring me as a hardware engineer intern at Enphase Energy in Petaluma California.

Thanks to Sharon Brasko and Connie Howard for helping me with purchases and with all the related paper work.

Thanks to all my friends from another advisors: Nadia Smith, Joel Flores Pino, Akrem Elrajoubi, Kirch Mackey, Ashfaqur Rahman, Ramchandra Kotecha, Janviere Umuhoza, Yusi Liu, Shuang Zhao, Xingcheng Zhao, Waleed Alhosaini, She Zhao, all the other friend which I cannot spell correctly their names.

Thanks to my mates while I was a teaching assistant: Mohammed Marie, Juan Aguilar, and Amad Nusir. Thanks to all the professors that I had assisted as a teaching assistant: Dr. Roy McCann, Mr. Robert Saunders, Dr. Omar Manasreh, and Dr. Mantooth.

Thanks to all the masters and Ph.D. students of Dr. Balda during the time I was in the lab: Jonathan Hayes, Corris Stewart, Andres Escobar Mejia, Collins Sassu, Elizabeth Merida Fernandez, David Guzman, Manuel Sanchez, Luis Mogollon Pinzon, Samuel Garcia Brown, Vinson Jones, Arthur Barnes, Roderick Garcia Montolla, Adithya Mallela, Obaid Aldosari, Witness Martin, Dimas Fiddiansyah, Erkin Bektenov, Sharthak Munasib, Thouhidul Islam, Joyotree Das, David Carballo, Edgar Escala, Daniel Schwartz, Rana Alizadeh, Sohail Nouri, Rafael Alejandro Franceschi, Nima Abdolmaleki, Shamar Christian, Roderick Gomez Jimenez, Desmon Simatupang, Mojtaba Ahanch, and Pierre Dorile.

Thanks to all the postdocs and visiting professors of Dr. Balda: Jesus Gonzalez-Llorente, Cheng Deng, Tao Yang, Sebastian Gomez Jorge, Roberto Carballo, Roberto Fantino, Guillermo Garcia, and German Oggier.

Thanks to Alejandro Oliva for his help when I just came to the USA, and for his help in the SST transaction paper. Thank you Obaid and German for making together a great team while working for the new topology papers. Thanks to Dr. Deng for his help in the microinverter project and for the work we did together for the passive integration transaction paper.

DEDICATION

This dissertation is dedicated to my grandmother Luisa Esther Ohaco who passed away while I was studying my Ph.D. Then, I also want to dedicate this work to my parents Alicia and Daniel, to my grandfather Cuco, and to my siblings Daniela, Emanuel, Rocio and Guido. Lastly, I want to dedicate this dissertation to my wife, Betina, who was my support during all these years of hard work.

TABLE OF CONTENT

LIST OF FIGURES

LIST OF TABLES

CHAPTER 1

Introduction and Contributions

1.1 FLYBACK CONVERTER

The flyback converter is one of the most popular isolated topologies for systems rated up to 200 W because of its simplicity, low cost, and wide voltage ratio [1]. Flyback converters are used in many applications like AC/DC power supplies for LED loads and battery chargers[2]–[4], photovoltaic microinverters [5], [6], and traditional DC/DC converters used for isolated switching power supplies [7]. A flyback converter consists of a transistor Q, a flyback transformer T with a magnetizing inductance L_m, a diode D, and an output capacitor C_o as displayed in Fig. 1.1, where the load is being modeled as a constant current source I_o [8].

When Q turns ON, the input voltage source V_{in} is connected across L_m, so the magnetizing current i_m increases linearly. Since the primary and secondary windings of the transformer are wounded in opposite directions, the positive voltage V_{in} across L_m will be reflected to the anode of diode D as a negative voltage, reverse biasing D as noted in Fig. 1.1(a). During the ON-period, the load is supplied exclusively by C_o. When Q turns OFF, the voltage across L_m reverses its polarity forward biasing D. During this period, the energy stored in L_m during the ON-period is released to charge the output capacitor C_o and supply the load needs.

Flyback converters can operate in three possible modes of operation: continuous conduction mode (CCM), boundary conduction mode (BCM), and discontinuous conduction mode (DCM). Those modes of operation are defined based on the state of the magnetizing current i_m. When the magnetizing current is always greater than zero, the flyback converter is operating in CCM as illustrated in Fig. 1.2 (a). Then, the flyback converter is operating in BCM as shown in Fig. 1.2 (b) when the magnetizing current reaches zero and immediately becomes positive. Lastly, when the

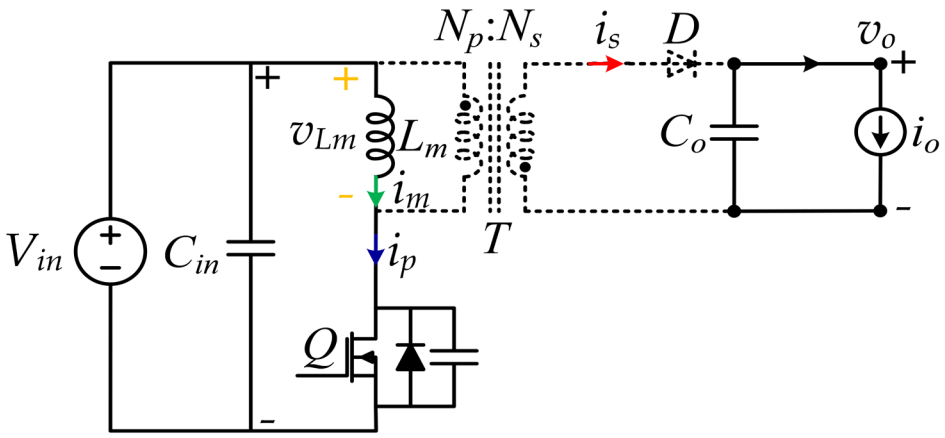

(a)

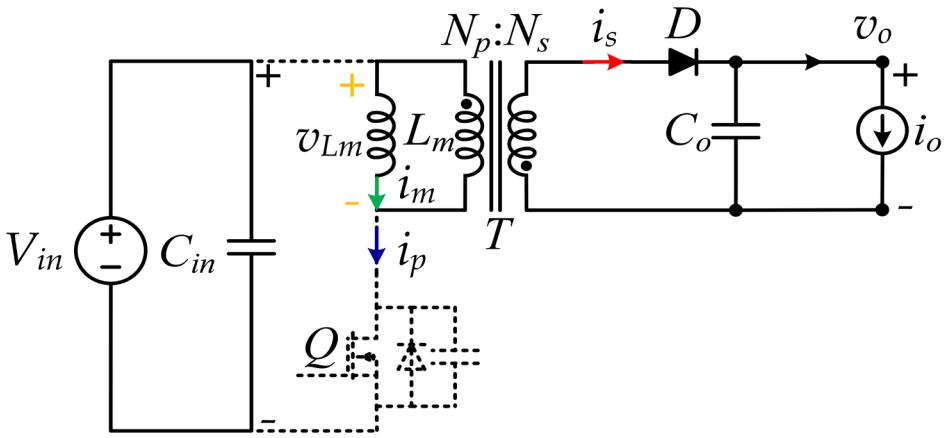

(b)

Fig. 1. 1. Flyback converter equivalent circuits when: (a) Q is ON, and (b) Q is OFF.

magnetizing current becomes zero for a measurable period of time, the flyback converter is operating in DCM as seen in Fig. 1.2 (c).

Fig. 1.3 shows the per-unit peak input current $I_{in,pk}$ and the per-unit RMS value of the input capacitor current $I_{Cin,RMS}$ for CCM and DCM modes of operation as function of a normalized switching frequency $f_{sw}/f_{critical}$. The critical switching frequency $f_{critical}$ is that one where a given flyback converter with certain parameters (L_m, N_p/N_s, and C_o) operates under BCM. The value of $f_{critical}$ can be calculated as [9]:

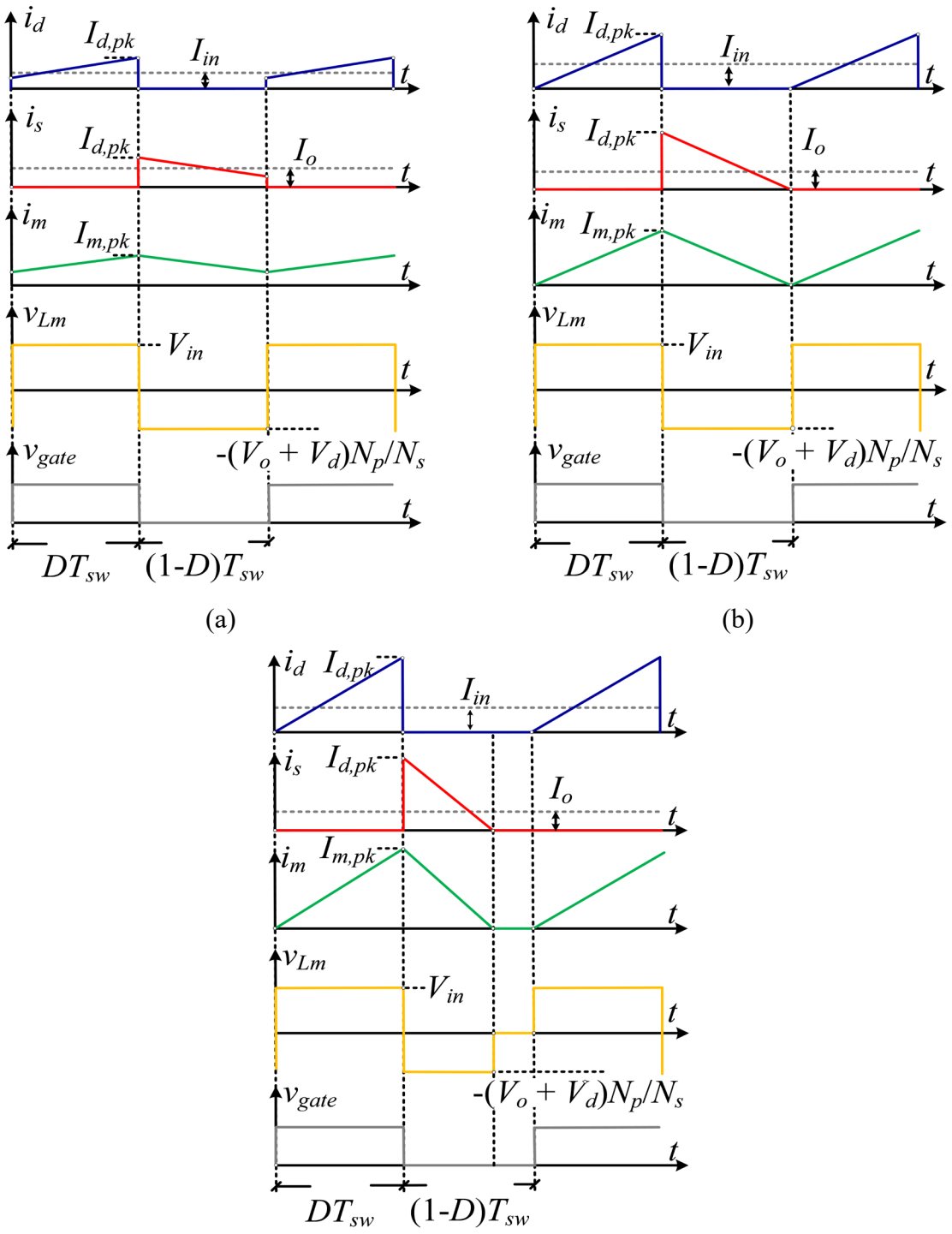

Fig. 1. 2. Theoretical waveforms of a flyback converter operating in: (a) continuous (CCM), (b) boundary (BCM), and discontinuous conduction (DCM) modes.

$$L_{critical} = \frac{v_o (1-D)^2}{2 i_o f_{sw}} \left(\frac{N_p}{N_s} \right)^2, \tag{1.1}$$

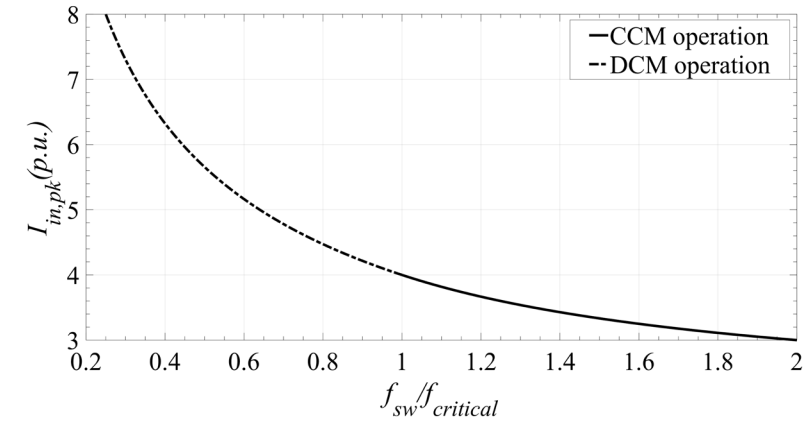

(a)

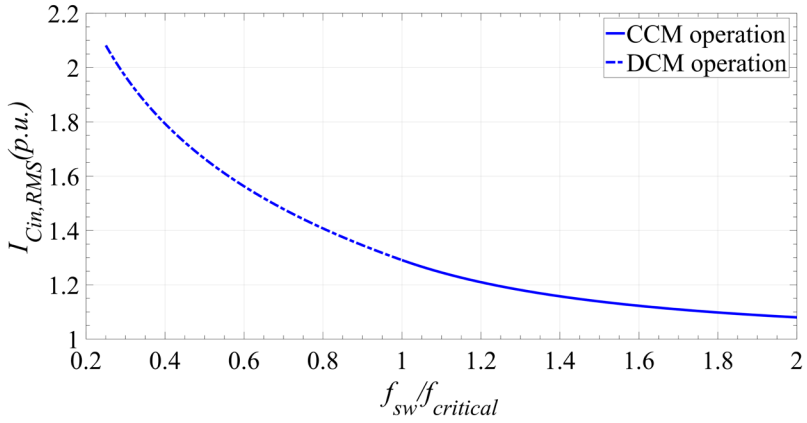

(b)

Fig. 1. 3. (a) Per-unit peak input current $I_{in,pk}$ (p.u.) as function of the switching frequency f_{sw}, and (b) per-unit RMS input capacitor current $I_{Cin,RMS}$ (p.u.) as function of f_{sw}.

where, D is the duty cycle of the converter defined as the ratio between the ON-period T_{ON} and the switching period T_{sw}.

If f_{sw} is greater than $f_{critical}$ the converter will operate in CCM, and if f_{sw} is lower than $f_{critical}$, the converter will operate in DCM. With reference to Fig. 1.3, the peak and RMS currents for the primary side devices decrease when the switching frequency increases, while for switching frequencies lower than $f_{critical}$ the peak and RMS values increase. Similarly, Fig. 1.4 shows that for operation in DCM, the diode requires to be rated for a higher level than for CCM. Also, the output capacitor is subjected to a higher current when the converter operates under DCM.

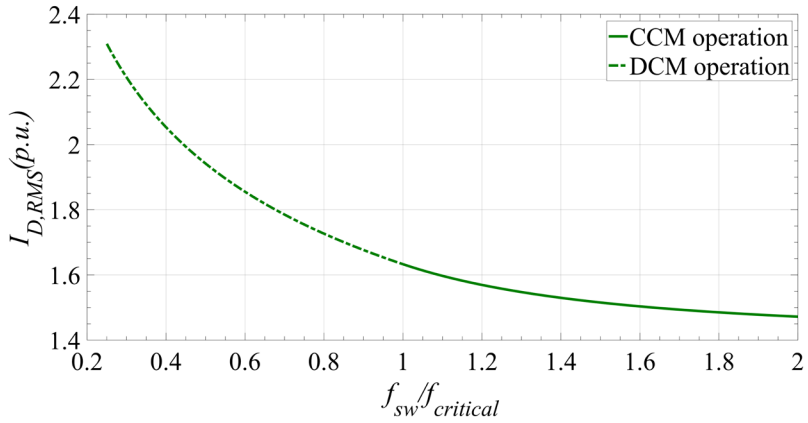

(a)

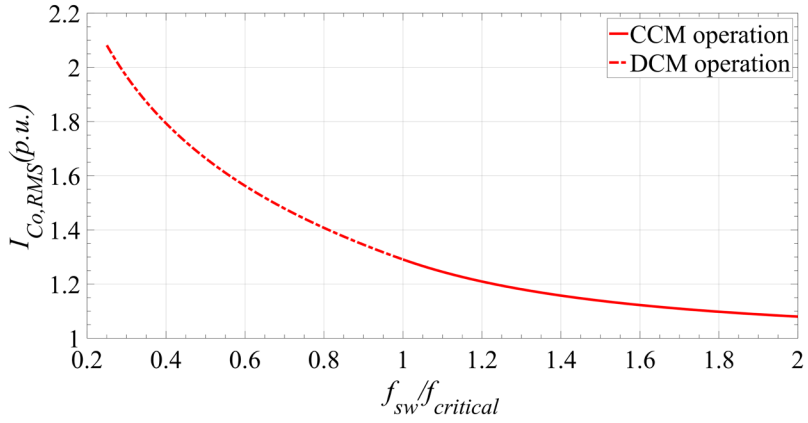

(b)

Fig. 1. 4. (a) Per-unit-diode RMS current $I_{D,RMS}$(p.u) as function of f_{sw}, and (b) RMS output capacitor current $I_{Co,RMS}$(p.u.) as function of the f_{sw}.

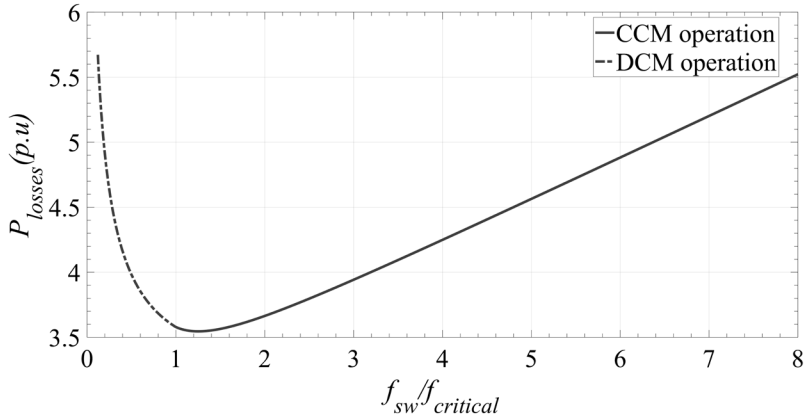

Fig. 1. 5. (a) Per-unit total flyback converter losses P_{losses}(p.u) as function of f_{sw}.

Flyback converters operating in BCM are broadly used for high-frequency applications since zero-current turn-ON for the switching device and zero-current turn-OFF for the diode are achieved

while keeping conduction losses and current stresses low in comparison with operation in the discontinuous conduction mode (DCM) [3], [9]. As illustrated in Fig. 1.5, total converter power losses (switching and conduction losses) are minimized when the switching frequency is close to the critical frequency. Also, soft-switching transitions during BCM operation reduce electromagnetic interference (EMI) and lead to lower power losses due to Joule effect than operation under continuous conduction mode (CCM), simplifying the snubber design, EMI filtering and thermal management [10]–[11]. Also, BCM operation leads to less voltage ripples than under DCM operation.

1.2 BOUNDARY CONTROL

A flyback converter is a non-minimum phase system due to the presence of a right-half plane zero in the control-to-output transfer function [12]. Using linear compensators to control such a system requires a low crossover frequency to guarantee stability which implies a slow control response [13]. Unfortunately, linear compensators are unsuccessful when there are large load variations since the model is only valid around an equilibrium point [14]; therefore, nonlinear controllers are used to improve the control dynamics.

By assuming that the magnetizing inductance current i_m and output voltage v_o are the converter variables of interest, the state trajectories are the curves in the plane (i_m, v_o) that a given flyback converter follows from a certain initial condition when the transistor Q turns ON and OFF. Fig. 1.6 shows the flyback state trajectories with the ON-trajectories being straight lines and the OFF-trajectories circles. The load line in Fig. 1.6 represents all the possible steady state points where the converter can operate.

Variable structure control (VSC) is a discontinuous nonlinear control strategy whose structure changes depending on the location of the state trajectories with respect to a designed switching

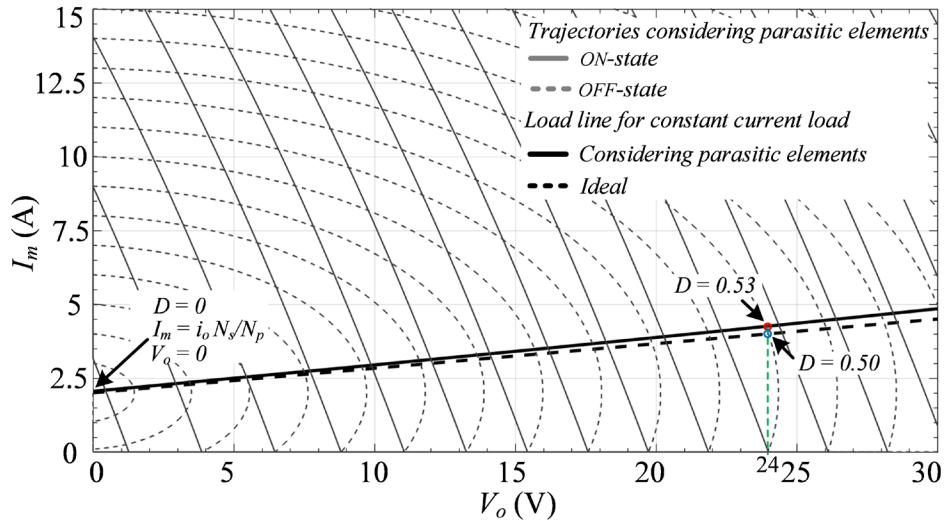

Fig. 1. 6. Flyback state trajectories and load line when the output current is constant.

surface (SS) [14]–[18]. Boundary control (BC) and sliding mode control (SMC) are VSC examples. Under SMC, the system remains close to the SS after reaching it. However, the SSs in BC may not be related with sliding regimes [14].

BC is a large-signal geometric control method that does not distinguish between start-up, transients and steady-state operation [12]–[16]. The intersection of the system trajectories with the selected SS defines whether the switch turns ON or OFF. First-order SSs are commonly used in BC because they are robust and simple to implement [18], [19]. However, the transient dynamics may require several switching cycles before reaching a steady state after start-up or transient conditions [20], [21]. As an example, Fig. 1.7 presents the transient response of a flyback converter when two first-order SS are used. When the transistor Q is ON, and the OFF-first-order SS is intersected, Q turns OFF. While Q is OFF and the ON-first-order SS is intersected, Q turns ON. Both ON and OFF-first-order SS contain the desired target operating point TP = (V_{TPn}, 0). As seen in Fig. 1.7, multiple ON and OFF switching transitions are required to get to TP.

Furthermore, the optimal slope for the first-order SS is dependent on the load and supply characteristics which reduce the overall system performance [12]. An ideal SS is the one that

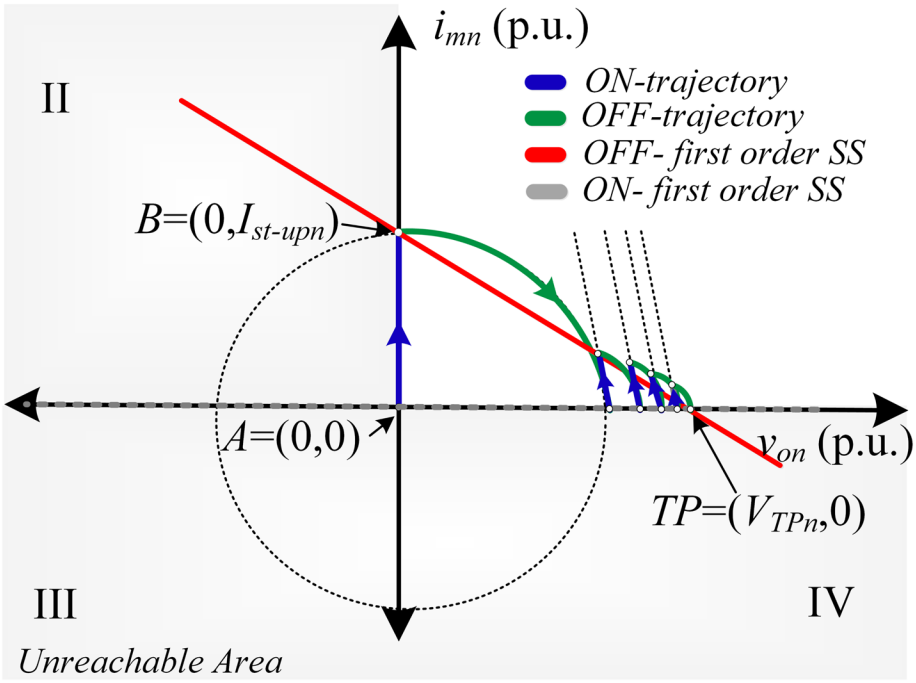

Fig. 1. 7. Flyback converter start-up response when first-order switching surfaces are used for the control.

guides the system to the desired steady state with the minimum number of switching actions [16]. The ideal SS is derived from the intersection of the system OFF-trajectory that contains the operating point with the ON-trajectory that leaves the operating point [14]–[16].

1.3 NATURAL SWITCHING SURFACES (NSS)

Multiple SSs have been proposed to estimate the ideal trajectories or natural response of converters. For example, second-order SSs derived from capacitor charge-balance equations with low ripple approximation have been proposed for buck converters operating under CCM [20] and DCM [22]. Also, a fixed-frequency second-order SS using a variable-width hysteresis loop was presented in [23]. A similar methodology was applied to single-phase [24]–[25] and three-phase inverters [26]. Other types of second-order SSs derived using the state-energy plane were proposed for single- and dual-output boost converters [12], [27]. Higher-order switching surfaces for

inverters were derived in [21] and [28], where logarithmic SSs were used to approximate the system trajectories. Another method to approximate the ideal trajectories was derived from the converter differential equations assuming a constant-current load [29]. Using those SSs called the Natural Switching Surfaces (NSS) warrants no output voltage overshoot for a step load variation under nominal design conditions, excellent response for any change of the load resistance and much easier trajectory derivation because of the absence of the exponential decay, spirals or hyperbolic terms related to the presence of the load resistance in the differential equations [15]. This method was first presented in [29] for buck converters and then extended to the inverters [30], boost [13], [31], buck-boost [32], dual active bridge [33], full bridge [34] and flyback converters [8], [35], [36].

1.4 ISSUES OF BOUNDARY CONTROL

The main drawback of BC is the dependence of the switching surfaces on the converter parameters [14], [16], which are exposed to changes due to component tolerances, aging effects, humidity and temperature [25]–[26]. Parameter variations, such as discrepancies between the design output capacitor value and the real one, impact on the steady-state performance [21]–[22] and lead to stability issues because of changes on the shape of the switching surfaces [31] and converter operating modes [12]. This dissertation presents a solution to those issues by deriving the NSSs and the control law for a flyback converter operating in BCM and considering parameter uncertainties. The proposed control law can provide a very precise estimation of the parameter variations in only a single switching action and then continuously adapt the control switching surfaces before a new switching action occurs. Therefore, the converter can reach the steady-state operation in a single switching action for sudden load changes even under extreme converter parameter variations.

Another problem of the BC is the extensive number of current and voltage sensors needed to control the converter. For the case of the flyback converter, two voltage (v_{in} and v_o) and three current sensors (i_p, i_s, and i_o) are needed to provide a satisfactory control. Three of those sensors require galvanic insulation, which increase cost and complexity. This dissertation proposes a novel sensorless natural switching surface control that allows to eliminate some of the sensors and still estimate converter parameter uncertainties to provide a satisfactory control response.

1.5 DISSERTATION ORGANIZATION

This dissertation is organized as follows. Chapter 2 presents the derivation of the NSS for a flyback converter where the target point is carefully selected to operate in BCM. Multiple start-up algorithms are proposed, and their performances are compared. Chapter 3 describes the derivation of the NSS for a flyback converter with parameter uncertainties. An adaptive control law is proposed and validated through simulations. Chapter 4 introduces an extensive study about the influence of parasitic elements, such as diode voltage drop, in the previously derived natural switching surfaces. Also, the effect of the parameter uncertainties on the steady-state and transient characteristics of the converter are analyzed. Then, an adaptive BCM NSS control law is proposed, simulated and tested experimentally. Also, the proposed NSS control is compared with a linear compensator. Chapter 5 presents a sensorless approach for the adaptive BCM NSS control law that eliminate the need of sensing some of variables in the secondary side of the transformer. Finally, Chapter 6 presents the conclusions and recommendations for future work.

1.6 REFERENCES

[1] M. Kazimierczuk, “Pulse-width Modulated DC–DC Power Converters”, First Edition, John Wiley & Sons, ISBN: 978-0-470-69465-7, 2008.

[2] Q. Wu and Z. Zhu, "An Adaptive High-Precision OCP Control Scheme for Flyback AC/DC Converters," *in IEEE Transactions on Power Electronics*, vol. 32, no. 12, pp. 8969-8973, Dec. 2017.

[3] C. Zhao, J. Zhang and X. Wu, "An Improved Variable On-Time Control Strategy for a CRM Flyback PFC Converter," *in IEEE Transactions on Power Electronics*, vol. 32, no. 2, pp. 915-919, Feb. 2017.

[4] T. Yan, J. Xu, F. Zhang, J. Sha and Z. Dong, "Variable-On-Time-Controlled Critical-Conduction-Mode Flyback PFC Converter," *in IEEE Transactions on Industrial Electronics*, vol. 61, no. 11, pp. 6091-6099, Nov. 2014.

[5] S. B. Kjaer, J. K. Pedersen and F. Blaabjerg, "A review of single-phase grid-connected inverters for photovoltaic modules," *in IEEE Transactions on Industry Applications*, vol. 41, no. 5, pp. 1292-1306, Sept.-Oct. 2005.

[6] A. C. Kyritsis, E. C. Tatakis and N. P. Papanikolaou, "Optimum Design of the Current-Source Flyback Inverter for Decentralized Grid-Connected Photovoltaic Systems," *in IEEE Transactions on Energy Conversion*, vol. 23, no. 1, pp. 281-293, March 2008.

[7] S. Ang, A. Oliva, “Power-Switching Converters”, Third Edition, CRC Press, ISBN: 978-1439815335, 2010.

[8] L. A. Garcia-Rodriguez, E. Williams, J. C. Balda, J. Gonzalez-Llorente and H. Chiacchiarini, "Control of a flyback converter operating in BCM using the natural switching surface," *2015 IEEE 6th International Symposium on Power Electronics for Distributed Generation Systems* (PEDG), Aachen, 2015, pp. 1-8.

[9] L. A. Garcia Rodriguez and J. C. Balda, "A comparison of isolated DC-DC converters for microinverter applications," *2013 Twenty-Eighth Annual IEEE Applied Power Electronics Conference and Exposition (APEC),* Long Beach, CA, USA, 2013, pp. 2084-2091.

[10] G. Spiazzi, D. Tagliavia and S. Spampinato, "DC-DC flyback converters in the critical conduction mode: a re-examination," *Conference Record of the 2000 IEEE Industry Applications Conference. Thirty-Fifth IAS Annual Meeting and World Conference on Industrial Applications of Electrical Energy (Cat. No.00CH37129)*, Rome, 2000, pp. 2426-2432 vol.4.

[11] B. T. Irving, Y. Panov and M. M. Jovanovic, "Small-signal model of variable-frequency flyback converter," *Applied Power Electronics Conference and Exposition, 2003. APEC '03. Eighteenth Annual IEEE, Miami Beach*, FL, USA, 2003, pp. 977-982 vol.2.

[12] T. T. Song and H. S. h. Chung, "Boundary Control of Boost Converters Using State-Energy Plane," *in IEEE Transactions on Power Electronics*, vol. 23, no. 2, pp. 551-563, March 2008.

[13] J. M. Galvez, M. Ordonez, F. Luchino and J. E. Quaicoe, "Improvements in Boundary Control of Boost Converters Using the Natural Switching Surface," *in IEEE Transactions on Power Electronics*, vol. 26, no. 11, pp. 3367-3376, Nov. 2011.

[14] P. T. Krein, Nonlinear Phenomena in Power Electronics: Attractors, Bifurcation, Chaos, and Nonlinear Control. New York: IEEE Press, 2001, ch. 8.

[15] R. Munzert and P. T. Krein, "Issues in boundary control [of power convertors]," *PESC Record. 27th Annual IEEE Power Electronics Specialists Conference*, Baveno, 1996, pp. 810-816 vol.1.

[16] M. Greuel, R. Muyshondt and P. T. Krein, "Design approaches to boundary controllers," PESC97. *Record 28th Annual IEEE Power Electronics Specialists Conference*. Formerly Power Conditioning Specialists Conference 1970-71. Power Processing and Electronic Specialists Conference 1972, St. Louis, MO, 1997, pp. 672-678 vol.1.

[17] R. A. DeCarlo, S. H. Zak and G. P. Matthews, "Variable structure control of nonlinear multivariable systems: a tutorial," *in Proceedings of the IEEE*, vol. 76, no. 3, pp. 212-232, Mar 1988.

[18] V. I. Utkin, "Sliding mode control design principles and applications to electric drives," *in IEEE Transactions on Industrial Electronics*, vol. 40, no. 1, pp. 23-36, Feb 1993.

[19] C. N. Onwuchekwa and A. Kwasinski, "Analysis of Boundary Control for Buck Converters With Instantaneous Constant-Power Loads," *in IEEE Transactions on Power Electronics*, vol. 25, no. 8, pp. 2018-2032, Aug. 2010.

[20] K. K. S. Leung and H. S. H. Chung, "Derivation of a second-order switching surface in the boundary control of buck converters," *in IEEE Power Electronics Lette*rs, vol. 2, no. 2, pp. 63-67, June 2004.

[21] J. Y. C. Chiu, K. K. S. Leung and H. S. H. Chung, "High-Order Switching Surface in Boundary Control of Inverters," *in IEEE Transactions on Power Electronics*, vol. 22, no. 5, pp. 1753-1765, Sept. 2007.

[22] K. K. S. Leung and H. S. h. Chung, "A Comparative Study of Boundary Control With First- and Second-Order Switching Surfaces for Buck Converters Operating in DCM," *in IEEE Transactions on Power Electronics*, vol. 22, no. 4, pp. 1196-1209, July 2007.

[23] W. T. Yan, C. N. M. Ho, H. S. H. Chung and K. T. K. Au, "Fixed-Frequency Boundary Control of Buck Converter With Second-Order Switching Surface," *in IEEE Transactions on Power Electronics*, vol. 24, no. 9, pp. 2193-2201, Sept. 2009.

[24] P. K. W. Chan, H. Shu-Hung Chung and S. Y. Hui, "A Generalized Theory of Boundary Control for a Single-Phase Multilevel Inverter Using Second-Order Switching Surface," *in IEEE Transactions on Power Electronic*s, vol. 24, no. 10, pp. 2298-2313, Oct. 2009.

[25] Y. He, H. S. H. Chung, C. N. M. Ho and W. Wu, "Use of Boundary Control With Second-Order Switching Surface to Reduce the System Order for Deadbeat Controller in Grid-Connected Inverter," *in IEEE Transactions on Power Electronics*, vol. 31, no. 3, pp. 2638-2653, March 2016.

[26] Y. He, H. S. h. Chung, C. N. M. Ho and W. Wu, "Direct Current Tracking Using Boundary Control With Second-Order Switching Surface for Three-Phase Three-Wire Grid-Connected Inverter," *in IEEE Transactions on Power Electronics*, vol. 32, no. 7, pp. 5723-5740, July 2017.

[27] T. Messikh, N. Rahim and M. Saad, "Boundary control of dual-output boost converter using state-energy plane," *in IET Power Electronics*, vol. 7, no. 9, pp. 2310-2321, September 2014.

[28] S. Chen, Y. M. Lai, S. C. Tan and C. K. Tse, "Boundary Control With Ripple-Derived Switching Surface for DC–AC Inverters," *in IEEE Transactions on Power Electronics*, vol. 24, no. 12, pp. 2873-2885, Dec. 2009.

[29] M. Ordonez, M. T. Iqbal and J. E. Quaicoe, "Selection of a curved switching surface for buck converters," *in IEEE Transactions on Power Electronics*, vol. 21, no. 4, pp. 1148-1153, July 2006.

[30] M. Ordonez, J. E. Quaicoe and M. T. Iqbal, "Advanced Boundary Control of Inverters Using the Natural Switching Surface: Normalized Geometrical Derivation," *in IEEE Transactions on Power Electronics*, vol. 23, no. 6, pp. 2915-2930, Nov. 2008.

[31] J. M. Galvez and M. Ordonez, "High Performance Boundary Control of Boost-Derived PFCs: Natural Switching Surface Derivation and Properties," *in IEEE Transactions on Power Electronics*, vol. 27, no. 8, pp. 3807-3816, Aug. 2012.

[32] J. M. Galvez, M. Ordonez, T. T. Nguyen and F. Luchino, "Boundary control of buck-boost converters: normalized trajectories and the Natural Switching Surface," *2012 IEEE Energy Conversion Congress and Exposition (ECCE)*, Raleigh, NC, 2012, pp. 358-363.

[33] G. G. Oggier, M. Ordonez, J. M. Galvez and F. Luchino, "Fast Transient Boundary Control and Steady-State Operation of the Dual Active Bridge Converter Using the Natural Switching Surface," *in IEEE Transactions on Power Electronics*, vol. 29, no. 2, pp. 946-957, Feb. 2014.

[34] G. G. Oggier and M. Ordonez, "Boundary Control of Full-Bridge ZVS: Natural Switching Surface for Transient and Steady-State Operation," *in IEEE Transactions on Industrial Electronics*, vol. 61, no. 2, pp. 969-979, Feb. 2014.

[35] L. A. G. Rodriguez, H. Chiacchiarini and J. C. Balda, “Control of a flyback converter with parametric uncertainties operating in BCM Using the natural switching surface*,” 2016 IEEE Biennial Congress of Argentina (ARGENCON)*, Buenos Aires, Argentina, 2016, pp. 1-7.

[36] L. A. Garcia Rodriguez, H. G. Chiacchiarini, D. Carballo Rojas and J. C. Balda, “Adaptive Boundary Control Using Natural Switching Surfaces for Flyback Converters Operating in the Boundary Conduction Mode with Parameter Uncertainties,” in *IEEE Transactions on Power Electronics*, vol. 34, no. 8, pp. 8118-8137, Aug. 2019.

CHAPTER 2

Control of a Flyback Converter Operating in BCM Using the Natural Switching Surface

L. A. Garcia-Rodriguez, E. Williams, J. C. Balda, J. Gonzalez-Llorente and H. Chiacchiarini, "Control of a flyback converter operating in BCM using the natural switching surface," *2015 IEEE 6th International Symposium on Power Electronics for Distributed Generation Systems (PEDG)*, Aachen, 2015, pp. 1-8.

2.1 ABSTRACT

The derivation and implementation of natural switching surface (NSS) control for a flyback converter operating in boundary conduction mode (BCM) is the main focus of this paper. The flyback converter has been wildly utilized in the area of power electronics and BCM operation has been proven to be successful in attaining high efficiencies. The NSS presents many benefits for the control of non-linear systems such as fast transient response under load-changing conditions. The NSS control technique has previously been implemented in non-isolated (e.g., buck and boost converters) and isolated (dual active bridge) converter topologies demonstrating excellent performances. The analytical derivation of the proposed switching surfaces is presented and validated through simulations using MATLAB/Simulink™ and a 65W prototype was experimentally tested.

Keywords—Flyback converter, non-linear control, boundary control, natural switching surface, boundary conduction mode.

2.2 INTRODUCTION

A flyback converter is commonly used in systems rated 20 W to 200 W due to its low part count, electrical isolation and wide voltage ratio [1]. In addition to the traditional applications in computers and TV sets, the flyback converter is utilized in photovoltaic microinverters where it operates over a wide range of operating conditions [2]–[4]. Linear compensators are unsuccessful for large load variations; therefore, nonlinear controllers, such as sliding mode controllers, are suitable for these converters [5]–[6].

In recent years, the transient response of typical boundary schemes in power converters has been improved by using the natural switching surfaces (NSS) [7], [8]. The NSS are the natural trajectories of states for each switching position of the converter [9]. The NSS has been studied for the basic non-isolated topologies [7], [8] and for isolated topologies like the dual active bridge [10]. In this work, the NSS and its control law are derived for any generic flyback converter. It is also proven that it is possible to design the converter to work in the boundary conduction mode (BCM) for any loading condition by properly selecting the target point of the trajectories.

The organization of this paper is as follows: the normalized system trajectories are derived in section 2.3; the selection of the operating conditions and target points are developed in section 2.4, the presented control laws are presented in section 2.5. Finally, the simulation and experimental results are given in section 2.6 and 2.7, and the conclusions and future work are provided in section 2.8.

2.3 NORMALIZED SYSTEM TRAJECTORIES

The system shown in Fig. 2.1 is a simplified version of a flyback converter which consists of an ideal transistor *Q*, a diode *D*, a flyback transformer, as well as input and output capacitors. The load is represented by a current source which states the worst-case scenario in terms of stability [8].

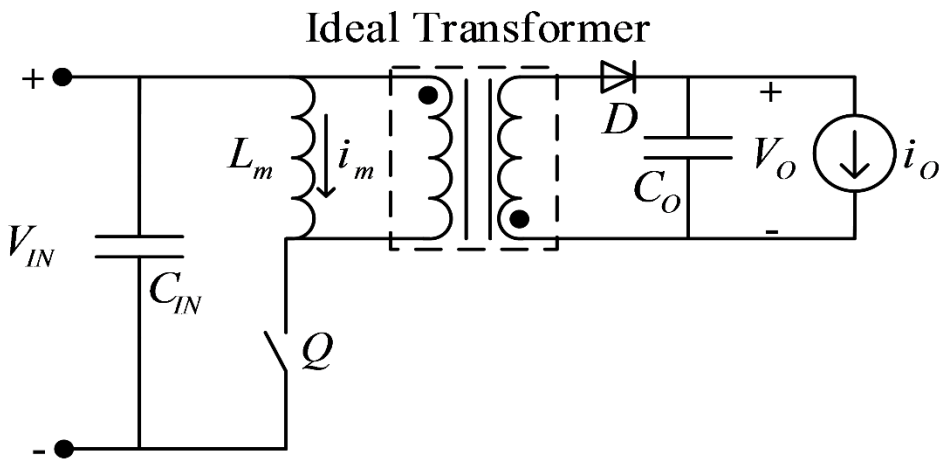

Fig. 2. 1. Flyback converter circuit.

The normalization of the system consists of a scale change of its differential equations which enables a general solution. The presence of a transformer makes it necessary to refer the converter parameters to one side; the secondary side is selected in this case. The normalization is performed using the output voltage as the reference voltage $V_r = V_o$, the characteristic impedance of the combined magnetizing inductance referred to the secondary side and the output capacitor, $Z_o = (1/n)\sqrt{L_m/C_o}$ as the reference impedance Z_r and the natural frequency $f_o = n\Big/\left(2\pi\sqrt{L_m C_o}\right)$ as the reference frequency f_r. The normalizing equations of the voltage, current and time variables as well as their derivatives for the secondary variables are as follows:

$$v_n = \frac{v}{V_r}, \qquad dv_n = \frac{dv}{V_r}, \tag{1}$$

$$i_n = i\frac{Z_r}{V_r}, \qquad di_n = di\frac{Z_r}{V_r}, \tag{2}$$

$$t_n = t.f_r, \qquad dt_n = dt.f_r, \tag{3}$$

where v, i, t are the standard voltage, current and time variables of the secondary side, and v_n, i_n, and t_n are the normalized versions. Due to the presence of a transformer, the normalizing equations

must be reflected back to the primary side to normalize a primary variable. The normalizing equations of primary variables are as follows:

$$v_n = \frac{v}{V_r}\frac{N_s}{N_p}, \qquad i_n = i\frac{Z_r}{V_r}\frac{N_p}{N_s}, \tag{4}$$

$$dv_n = dv\frac{N_s}{V_r N_p}, \qquad di_n = di\frac{Z_r}{V_r}\frac{N_p}{N_s}. \tag{5}$$

The following subsections present the derivation of the normalized ON- and OFF-state trajectories.

2.3.A OFF-State Trajectory

During the OFF-state of transistor *Q*, diode *D* conducts and the energy stored in the air gap of the transformer during the ON-state is transferred to the load. The voltage applied to the magnetizing inductance is the output voltage multiplied by the transformer turns ratio. The following are the differential equations that describe this mode of operation:

$$L_m\frac{di_m}{dt} = -v_o\frac{N_p}{N_s}, \tag{6}$$

$$C_o\frac{dv_o}{dt} = i_m\frac{N_p}{N_s} - i_o. \tag{7}$$

Using equations (1) through (5), the normalization of the differential equations (6) and (7) becomes:

$$\frac{di_{mn}}{dt_n} = -2\pi v_{on}, \tag{8}$$

$$\frac{dv_{on}}{dt_n} = 2\pi\left(i_{mn} - i_{on}\right). \tag{9}$$

Differentiating both sides of (8) and replacing it in (9) yields a differential equation having the following solution:

$$i_{mn}(t_n) = i_{on} + \left(i_{mn}\left(0^-\right) - i_{on}\right)\cos\left(2\pi t_n\right) + \frac{\dfrac{di_{mn}\left(0^-\right)}{dt_n}}{2\pi}\sin\left(2\pi t_n\right). \tag{10}$$

By applying the trigonometric property $A\cos(x) + B\sin(x) = \sqrt{A^2 + B^2}\,\sin\left(x + \tan^{-1}\left(\frac{A}{B}\right)\right)$ to (10), taking the derivative of the resulting expression and applying the property $\cos\left(\sin^{-1}(x)\right) = \sqrt{1 - x^2}$, the result is an equation which does not depend on the normalized time. Then, the OFF-state trajectory can be expressed as:

$$\lambda_{OFF} := v_{on}^2 + \left(i_{mn} - i_{on}\right)^2 - A^2 - B^2 = 0, \tag{11}$$

where $A = i_{mn}\left(0^-\right) - i_{on}$ and $B = \frac{1}{2\pi}\frac{di_{mn}\left(0^-\right)}{dt_n}$. Therefore, the OFF-state trajectory is a circle with its center at (i_{mn}, v_{on}) = (i_{on}, 0) and a radius that is a function of the specifications of the converter.

2.3.B ON-State Trajectory

When the transistor Q is ON, the magnetizing inductance is connected to the input source and the diode at the secondary side is reversed bias. The differential equations for this stage and their normalized versions are:

$$V_{IN} = \frac{L_m di_m}{dt}, \qquad -i_o = C_o\frac{dv_o}{dt}, \tag{12}$$

$$2\pi V_{INn} = \frac{di_{mn}}{dt_n}, \qquad -2\pi i_{on} = \frac{dv_{on}}{dt_n}. \tag{13}$$

Equation (13) shows that when the transistor is ON, the magnetizing current and the output voltage vary linearly with time. The slope of the straight line is obtained by dividing the two normalized equations:

$$\frac{di_{mn}}{dv_{on}} = -\frac{V_{INn}}{i_{on}}. \tag{14}$$

By integrating (14), the natural trajectory of the flyback converter when the transistor is ON is given by:

$$\lambda_{ON} := i_{mn} + \frac{V_{INn}}{i_{on}} v_{on} - K = 0, \tag{15}$$

where K is a constant which defines the point where the trajectory intersects the normalized magnetizing current axis. This constant K is selected in such a way that the ON-state trajectory intersects the target operating point.

2.3.C Graphical Analysis of the NSS Trajectories

Fig. 2.2 presents graphical renditions of the NSS trajectories previously derived. These graphs are for a generic flyback converter, with arbitrary trajectory placement in the i_{mn} vs. v_{on} plane. As previously described, the ON-state trajectory is a descending sloping line and the OFF-state trajectory is a circle, arbitrarily pictured here with a center at (0, 0). This subsection shows the interaction of the two trajectories with each other and their relationship with the converter operation.

Evaluating the i_{mn} vs. v_{on} plane and analysing the operation of a flyback converter, immediately quadrants of the plane can be recognized as unobtainable or undesirable operation zones based on the polarity of the variables. For example, i_{mn} can only be positive for the flyback converter to be operating correctly. Therefore, i_{mn} would not be reachable in quadrants III or IV. Also, v_{on} would not be negative either. This would imply that the load was transferring power to the input of the converter, which is physically impossible due to the presence of D. Therefore, v_{on} should not operate in quadrants II or III. That leaves only quadrant I as the operational quadrant which

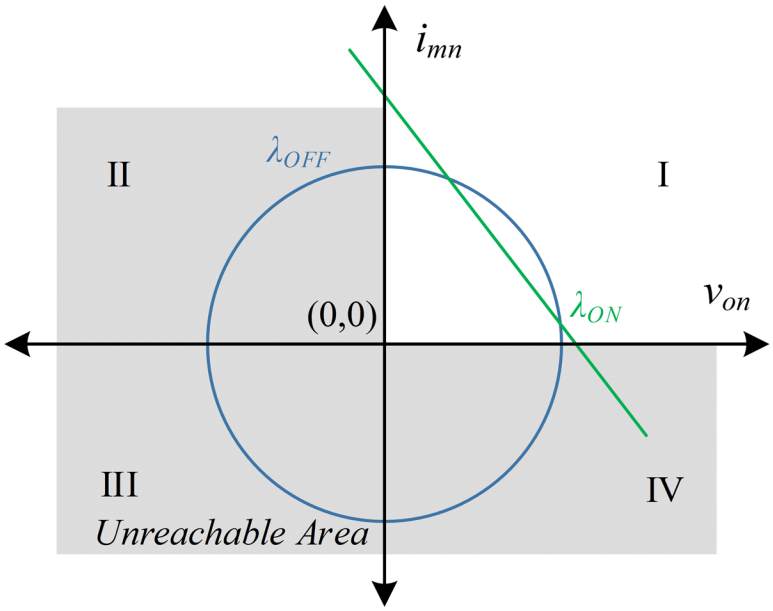

Fig. 2. 2. Normalized natural surfaces for a flyback converter.

satisfies both variables' conditions. In quadrant I, i_{mn} and v_{on} are both positive and the flyback converter would be transferring power to the load. The undesired quadrants have been grayed out in Fig 2.2.

Movement along the trajectories during steady-state can be determined by considering the flyback's operation in each state. As previously discussed, during the ON-state i_{mn} is increasing, storing energy in the transformer magnetizing inductance field from the input source, and v_{on} is decreasing, due to the load consuming the energy stored in the output capacitor. Therefore, the converter operating point would slide up the trajectory during the ON-state, as shown in Fig. 2.3. During the OFF-state, i_{mn} is decreasing, supplying the transformer's stored energy to the load and output capacitor, while v_{on} is increasing, due to the transformer's supplied energy. Therefore, the converter operating point would slide down the trajectory during the OFF-state.

If the converter's trajectory was to reach an axis, the converter would then evolve on that axis. Therefore, reaching the i_{mn} axis, the converter would change i_{mn} while the output voltage remained

at zero. Likewise, reaching the v_{on} axis, the converter would change v_{on} while keeping the magnetizing current zero. This is due to the unobtainable quadrants.

2.3.D NSS Trajectories and Modes of Operation

The interaction between the ON- and OFF-state trajectories determines which mode the flyback converter operates in, whether Continuous (CCM), Boundary, and Discontinuous (DCM) Modes of Operation. From this knowledge, a control law to force the converter into BCM, as desired, can be designed. When the two trajectories intersect, the flyback converter switches from the ON- to OFF-state or vice versa. Therefore, this intersection actually determines when the flyback converter's transistor Q actually switches.

There are three possibilities where the trajectories can intersect, correlating to the three modes of operation. Fig. 2.3 depicts the three choices. Fig. 2.3(a) shows the converter trajectories in CCM, where the magnetizing current never reaches zero. Fig. 2.3(b) illustrates when the magnetizing current just reaches zero before turning transistor Q ON again, which correlates to BCM. Lastly, Fig. 2.3(c) shows DCM operation, allowing the converter to evolve along the v_{on} axis with zero magnetizing current before changing back to the ON-state. Fig. 2.3(b) depicts the intended converter operation, since BCM operation is desired.

2.4 SELECTION OF THE OPERATING CONDITIONS AND TARGET POINTS

2.4.A Conventional Approach

The approach presented in [8] defines the initial conditions of the ON- and OFF-state trajectories based on the target operating point of the converter. The target for the output voltage is equal to the reference voltage $v_{on} = V_{rn} = 1$, and the target for the magnetizing current is based on the required output power. Assuming that the converter is ideal, the initial conditions of (11) are:

$$I_{mn,target} = \frac{i_{on}V_{rn}}{D_n V_{INn}} = i_{on}\left(1+\frac{1}{V_{ccn}}\right), \tag{16}$$

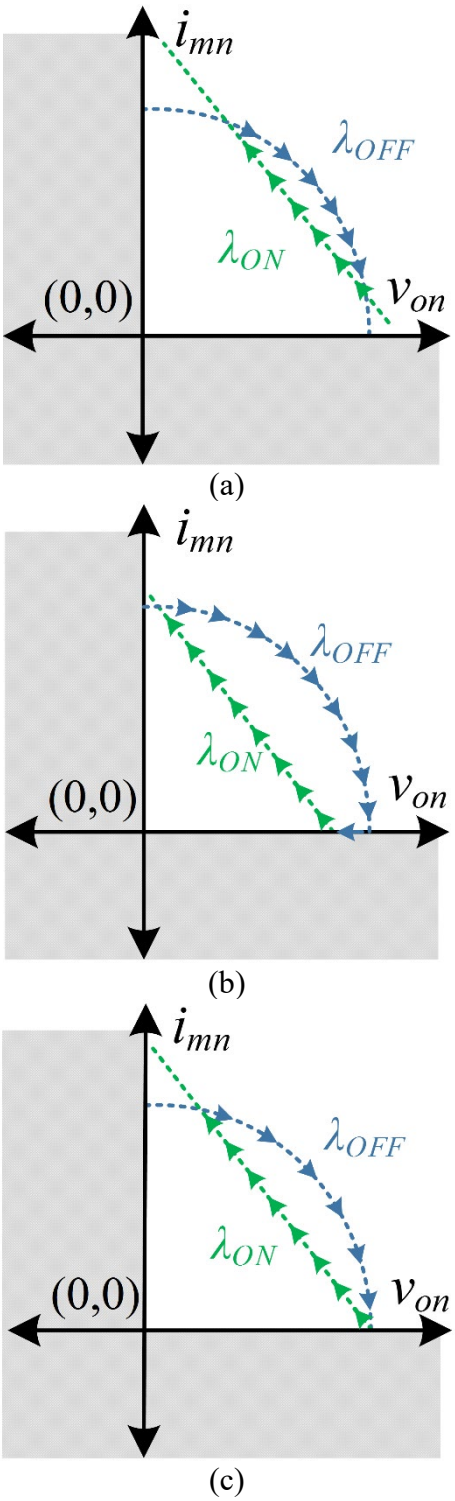

Fig. 2. 3. NSS trajectories and modes of operation: (a) CCM, (b) BCM, and (c) DCM.

$$\frac{di_{mn}(0^-)}{dt_n} = -2\pi, \tag{17}$$

where $D_n = \frac{V_{on}}{V_{INn} + V_{on}}$ is the normalized duty cycle for the flyback converter. The OFF-state trajectory is obtained by replacing (16) and (17) into (11):

$$\lambda_{OFF} := v_{on}^2 + \left(i_{mn} - i_{on}\right)^2 - 1 - \left(\frac{i_{on}}{V_{ccn}}\right)^2 = 0, \tag{18}$$

Similarly, evaluating (15) at the target point (i_{mn}, v_{on}) = ($i_{mn,target}$, 1), the trajectory for the ON-state is obtained as follows:

$$\lambda_{ON} := i_{mn} + \frac{V_{ccn}}{i_{on}} v_{on} - \left(i_{on} + \frac{i_{on}}{V_{ccn}} + \frac{V_{ccn}}{i_{on}}\right) = 0. \tag{19}$$

A control approach derived from similar equations than (18) and (19) but for a boost converter was presented in [9]. That control approach leads to an operating area close to the target operating point. This would cause the operation mode of the converter to mainly be CCM which would not be the desired case for applications that require high efficiencies.

2.4.B Proposed Approach

A control law to keep the operation of a flyback converter in BCM operation for all load conditions is desired. The goal of this section is to identify a known target operating point and define the trajectories' design parameters and unknowns to include this point.

From Fig. 2.3(b), it is identified that if the target operating point is set to be at the reference output voltage and zero magnetizing current, the converter will work in BCM for all load conditions. Replacing this known trajectory point (i_{mn}, v_{on}) = (0, 1), in (15), the constant K in the ON-state trajectory is given by:

$$K = \frac{V_{INn}}{i_{on}}. \tag{20}$$

Therefore, the BCM ON-state trajectory is

$$\lambda_{ON} := i_{mn} + \frac{V_{INn}}{i_{on}} v_{on} - \frac{V_{INn}}{i_{on}} = 0. \tag{21}$$

Moving onto the OFF-state trajectory, A and B can be simplified with the known trajectory point. Knowing that $v_{on} = 1$, (8) can be simplified to

$$\frac{di_{mn}\left(0^-\right)}{dt_n} = -2\pi. \tag{22}$$

Then, A and B can be expressed as:

$$A = -i_{on}, \qquad B = -1. \tag{23}$$

Substituting (23) into (11), the complete BCM OFF-state trajectory is defined as

$$\lambda_{OFF} := v_{on}^2 + \left(i_{mn} - i_{on}\right)^2 - 1 - i_{on}^2 = 0. \tag{24}$$

2.5 STEADY-STATE BCM CONTROL LAW

The goal of a control law is to force the converter to move to or stay on the identified BCM trajectories. Knowing the movements along the trajectories for each state of transistor Q and the above conditions, a control law can be developed. The control law decides between two options: either Q should be ON or Q should be OFF. The decision is based on the current state of transistor Q and the relative location of the current operating point to the BCM trajectories.

Fig. 2.4(a) depicts the control law and possible converter trajectories for when Q is ON. As previously discussed, while Q is ON, the converter will move up the plane. If the converter is currently operating below the OFF-trajectory, Q is kept ON while the converter continues to move up the plane until the OFF-state trajectory is reached. Once the OFF-state trajectory is reached, Q is

switched OFF. If the converter is operating anywhere above the OFF-trajectory, then transistor Q should be turned OFF.

Fig. 2.4(b) shows the control law and possible converter trajectories for when Q is OFF. Remembering the desire to operate in BCM, the first part of the law is that Q is not allowed to

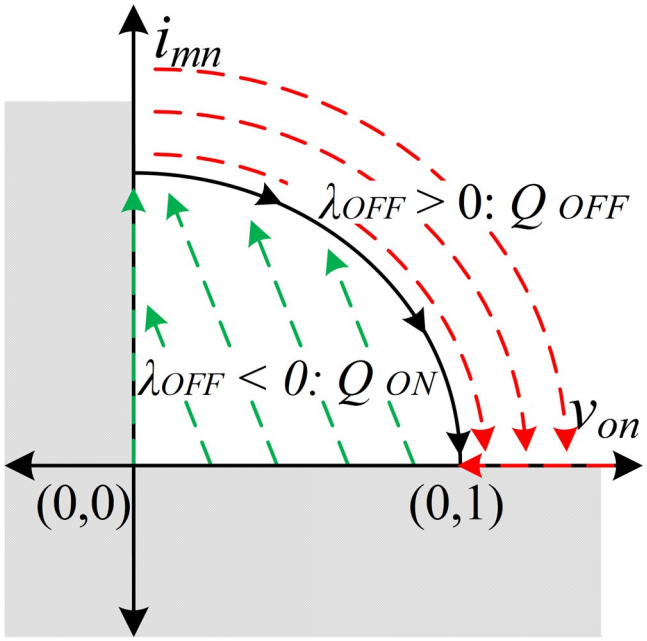

(a)

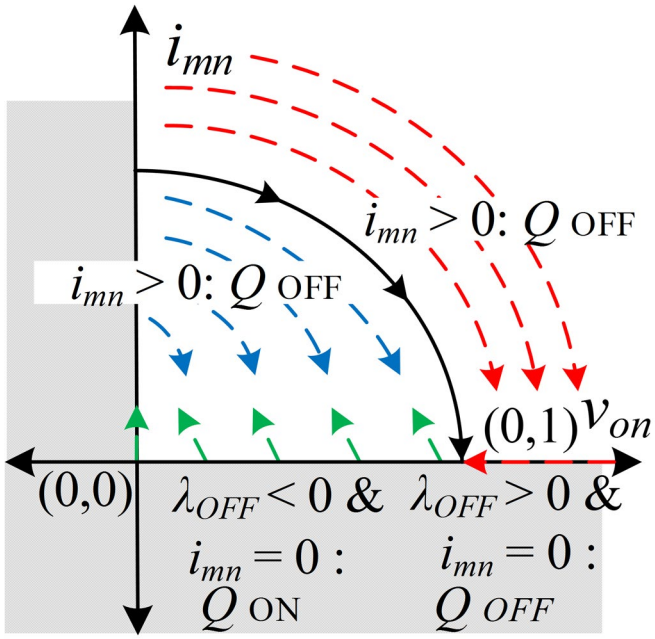

(b)

Fig. 2. 4. BCM control law trajectories: (a) Q is ON, (b) Q is OFF.

switch back ON until $i_{mn} = 0$, once it has been switched OFF. Therefore, if the converter is operating anywhere above the v_{on} axis ($i_{mn} > 0$), Q is kept OFF until the converter reaches the v_{on} axis. Once the v_{on} axis is reached, the current operating point is compared to the OFF-state trajectory. If the converter is operating greater than the OFF-state trajectory, Q is kept OFF, allowing the converter to evolve down the v_{on} axis to the OFF-state trajectory. If the converter is operating below or at the OFF-state trajectory, Q is switched ON, allowing the converter to ride the ON-state trajectory back up to the OFF-state trajectory as previously described.

Fig. 2.5 shows a complete flow diagram for the developed BCM control law that forces the converter to move to and operate on the BCM trajectories in one switching cycle, no matter where the converter is currently operating. This allows the flyback converter to operate in BCM continuously for any loading condition during steady-state. In a transient condition, where the input voltage or load changes, the worst case scenario would be that the converter recovers in one switching cycle. During that one transient switching cycle, a DCM operation with a slightly over voltage output or a BCM of operation with a slightly under voltage output could be experienced. This is because the desired ON- and OFF-state trajectories change with converter parameter changes. Taking only one switching cycle to recover provides remarkable stability and transient response time for all converter conditions.

Another significant benefit of keeping Q OFF until $i_{mn} = 0$ after switching is that the possibliity of chattering is eliminated because only two definite switching locations are identified: at the intersection of the ON- and OFF-state trajectories and on the v_{on} axis.

2.5.A Steady-State Switching Frequency Derivation

The switching frequency of a converter is very important in considerations for EMI and component selection including microcontroller or processor, semiconductor devices, current

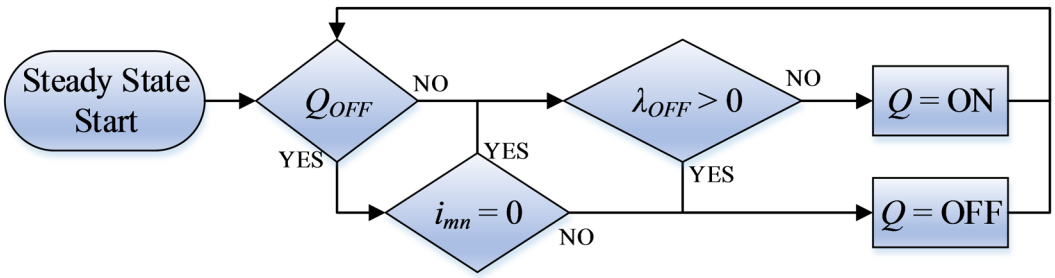

Fig. 2. 5. BCM control law flow diagram.

sensors, and analog-to-digital (ADC) converters. This section will derive an accurate approximation for the steady-state switching frequency using the proposed control laws. The switching frequency is dependent upon the average input and output voltages, turns ratio of the transformer, and the transformer's magnetizing inductance.

The normalized switching period, T_{SWn}, can be described as

$$T_{SWn} = T_{ONn} + T_{OFFn}, \tag{25}$$

where T_{ONn} and T_{OFFn} are the normalized values for the ON and OFF times, respectively; T_{ONn} and T_{OFFn} can be calculated from the differential equations for i_{mn} in each state:

$$T_{ONn} = \frac{\Delta i_{mn}}{2\pi V_{INn}}, \tag{26}$$

$$T_{OFFn} = \frac{\Delta i_{mn}}{2\pi V_{on}}. \tag{27}$$

Noting that Δi_{mn} is equal for both ON- and OFF-states, the normalized switching period is obtained by replacing (26) and (27) into (25):

$$T_{SWn} = \frac{\Delta i_{mn}}{2\pi}\left(1 + \frac{1}{V_{INn}}\right). \tag{28}$$

Therefore, the switching frequency is

$$f_{SWn} = \frac{2\pi}{\Delta i_{mn} T_o \left(1 + \frac{1}{V_{inn}}\right)}. \tag{29}$$

The magnetizing current variation, Δi_{mn}, can be obtained from the intersection point of the ON- and OFF-state trajectories in steady-state operation. One extreme is where $i_{mn} = 0$, which corresponds to $V_{on} = 1$. The other intersection defines Δi_{mn} and here it is realized that V_{on} is close, but not equal to 1. To find this intersection, and therefore Δi_{mn}, the ON- and OFF-state trajectories will be solved for V_{on} by setting them equal to each other in order to eliminate V_{on}. Δi_{mn} is then solved for

$$\Delta i_{mn} = 2 i_{on} \left(1 + \frac{1}{V_{INn}} \right). \tag{30}$$

Substituting (30) into (29), and replacing the normalized converter values in terms of the non-normalized ones, the switching frequency can be described as

$$f_{sw} = \frac{V_o \left(\frac{N_p}{N_s} \right)^2}{2 i_o L_m \left(1 + \frac{V_o N_p}{V_{IN} N_s} \right)^2}. \tag{31}$$

2.6 SIMULATION RESULTS

2.6.A Steady-State BCM Control Law

The control law proposed above was implemented in MATLAB/Simulink©. The flyback was simulated at 100 W, with device parameters equivalent to chosen devices used in the experimental testing, detailed in Table 2.I.

Fig. 2.6(a) shows the simulation results for the ON- and OFF-state trajectories of the steady-state BCM control law implementation for one switching cycle. From this figure, it is notable that the ON-state trajectory is a straight line and the OFF-state trajectory is an arc of a circle (the circle is distorted in the figure due to axis scaling). The converter changes from the OFF-state to the ON-state

TABLE 2. I. EXPERIMENTAL AND SIMULATION CONVERTERS PARAMETERS

Parameter	Value
V_o	200 V
I_o	0.5 A
P_o	100 W
L_m	28 μH
C_o	100 μF
V_{in}	24 V

once the converter reaches $i_{mn} = 0$, meaning the converter is operating in BCM as desired. Fig. 2.6(b) displays the steady-state primary and secondary current while Fig. 2.6(c) the steady-state output voltage. The primary and secondary currents are clearly operating in BCM; once the secondary current reaches zero, the primary current instantly starts increasing. The output voltage has a ripple less than 0.09 V (also shown by Fig. 2.6(a)), which corresponds to less than 0.05%. The average value is equal to 199.97 V, which is only a 0.015% error from the desired 200 V reference. From (2), the switching frequency is approximated to be 34.77 kHz for these operating conditions. The switching frequency is measured to be 34.81 kHz from the simulations, yielding an error of 0.12%.

2.6.B Transient Response of the BCM Control Law

A transient response happens when the input voltage or loading condition changes. The transient lasts for only one switching cycle, assuming the change is completed in one switching cycle, due to the proposed control law forcing the converter to the NSS. This allows for an extremely fast transient response. Depending on when the voltage or load changes constitutes how the converter will react. The only two options for the converter operation with the proposed control law is to continue in BCM or to operate in DCM for one switching cycle.

If the OFF-trajectory radius is decreased (by a change in output current or input voltage) while the converter is operating past the new radius value, the converter will operate in DCM for one

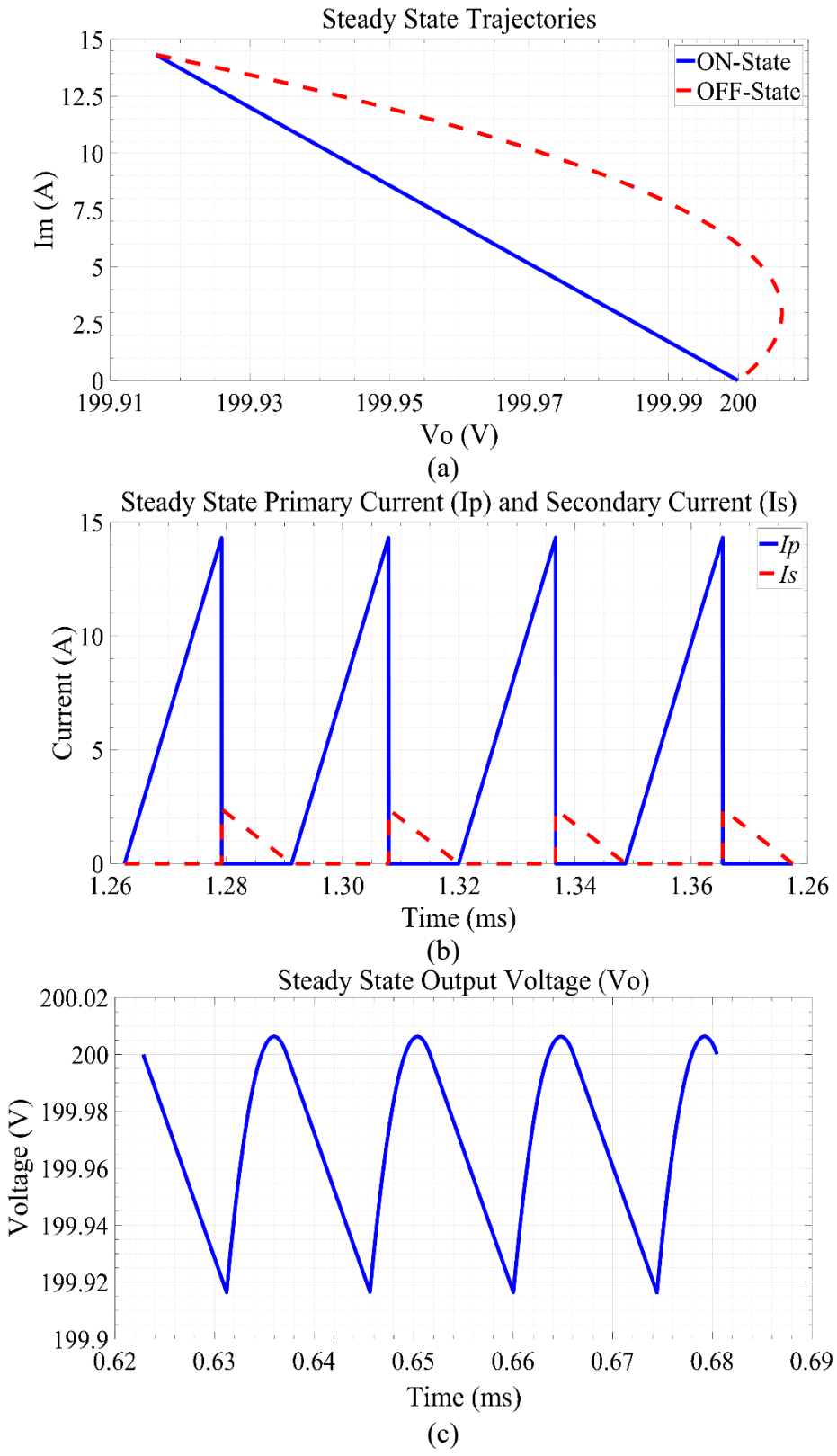

Fig. 2. 6. (a) Steady-state simulation of trajectories, (b) primary and secondary currents and (c) output voltage.

switching cycle. This is due to the fact that to get back to a lower radius trajectory, the converter must evolve down the v_{on} axis. This will result in a slightly larger overshoot of the output voltage compared to steady-state for one switching cycle. If the change occurs while the converter is operating below the new OFF-trajectory radius, no transient will occur. Fig. 2.7(a) presents an example of a DCM transient. The key point of this figure is the transient trajectory which evolves

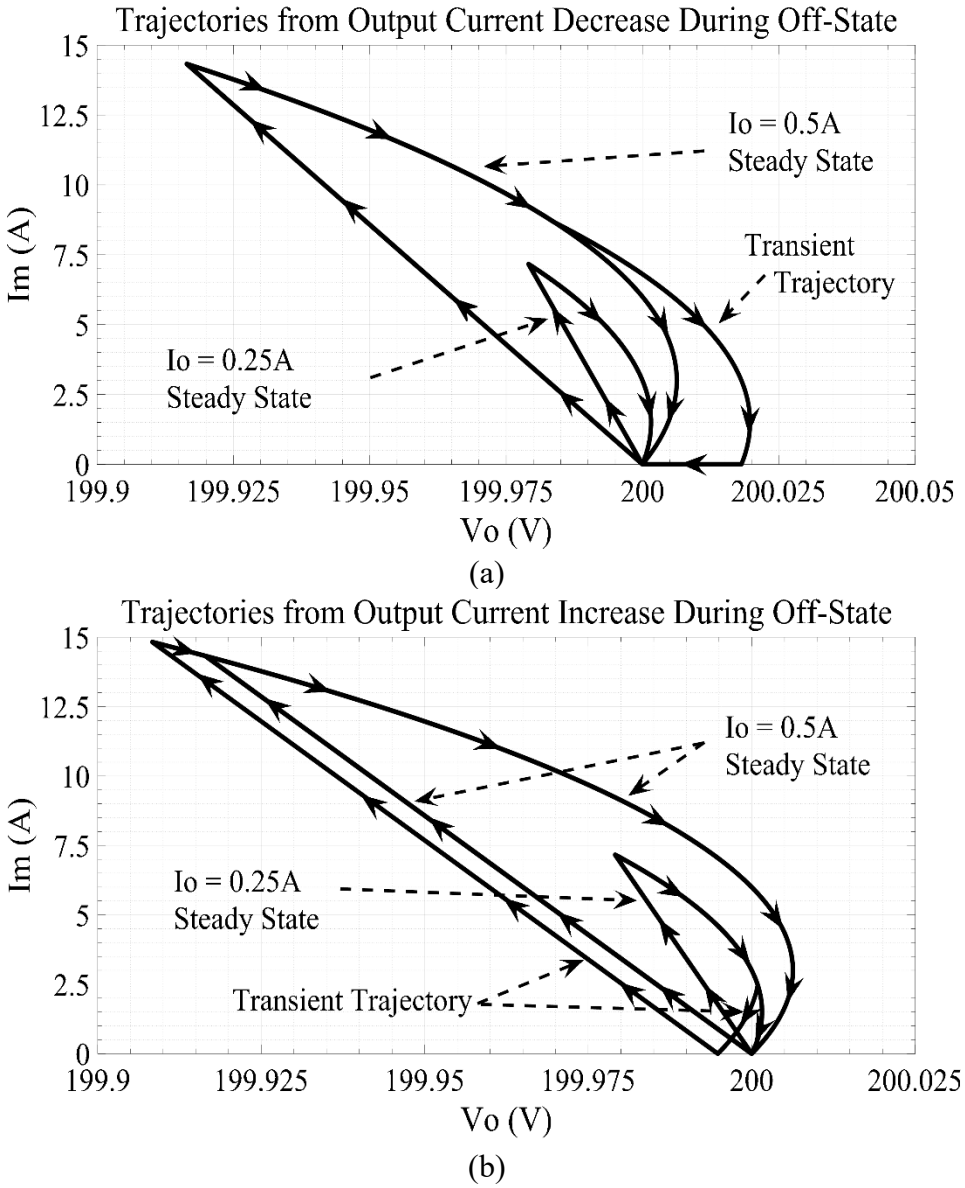

Fig. 2. 7. Transient trajectory: (a) DCM, and (b) BCM.

down the v_{on} axis. This is not the only situation where a DCM operation could occur, but just one example.

In comparison, if the OFF-trajectory radius is extended, the converter will still operate in BCM. If the change is during the ON-state, no transient will be experienced. If the change is during the OFF-state however, the converter will undershoot the new trajectory. In the next switching cycle, the converter will recover and operate back ON the desired trajectories. This will result in a slightly lower output voltage and higher peak input current compared to steady-state value for one switching cycle. Fig. 2.7(b) shows an example of an undershooting BCM transient. The undershooting transient is observable with the larger peak current.

Analyzing the undershooting BCM transient, a modification of the control law could be potentially proposed. During the OFF-trajectory, if Q was turned ON at the instant the OFF-trajectory crossed the ON-trajectory, the undershooting voltage and increase peak current would be avoided. This would force the converter to operate in CCM, never reaching 0 A during the transient. While this is a viable solution to improve the transient, the modification was omitted due to creating potential chattering issues during steady-state conditions and increasing control complexity.

Another note about Fig. 2.7 is that during steady-state, both loading conditions operated in BCM automatically. This was intended and one of the main points of the proposed control method.

2.6.C Start-Up Operation and Max Input Current Protection

Using the proposed BCM control law during start up, the flyback converter would experience an extreme input and magnetizing current peak. This is due to the control law bringing the output voltage to the reference value in one switching cycle; this would obviously require a large amount of energy since the converter is starting with 0 V output. The start-up trajectory is shown in Fig. 2.8(a). Here, the peak input current reaches 375 A, which is obviously unacceptable for typical

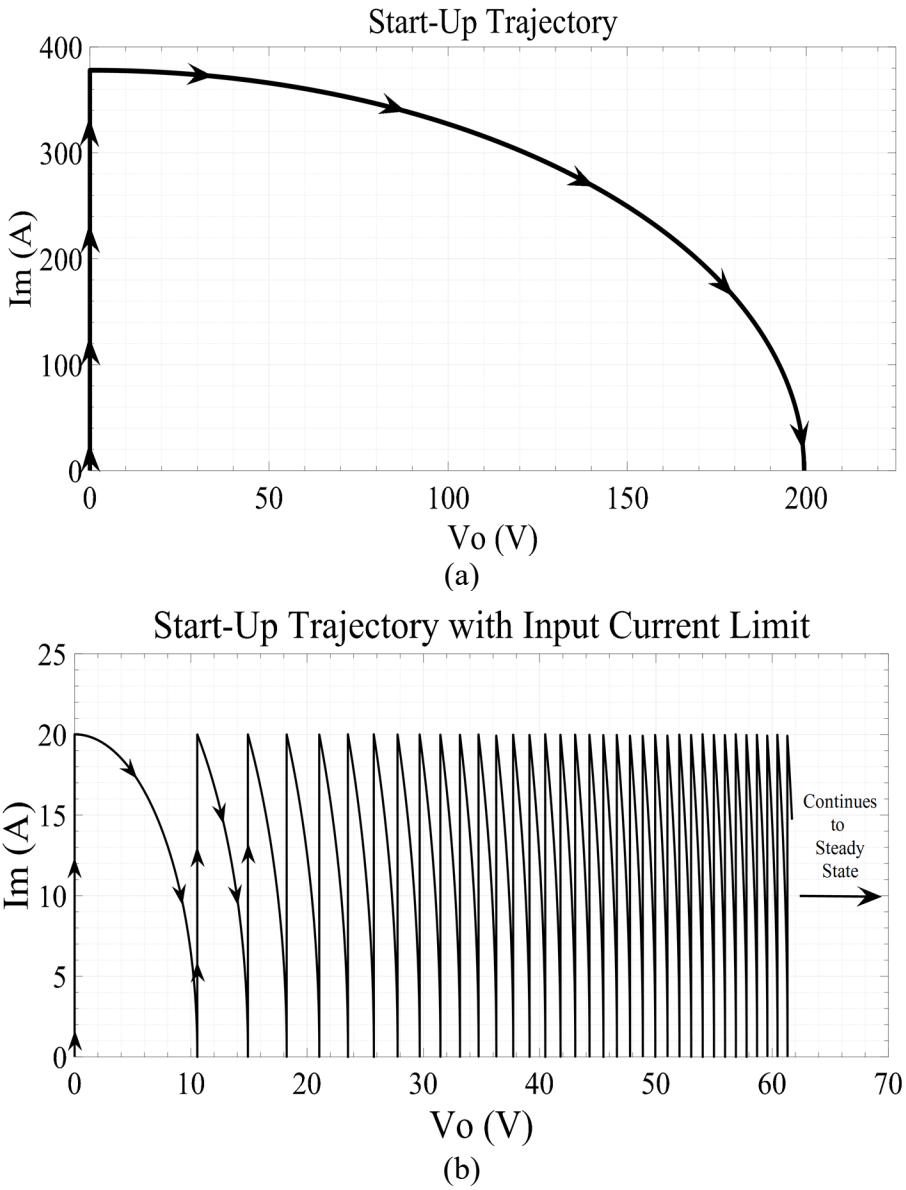

Fig. 2. 8. Start-up trajectory: (a) conventional approach, (b) with BCM input current limit.

devices. The settling time (defined here as the time for the output voltage to be bounded within 5% of its desired value) is only 0.841 ms, shown in Fig. 2.9.

To fix the large start-up input current, a maximum input current level can be set. This is a desirable addition to the control law because it protects the input devices (such as the transistor and transformer) from exceeding the current ratings and damaging the devices. Therefore, a peak input

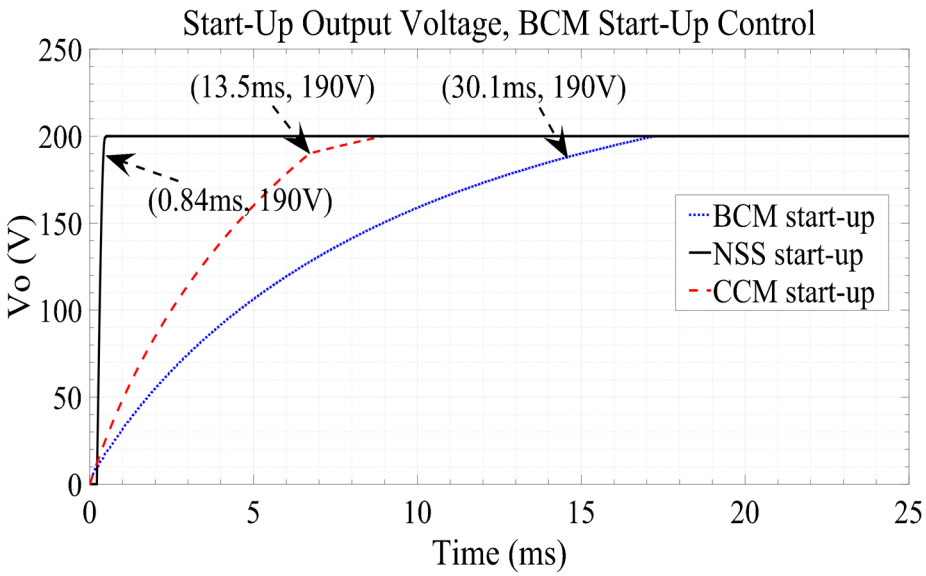

Fig. 2. 9. Start-up output voltage.

current value can be selected based of the device ratings. For this specific controller design, the peak input current was set to a non-normalized value of 20 A. Fig. 2.10(a) shows the updated control law flow diagram with the peak limitation addition. Fig. 2.8(b) shows the start-up trajectory with the current maximum implemented. As expected, the current never exceeds 20 A. The converter now takes multiple switching cycles to reach the desired voltage reference. As described before, the load of the converter is modeled as purely resistive; therefore, the output current is actually a function of the output voltage. In the start-up situation, the output current is increasing with the output voltage until the desired voltage reference is reached. Here, the controller is still operating in BCM during the start-up, forcing the magnetizing current to zero before turning Q back ON. Fig. 2.9 shows the effects of limiting the input current. The converter's output voltage settling time drastically increased from 0.841 ms to 30.1 ms, which is an undesirable effect.

To decrease the settling time, the start-up control was modified to operate in CCM, with a set Δi_{mn}, instead of operating in BCM. This allowed for a larger amount of energy to transfer faster, while still limiting the peak current. The current i_{mn} oscillated between the defined peaks, $i_{mn,pk}$ and

$i_{mn,pk}$ - Δi_{mn}. This control was chosen to be implemented any time the converter is operating below the settling range (5% of V_r, which in this converter is 190 V). The transition location between the CCM and BCM control method was selected arbitrarily and could be changed for each application, depending on the expected peak current and settling times. The longer the CCM control method operates during start up (the closer the transition is to steady-state operation), the faster the settling time will be. A potential issue though is getting the transition too close to steady-state operation and causing a chattering situation in the converter where the control law is switching from BCM to CCM operation due to a transient situation. Therefore, the 5% of V_r boundary was selected. For this converter design, Δi_{mn} = 5 A. Again, this was an arbitrary selection. The smaller the Δi_{mn}, the faster the settling time will be. The negative effect of a smaller Δi_{mn} is a higher switching frequency, which

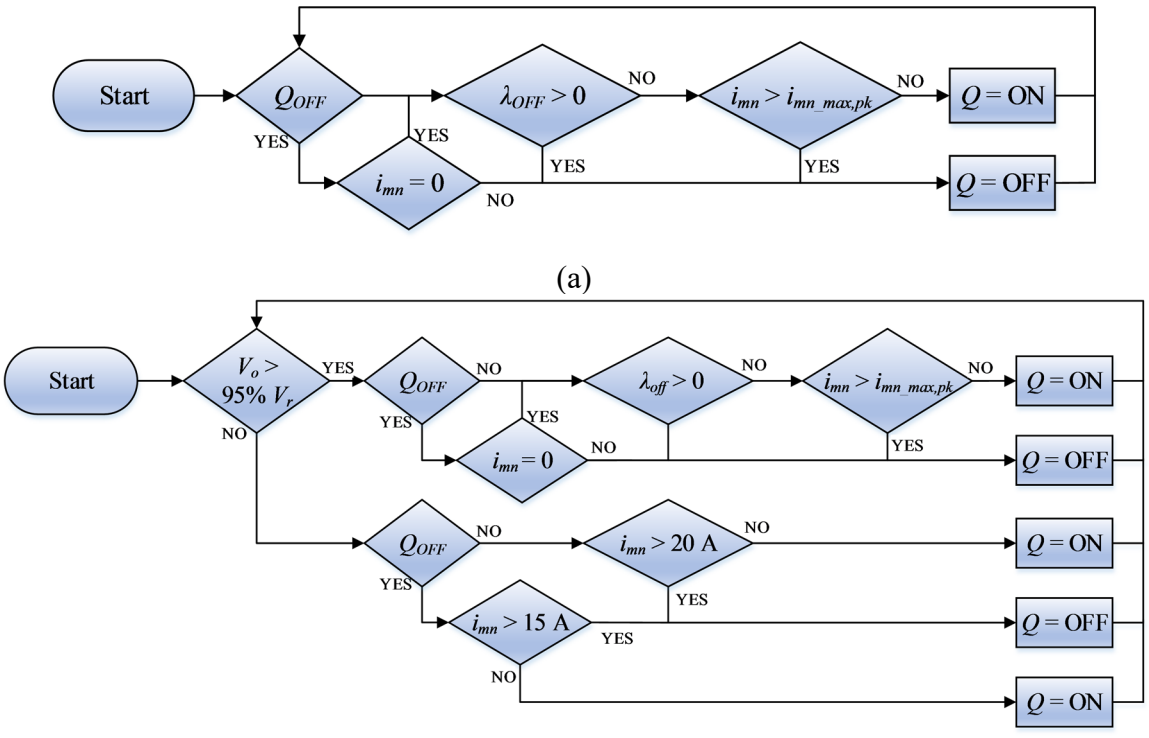

Fig. 2. 10. BCM control law flow diagram with input current limit, (a) BCM start-up, and (b) CCM start-up.

could affect EMI, increase start-up losses, and cause higher average power dissipation through the devices.

Fig. 2.10(b) depicts the updated flow diagram for the CCM start-up method. Figs. 2.8(c) and (d) display the start-up trajectory with the CCM start-up control. Fig. 2.8(c) shows the first few switching cycles of start-up. It is clear that the converter is now operating in CCM with a Δi_{mn} of 5 A and peak of 20 A. Fig. 2.8(d) highlights the transition from CCM to BCM at 190V (5% of V_r). From there, BCM control continues to and during steady-state. The benefit of this modified control is shown in Fig. 2.9. The settling time decreased to 13.5 ms, a 55.1% reduction compared to the BCM start-up of Fig. 2.8(b).

2.7 EXPERIMENTAL RESULTS

A 90W 24/200V flyback converter with the parameters of Table 2.I was prototyped. The proposed BCM controller was implemented using the DSP TMS320F28335 from Texas Instruments.

Fig. 2.11(a) shows the start-up output voltage and current waveforms and the gate signal when the start-up controller limiting the BCM input current is implemented. It can be seen that a non-overshoot output voltage response with a settling time in the order of 30 ms is obtained which agrees with the simulation results of section V. As desired, the operation of the converter is always at BCM which is the most efficient operation point for a flyback converter [3].

The converter responds satisfactorily under sudden changes in input voltage and load. For example, Fig. 2.11(b) depicts the output voltage and load current when the converter is put though a rapid load variation. In that case the resistive load changes from 1000 Ω to 500 Ω.

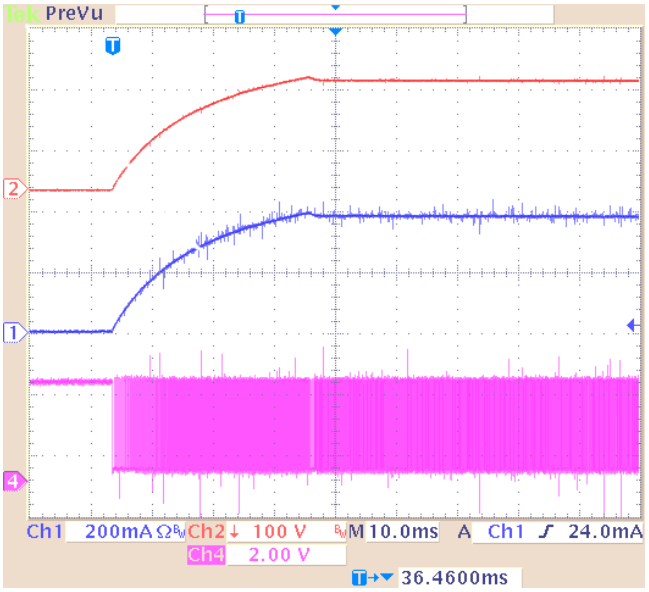

(a)

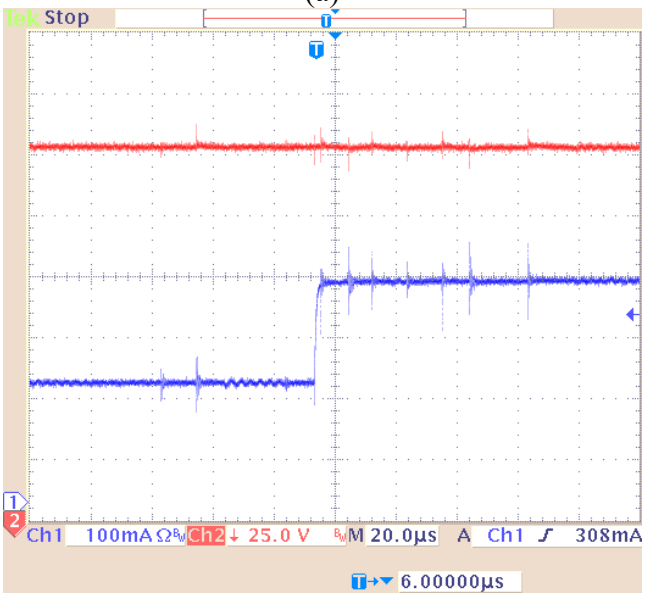

(b)

Fig. 2. 11. (a) Start-up output voltage and current, and gate signal for the BCM Control Law with BCM current limit, (b) output voltage transient under a sudden change in output current.

2.8 CONCLUSIONS

The Natural Switching Surfaces for a flyback converter were obtained from the normalized converter equations. The derived nonlinear control law showed no overshoot, zero steady-state error and adequate response to sudden load changes. By careful selection of the target operating point, the operational mode of the flyback converter can be defined. Trajectories for the ON- and OFF-states were derived for both CCM and BCM. The simulation and experimental results for a 65W, 24/180V prototype validated the proposed techniques. Since the control law reaches the reference voltage in one switching action, there is a large current peak during the start-up which can be destructive for the converter components. Therefore, several modifications of the control law were implemented under start-up conditions which showed an excellent performance.

2.9 ACKNOWLEDGMENTS

The authors are grateful for the financial support from the NSF-EPSCoR Vertically Integrated Center for Transformative Energy Research (www.victercenter.com). Dr. Chiacchirini is grateful to Consejo Nacional de Investigaciones Científicas y Técnicas (CONICET) and Universidad Nacional del Sur. Mr. Jesus Gonzalez-Llorente is grateful to Departamento Administrativo de Ciencia, Tecnología e Innovación (COLCIENCIAS) and Dirección de Investigación e Innovación (DII) of Universidad Sergio Arboleda.

2.10 REFERENCES

[1]. M. Kazimierczuk, Pulse-width Modulated DC–DC Power Converters, First Edit. John Wiley & Sons, 2008.

[2]. S. Ozturk and I. Cadirci, "DSPIC microcontroller based implementation of a flyback PV microinverter using Direct Digital Synthesis," in *Energy Conversion Congress and Exposition (ECCE)*, 2013 IEEE, 2013, pp. 3426–3433.

[3]. L. Garcia-Rodriguez, E. Williams, J. C. Balda, J. Gonzalez-Llorente, E. Lindstrom, and A. Oliva, "Dual-stage microinverter design with a GaN-based interleaved flyback converter stage," in *Energy Conversion Congress and Exposition (ECCE)*, 2013 IEEE, 2013, pp. 4496–4502.

[4]. D. C. Martins and R. Demonti, "Grid connected PV system using two energy processing stages," in Photovoltaic Specialists Conference, 2002. *Conference Record of the Twenty-Ninth IEEE*, 2002, pp. 1649–1652.

[5]. M. Seker and E. Zergeroglu, "A new sliding mode controller for the DC to DC flyback converter," in *Automation Science and Engineering (CASE)*, 2011 IEEE Conference on, 2011, pp. 720–724.

[6]. M. Salimi, J. Soltani, A. Zakipour, and V. Hajbani, "Sliding mode control of the DC-DC flyback converter with zero steady-state error," in *Power Electronics, Drive Systems and Technologies Conference (PEDSTC)*, 2013 4th, 2013, pp. 158–163.

[7]. M. Ordonez, M. T. Iqbal, and J. E. Quaicoe, "Selection of a curved switching surface for buck convert ers," *Power Electron. IEEE Trans*., vol. 21, no. 4, pp. 1148–1153, 2006.

[8]. J. M. Galvez, M. Ordonez, F. Luchino, and J. E. Quaicoe, "Improvements in Boundary Control of Boost Converters Using the Natural Switching Surface," Power Electron. IEEE Trans., vol. 26, no. 11, pp. 3367–3376, 2011.

[9]. K . K. S. Leung and H. S.-H. Chung, "Derivation of a second-order switching surface in the boundary control of buck converters," *Power Electron. Lett. IEEE*, vol. 2, no. 2, pp. 63–67, 2004.

[10]. G. G. Oggier and M. Ordonez, "Boundary Control of Full-Bridge ZVS: Natural Switching Surface for Transient and Steady-State Operation," *Ind. Electron. IEEE Trans.*, vol. 61, no. 2, pp. 969–979, 2014.

2.11 APPENDICES

2.11.A Paper Permissions

11/5/2019 Rightslink® by Copyright Clearance Center

Copyright Clearance Center RightsLink®

Home | Help | Email Support | Sign in | Create Account

IEEE Requesting permission to reuse content from an IEEE publication

Control of a flyback converter operating in BCM using the natural switching surface

Conference Proceedings:
2015 IEEE 6th International Symposium on Power Electronics for Distributed Generation Systems (PEDG)

Author: Luciano A. Garcia-Rodriguez

Publisher: IEEE

Date: June 2015

Copyright © 2015, IEEE

Thesis / Dissertation Reuse

The IEEE does not require individuals working on a thesis to obtain a formal reuse license, however, you may print out this statement to be used as a permission grant:

Requirements to be followed when using any portion (e.g., figure, graph, table, or textual material) of an IEEE copyrighted paper in a thesis:

1) In the case of textual material (e.g., using short quotes or referring to the work within these papers) users must give full credit to the original source (author, paper, publication) followed by the IEEE copyright line © 2011 IEEE.
2) In the case of illustrations or tabular material, we require that the copyright line © [Year of original publication] IEEE appear prominently with each reprinted figure and/or table.
3) If a substantial portion of the original paper is to be used, and if you are not the senior author, also obtain the senior author's approval.

Requirements to be followed when using an entire IEEE copyrighted paper in a thesis:

1) The following IEEE copyright/ credit notice should be placed prominently in the references: © [year of original publication] IEEE. Reprinted, with permission, from [author names, paper title, IEEE publication title, and month/year of publication]
2) Only the accepted version of an IEEE copyrighted paper can be used when posting the paper or your thesis on-line.
3) In placing the thesis on the author's university website, please display the following message in a prominent place on the website: In reference to IEEE copyrighted material which is used with permission in this thesis, the IEEE does not endorse any of [university/educational entity's name goes here]'s products or services. Internal or personal use of this material is permitted. If interested in reprinting/republishing IEEE copyrighted material for advertising or promotional purposes or for creating new collective works for resale or redistribution, please go to http://www.ieee.org/publications_standards/publications/rights/rights_link.html to learn how to obtain a License from RightsLink.

If applicable, University Microfilms and/or ProQuest Library, or the Archives of Canada may supply single copies of the dissertation.

BACK CLOSE

UNIVERSITY OF
ARKANSAS
College of Engineering

Department of Electrical Engineering

1 University Avenue, 3217 Bell Engineering Center, Fayetteville, AR 72701, (479) 575-3005, (479) 575-7967 (fax)

November 6, 2019

To whom it may concern,

This letter is to verify that Mr. Luciano Andrés Garcia Rodriguez, ID 010593736, is the first author and did at least 51% of the work for the paper titled "Control of a Flyback Converter Operating in BCM Using the Natural Switching Surface".

Kind Regards,

Dr. Juan Carlos Balda

University Professor, Department Head and Major Advisor to Mr. Luciano Andrés Garcia Rodriguez

CHAPTER 3

Control of a Flyback Converter with Parametric Uncertainties Operating in BCM Using the Natural Switching Surface

L. A. G. Rodriguez, H. Chiacchiarini and J. C. Balda, "Control of a flyback converter with parametric uncertainties operating in BCM Using the natural switching surface," *2016 IEEE Biennial Congress of Argentina (ARGENCON)*, Buenos Aires, Argentina, 2016, pp. 1-7.

3.1 ABSTRACT

The derivation and implementation of the natural switching surfaces (NSS) considering parametric uncertainties for a flyback converter operating at boundary conduction mode (BCM) is the main focus of this paper. The NSS presents many benefits for the control of non-linear systems; for example fast transient response under load-changing conditions. However, the performance considerable worsens when real parameters of the converter are slightly different from the designed ones. Therefore, a novel control strategy that considers the effect of parameter uncertainties is presented. This control law can estimate and adapt the control trajectories in one switching action to obtain excellent performances even under extreme parameter uncertainties. The analytical derivation of the proposed adaptive switching surfaces are presented.

3.2 RESUMEN

La derivación e implementación de las superficies naturales de conmutación (NNS) considerando incertidumbres paramétricas para un convertidor flyback operando en modo de conducción críticamente continuo (BCM) es el principal foco de este trabajo. NSS presenta muchos beneficios para el control de sistemas no lineales; por ejemplo rápida respuesta transitoria

bajo condiciones de carga variable. Sin embargo, el rendimiento empeora considerablemente cuando los parámetros reales del convertidor son un poco distintos a los parámetros diseñados. Este trabajo presenta una estrategia novedosa de control que considera el efecto de incertidumbres paramétricas. Esta ley de control puede estimar y adaptar las trayectorias de control para obtener un excelente desempeño incluso bajo incertidumbres paramétricas extremas. Se presenta la derivación analítica de las superficies adaptivas de conmutación propuestas.

3.3 INTRODUCTION

A flyback converter is commonly used in systems rated 20 W to 200 W due to its low part count, electrical isolation and wide voltage ratio [1]. In addition to the traditional applications in computers and TV sets, the flyback converter is used in photovoltaic microinverters where it operates over a wide range of operating conditions [2]–[4]. Linear compensators are unsuccessful when there are large load variations; therefore, nonlinear controllers, such as sliding mode controllers, are suitable for these converters [5]–[6].

In recent years, the transient response of typical boundary schemes in power converters has been improved by using the natural switching surfaces (NSS) [7]–[8]. The NSS are the natural trajectories of states for each switching position of the converter [9]. The NSS has been studied for the basic non-isolated topologies [7]–[8] and for isolated topologies like the dual active bridge [10]. In this work, the NSS and its control law are derived for any generic flyback converter. It is also proven that it is possible to design the converter to work in the boundary conduction mode (BCM) for any loading condition by properly selecting the target point of the trajectories. The nominal case for NSS BCM control of flyback converters was addressed in [1].

The organization of this paper is as follows: the normalized system trajectories are derived in section 3.4; the selection of the operating conditions and target points are developed in section 3.5

and the control laws are presented in section 3.6. Finally, the simulation results are presented in section 3.7 and 3.8, and the conclusions and future work are provided in section 3.9.

3.4 NORMALIZED SYSTEM TRAJECTORIES CONSIDERING PARAMETRIC UNCERTAINTIES

The system shown in Fig. 3.1 is a simplified version of a flyback converter which consists of an ideal transistor Q, a diode D, a flyback transformer with magnetizing inductance L_m, as well as input and output capacitors, C_{in} and C_o. These parameters are the real parameters of the converter which may differ from the designed nominal ones. The components which determine the dynamics of a flyback converter are the magnetizing inductance and the output capacitance [11]. The designed output capacitance is called $\overline{C}_o$ while the design magnetizing inductance is $\overline{L}_m$. The load is represented by a current source which states the worst case scenario in terms of stability [8]. The normalization of the system consists of a scale change of its differential equations which enables a general solution. The presence of a transformer makes it necessary to relate the converter parameters to one side; the secondary side is selected in this case. The normalization is performed

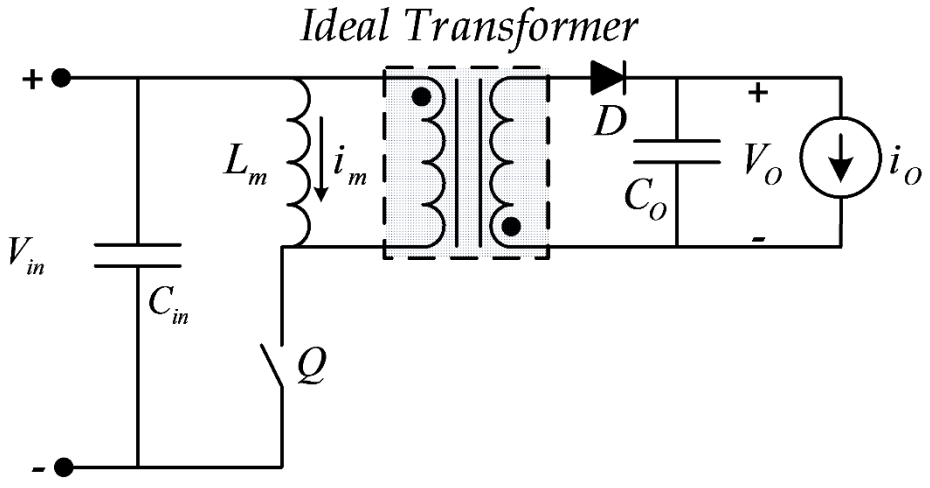

Fig. 3. 1. Flyback converter circuit.

using the output voltage as the reference voltage $V_r = V_o$, the characteristic nominal impedance of the combined designed magnetizing inductance referred to secondary side and the nominal designed output capacitor, $\overline{Z}_o = (1/n)\sqrt{\overline{L}_m/\overline{C}_o}$ as the reference impedance Z_r and the natural frequency $\overline{f}_o = n\Big/\left(2\pi\sqrt{\overline{L}_m\overline{C}_o}\right)$ as the reference frequency f_r. The normalizing equations of the voltage, current and time variables as well as their derivatives for the secondary variables are as follows:

$$v_n = v/V_r\,, \quad dv_n = dv/V_r\,, \tag{1}$$

$$i_n = i.Z_r/V_r, \quad di_n = di.Z_r/V_r, \tag{2}$$

$$t_n = t.f_r, \quad dt_n = dt.f_r. \tag{3}$$

Where v, i, and t are the standard voltage, current and time variables of the secondary side, and v_n, i_n, and t_n are the normalized versions. Due to the presence of a transformer, the normalizing equations must be reflected back to the primary side to normalize a primary variable. The normalizing equations of primary variables are as follows:

$$v_n = v/(n.V_r), \quad i_n = i.n.Z_r/V_r\,, \tag{4}$$

$$dv_n = dv/(nV_r), \quad di_n = di.n.Z_r/V_r\,. \tag{5}$$

The following subsections present the derivation of the normalized ON- and OFF-state trajectories.

3.4.A OFF-State Trajectory

During the OFF-state of transistor Q, diode D conducts, and the energy stored in the air gap of the transformer during the ON-state is transferred to the load. The voltage applied to the magnetizing inductance is the output voltage multiplied by the transformer turns ratio. The

following are the differential equations that describe this mode of operation, where L_m, C_o are the real parameters of the converter:

$$L_m \frac{di_m}{dt} = -nv_o, \tag{6}$$

$$C_o \frac{dv_o}{dt} = ni_m - i_o. \tag{7}$$

Using equations (1) through (5), the normalization of the differential equations (6) and (7) becomes:

$$\frac{di_{mn}}{dt_n} = -2\pi \frac{\overline{L}_m}{L_m} v_{on}, \tag{8}$$

$$\frac{dv_{on}}{dt_n} = 2\pi \frac{\overline{C}_o}{C_o}\left(i_{mn} - i_{on}\right). \tag{9}$$

Differentiating both sides of (8) and replacing it in (9) yields a differential equation with the following solution:

$$i_{mn}\left(t_n\right) = i_{on} + \left(i_{mn}\left(0^-\right) - i_{on}\right)\cos\left(2\pi\sqrt{\alpha\beta}t_n\right) + \frac{\dfrac{di_m\left(0^-\right)}{dt_n}}{2\pi\sqrt{\alpha\beta}}\sin\left(2\pi\sqrt{\alpha\beta}t_n\right). \tag{10}$$

Where $\alpha = \overline{L}_m / L_m$, and $\beta = \overline{C}_o / C_o$. By applying the trigonometric property $A\cos\left(x\right) + B\sin\left(x\right) = \sqrt{A^2 + B^2}\,\sin\left(x + \tan^{-1}\left(A/B\right)\right)$ to (10), taking the derivative of the resulting expression and applying the property $\cos\left(\sin^{-1}\left(x\right)\right) = \sqrt{1 - x^2}$, the result is an equation that does not depend on the normalized time. Then, the OFF-state trajectory can be expressed as:

$$\lambda_{OFF} := v_{on}^2 \frac{\alpha}{\beta} + \left(i_{mn} - i_{on}\right)^2 - A^2 - B^2 = 0. \tag{11}$$

Where $A = i_{mn}\left(0^{-}\right) - i_{on}$ and $B = \frac{1}{2\pi\sqrt{\alpha\beta}} \frac{di_{mn}\left(0^{-}\right)}{dt_n}$. Therefore, in the case where the designed parameters are the same than the real ones ($\alpha/\beta = 1$), the OFF-state trajectory is a circle with its center at (i_{mn}, v_{on}) = (i_{on}, 0) and a radius that is a function of the specifications of the converter [11]. However, in case the real parameters differ from the designed ones, the normalized ON-trajectory becomes an ellipse.

3.4.B ON-State Trajectory

When the transistor *Q* is ON, the magnetizing inductance is connected to the input source and the diode at the secondary side is reversed bias. The differential equations for this stage and their normalized versions are:

$$V_{in} = \frac{L_m di_m}{dt}, \qquad -i_o = C_o \frac{dv_o}{dt}, \tag{12}$$

$$2\pi \frac{\overline{L}_m}{L_m} V_{inn} = \frac{di_{mn}}{dt_n}, \qquad -2\pi \frac{\overline{C}_o}{C_o} i_{on} = \frac{dv_{on}}{dt_n}. \tag{13}$$

Equation (13) shows that when the transistor is ON, the magnetizing current and the output voltage vary linearly with time. By dividing the two normalized equations, it is obtained:

$$\frac{di_{mn}}{dv_{on}} = -\frac{\alpha}{\beta} \frac{v_{inn}}{i_{on}}. \tag{14}$$

By integrating (14), the natural trajectory of the flyback converter when the transistor is ON is given by:

$$\lambda_{ON} := i_{mn} + \frac{\alpha}{\beta} \frac{v_{inn}}{i_{on}} v_{on} - H = 0, \tag{15}$$

where *K* is a constant which is selected in such a way that the ON-state trajectory intersects the target operating point.

3.4.C Graphical Analysis of the NSS Trajectories with Parametric Uncertainties

Fig. 3.2 presents graphical renditions of the NSS trajectories previously derived. These graphs are for a generic flyback converter, with arbitrary trajectory placement in the i_{mn} vs. v_{on} plane. As previously described, the ON-state trajectory is a descending sloping line and the OFF-state trajectory is a circle with a center at (0, i_{on}) for the case when $\alpha/\beta = 1$ and an ellipse for the case when $\alpha/\beta \neq 1$. This subsection shows the interaction of the two trajectories and their relation with the converter operation.

By evaluating the i_{mn} vs. v_{on} plane and analysing the operation of a flyback converter, quadrants of the plane can immediately be recognized as unobtainable or undesirable operation zones based on the polarity of the variables. For example, i_{mn} must be positive for the flyback converter to

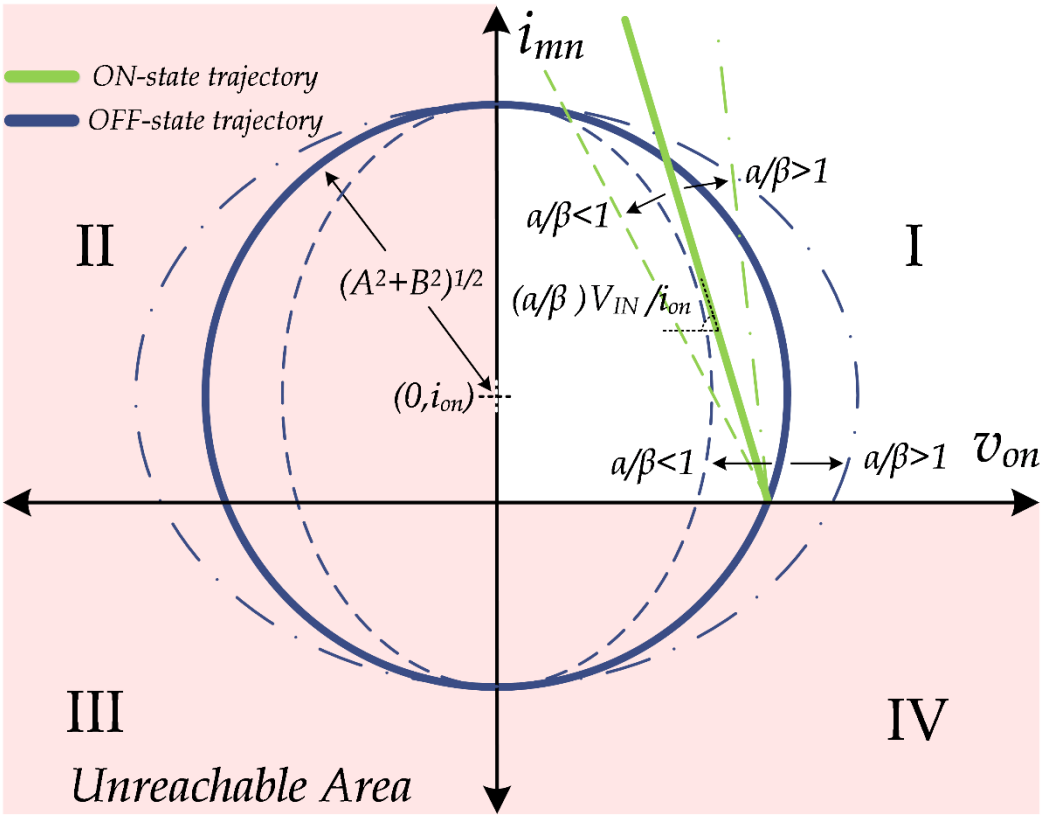

Fig. 3. 2. Normalized natural surfaces for a flyback converter considering parametric uncertainties.

operate correctly. Therefore, i_{mn} would not be attainable in quadrants III or IV. Likewise, the converter could not operate if v_{on} were negative. If the converter were operating when v_{on} were negative, it would imply that the load would be transferring power to the input of the converter, which is physically impossible due to the presence of D. Therefore, v_{on} should not operate in quadrants II or III. This leaves quadrant I as the only operational quadrant that satisfies both variables' conditions. In quadrant I, i_{mn} and v_{on} are both positive and the flyback converter would be transferring power to the load. The undesirable quadrants have been grayed out in Fig. 3.2.

Movement along the trajectories during steady-state can be determined by considering the flyback's operation in each state. As previously discussed, during the ON-state i_{mn} is increasing, storing energy in the transformer magnetizing inductance field from the input source, and v_{on} is decreasing, due to the load consuming the energy stored in the output capacitor. Therefore, the converter operating point would slide up the trajectory during the ON-state, as shown in Fig. 3.3. During the OFF-state, i_{mn} is decreasing, supplying the transformer's stored energy to the load and output capacitor, while v_{on} is increasing, due to the transformer's supplied energy. Therefore, the converter operating point would slide down the trajectory during the OFF-state.

If the converter's trajectory were to reach an axis, the converter would then evolve on that axis. Therefore, reaching the i_{mn} axis, the converter would change i_{mn} while the output voltage remained at zero. Likewise, reaching the v_{on} axis, the converter would change v_{on} while keeping the magnetizing current at zero. This is due to the unobtainable quadrants.

3.4.D NSS Trajectories and Modes of Operation

The interaction between the ON- and OFF-state trajectories determines the instant when a transition between one state and the other occurs. Fig. 3.3(a) shows the normalized trajectories derived for a flyback converter operating at boundary conduction mode (BCM) [11]. At the converter start-up, i_{mn} and v_{on} are zero. When Q turns ON, i_{mn} starts increasing while v_{on} keeps being zero.

When the ON-trajectory intersects the OFF-trajectory (0, $I_{st\text{-}up}$), Q turns OFF and the magnetizing current decreases while the output voltage increases. At steady-state conditions, the current and voltage ripples of the flyback converter are determined by the intersection of the ON- and OFF-trajectories. Fig. 3.3(b) depicts the time evolution of v_{on} and i_{mn}.

In case the load changes, the center and radius of the OFF-trajectory is modified producing new intersection points with the ON-trajectory. The intersections of the ON- and OFF-trajectories define the new current and voltage ripples in which the converter will operate.

3.5 SELECTION OF THE OPERATING CONDITIONS AND TARGET POINTS

3.5.A Conventional Approach

The approach presented in [8], for the case of a boost converter, defines the initial conditions of the ON- and OFF-state trajectories based on the target operating point of the converter. The target for the output voltage is equal to the reference voltage $v_{on} = V_{rn} = 1$, and the target for the magnetizing current is based on the required output power. Assuming that the converter losses are zero, the initial conditions of (11) are:

$$I_{mn,target} = \frac{i_{on} V_{rn}}{D_n V_{inn}} = i_{on}\left(1 + \frac{1}{V_{ccn}}\right), \tag{16}$$

$$\frac{di_{mn}\left(0^{-}\right)}{dt_n} = -2\pi\alpha, \tag{17}$$

where $D_n = V_{on}/(V_{inn} + V_{on})$ is the normalized duty cycle for the flyback converter. The OFF-state trajectory is obtained by replacing (16) and (17) into (11):

$$\lambda_{OFF} := v_{on}^2 \frac{\alpha}{\beta} + \left(i_{mn} - i_{on}\right)^2 - \frac{\alpha}{\beta} - \left(\frac{i_{on}}{V_{ccn}}\right)^2 = 0. \tag{18}$$

Similarly, evaluating (15) at the target point $(i_{mn}, v_{on}) = (i_{mn,target}, 1)$, the trajectory for the ON-state is obtained as follows:

$$\lambda_{ON} := i_{mn} + \frac{\alpha}{\beta}\frac{V_{ccn}}{i_{on}} v_{on} - \left(i_{on} + \frac{i_{on}}{V_{ccn}} + \frac{\alpha}{\beta}\frac{V_{ccn}}{i_{on}}\right) = 0. \tag{19}$$

This control approach leads to an operating area close to the target operating point. This would cause the operation mode of the converter to mainly be CCM, which would not be the desired case for flyback converter applications that require high efficiencies.

3.5.B Proposed Approach

A control law to keep the operation of a flyback converter in BCM operation for all load conditions is desired. The goal of this section is to identify a known target operating point and define the trajectories' design parameters and unknowns to include this point.

From Fig. 3.3(a), it is identified that if the target operating point is set to be at the reference output voltage and zero magnetizing current, the converter will work in BCM for all load conditions. Replacing this known trajectory point $(i_{mn}, v_{on}) = (0, 1)$, in (15), the constant K in the ON-state trajectory is given by:

$$K = \frac{\alpha}{\beta}\frac{V_{inn}}{i_{on}}. \tag{20}$$

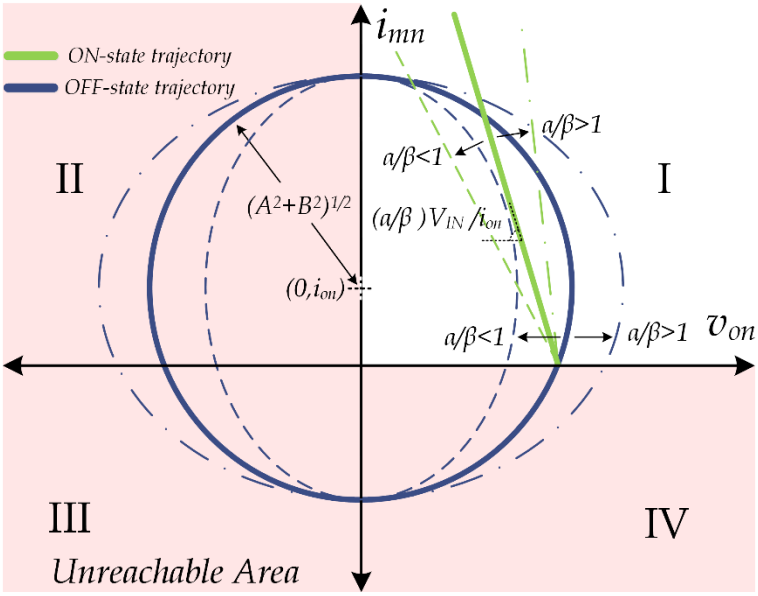

(a)

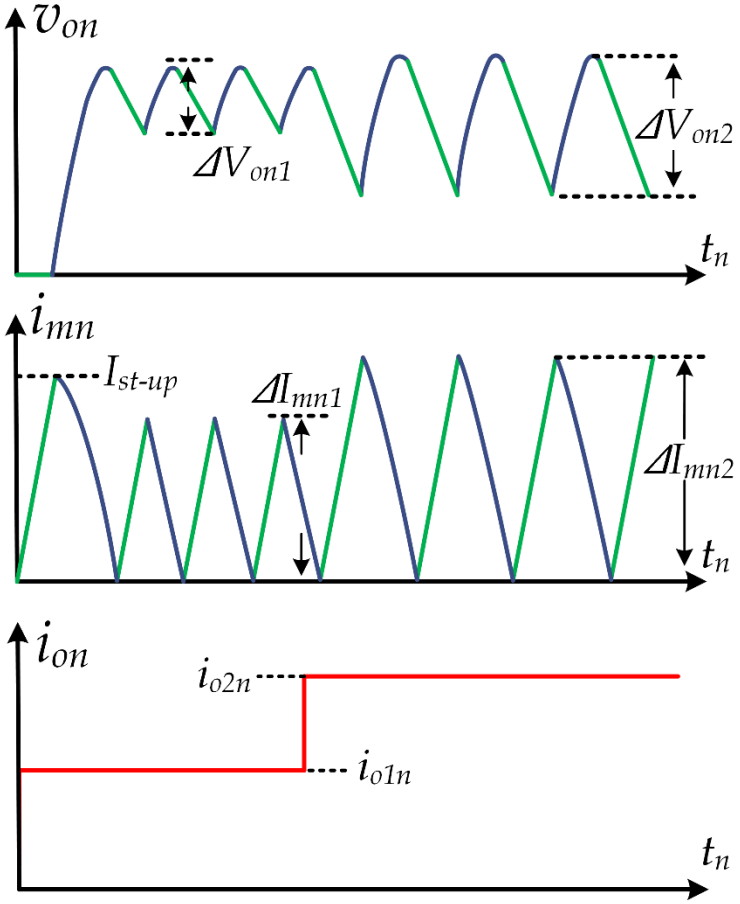

(b)

Fig. 3. 3. (a) NSS trajectories for the flyback converter operating at BCM when $\alpha/\beta = 1$, and (b) Normalized output voltage v_{on}, magnetizing inductance current i_{mn} and output current i_{on}.

Therefore, the BCM ON-state trajectory is

$$\lambda_{ON} := i_{mn} + \frac{\alpha}{\beta}\frac{V_{inn}}{i_{on}}v_{on} - \frac{\alpha}{\beta}\frac{V_{inn}}{i_{on}} = 0. \tag{21}$$

Moving onto the OFF-state trajectory, A and B can be simplified with the known trajectory point. Knowing that $v_{on} = 1$, (8) can be simplified to

$$\frac{di_m\left(0^-\right)}{dt_n} = -2\pi\alpha. \tag{22}$$

Then, A and B can be expressed as:

$$A = -i_{on}, \qquad B = -\sqrt{\alpha/\beta}. \tag{23}$$

Substituting (23) into (11), the complete BCM OFF-state trajectory is defined as

$$\lambda_{OFF} := v_{on}^2\frac{\alpha}{\beta} + \left(i_{mn} - i_{on}\right)^2 - \frac{\alpha}{\beta} - i_{on}^2 = 0. \tag{24}$$

3.6 STANDARD STEADY-STATE BCM CONTROL LAW

This section explains how the control law is derived based on the trajectories of equations (21) and (24). The goal of a control law is to force the converter to move to or stay on the identified BCM trajectories. Knowing the movements along the trajectories for each state of transistor Q and the above conditions, the control law is developed. The control law decides between two options: either Q should be ON or Q should be OFF. The decision is based on the current state of transistor Q and the relative location of the current operating point to the BCM trajectories.

While Q is ON, the converter will move up the plane. If the converter is currently operating below the OFF-trajectory, Q is kept ON while the converter continues to move up the plane until the OFF-state trajectory is reached. Once the OFF-state trajectory is reached, Q is switched OFF. If

the converter is operating anywhere above the OFF-trajectory, then transistor Q should be turned OFF.

Since the desire is to operate in BCM, the first part of the law is that Q is not allowed to switch back ON until $i_{mn} = 0$, once it has been switched OFF. Therefore, if the converter is operating anywhere above the v_{on} axis ($i_{mn} > 0$), Q is kept OFF until the converter reaches the v_{on} axis. Once the v_{on} axis is reached, the current operating point is compared to the OFF-state trajectory. If the converter is operating at a level greater than the OFF-state trajectory, Q is kept OFF, allowing the converter to evolve down the v_{on} axis to the OFF-state trajectory. If the converter is operating below or at the OFF-state trajectory, Q is switched ON, allowing the converter to ride the ON-state trajectory back up to the OFF-state trajectory as previously described.

Fig. 3.4 shows a complete flow diagram for the BCM control law [11], which forces the converter to move and operate on the BCM trajectories in one switching cycle, no matter where the converter is currently operating. This allows the flyback converter to operate in BCM continuously for any loading condition during steady-state. In a transient condition, where the input voltage or load changes, the worst-case scenario would be that the converter recovers in one switching cycle. During that one transient switching cycle, a DCM operation with a slightly over voltage output or a BCM of operation with a slightly under voltage output could be experienced. This is because the desired ON- and OFF-state trajectories change when converter parameters change. The rapid recovery time of one switching cycle provides remarkable stability and transient response time for all converter conditions.

3.6.A Derivation of Steady-State Parameters

The proposed control method maintains the flyback converter operating at BCM under all load conditions. Therefore, the switching frequency changes based on changes in the load condition

and converter parameters. The switching frequency of a converter is a very important consideration when selecting EMI and components such us microcontroller or processor, semiconductor devices, current sensors, and analog-to-digital (ADC) converters. This section will derive an accurate approximation for the steady-state switching frequency using the proposed control laws. The switching frequency is dependent upon the average input and output voltages, the turns ratio of the transformer, and the transformer's magnetizing inductance. Therefore, knowing the power and voltage operating range, a range in operating frequency can be derived.

As seen in Fig. 3.3 (b), the intersection points between the ON- and OFF-trajectories can determine the output voltage and magnetizing current ripples which are expressed as:

$$\Delta v_{on} = \frac{2V_{inn}}{1+\frac{\alpha}{\beta}\left(\frac{V_{inn}}{i_{on}}\right)^2}, \tag{25}$$

$$\Delta i_{mn} = \frac{\alpha\beta V_{inn} i_{on}^2 + \alpha^2 V_{inn}^3 - 2\alpha V_{inn}^2 \beta i_{on}^2}{\beta^2 i_{on}^3 + \alpha\beta V_{inn}^2 i_{on}}. \tag{26}$$

Replacing (25) into (9) and (13), the time intervals when Q is ON (T_{ON}) and OFF (T_{OFF}) can be found. The normalized switching period, T_{SWn}, can be described as

$$T_{SWn} = T_{ONn} + T_{OFFn}, \tag{27}$$

where T_{ONn} and T_{OFFn} are the normalized values for the ON and OFF times, respectively; T_{ONn} and T_{OFFn} can be calculated from the differential equations for i_{mn} in each state:

$$T_{ONn} = \frac{\Delta v_{on}}{2\pi\left(i_{mn} - i_{on}\right)\beta}, \tag{28}$$

$$T_{OFFn} = \frac{\Delta v_{on}}{2\pi i_{on}\beta}. \tag{29}$$

Noting that Δv_{on} is equal for both ON- and OFF-states, the normalized switching period is obtained by inserting (28) and (29) into (27):

$$T_{SWn} = \frac{\Delta v_{on}}{2\pi\left(i_{mn} - i_{on}\right)\beta} + \frac{\Delta v_{on}}{2\pi i_{on}\beta}. \tag{30}$$

Therefore, the switching frequency is

$$f_{SWn} = \frac{2\pi\left(i_{mn} - i_{on}\right)i_{on}\beta}{\Delta v_{on} i_{mn}}. \tag{31}$$

Substituting (25) with (31), and replacing the normalized converter values in terms of the non-normalized ones, the switching frequency can be described as

$$f_{SW} = \frac{\pi\left(i_{mn} - i_{on}\right)\left(\beta i_{on}^2 + \alpha V_{inn}^2\right)}{V_{inn} i_{mn} i_{on}}. \tag{32}$$

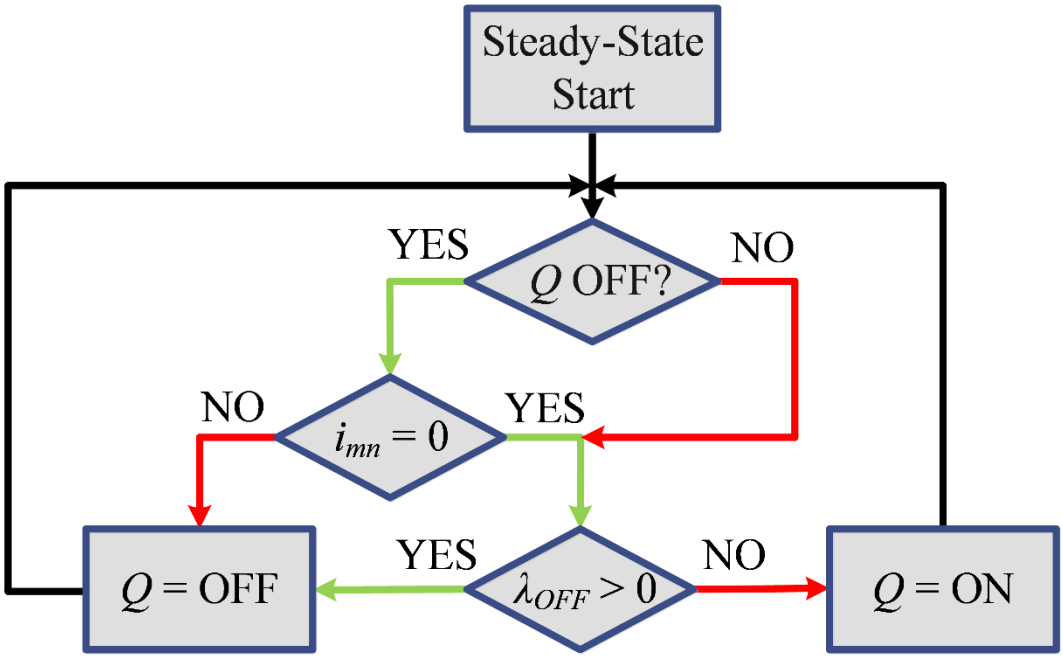

Fig. 3. 4. BCM control law flow diagram.

3.7 SIMULATION RESULTS

3.7.A Steady-State BCM Control Law

The control law proposed above was implemented in MATLAB/Simulink©. The flyback was simulated at 100 W, with device parameters equivalent to those of chosen devices used in the experimental setup under development, detailed in Table 3. I.

Fig. 3.5 shows simulation results for the transient response of a flyback converter with the parameters shown in Table 3.I. Fig. 3.5(a) and Fig. 3.5(b) represent the ideal case when the designed parameters of the converter are the same than the real parameters ($\alpha/\beta = 1$). It can be seen that the flyback converter is operating at boundary conduction mode (BCM) and the steady state is reached in just one switching action. The output capacitor was intentionally selected small enough so the ripple at the voltage output can be clearly appreciated. A sudden load change occurs at 0.5 ms, but the controller keeps the converter operating at BCM.

Fig. 3.6(a) and Fig. 3.6(b) present the case when $\alpha/\beta > 1$. This case was performed by keeping the same magnetizing inductance of the transformer while reducing the amount of output capacitance from 2 μF to 1 μF. It can be seen that the output voltage overpeak exceeds the target voltage (100 V) for almost 50%. This is due to the fact that the magnetizing inductance stored the amount of energy necessary to charge 100 V in one switching action into the output capacitor of 2 μF instead of 1 μF. The extra charge provided during the ON-time produces an overvoltage at C_o. When $\alpha/\beta > 1$, the operating mode of the flyback converter is discontinuous conduction mode (DCM) instead of BCM.

The transient response when $\alpha/\beta < 1$ is shown in Fig. 3.7(a) and Fig. 3.7(b). This case was obtained increasing the output capacitance from 2 μF to 4 μF while maintaining the same

TABLE 3. I PARAMETERS FOR THE SIMULATED CONVERTER

Parameter	Value
V_o	100 V
I_o	1 A
P_o	100 W
L_m	28 uH
C_o	2 uF
V_{in}	24 V
N_s/N_p	6

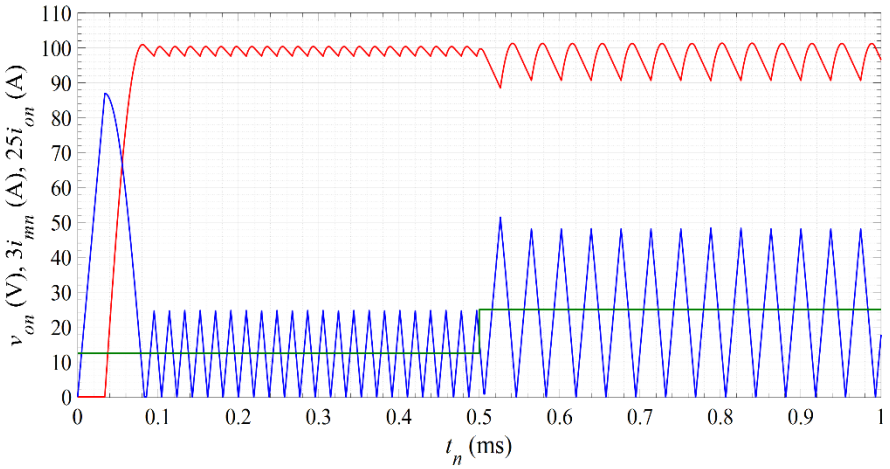

(a)

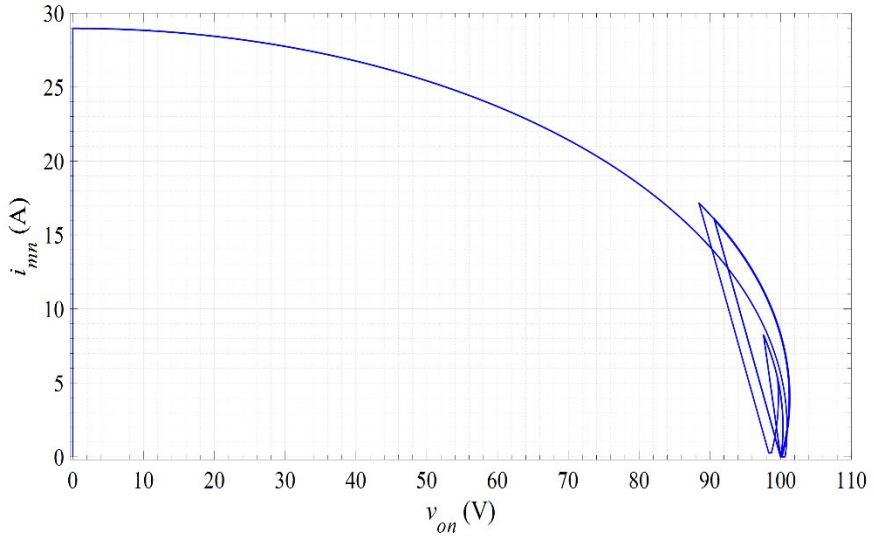

(b)

Fig. 3. 5. (a) Transient response, and (b) i_{mn} vs. v_{on} state plane trajectory plot when $\alpha/\beta = 1$.

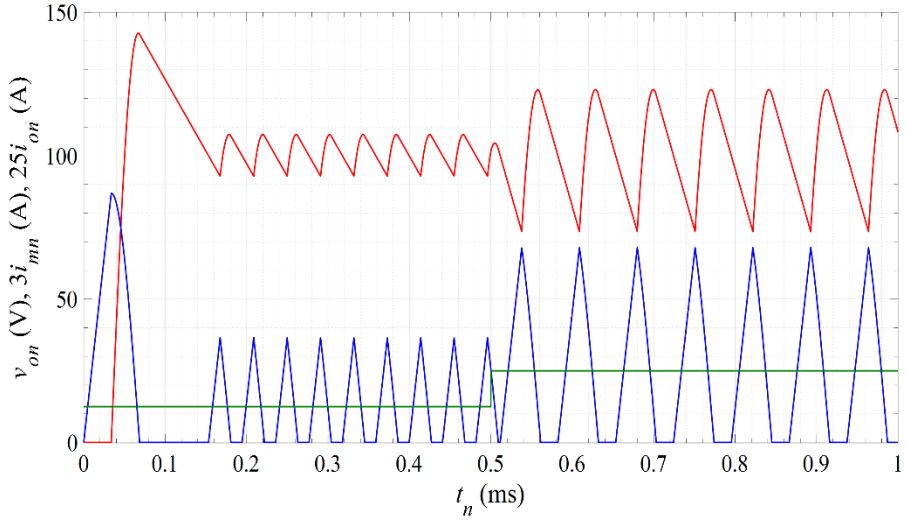

(a)

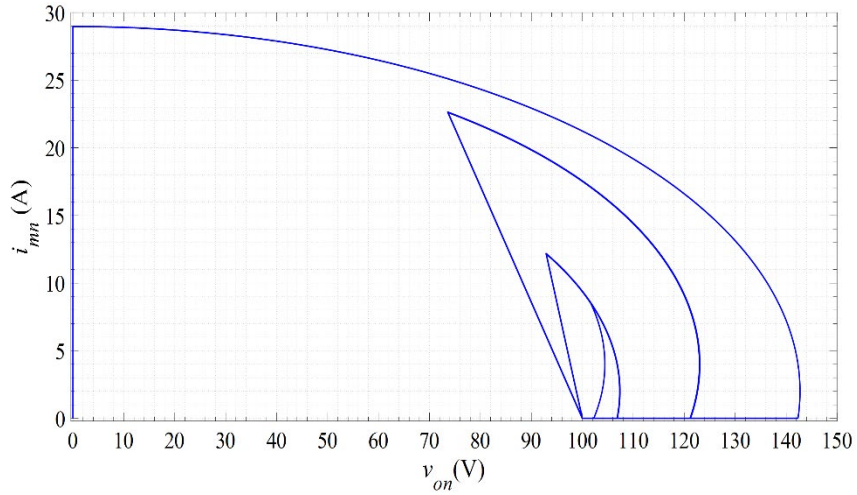

(b)

Fig. 3. 6. (a) Transient response, and (b) i_{mn} vs. v_{on} state plane trajectory plot when $\alpha/\beta > 1$.

magnetizing inductance. Since the output capacitance is larger than the expected one, it takes more than one switching action to get the steady state reference voltage.

The simulation results demonstrated that the performance of the BCM NSS presented in [11] is satisfactory when the difference between the nominal and real parameters is not very big.

3.8 PROPOSED ADAPTIVE BCM NSS CONTROL LAW

One of the problems of the NSS control is that the response may not be as good as expected when the real parameters of the converter $\overline{L}_m$ and $\overline{C}_o$ are not equal to the designed ones L_m and C_o. This happens because the control trajectories are obtained normalizing the differential equations of the converter with base values that differ from the real ones.

This section presents a novel BCM NSS controller that is able to compensate the parametric uncertainties. The proposed controller responds adapting the ratio α/β whenever it detects that the

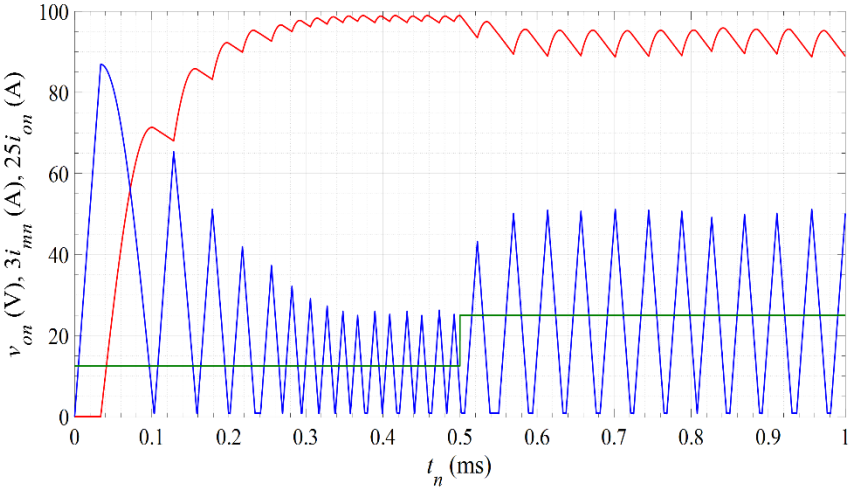

(a)

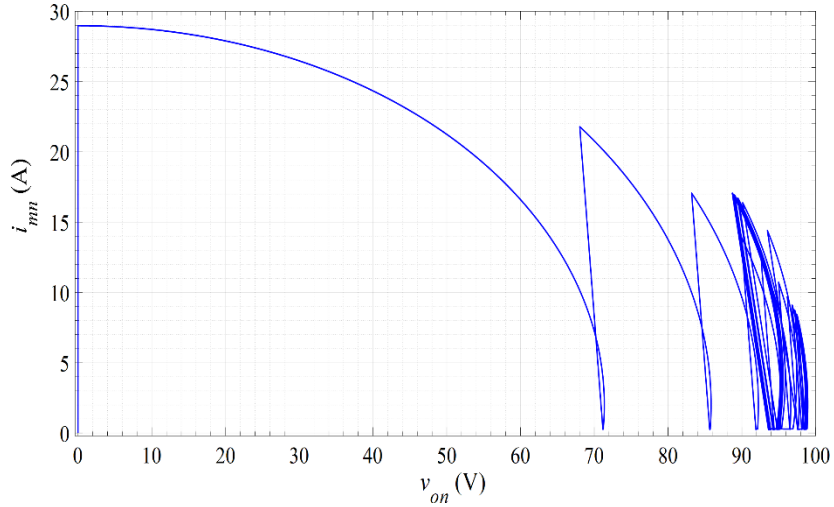

(b)

Fig. 3. 7. (a) Transient response, and (b) state plane trajectory plot when $\alpha/\beta < 1$.

system is not evolving on the specified trajectories. The adaptation is performed at the end of each switching cycle.

It should be noted that the trajectories presented in equations (21) and (24) are the trajectories that allows to get the ideal BCM NSS response for a flyback converter with parametric uncertainties ratio equals to α/β. Therefore, knowing the uncertainties ratio for a specific flyback converter and applying the control laws based on (21) and (24) leads to the compensation of the uncertainties problem because those trajectories contain the desired target point.

When the uncertainties ratio α/β equals one, the first time when the OFF-trajectory intersects the $i_{mn} = 0$ axes is at $v_{on} = 1$, which is the target point. If the intersection of OFF-trajectory of (24) with the $i_{mn} = 0$ axes is found, it can be seen that if α/β is not equal to 1, the voltage v_{on} will not be equal to 1 as seen in Figs. 3.6(a) and Fig. 3.7 (a). The value of v_{on} when i_{mn} is zero for the first time can be calculated replacing $i_{mn} = 0$ into (24) as:

$$v_{on} = \sqrt{\frac{\beta}{\alpha}}. \tag{33}$$

Therefore, the first intersection of the OFF-trajectory can be used as valuable information to produce a feed-forward term that can ideally compensate the uncertainties ratio in one switching action. Fig. 3.8 presents the flow diagram of the proposed adaptive control method. At start-up condition, the uncertainties ratio α/β is considered equal to one. The transistor will be turn ON until the OFF-trajectory is reached. Then, the transistor is kept OFF until the current i_{mn} equals zero. The voltage v_{on} at the first zero of i_{mn} will be the feed-forward term which will adapt the OFF-trajectory in order to compensate for the uncertainties in the parameters. After the feed-forward term is replaced on the control trajectories, during the next switching action the steady-state loop will gradually adapt the controller every time the magnetizing current equals zero. The latest improve

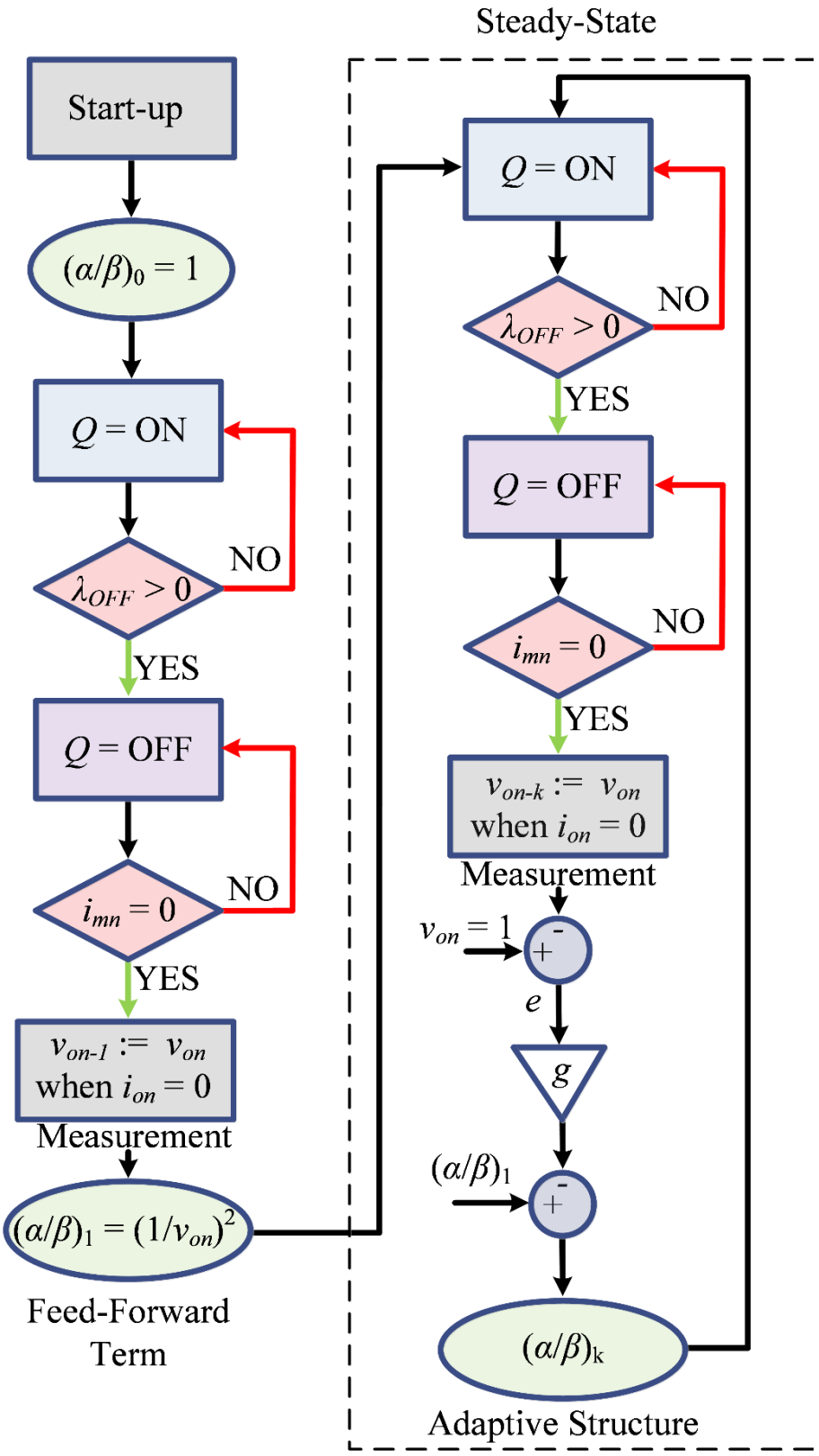

Fig. 3. 8. Adaptive BCM NSS control flow diagram.

the robustness of the controller in case an estimation error is introduced with the feed-forward term.

3.9 CONCLUSIONS AND FUTURE WORK

The Natural Switching Surfaces for a flyback converter were obtained from the normalized converter equations. The derived nonlinear control law forces BCM in one switching cycle for all initial conditions. When sudden load changes are produced, the controller instantaneously reacts to compensate for the load change within a switching action.

Simulations showed that for the nominal system, the closed loop response has no overshoot, zero steady-state error and an adequate response to sudden load changes. For the case of parameter uncertainties, the performance of the closed loop system controlled with the nominal controller degrades. To improve the performance, an adaptive scheme can be built by adjusting the relation alfa/beta at the end of each switching cycle, after analyzing the locus of the true OFF-trajectory. The simulations which validated the proposed control techniques were performed for a 100 W, 24/100 V converter, whose prototype is under construction.

Since the control law reaches the reference voltage in one switching action, there is a large current peak during the start-up which can be destructive for the converter components. Therefore, several modifications of the control law were implemented under start-up conditions which showed an excellent performance.

3.10 ACKNOWLEDGMENTS

The authors are grateful for the financial support from the NSF-EPSCoR Vertically Integrated Center for Transformative Energy Research (www.victercenter.com). Dr. Chiacchirini is grateful

to Consejo Nacional de Investigaciones Científicas y Técnicas (CONICET) and Universidad Nacional del Sur.

3.11 REFERENCES

[1]. M. Kazimierczuk, Pulse-width Modulated DC–DC Power Converters, First Edit. John Wiley & Sons, 2008.

[2]. S. Ozturk and I. Cadirci, "DSPIC microcontroller based implementation of a flyback PV microinverter using Direct Digital Synthesis," in Energy Conversion Congress and Exposition (ECCE), 2013 IEEE, 2013, pp. 3426–3433.

[3]. L. Garcia-Rodriguez, E. Williams, J. C. Balda, J. Gonzalez-Llorente, E. Lindstrom, and A. Oliva, "Dual-stage microinverter design with a GaN-based interleaved flyback converter stage," in Energy Conversion Congress and Exposition (ECCE), 2013 IEEE, 2013, pp. 4496–4502.

[4]. D. C. Martins and R. Demonti, "Grid connected PV system using two energy processing stages," in Photovoltaic Specialists Conference, 2002. Conference Record of the Twenty-Ninth IEEE, 2002, pp. 1649–1652.

[5]. M. Seker and E. Zergeroglu, "A new sliding mode controller for the DC to DC flyback converter," in Automation Science and Engineering (CASE), 2011 IEEE Conference on, 2011, pp. 720–724.

[6]. M. Salimi, J. Soltani, A. Zakipour, and V. Hajbani, "Sliding mode control of the DC-DC flyback converter with zero steady-state error," in Power Electronics, Drive Systems and Technologies Conference (PEDSTC), 2013 4th, 2013, pp. 158–163.

[7]. M. Ordonez, M. T. Iqbal, and J. E. Quaicoe, "Selection of a curved switching surface for buck converters," Power Electron. IEEE Trans., vol. 21, no. 4, pp. 1148–1153, 2006.

[8]. J. M. Galvez, M. Ordonez, F. Luchino, and J. E. Quaicoe, "Improvements in Boundary Control of Boost Converters Using the Natural Switching Surface," Power Electron. IEEE Trans., vol. 26, no. 11, pp. 3367–3376, 2011.

[9]. K. K. S. Leung and H. S.-H. Chung, "Derivation of a second-order switching surface in the boundary control of buck converters," Power Electron. Lett. IEEE, vol. 2, no. 2, pp. 63–67, 2004.

[10]. G. G. Oggier and M. Ordonez, "Boundary Control of Full-Bridge ZVS: Natural Switching Surface for Transient and Steady-State Operation," Ind. Electron. IEEE Trans., vol. 61, no. 2, pp. 969–979, 2014.

[11]. L. A. Garcia-Rodriguez, E. Williams, J. C. Balda, J. Gonzalez-Llorente and H. Chiacchiarini, "Control of a flyback converter operating in BCM using the natural switching surface," *2015 IEEE 6th International Symposium on Power Electronics for Distributed Generation Systems (PEDG)*, Aachen, 2015, pp. 1-8 .

3.12 APPENDICES

3.12.A Paper Permissions

11/5/2019 Rightslink® by Copyright Clearance Center

Copyright Clearance Center RightsLink®

Home | Help | Email Support | Sign in | Create Account

IEEE Requesting permission to reuse content from an IEEE publication

Control of a flyback converter with parametric uncertainties operating in BCM Using the natural switching surface

Conference Proceedings: 2016 IEEE Biennial Congress of Argentina (ARGENCON)

Author: Luciano A. Garcia Rodriguez

Publisher: IEEE

Date: June 2016

Copyright © 2016, IEEE

Thesis / Dissertation Reuse

The IEEE does not require individuals working on a thesis to obtain a formal reuse license, however, you may print out this statement to be used as a permission grant:

Requirements to be followed when using any portion (e.g., figure, graph, table, or textual material) of an IEEE copyrighted paper in a thesis:

1) In the case of textual material (e.g., using short quotes or referring to the work within these papers) users must give full credit to the original source (author, paper, publication) followed by the IEEE copyright line © 2011 IEEE.
2) In the case of illustrations or tabular material, we require that the copyright line © [Year of original publication] IEEE appear prominently with each reprinted figure and/or table.
3) If a substantial portion of the original paper is to be used, and if you are not the senior author, also obtain the senior author's approval.

Requirements to be followed when using an entire IEEE copyrighted paper in a thesis:

1) The following IEEE copyright/ credit notice should be placed prominently in the references: © [year of original publication] IEEE. Reprinted, with permission, from [author names, paper title, IEEE publication title, and month/year of publication]
2) Only the accepted version of an IEEE copyrighted paper can be used when posting the paper or your thesis on-line.
3) In placing the thesis on the author's university website, please display the following message in a prominent place on the website: In reference to IEEE copyrighted material which is used with permission in this thesis, the IEEE does not endorse any of [university/educational entity's name goes here]'s products or services. Internal or personal use of this material is permitted. If interested in reprinting/republishing IEEE copyrighted material for advertising or promotional purposes or for creating new collective works for resale or redistribution, please go to http://www.ieee.org/publications_standards/publications/rights/rights_link.html to learn how to obtain a License from RightsLink.

If applicable, University Microfilms and/or ProQuest Library, or the Archives of Canada may supply single copies of the dissertation.

BACK CLOSE

UNIVERSITY OF
ARKANSAS
College of Engineering

Department of Electrical Engineering

1 University Avenue, 3217 Bell Engineering Center, Fayetteville, AR 72701, (479) 575-3005, (479) 575-7967 (fax)

November 6, 2019

To whom it may concern,

This letter is to verify that Mr. Luciano Andrés Garcia Rodriguez, ID 010593736, is the first author and did at least 51% of the work for the paper titled "Control of a Flyback Converter with Parametric Uncertainties Operating in BCM Using the Natural Switching Surface".

Kind Regards,

Dr. Juan Carlos Balda

University Professor, Department Head and Major Advisor to Mr. Luciano Andrés Garcia Rodriguez

CHAPTER 4

Adaptive Boundary Control Using Natural Switching Surfaces for Flyback Converters Operating in the Boundary Conduction Mode with Parameter Uncertainties

L. A. Garcia Rodriguez, H. G. Chiacchiarini, D. Carballo Rojas and J. C. Balda, "Adaptive Boundary Control Using Natural Switching Surfaces for Flyback Converters Operating in the Boundary Conduction Mode with Parameter Uncertainties," *IEEE Transactions on Power Electronics*, vol. 34, no. 8, pp. 8118-8137, Aug. 2019.

4.1 ABSTRACT

The derivation and implementation of the natural switching surfaces (NSS) considering certain parametric uncertainties for a flyback converter operating in the boundary conduction mode (BCM) is the main focus of this paper. The NSS with nominal parameters presents many benefits for the control of nonlinear systems; for example fast transient response under load-changing conditions. However, the performance worsens considerably when the converter actual parameters are different from the ones used in the design process. Therefore, a novel control strategy for NSS considering the effects of parameter uncertainties is proposed. This control law can estimate and adapt the control trajectories in a minimum number of switching cycles to obtain excellent performances even under extreme parameter uncertainties. The analytical derivation of the proposed adaptive switching surfaces is presented together with simulations and experimental results showing adequate performance under different tests, including comparisons with a standard PI controller.

Index Terms— Flyback converter, critical conduction mode (CRM), boundary conduction mode (BCM), variable structure control (VSC), boundary control (BC), switching surface control

(SSC), natural switching surface (NSS), parametric uncertainties, adaptive controller, nonlinear control.

4.2 INTRODUCTION

The flyback converter is one of the most used topologies in systems rated up to 200 W due to many benefits such as low part count, low cost, electrical isolation, and wide voltage ratio [1]. In addition to the traditional applications in computers and TV sets, flyback converters are used in AC/DC power supplies for LED loads and battery chargers [2]–[4], and in photovoltaic microinverters [5], [6]. Flyback converters operating in the boundary conduction mode (BCM) are broadly used for high-frequency applications since zero-current turn-ON for the switching device and zero-current turn-OFF for the diode are achieved while keeping conduction losses and current stresses low in comparison with operation in the discontinuous conduction mode (DCM) [3], [7]. The soft-switching transitions during the BCM operation reduce the electromagnetic interference (EMI) and lead to lower power losses due to Joule effect than operation in continuous conduction mode (CCM), simplifying the snubber design, EMI filtering and thermal management [8], [9]. Also, operation in BCM leads to less voltage ripple than operation in DCM.

A flyback converter is a non-minimum phase system due to the presence of a right-half plane zero in the control-to-output transfer function [10]. Using linear compensators to control such a system requires a low crossover frequency to guarantee stability which implies a slow control response [11]. Unfortunately, linear compensators are unsuccessful when there are large load variations since the model is only valid around an equilibrium point [12]; therefore, nonlinear controllers are used to improve the control dynamics. Variable structure control (VSC) is a discontinuous nonlinear control strategy whose structure changes depending on the location of the state trajectories with respect to a designed switching surface (SS) [12]–[16]. Boundary control

(BC) and sliding mode control (SMC) are VSC examples. Under SMC, the system remains close to the SS after reaching it. However, the SSs in BC may not be related with sliding regimes [12].

BC is a large-signal geometric control method that does not distinguish between start-up, transients and steady-state operation [12]–[14]. The intersection of the system trajectories with the selected SS defines whether the switch turns ON or OFF. First-order SSs are commonly used in BC because they are robust and simple to implement [16], [17]. However, the transient dynamics may require several switching cycles before reaching a steady state after start-up or transient conditions [18], [19]. Furthermore, the optimal slope for the first-order SS is dependent on the load and supply characteristics which reduce the overall system performance [10]. An ideal SS is the one that guides the system to the desired steady state with the minimum number of switching actions [14]. The ideal SS is derived from the intersection of the system OFF-trajectory that contains the operating point with the ON-trajectory that leaves the operating point [12]–[14].

Multiple SSs have been proposed to estimate the ideal trajectories or natural response of converters. For example, second-order SSs derived from capacitor charge-balance equations with low ripple approximation have been proposed for buck converters operating in CCM [18] and DCM [20]. Also, a fixed-frequency second-order SS using a variable-width hysteresis loop was presented in [21]. A similar methodology was applied to single-phase [22], [23] and three-phase inverters [24]. Other types of second-order SSs derived using the state-energy plane were proposed for single- and dual-output boost converters [10], [25]. Higher-order switching surfaces for inverters were derived in [19] and [26], where logarithmic SSs were used to approximate the system trajectories. Another method to approximate the ideal trajectories was derived from the converter differential equations assuming a constant-current load [27]. Using those SSs called the Natural Switching Surfaces (NSS) warrants no output voltage overshoot for a step load variation

under nominal design conditions, excellent response for any change of the load resistance and much easier trajectory derivation because of the absence of the exponential decay, spirals or hyperbolic terms related to the presence of the load resistance in the differential equations [13]. This method was first presented in [27] for buck converters and then extended to the inverters [28], boost [11], [29], buck-boost [30], dual active bridge [31], full bridge [32] and flyback converters [33], [34].

The main drawback of BC is the dependence of the switching surfaces on the converter parameters [12], [14], which are exposed to changes due to tolerance, aging effect, humidity and temperature [23], [24]. Parameter variations impact on the steady-state performance [19], [20] and lead to stability issues because of changes on the shape of the switching surfaces [29] and converter operating modes [10]. This paper presents a solution to those issues by deriving the NSSs and the control law for a flyback converter operating in BCM and considering parameter uncertainties. The proposed control law can provide a very precise estimation of the parameter variations in only a single switching action and then continuously adapt the control switching surfaces before a new switching action occurs. Therefore, the converter can reach the steady-state operation in a single switching action for sudden load changes even under extreme converter parameter variations.

This paper is organized as follows. The normalized system trajectories considering parametric uncertainties are derived in Section 4.3. Then, the start-up and steady-state characteristics are presented in Section 4.4. The adaptive control laws are developed in Section 4.5. The design procedure and an example are given in Section 4.6. The feasibility of the proposed control law is validated through simulation results in Section 4.7 and experimental results in Section 4.8. Finally, Section 4.9 presents the conclusions.

4.3 DERIVATION OF NORMALIZED SYSTEM TRAJECTORIES CONSIDERING PARAMETRIC UNCERTAINTIES

The circuit shown in Fig. 4.1 represents a flyback converter either for resistive load R_o or for constant-current load I_o. It includes the following circuit and parasitic elements:

- Q: transistor,
- d: diode,
- T: transformer,
- $n = N_p/N_s$: transformer turns ratio,
- L_m: transformer magnetizing inductance,
- L_k: transformer leakage inductance,
- C_{in}: input capacitor,
- C_o: output capacitor,
- R_{Lp}: primary-side winding resistance,
- R_{ON}: switch ON resistance,
- $R_p = R_{Lp} + R_{ON}$: total primary resistance,
- R_d: diode ON resistance,
- R_{Ls}: secondary-side winding resistance,
- $R_s = R_d + R_{Ls}$: total secondary resistance,
- V_d: diode forward voltage drop.

The stationary and transient responses of the circuit for both load conditions can be obtained from the circuit equations. For the case of a resistive load, after some basic calculations, the following steady-state solution can be obtained:

$$\left(V_{in} - I_m R_p\right) D = n\left(V_o + V_d + n I_m R_s\right)\left(1 - D\right), \tag{1}$$

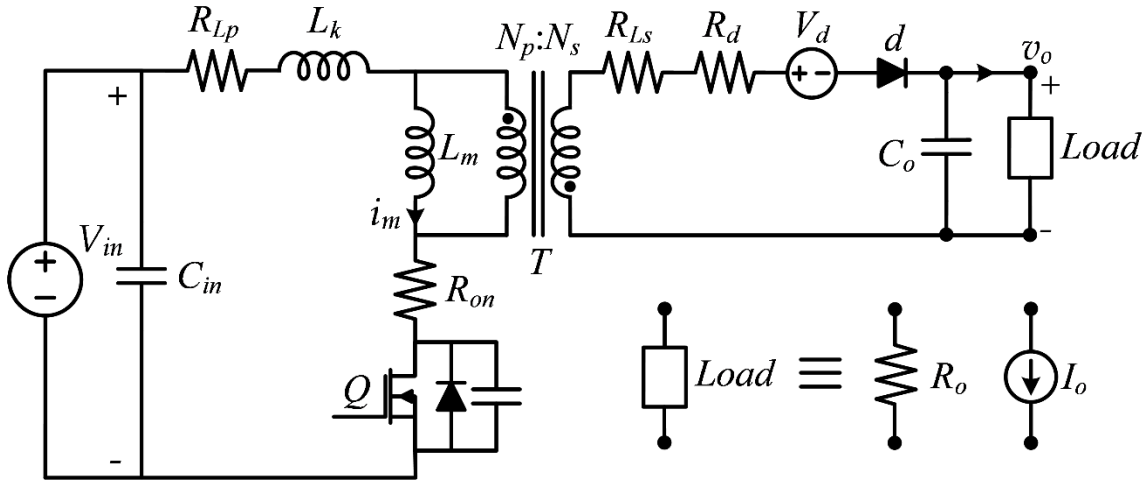

Fig. 4. 1. Flyback converter with parasitic elements.

$$I_m n(1-D) = V_o / R_o \,. \tag{2}$$

By solving for the duty cycle D from (2) and replacing it in (1), the flyback converter load line for a resistive load is given by:

$$I_m R_p R_o + \frac{V_o}{I_m}\left(V_o + \frac{V_{IN}}{n} + V_d\right) = V_o\left(\frac{R_p}{n} - nR_s\right) + V_{IN}R_o. \tag{3}$$

Fig. 4.2 (a) shows the load line from (3), and ON and OFF-BCM flyback trajectories obtained by solving the circuit equations for the ON- and OFF-switch states for different arbitrary initial conditions. The load resistor R_o is 48 Ω and the input voltage source V_{in} is 6 V. The value of the parasitic elements of the flyback components are shown in Table 4.I and they represent the same actual parameters from the components used for the simulation and experimental results included in this work.

For the constant-current load, the following steady-state solution can be derived after some basic calculations:

$$\left(V_{in} - I_m R_p\right)D = n(1-D)\left(V_o + V_d + nI_m R_s\right), \tag{4}$$

$$I_o = n(1-D)I_m \,. \tag{5}$$

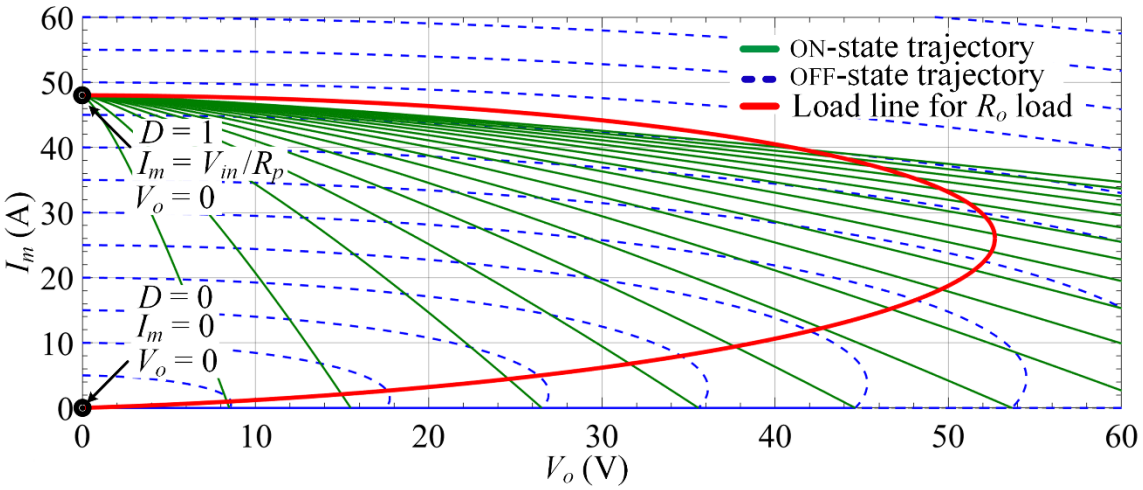

(a)

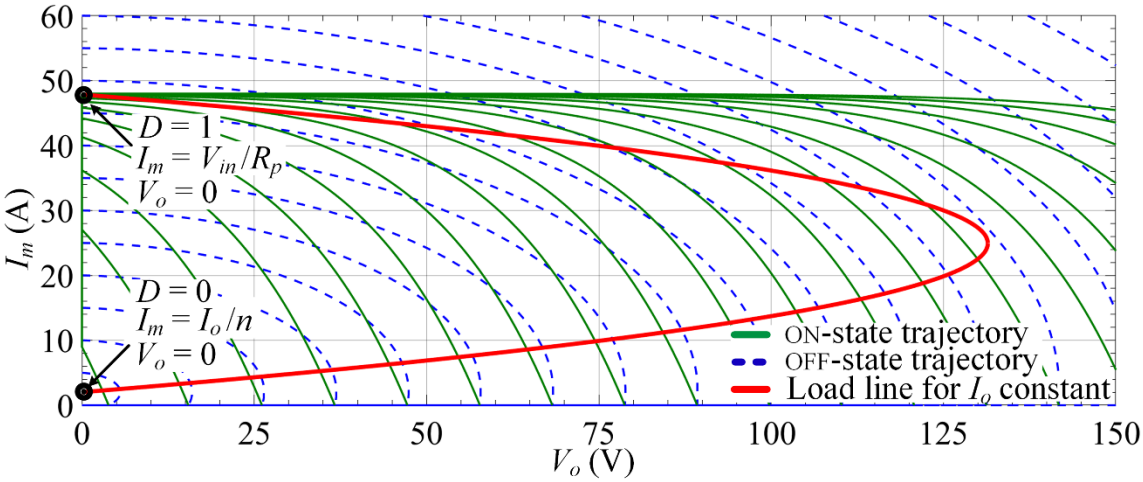

(b)

Fig. 4. 2. Load line for a flyback converter with (a) a resistive load, and (b) a constant-current load.

TABLE 4. I FLYBACK CONVERTER PARASITIC ELEMENTS

Component	Parasitic Element	Value
Transformer	L_k	1.58 µH
	R_{Lp}	0.048 Ω
	R_{Ls}	0.110 Ω
Transistor	R_{ON}	0.077 Ω
Diode	V_d	0.58 V
	R_d	0.02 Ω

By solving for the duty cycle D from (5) and replacing it into (4), the load line for a flyback with constant-current load is obtained as:

$$I_m R_p + \frac{V_{in} i_o}{n I_m} + \frac{(V_o + V_d) I_o}{I_m} = I_o \left(\frac{R_p}{n} - n R_s \right) + V_{IN} . \quad (6)$$

Fig. 4.2(b) shows the load line for a constant-current load and the ON and OFF trajectories when the actual converter parameters from Table 4.I are used. The constant-current load I_o was set to 0.5 A and the input voltage to V_{in} = 6 V.

The load lines considering parasitic components derived for the resistive and constant-current load cases are compared below to the load lines obtained without parasitic components to show that the ideal model and the model considering parasitic elements behave very similarly under steady-state conditions. The ideal load line for the resistive load case is obtained by making the parasitic elements equal to zero on (3) as:

$$V_o^2 n + V_o V_{in} = I_m V_{in} R_o n . \quad (7)$$

Fig. 4.3(a) shows the ideal and real load lines, and the ON and OFF real BCM trajectories. It is possible to see that they are very similar during most of the operating range. If the particular case with V_o = 24 V, V_{in} = 6 V and the turns ratio N_p/N_s = 4 is considered, the ideal duty cycle D is 0.5. However, D should be 0.53 under conditions with actual parameters, which represents a 6% of duty cycle variation.

The actual and the ideal flyback load lines for the case of a constant-current load are shown in Fig. 4.3(b). Like the case of a resistive load, the actual and ideal load lines for a constant-current load are similar for the duty cycle range ($0 < D < 0.8$). For example, if V_o = 24 V, V_{in} = 6 V and the turns ratio N_p/N_s = 4 is considered, the ideal duty cycle D is 0.5 while D = 0.53 is needed when actual components are used.

It is concluded that flyback circuits with typical parasitic components can be analyzed under ideal conditions (no parasitic components) without producing relevant errors.

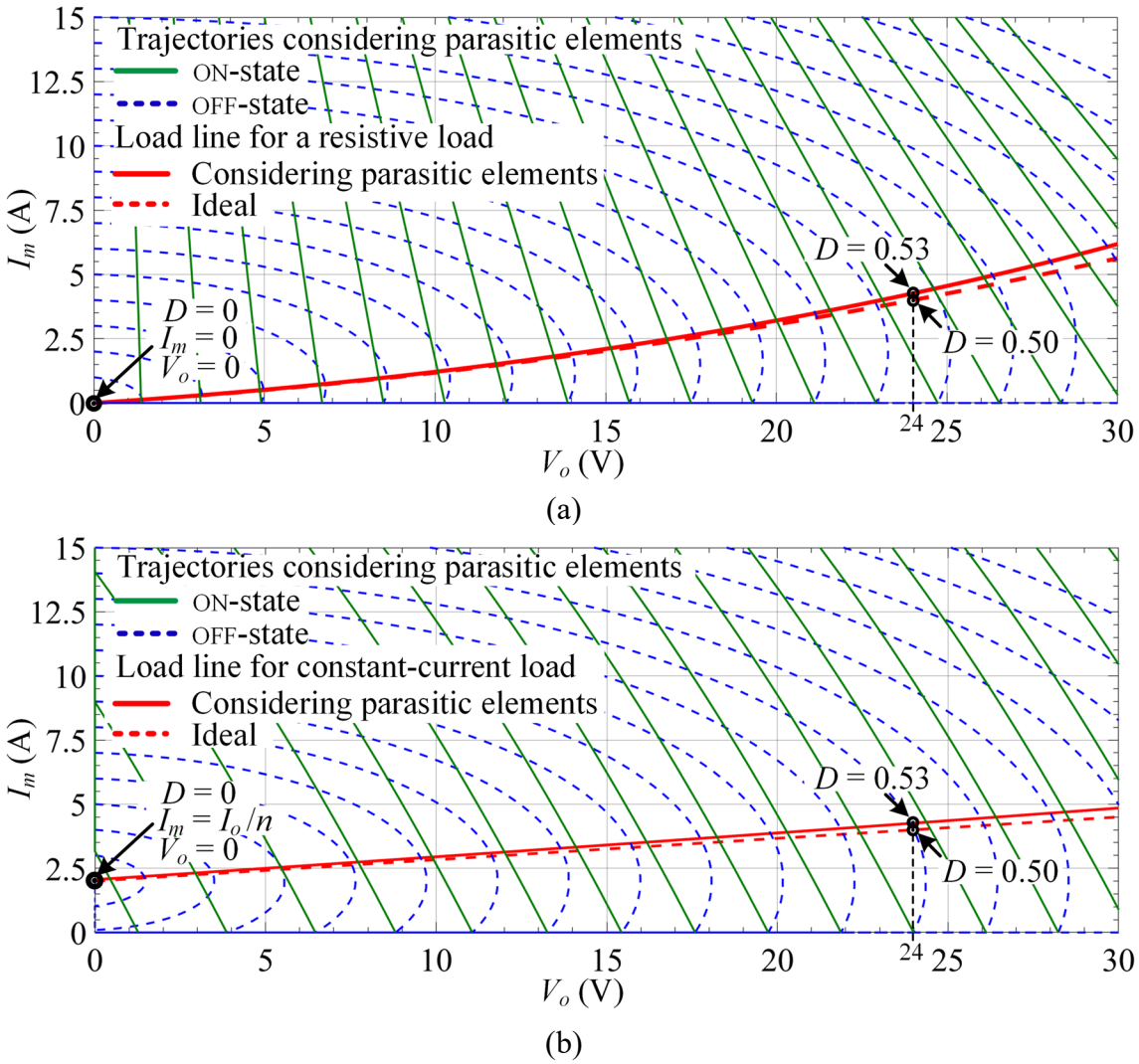

Fig. 4. 3. Actual and ideal flyback converter load lines for (a) a resistive load, and (b) a constant-current load.

The system shown in Fig. 4.4 is a simplified version of a flyback converter which consists of an ideal transistor Q, and ideal diode d, flyback transformer T with magnetizing inductance L_m, as well as input and output capacitors, C_{in} and C_o. These parameters are the converter actual parameters which may differ from the nominal ones used in the design process. The components which determine the dynamics of a flyback converter are the magnetizing inductance and output capacitance [33]. The nominal output capacitance is $\overline{C}_o$ and the nominal magnetizing inductance is $\overline{L}_m$. The load is represented by a constant-current load which states the worst-case scenario in

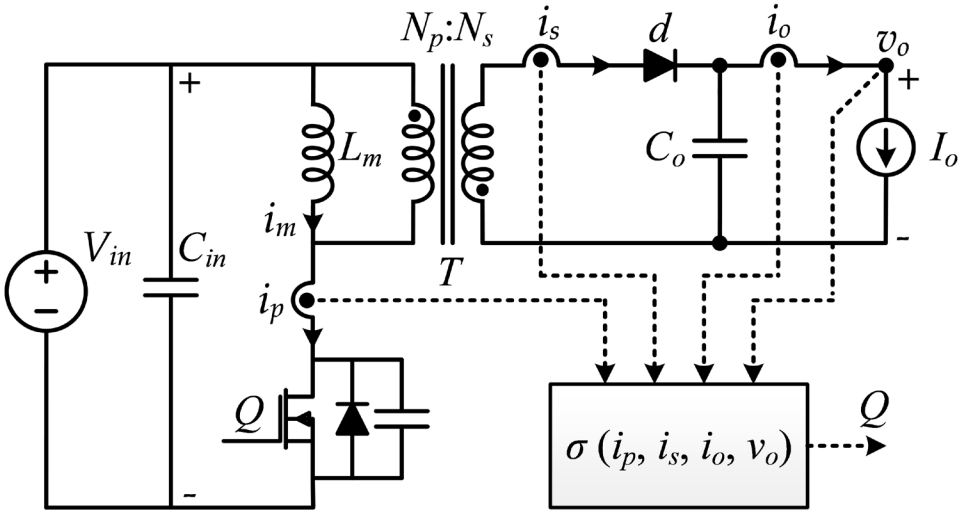

Fig. 4. 4. Flyback converter circuit including current and voltage sensors.

terms of stability [11]. The normalization of the system consists of a scale change of variables on its differential equations which enables a general solution [27]. The presence of a transformer makes it necessary to relate the converter parameters to one side; the secondary side is selected in this case. The normalization is performed using the nominal output voltage as the reference voltage $V_r = v_o$, the characteristic nominal impedance of the combined nominal magnetizing inductance referred to the secondary side and the nominal output capacitor, $\overline{Z}_o = (1/n)\sqrt{\overline{L}_m/\overline{C}_o}$ as the reference impedance Z_r and the natural frequency $\overline{f}_o = n\Big/\left(2\pi\sqrt{\overline{L}_m\overline{C}_o}\right)$ as the reference frequency f_r. The normalizing equations of the voltage, current and time variables as well as their derivatives for the secondary variables are as follows:

$$v_n = v/V_r, \quad dv_n = dv/V_r, \tag{8}$$

$$i_n = i.Z_r/V_r, \quad di_n = di.Z_r/V_r, \tag{9}$$

$$t_n = t.f_r, \quad dt_n = dt.f_r, \tag{10}$$

where v, i, and t are the standard voltage, current and time variables of the secondary side, and v_n,

i_n, and t_n are their normalized versions. The normalizing equations must be reflected back to the primary side to normalize primary variables as follows:

$$v_n = v/\left(n.V_r\right), \quad i_n = i.n.Z_r/V_r, \tag{11}$$

$$dv_n = dv/\left(nV_r\right), \quad di_n = di.n.Z_r/V_r. \tag{12}$$

The next subsections present the derivation of the normalized OFF- and ON-state general natural trajectories on the plane i_{mn} vs. v_{on}, which depend on generic initial conditions, input voltage and output current. Later, specific natural trajectories containing the point $i_{mn} = 0$, $v_{on} = V_{TPn}$ will be analyzed. This specific point characterizes the operation in BCM. As will be explained in the sequel, voltage V_{TPn} is set as the desired target point voltage which leads to the converter producing the required root-mean-square value (RMS) of the voltage output.

4.3.A OFF-State Trajectory

Diode *d* conducts during the OFF-state of transistor *Q* and the energy stored in the transformer during the ON-state is transferred to the load. The voltage applied to the magnetizing inductance is the output voltage multiplied by the transformer turns ratio. The following expressions are the differential equations that describe this mode of operation, where L_m and C_o are the actual parameters of the converter:

$$L_m \frac{di_m}{dt} = -nv_o, \tag{13}$$

$$C_o \frac{dv_o}{dt} = ni_m - i_o. \tag{14}$$

Using (1) through (5), the normalization of (6) and (7) becomes:

$$\frac{di_{mn}}{dt_n} = -2\pi \frac{\overline{L}_m}{L_m} v_{on}, \tag{15}$$

$$\frac{dv_{on}}{dt_n} = 2\pi \frac{\overline{C}_o}{C_o}\left(i_{mn} - i_{on}\right). \tag{16}$$

Differentiating both sides of (8) and replacing it in (9) yields a differential equation with the following solution:

$$i_{mn}\left(t_n\right) = i_{on} + A\cos\left(2\pi\sqrt{\alpha\beta}t_n\right) + B\sin\left(2\pi\sqrt{\alpha\beta}t_n\right), \tag{17}$$

where $\alpha = \overline{L}_m / L_m$, $\beta = \overline{C}_o / C_o$, $A = i_{mn}\left(0^-\right) - i_{on}$ and $B = \dfrac{1}{2\pi\sqrt{\alpha\beta}} \dfrac{di_{mn}\left(0^-\right)}{dt_n}$. By applying the trigonometric property $A\cos\left(x\right) + B\sin\left(x\right) = \sqrt{A^2 + B^2}\,\sin\left(x + \tan^{-1}\left(A/B\right)\right)$ to (17), taking the derivative of the resulting expression and using the property $\cos\left(\sin^{-1}\left(x\right)\right) = \sqrt{1 - x^2}$, the result is an equation that does not depend on the normalized time. Then, the OFF-state trajectory can be expressed as follows:

$$\lambda_{OFF} := v_{on}^2 \frac{\alpha}{\beta} + \left(i_{mn} - i_{on}\right)^2 - A^2 - B^2 = 0. \tag{18}$$

Therefore, in the case where the nominal parameters are the same as the actual ones ($\alpha/\beta = 1$), λ_{OFF} is a circle with its center at (i_{mn}, v_{on}) = (i_{on}, 0) and a radius that is a function of the specifications of the converter [33]. However, λ_{OFF} becomes an ellipse in the case where the actual parameters differ from those used in the design process.

4.3.B ON-State Trajectory

The magnetizing inductance is connected to the input source and the diode in the secondary side is reversed bias when the transistor Q is ON. The differential equations for this stage and their normalized versions are:

$$v_{in} = L_m \frac{di_m}{dt}, \tag{19}$$

$$-i_o = C_o \frac{dv_o}{dt}, \tag{20}$$

$$2\pi\alpha v_{inn} = \frac{di_{mn}}{dt_n}, \tag{21}$$

$$-2\pi\beta i_{on} = \frac{dv_{on}}{dt_n}. \tag{22}$$

From (21) and (22), when Q is ON, the normalized magnetizing current and output voltage vary linearly with time. Dividing these two normalized equations yields:

$$\frac{di_{mn}}{dv_{on}} = -\frac{\alpha}{\beta}\frac{v_{inn}}{i_{on}}. \tag{23}$$

By integrating (14), the natural trajectory of the flyback converter when the transistor Q is ON is given by:

$$\lambda_{ON} := i_{mn} + \frac{\alpha}{\beta}\frac{v_{inn}}{i_{on}} v_{on} - H = 0, \tag{24}$$

where H is a constant that depends on the initial conditions selected for starting the ON-state. In particular, if the initial conditions for the λ_{OFF} trajectory are properly imposed (i.e., designing the controller adequately), the natural OFF-trajectory will intersect the state space target point (0, v_{on}), and H in λ_{ON} can also be selected such that λ_{ON} intersects the same target point.

The loci λ_{OFF} and λ_{ON} are the natural trajectories of the system when the switch is OFF and ON, respectively. Those natural trajectories start from the initial conditions which correspond to the time instants when the switch commutes. By properly selecting the switching times, specific natural trajectories can be selected to be the NSS that lead the converter to the target operating condition.

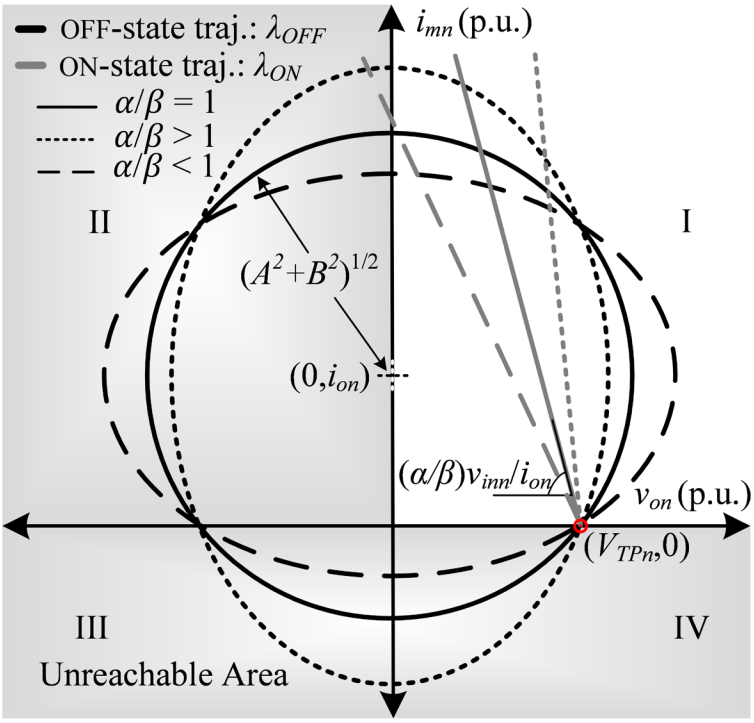

Fig. 4. 5. Normalized natural surfaces for a flyback converter operating in BCM under parametric uncertainties.

4.3.C Graphical Analysis of the NSS Trajectories with Parametric Uncertainties

Fig. 4.5 presents the graphical renditions of the NSS trajectories previously derived. These graphs show different elliptic trajectories λ_{OFF} all passing through the point (V_{TPn}, 0) for the BCM operation presented in the next subsection. As previously described, λ_{ON} is a descending sloping line and λ_{OFF} is a circle with a center at (0, i_{on}) for the case when $\alpha/\beta = 1$ and an ellipse for the case when $\alpha/\beta \neq 1$. This subsection shows the interaction of the two trajectories and their relationship with the converter operation.

Analyzing the operation of the flyback converter on the i_{mn} vs. v_{on} plane, quadrants of the plane can immediately be recognized as unobtainable or undesirable operation zones based on the polarity of the variables. For example, i_{mn} must be positive for the flyback converter to operate correctly. Therefore, i_{mn} would not be attainable in quadrants III or IV. Likewise, the converter

could not operate if v_{on} was negative. If the converter was operating when v_{on} were negative, it would imply that the load would be transferring power to the input of the converter, which is physically impossible due to the presence of the diode *d*. Therefore, v_{on} should not operate in quadrants II or III. This leaves quadrant I as the only operational quadrant that satisfies the constraints for both variables. In quadrant I, i_{mn} and v_{on} are both positive and the flyback converter would be transferring power to the load. The unreachable quadrants have been grayed out in Fig. 4.5.

If the converter's trajectories were to reach an axis, the converter would then evolve on that axis. Therefore, the converter upon reaching the i_{mn} axis would change i_{mn} while the output voltage remained at zero. Likewise, the converter upon reaching the v_{on} axis would change v_{on} while keeping the magnetizing current at zero. This is due to the unobtainable quadrants.

4.3.D Selection of the Target Point for Operation in BCM

The free parameters of λ_{ON} and λ_{OFF} in (11) and (15) should be selected for the natural trajectories to contain a target operating point that maintains the converter operating in BCM for all loading conditions. Selecting the target normalized magnetizing current as zero assures BCM operation. The target for the normalized output voltage is selected as V_{TPn}, whose value will be calculated so the desired output RMS voltage equals to the reference voltage V_r. The expression of V_{TPn} will be derived in the next sections.

Replacing the target point (i_{mn}, v_{on}) = (0, V_{TPn}) in (24), the constant *H* in λ_{ON} is given by:

$$H = \frac{\alpha}{\beta}\frac{V_{inn}}{i_{on}}V_{TPn}. \tag{25}$$

Therefore, the normalized BCM ON-state trajectory noted as σ_{ON} is given by:

$$\sigma_{ON} := i_{mn} + \frac{\alpha}{\beta}\frac{v_{inn}}{i_{on}}v_{on} - \frac{\alpha}{\beta}\frac{v_{inn}}{i_{on}}V_{TPn} = 0. \tag{26}$$

Moving onto λ_{OFF}, A and B can be evaluated from the known target point as the initial conditions:

$$i_{mn}\left(0^{-}\right) = 0, \quad di_{mn}\left(0^{-}\right)\Big/dt_n = -2\pi.\alpha.V_{TPn}. \tag{27}$$

Then, A and B can be expressed as:

$$A = -i_{on}, \quad B = -V_{TPn}\sqrt{\alpha/\beta}\,. \tag{28}$$

Substituting (28) into (11), the complete normalized BCM OFF-state trajectory which is named as σ_{OFF} is defined as follows:

$$\sigma_{OFF} := \frac{\alpha}{\beta}v_{on}^2 + \left(i_{mn} - i_{on}\right)^2 - \frac{\alpha}{\beta}v_{TPn}^2 - i_{on}^2 = 0. \tag{29}$$

4.3.E BCM Control Law

This section explains the derivation of the control law based on the BCM trajectories from (26) and (29). The goal of the control law is to force the converter to move to and stay on the identified BCM trajectories. The control law is developed by knowing the movements along the trajectories for each state of transistor Q and the above conditions. Basically, the control law decides between two options: either Q should be turned ON or OFF. The decision is based on the current state of transistor Q and the relative location of the current operating point with respect to the BCM trajectories.

While Q is ON, the converter moves up the i_{mn} vs. v_{on} plane. If the converter is currently operating below σ_{OFF}, Q is kept ON if $v_{on} \leq V_{TPn}$ while the converter continues to move up the plane until σ_{OFF} is reached. Then, Q is turned OFF. If the converter were operating anywhere above σ_{OFF}, Q should be turned OFF.

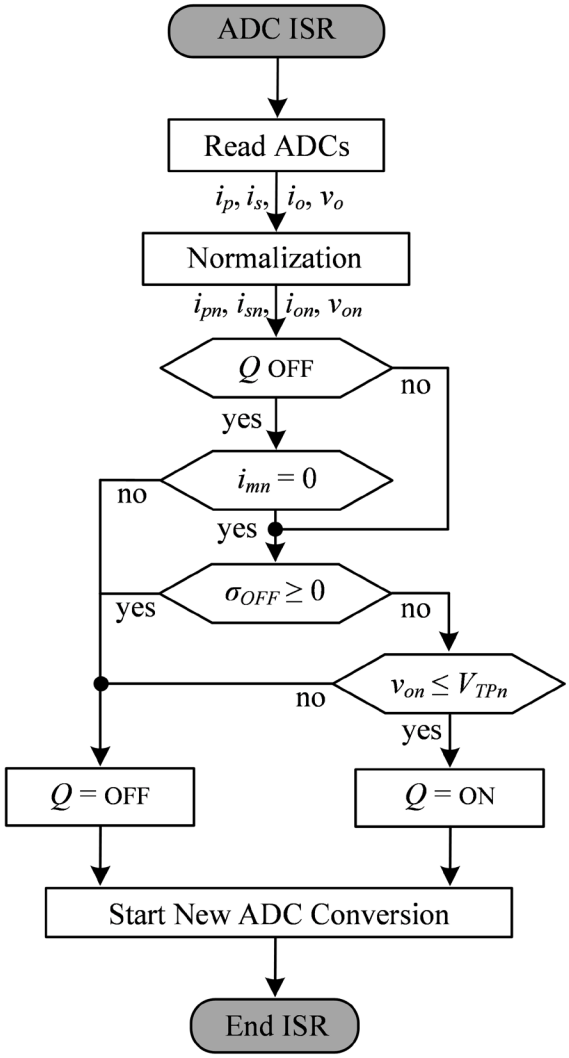

Fig. 4. 6. Flow diagram of the BCM control law.

Since the objective is to operate in BCM, Q is not allowed to switch back ON until $i_{mn} = 0$ p.u., once it has been switched OFF. Therefore, if the converter is operating anywhere above the v_{on} axis ($i_{mn} > 0$ p.u.) and Q is OFF, Q is kept OFF until the converter reaches the v_{on} axis. Once the v_{on} axis is reached, the current operating point is compared to σ_{OFF}. If the converter is operating at a point higher than σ_{OFF}, Q is kept OFF, allowing for the converter to evolve down the v_{on} axis to the OFF-state trajectory. After the converter is operating below or at σ_{OFF}, Q is switched ON if $v_{on} \leq V_{TPn}$, allowing for the converter to ride the ON-state trajectory back up to the OFF-state trajectory as previously described.

Fig. 4.6 shows a complete flow diagram of the BCM control law [33], which forces the converter to move and operate under the BCM trajectories in one switching cycle, no matter where the converter is currently operating. This allows the flyback converter to operate in BCM continuously for any load during steady-state conditions. Under transient conditions where the input voltage or load changes when Q is OFF, the worst-case scenario would be that the converter recovers in two switching cycles. During that transient, a DCM operation with a slightly overvoltage at the output or BCM operation with a slightly undervoltage at the output could be experienced. This is because the desired ON- and OFF-state trajectories change when the converter parameters change. If the disturbance occurs while Q is ON, the converter will reach the target point in only a single switching cycle. The rapid recovery time of one switching cycle provides remarkable stability and transient response time for all converter conditions.

4.4 START-UP AND STEADY-STATE CHARACTERISTICS

The normalized trajectories and main waveforms for a flyback converter operating in BCM when $\alpha/\beta = 1$ are shown in Fig. 4.7 [33]. At the converter start-up, initially i_{mn}, v_{on} and i_{on} are zero (see point A in Fig. 4.7). When Q turns ON, i_{mn} starts increasing while v_{on} stays at zero. When σ_{ON} intersects σ_{OFF} at point B = (0 p.u., $I_{st\text{-}upn}$), Q turns OFF so i_{mn} decreases while v_{on} increases. As soon as v_{on} starts rising, i_{on} moves towards its rated level I_{o1n} if the load is connected. Therefore, the first intersection of σ_{OFF} with the v_{on} axis will be at V_{xn}, whose level is lower than the target point V_{TPn} because σ_{OFF} was calculated for $i_{on} = 0$ p.u.. When $i_{mn} = 0$ p.u., Q turns ON at point C = (V_{xn}, 0 p.u.) until σ_{OFF} is reached at point D where Q turns OFF. The next intersection with the v_{on} axis is at the target point TP = (V_{TPn}, 0 p.u.) where steady-state conditions are reached and the flyback operates between points E and TP. In case of a sudden load change while Q is ON, the controller will be able to reach steady-state conditions in only one switching cycle. In that case,

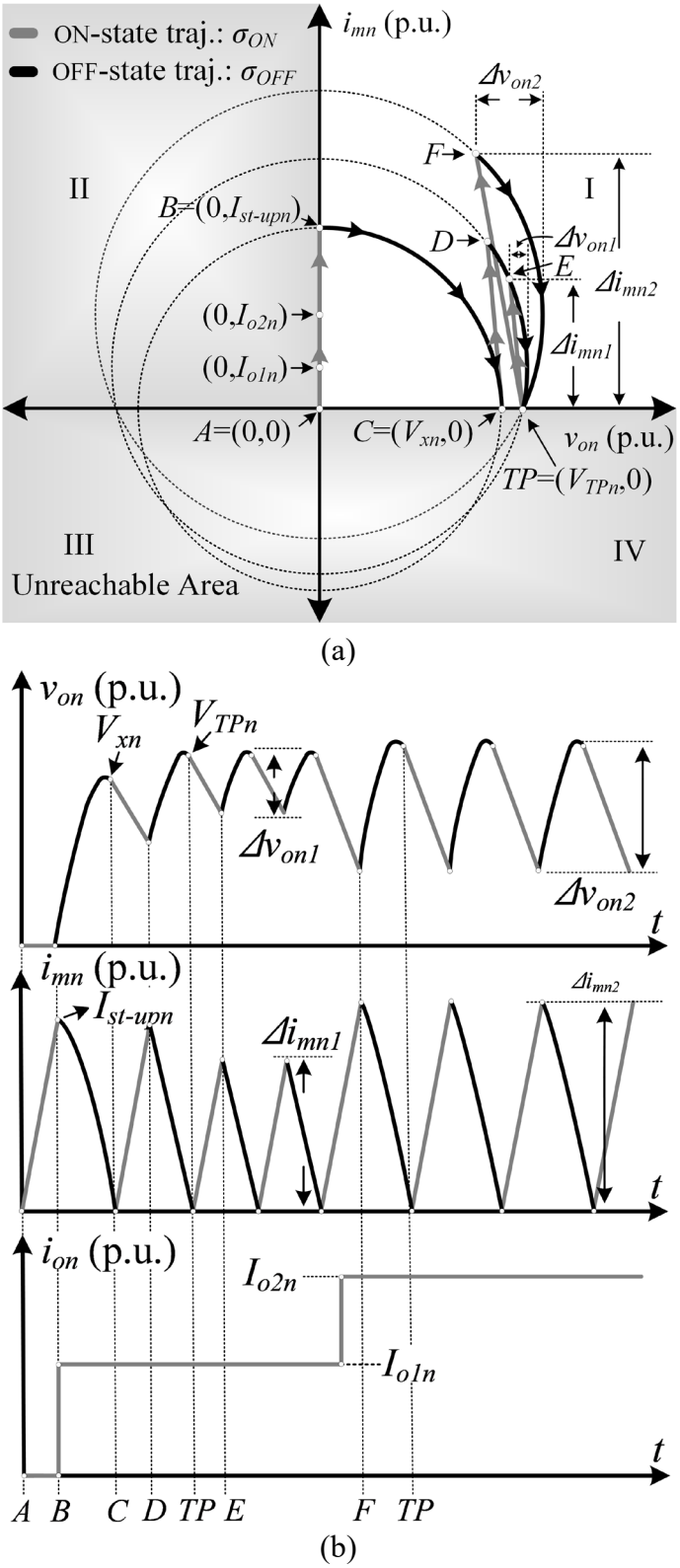

Fig. 4. 7. (a) NSS trajectories for the flyback converter operating in BCM when $\alpha/\beta = 1$, and (b) Normalized output voltage v_{on}, magnetizing inductance current i_{mn} and output current i_{on}.

the converter will be operating from points *F* to *TP*. The expressions for the start-up and steady-state conditions of Fig. 4.7 are calculated, and their dependence to the converter parameter uncertainties is analyzed in the following subsections.

4.4.A Start-Up Peak Current

The normalized start-up peak current $I_{st\text{-}upn}$ with start-up initial conditions (i_{on}, v_{on}) = (0, 0) p.u. can be determined by evaluating σ_{OFF} (29) yielding:

$$I_{st-upn} = \sqrt{\alpha/\beta}V_{TPn}. \tag{30}$$

Fig. 4.8 shows $I_{st\text{-}upn}$ as function of α/β when V_{TPn} = 1 p.u.. $I_{st\text{-}upn}$ = 1 p.u. that only happens under ideal conditions (α/β = 1). De-normalizing (30) by using (1) and (4), the start-up peak current $I_{st\text{-}up}$ can be calculated as follows:

$$I_{st-up} = \sqrt{\frac{\alpha}{\beta}\frac{\overline{C}_o}{\overline{L}_m}}V_{TP}. \tag{31}$$

$I_{st\text{-}up}$ is proportional to the square root of $\overline{C}_o/\overline{L}_m$ and V_{TP}; so $I_{st\text{-}up}$ could be very high for high-voltage and low-ripple applications. This is because, $I_{st\text{-}up}$ is the necessary magnetizing current to reach the target point in a single switching action when i_{on} = 0 p.u.. If necessary, the start-up current can be limited to a lower value I_{max} at the expense of reaching the target point under start-up conditions in more than a single switching action. Normally under start-up conditions, α/β = 1 since the flyback converter is supposed to have the parameters used in the design process.

4.4.B Start-Up Output Voltage

If the load is connected during start-up, the first intersection with the v_{on} axis will not be at the target point V_{TPn}. Instead it will be at a lower point defined as the start-up output voltage V_{xn}. Also, V_{xn} will be lower than V_{TPn} if the start-up current is limited to I_{maxn}, even if the load is disconnected.

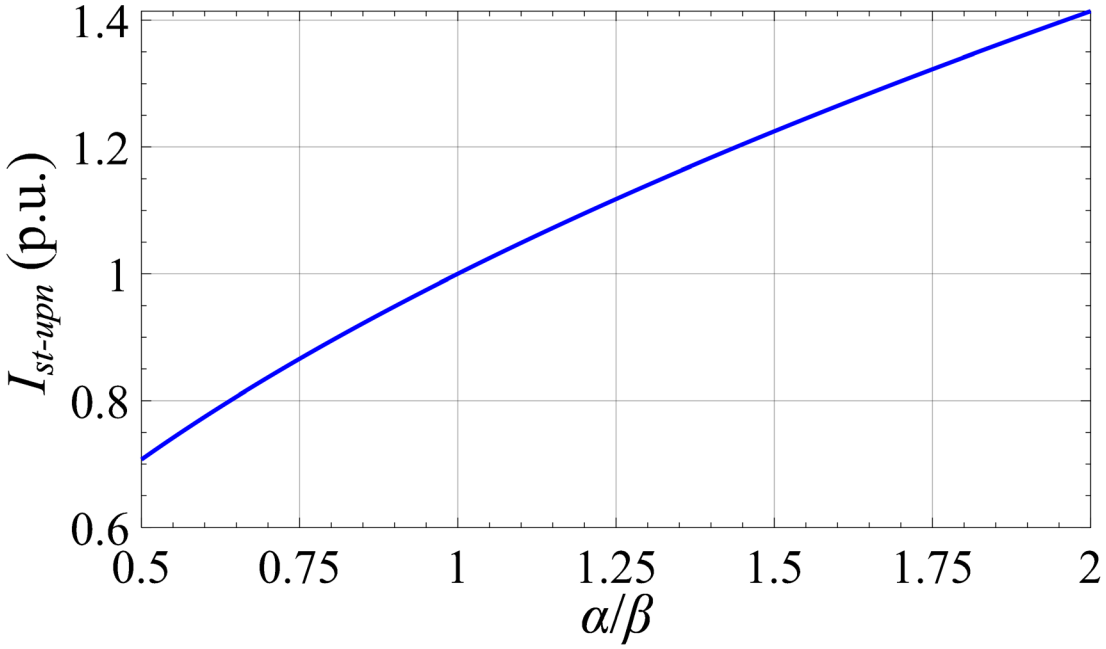

Fig. 4. 8. Normalized start-up current $I_{st\text{-}upn}$ to reach the target point V_{TPn} = 1 p.u. with minimum number of switching actions.

Modifying the initial conditions of (11), the normalized start-up output voltage V_{xn} can be derived as follows:

$$V_{xn} = \sqrt{\frac{I_{maxn}\left(I_{maxn} - 2i_{on}\right)}{\alpha/\beta}}. \tag{32}$$

The use and importance of V_{xn} on the design of the proposed adaptive boundary controller will be addressed in the following section. By de-normalizing (32), the start-up voltage V_x is given by:

$$V_x = \sqrt{I_{max}\frac{\overline{L}_m}{\overline{C}_o}\frac{\beta}{\alpha}\left(I_{max} - \frac{2i_o}{n}\right)}. \tag{33}$$

4.4.C Output Voltage Ripple

Under steady-state conditions, the voltage ripple Δv_{on} is defined by the difference between the maximum and minimum points of the voltage waveform. An expression for v_{on} as function of i_{mn}

can be obtained from σ_{OFF} as follows:

$$v_{on} = \sqrt{V_{TPn}^2 + 2\frac{\beta}{\alpha} i_{mn} i_{on} - \frac{\beta}{\alpha} i_{mn}^2}. \tag{34}$$

Since the locus of σ_{OFF} is an ellipse whose principal axes are aligned with the i_{mn}, v_{on} axes, the normalized maximum output voltage $V_{on,max}$ is obtained for $i_{mn} = i_{on}$ as:

$$V_{on,max} = \sqrt{V_{TPn}^2 + \frac{\beta}{\alpha} i_{on}^2}. \tag{35}$$

De-normalizing (35), the maximum output voltage $V_{o,max}$ can be then expressed as:

$$V_{o,max} = \sqrt{V_{TP}^2 + \frac{\overline{L}_m}{\overline{C}_o} \frac{\beta}{\alpha} \frac{i_o^2}{n^2}}. \tag{36}$$

The minimum value for the normalized output voltage $V_{on,min}$ is obtained from the intersection of σ_{OFF} with σ_{ON} as:

$$V_{on,min} = \frac{V_{TPn} v_{inn}^2 \frac{\alpha}{\beta} - i_{on}^2 \left(V_{TPn} + 2 v_{inn} \right)}{i_{on}^2 + v_{inn}^2 \frac{\alpha}{\beta}}. \tag{37}$$

Then, the normalized output voltage ripple is calculated as:

$$\Delta v_{on} = \sqrt{V_{TPn}^2 + i_{on}^2 \frac{\beta}{\alpha}} + \frac{i_{on}^2 \left(V_{TPn} + 2 v_{inn} \right) - V_{TPn} \frac{\alpha}{\beta} v_{inn}^2}{i_{on}^2 + \frac{\alpha}{\beta} v_{inn}^2}. \tag{38}$$

Fig. 4.9 illustrates (38) as function of i_{on} for different values of α/β when V_{inn} = 1 p.u.. For low output voltage ripple applications (Δv_o < 5% of V_r), i_{on} should not exceed 0.1 p.u. under ideal conditions. If $\alpha/\beta > 1$, Δv_{on} will decrease since the actual values of C_o will be greater than that used in the design process.

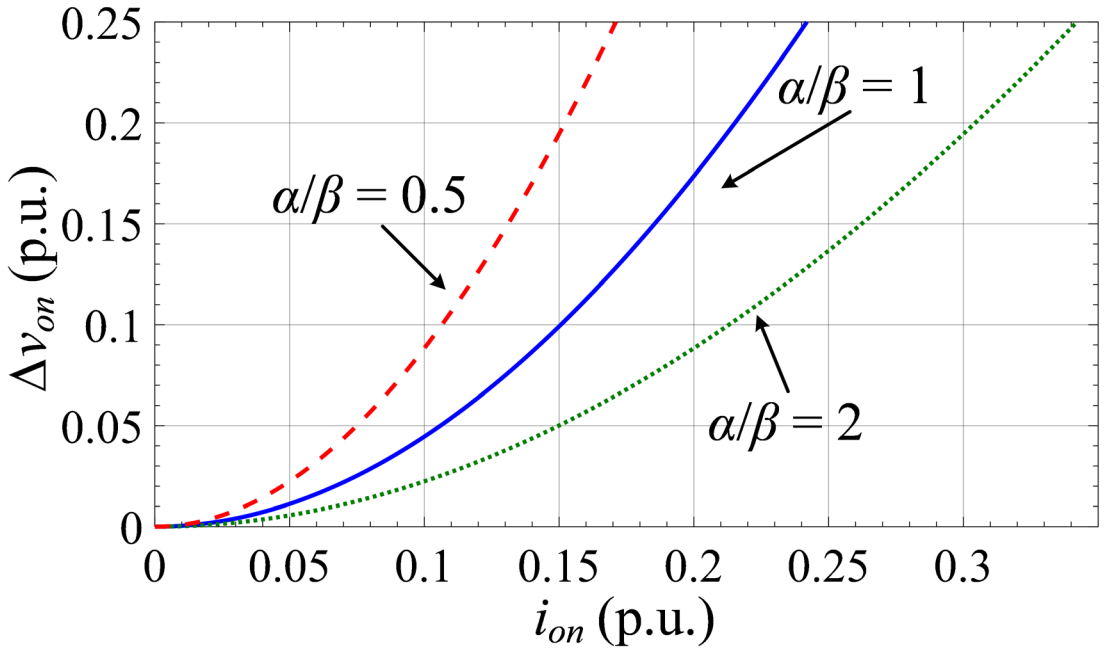

Fig. 4. 9. Normalized output voltage ripple Δv_{on} with v_{inn} = 1 p.u..

4.4.D Normalized Output Voltage Target Point

The target point of the output voltage V_{TPn} should be selected so that the normalized average output voltage $V_{on,ave}$ = 1 p.u. $V_{on,ave}$ should be obtained by integrating v_{on} over a normalized switching period T_{swn}; but the exact evaluation of $V_{on,ave}$ is cumbersome. However, the integral complexity is reduced if the RMS of v_{on} is calculated instead of the average value, and also, it is possible to obtain an approximated expression which is useful for low ripple cases. Furthermore, the RMS and the average values will be similar since Δv_{on} is small in comparison with the output voltage.

Considering the complexity of the exact evaluation of V_{AVE}, different simplified calculations can be made to obtain an approximated expression for V_{AVE}.

Among them:

1) Evaluating V_{RMS} instead of $V_{AVE;}$

2) $V_{AVE} \approx \delta\left(V_{on,min} + V_{TPn}\right)/2 + \left(1-\delta\right)\left(V_{on,max} + V_{TPn}\right)/2$, where δ is the fraction of time where V_{on} is lower than V_{TPn};

3) $V_{AVE} \approx \left(V_{on,max} + V_{on,min}\right)/2$;

4) $V_{AVE} \approx \left(V_{TPn} + V_{on,min}\right)/2$.

In all cases, $V_{on,max}$ is the output voltage corresponding to the time in which i_{mn} matches i_{on} reflected back to the primary side, and $V_{on,min}$ is the voltage value obtained at the time when Q is turned OFF.

Those alternative expressions are compared with a numerical evaluation of V_{AVE} in Fig. 4.10 for a specific design and fixed target operation point $V_{TPn} = 1$, and it is seen that the alternatives 1) and 2) are better approximations to V_{AVE} than 3) and 4).

Based on these results, V_{RMS} can be considered a good approximation for V_{AVE} and it is shown below that it can be calculated in closed form rather easily.

Although expression 2) seems to be accurate enough and easier than V_{RMS}, when $V_{on,min}$ and $V_{on,max}$ are included as functions of the other variables and parameters, the complexity increases. Also, parameter δ needs to be defined on an empirical basis.

Therefore, the RMS $V_{o,RMS}$ is calculated as follows:

$$V_{on,RMS} = \sqrt{\frac{1}{T_{swn}} \int_0^{T_{swn}} \left(v_{on}\left(t_n\right)\right)^2 dt_n} = \sqrt{\frac{1}{T_{swn}}\left(I_1 + I_2\right)}, \tag{39}$$

where $I_1 = \int_0^{I_{mn,max}} \left(V_{TPn} - \frac{\beta}{\alpha}\frac{i_{on}}{v_{inn}} i_{mn}\right)^2 \frac{di_{mn}}{2\pi\alpha v_{inn}}$ and $I_2 = \int_{I_{mn,max}}^{0} \left(\sqrt{V_{TPn}^2 + 2 i_{mn} i_{on}\frac{\beta}{\alpha} - i_{mn}^2 \frac{\beta}{\alpha}}\right)^2 \frac{di_{mn}}{-2\pi\alpha V_r}$.

$V_{on,RMS} = 1$ p.u. is replaced in (39) since the desired output voltage is equal to the reference level V_r. Solving for V_{TPn}, the expression in (40) is obtained.

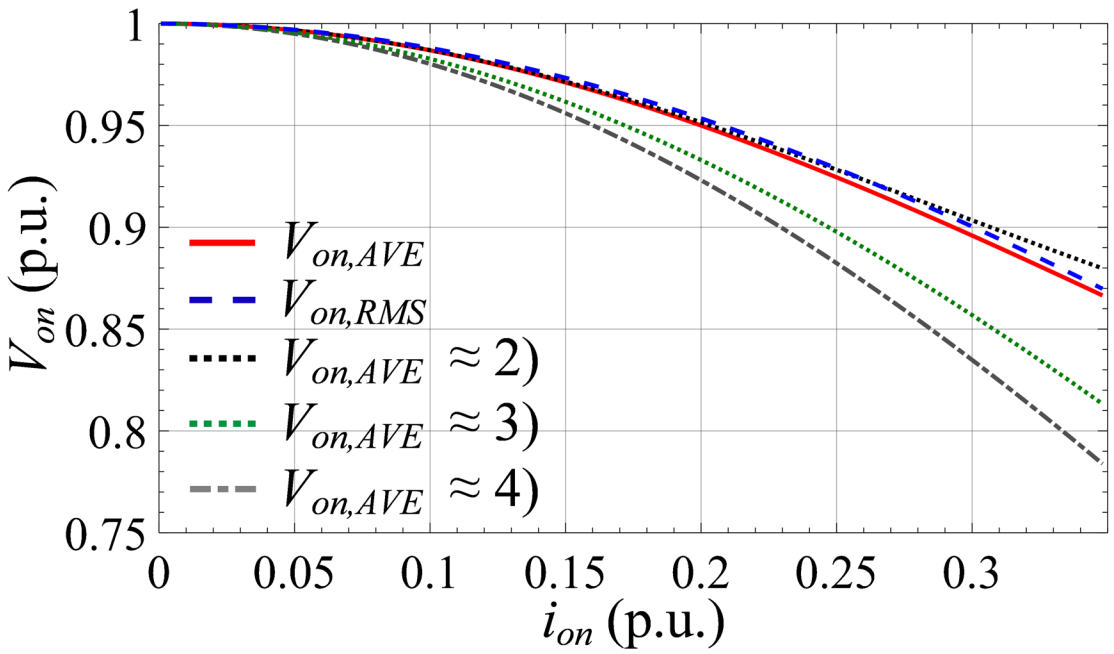

Fig. 4. 10. RMS, average and approximations for the output voltage v_{on}.

$$V_{TPn} = \frac{\left(\frac{\alpha}{\beta}v_{inn}^2 + i_{on}^2\right)\left(v_{inn}+1\right)\left(3v_{inn}^3\frac{\alpha}{\beta} + \sqrt{3v_{inn}^3\frac{\alpha}{\beta}\left(3v_{inn}\frac{\alpha}{\beta} - 2v_{inn}i_{on}^2 + 2i_{on}^2\right) + 3i_{on}^4\left(-3v_{inn}^2 + 2v_{inn} + 1\right)}\right)}{i_{on}^4\left(3v_{inn}+1\right) + 3v_{inn}^4\left(\frac{\alpha}{\beta}\right)^2 + 3v_{inn}^5\left(\frac{\alpha}{\beta}\right)^2 + 2v_{inn}^3\frac{\alpha}{\beta}i_{on}^2} - v_{inn} \tag{40}$$

Fig. 4.11 shows V_{TPn} as function of i_{on} when $\alpha/\beta = 1$ and 0.8 p.u. < v_{inn} < 1.2 p.u., and Fig. 4.12 displays V_{TPn} as function of i_{on} when $v_{inn} = 1$ p.u. and $0.5 < \alpha/\beta < 2$. If $i_{on} < 0.1$ p.u., V_{TPn} should only change about 1% to keep the RMS output voltage at the rated level. Therefore, while keeping $V_{TPn} = 1$, $V_{on,RMS}$ will decrease by about 1.5% when $i_{on} < 0.1$ p.u., and less than 0.05% when $i_{on} <$ 0.05 p.u. as seen in Fig. 4.13 and Fig. 4.14. Therefore, V_{TPn} could remain at 1 for a design where $\Delta v_{on} < 5\%$ and $i_{on} < 0.1$ p.u. without having a large output error. Otherwise, the target point can be evaluated as a function of the load condition using (40) or using the following simplified

approximation valid for low ripple cases which were obtained by first assuming $v_{inn} \approx 1$ which simplifies the square root term on (40), and then considering zero the terms i_{on}^4 :

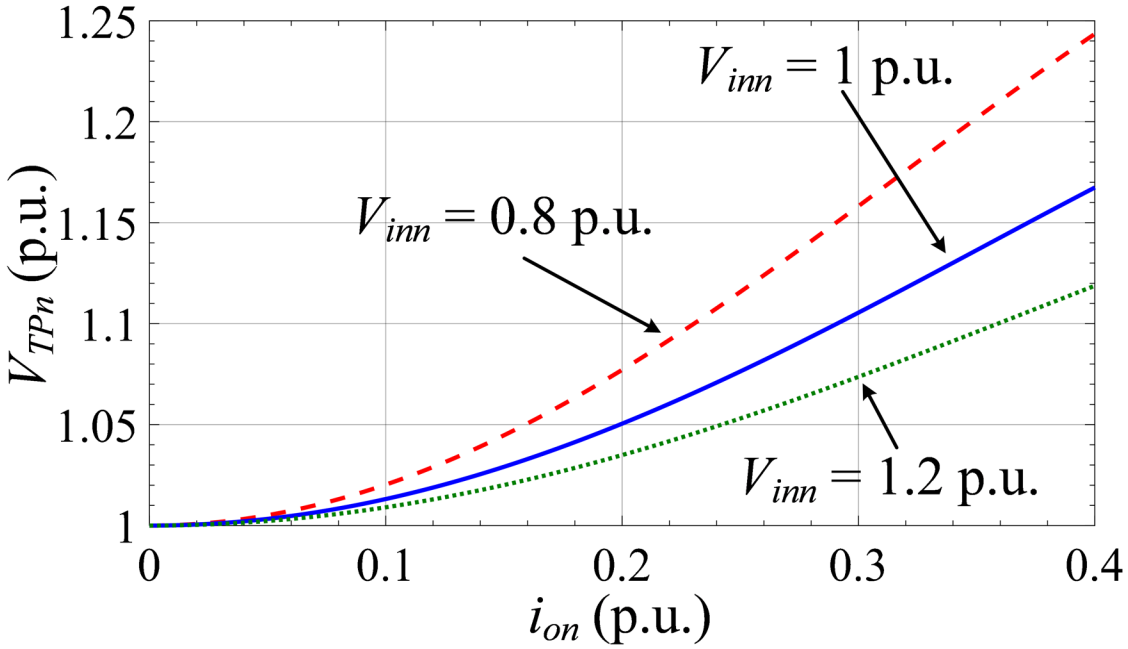

Fig. 4. 11. Normalized output voltage target point V_{TPn} to obtain $V_{on,RMS} = 1$ p.u. with $\alpha/\beta = 1$ and v_{inn} changing.

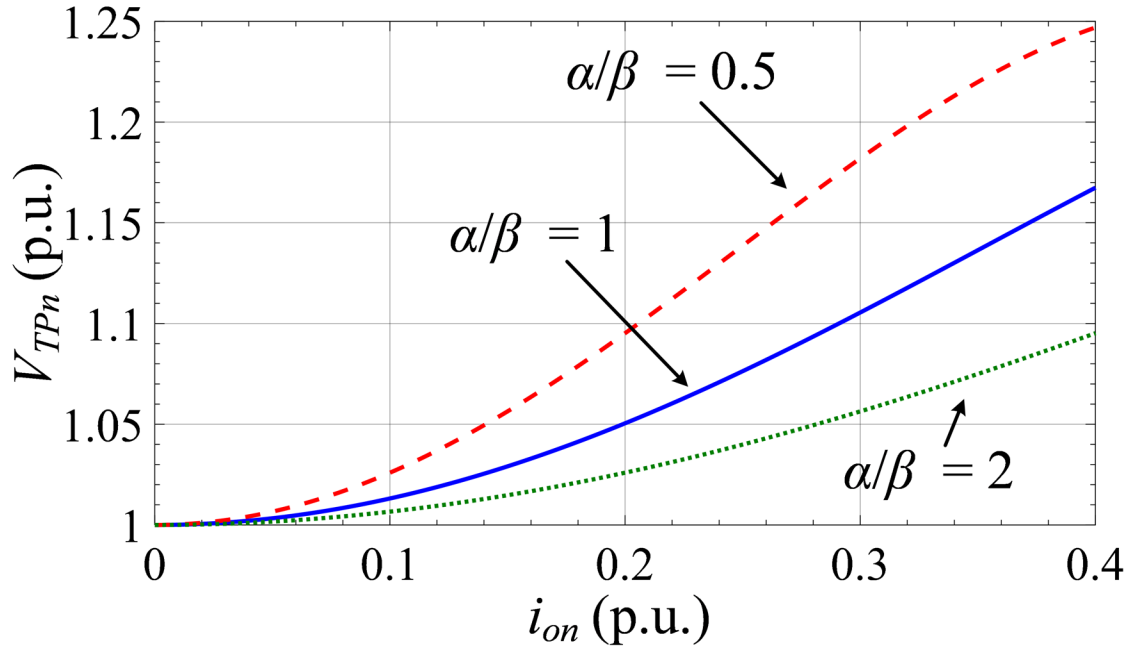

Fig. 4. 12. Normalized output voltage target point V_{TPn} to obtain $V_{on,RMS} = 1$ p.u. with $v_{inn} = 1$ p.u. and α/β changing.

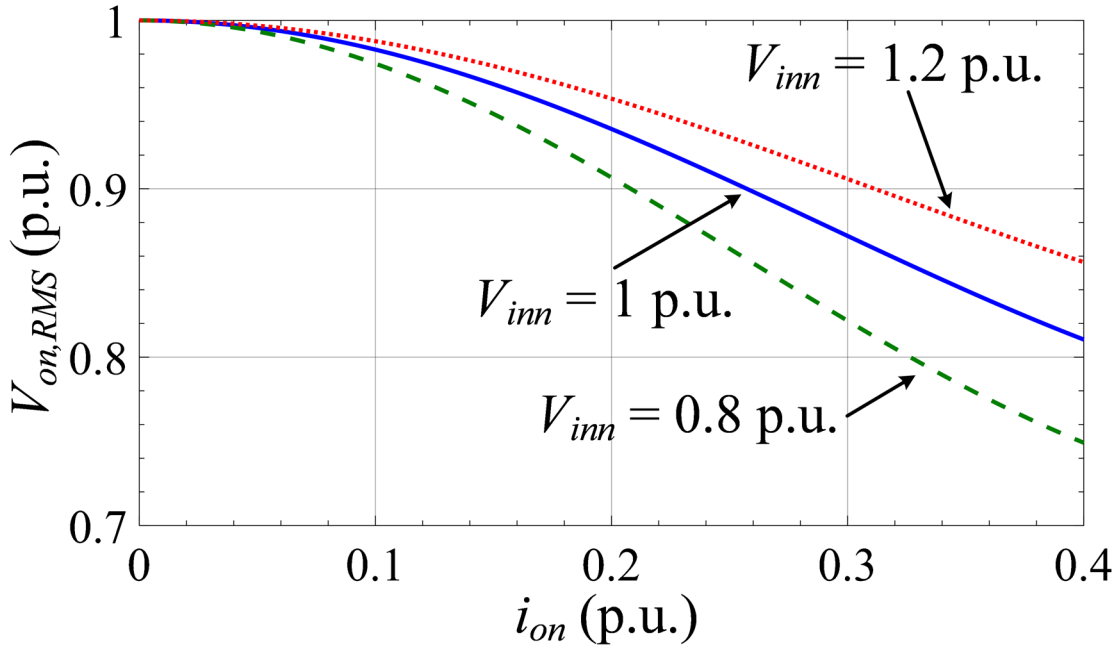

Fig. 4. 13. Normalized RMS output voltage when V_{TPn} = 1 p.u. with α/β = 1 and v_{inn} changing.

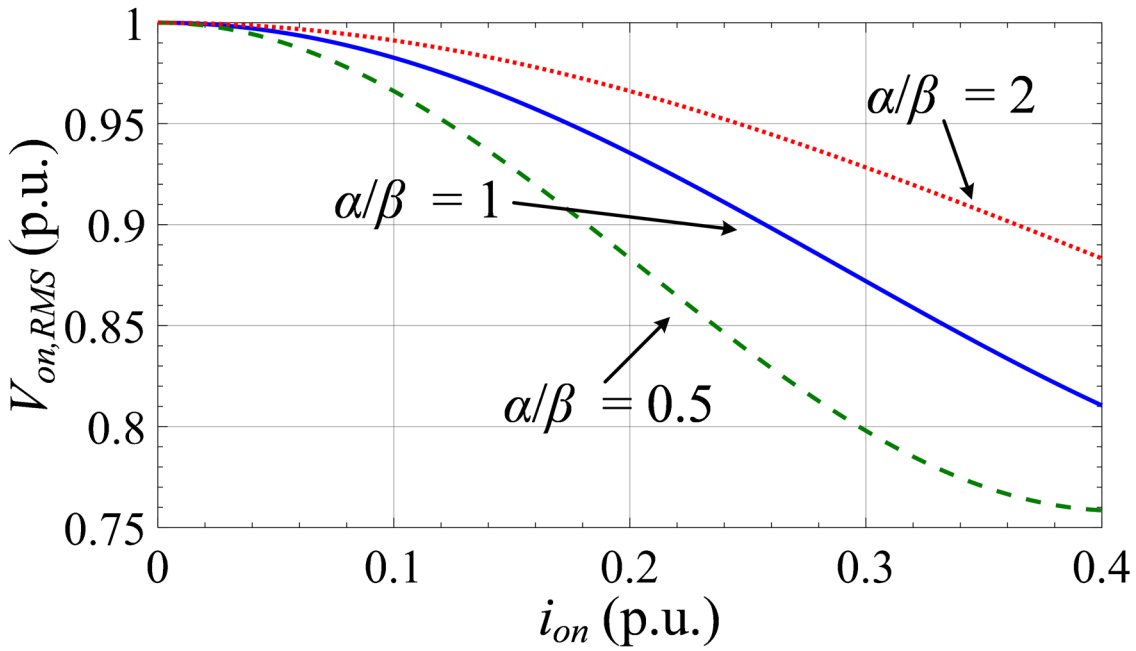

Fig. 4. 14. Normalized RMS output voltage when V_{TPn} = 1 p.u. with v_{inn} = 1 and α/β changing.

$$V_{TPn} = \left(3\frac{\alpha}{\beta} + 5i_{on}^2\right) \Big/ \left(3\frac{\alpha}{\beta} + i_{on}^2\right). \tag{41}$$

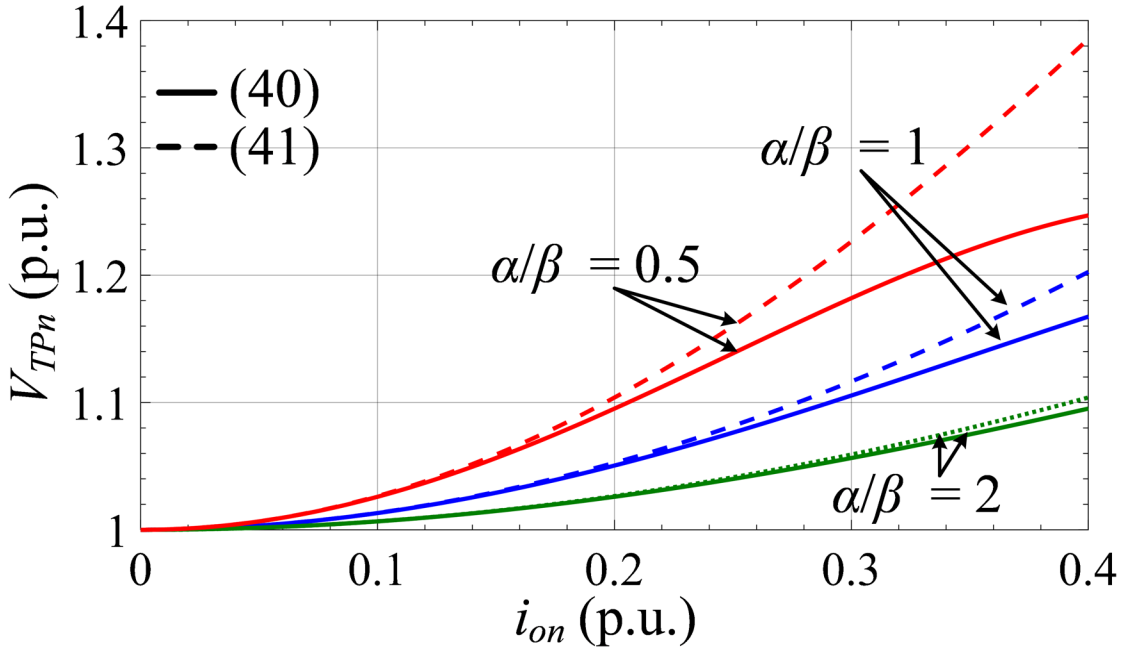

Fig. 4. 15. Normalized output voltage target point plotted from (40) and its low-ripple approximation from (41).

Fig. 4.15 shows V_{TPn} as function of i_{on} using expression (40) and compared to the approximation (41) for different values of α/β illustrating that the approximation works very well under low-ripple conditions.

4.4.E Normalized Magnetizing Inductance Current Ripple

The current ripple through the magnetizing inductance Δi_{mn} is equal to the peak current $I_{mn,max}$ which can be calculated by replacing $V_{on,min}$ on the BCM trajectory σ_{ON} and then solving for the magnetizing current yielding:

$$I_{mn,max} = \Delta i_{mn} = 2\frac{\alpha}{\beta} i_{on} v_{inn} \left(V_{TPn} + v_{inn}\right) \Big/ \left(i_{on}^2 + \frac{\alpha}{\beta} v_{inn}^2\right). \tag{42}$$

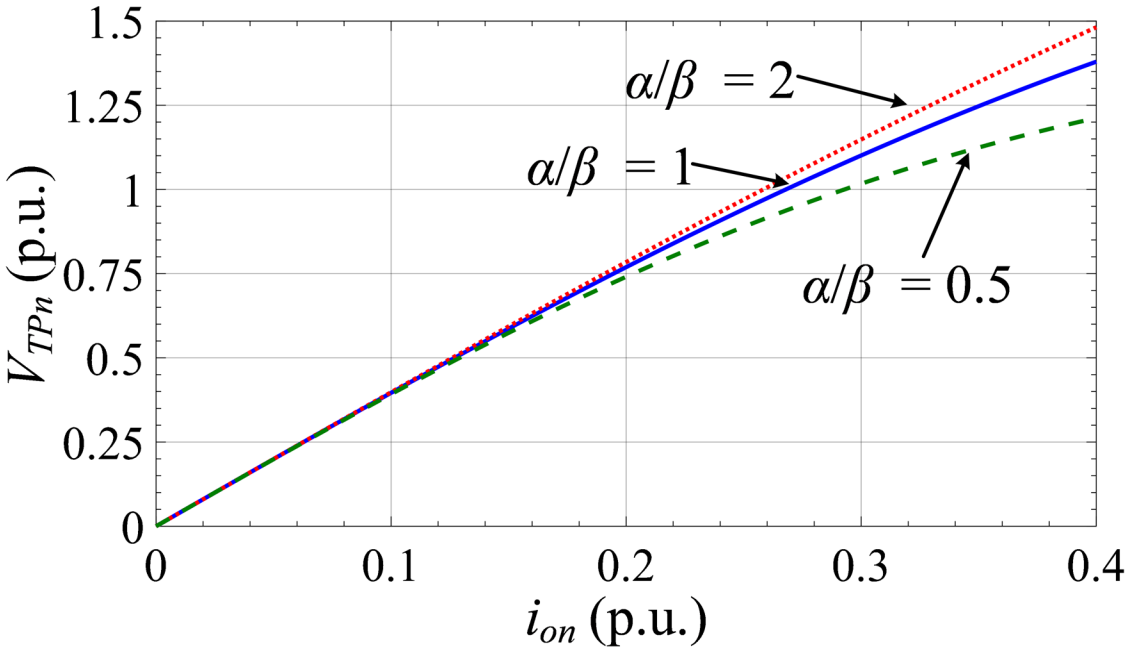

Fig. 4. 16. Normalized magnetizing current ripple ΔI_{mn} with v_{inn} = 1 p.u. and α/β changing.

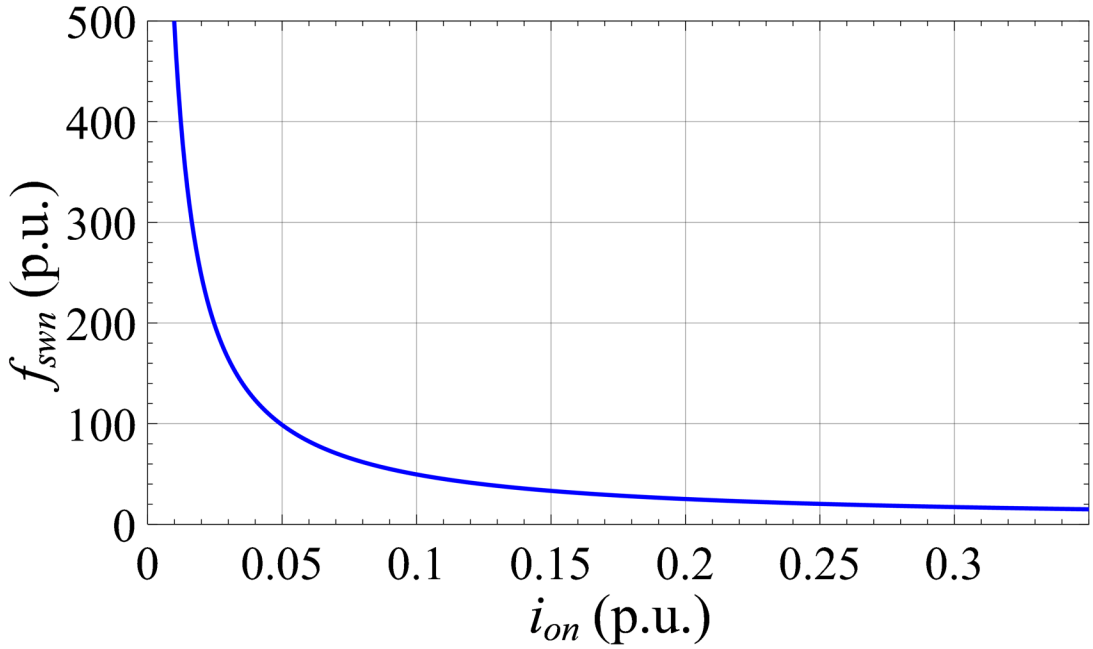

Fig. 4. 17. Normalized switching frequency f_{swn} as function of the load current i_{on}.

Fig. 4.16 shows the plot of (42) when v_{inn} = 1 p.u. and α/β changes. De-normalizing (42), the maximum magnetizing inductance current $I_{m,max}$ for a given operating steady-state condition can be calculated by:

$$I_{m,max} = 2\frac{\alpha}{\beta} i_o v_{in} \left(V_r + \frac{v_{in}}{n} \right) \Big/ \left(i_o^2 \frac{\overline{L}_m}{\overline{C}_o} + \frac{\alpha}{\beta} v_{in}^2 \right). \tag{43}$$

4.4.F Switching Frequency

The converter switching frequency f_{sw} will change based on the load, input voltage and parameter variations because of the operation in BCM. The derivation of f_{sw} is done by calculating the normalized switching period T_{swn} from the ON- and OFF-time periods obtained from (8) and (21); in particular:

$$T_{swn} = T_{ONn} + T_{OFFn} = \frac{\Delta i_{mn}}{2\pi\alpha} \left(\frac{1}{v_{inn}} + \frac{1}{V_r} \right). \tag{44}$$

By de-normalizing (44), f_{sw} is obtained as:

$$f_{sw} = f_{swn} f_r = \left(\alpha v_{in} V_r \right) \Big/ \left(\overline{L}_m \Delta i_m \left(V_r + v_{in}/n \right) \right). \tag{45}$$

Fig. 4.17 displays the normalized switching frequency f_{swn} as function of the load current. The switching frequency for BCM operation increases when the load current decreases. Due to the converter topology, the averaged diode current must be equal to the averaged load current for a constant averaged output voltage. So, the same must happen with the averaged diode current, which depends linearly on the peak magnetizing current, if the load current decreases. During the whole OFF interval, the diode current decreases at an approximately constant rate which depends on the output voltage, and the switching frequency increases inversely proportional to the peak of the magnetizing current.

As the maximum switching frequency is limited by the used hardware, BCM operation cannot be sustained for load currents falling below a certain limit. For lower load currents, DCM operation is necessary.

4.5 ADAPTIVE BCM CONTROL LAW

As analyzed in the previous section, the transient and steady- state responses of the converter under NSS control may not be as good as theoretically expected when the actual parameters of the flyback L_m and C_o are not equal to the nominal values $\overline{L}_m$ and $\overline{C}_o$ used in the design. This occurs because the derived BCM control trajectories are obtained by normalizing the differential equations of the converter with base values that may differ from the actual ones. This section presents a novel BCM NSS control method that compensates for the parametric uncertainties of the converter. The proposed controller (29) responds by adapting the ratio α/β whenever it detects that the system is not evolving on the ideal trajectories. The adaptation is performed at the end of each switching cycle using the following rule which produces small adjustments on α/β proportional to the difference between the normalized target point V_{TPn} and V_{xn}:

$$\alpha/\beta\left(n+1\right)=\alpha/\beta\left(n\right)+\left(V_{TPn}-V_{xn}\left(n\right)\right)K, \tag{46}$$

where the constant K is a real number selected by the designer, $\alpha/\beta(n)$ and $V_{xn}(n)$ are the actual values of the parameter ratio and measured target point voltage to obtain the future value $\alpha/\beta(n+1)$. A brief description and justification of the adaptation algorithm is presented below.

The proposed BCM trajectories (26) and (29) model the converter uncertainties with the introduction of the parameter α/β, so an ideal control performance could be always obtained if α/β is precisely estimated. The first estimation of α/β is performed during the start-up and then small adjustments will be implemented based on the measured error to the desired target point after each switching cycle. The complete control scheme is shown in Fig. 4.18 and explained in the following. After each analog-to-digital conversion (ADC) the normalization is performed using (1) through (5). The measured variables are the transformer primary- and secondary-side currents i_p and i_s, output current i_o and output voltage v_o. The magnetizing current i_m is obtained from i_p and i_s. When

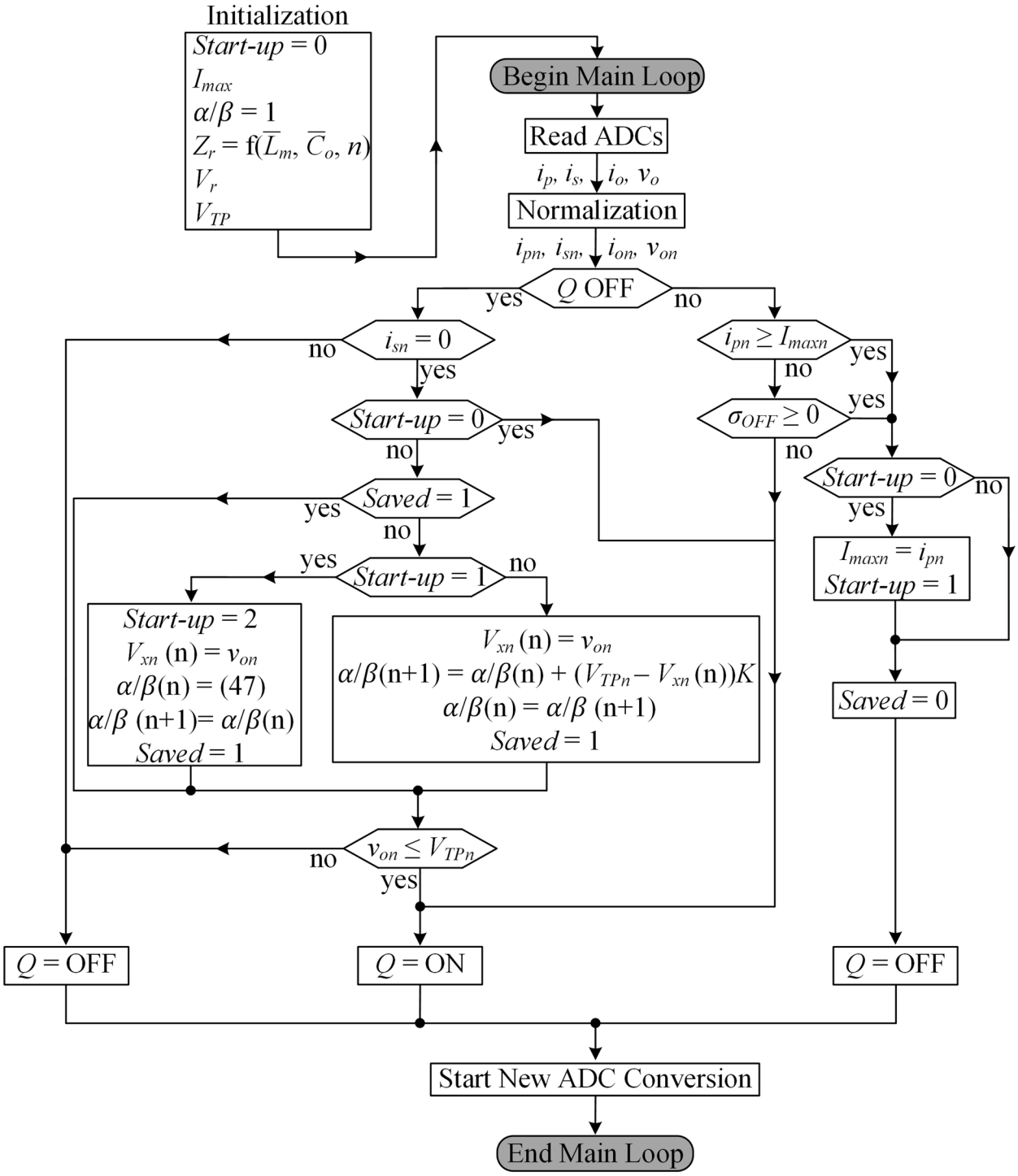

Fig. 4. 18. Flow diagram of the adaptive BCM NSS control law.

Q is ON, i_{mn} equals the normalized transformer primary side current i_{pn}, and when Q is OFF, i_{mn} is the secondary side one i_{sn}. The reference voltage V_r, the reference impedance Z_r, the maximum

start-up current I_{max}, and the voltage target point V_{TP} ($V_{TP} \approx V_r$ for low-ripple applications as presented in Section III-D) are the only constants required for the controller. At the beginning (see point *A* in Fig. 4.7), i_{mn}, i_{on} and v_{on} are zero, α/β is one, producing a negative value in the calculation of σ_{OFF}. Those are the initial conditions of the converter. The transistor remains ON until either σ_{OFF} is intersected ($\sigma_{OFF} \geq 0$) or the start-up current limit is reached ($i_{mn} \geq I_{maxn}$). *Start-up* is a variable used to determine if the converter is under start-up or steady-state conditions; initially, *Start-up* = 0 until *Q* turns OFF the first time.

Just before turning *Q* OFF for the first time (see point *B* in Fig. 4.7), the normalized start-up current $I_{st\text{-}upn}$ is saved in the variable I_{maxn} and the variable *start-up* is set to one. Later, I_{maxn} will be used for the initial estimation of α/β. Transistor *Q* will be kept OFF until the v_{on} axis is reached and $v_{on} \leq V_{TPn}$ (see point *C* in Fig. 4.7). As soon as the v_{on} axis is intersected, v_{on} will be saved into the variable V_{xn} and start-up is set equal two. Then, the first estimation for α/β is derived using (32):

$$\alpha/\beta = \frac{I_{maxn}\left(I_{maxn} - 2i_{on}\right)}{V_{xn}^2}. \tag{47}$$

The next time σ_{OFF} is calculated, it will be using the just updated α/β obtained from (47). Then, *Q* will turn ON again after v_{on} is less than the target point V_{TPn}. Therefore, the flyback in case of an overvoltage will operate in DCM during that transient. The overvoltage is related to cases where the true value of α/β is lower than the current estimation (see Fig. 4.11); otherwise, *Q* will turn ON right after i_{mn} reaches zero and the new α/β is calculated.

Similarly, to start-up conditions, *Q* will stay ON until $i_{mn} \geq I_{max}$ or $\sigma_{OFF} \geq 0$ but now it is not necessary to save anymore the peak value of the magnetizing current for the α/β calculation. After *Q* turns OFF and when i_{mn} reaches zero p.u., v_{on} is saved into V_{xn}.

The convergence and performance of the adaptation rule (46) are analyzed next. By

differentiating (41) with respect to α/β, the following is obtained:

$$dV_{TPn}/d(\alpha/\beta) = -12i_{on}^2 \Big/ \left(3\alpha/\beta + i_{on}^2\right)^2 = -G(n) < 0. \tag{48}$$

As this kind of converters do not operate adequately when the output current is zero because the output capacitor which holds the output voltage cannot be discharged, it is reasonable to consider that the output current is always greater than a minimum operating value $i_{on,min}$. So, it will always be $G(n) \geq G_{min}$, where G_{min} is obtained evaluating (48) at $i_{on,min}$. Also, a maximum value G_{max} can be evaluated from (48) by considering the maximum possible value of the output current $i_{on,max}$, and the minimum possible value for α/β. Since $i_{on,max}$ should be at most equal to 1 and α/β will never reach zero because it would imply to consider a null nominal magnetizing inductance in the design, it can be shown that for $\alpha/\beta > 0.1$, G will never be greater than 10, and usually will be lower than 4 considering a 50% error in the nominal parameters.

Approximating (48) as function of the actual and future values of V_{xn} and α/β yields:

$$\frac{V_{xn}(n+1) - V_{xn}(n)}{\alpha/\beta(n+1) - \alpha/\beta(n)} = -G(n). \tag{49}$$

By solving $\alpha/\beta(n+1) - \alpha/\beta(n)$ from (46), replacing it into (49), and rearranging the actual and future terms, the following expression is obtained:

$$V_{xn}(n+1) - V_{xn}(n)\left(1 + KG(n)\right) + V_{TPn}KG(n) = 0. \tag{50}$$

By applying the Z-transform to (50), assuming that the gain G is constant and the input V_{TPn} is a step signal, and solving for $V_{xn}(z)$, the stability of the target point can be analyzed:

$$V_{xn}(z) = -\frac{V_{TPn}KG}{z - (1 + KG)}. \tag{51}$$

By analyzing the poles of (51), the target point is exponentially stable without oscillatory behavior if and only if $0 < 1 + K.G < 1$ or, equivalently, $-1/G < K < 0$. So, considering the worst case, the

TABLE 4. II FLYBACK CONVERTER PARAMETERS

Parameter	Value
v_o	24 V
i_o	0.5 A
v_{IN}	6 V
Δv_o	4V
Δi_m	10 A
f_{sw}	7 kHz

gain K should be

$$-1/G_{\max} < K < 0 \tag{52}$$

to assure exponential stability, and therefore V_{xn} will converge towards V_{TPn} which also implies from (46) that α/β will converge to a constant final value. That can be also noted from the final value theorem applied to (51) and considering that V_{TPn} is a step signal:

$$\lim_{z\to 1}\left(-(z-1)V_{TPn}\frac{z}{z-1}\frac{KG}{z-1-KG}\right)=V_{TPn}. \tag{53}$$

When considering $G = G_{min}$ in (50), the dynamic response will be the slowest one and will provide an upper bound for any other dynamics obtained with other gains G such that $G_{max} > G > G_{min}$ for the same initial conditions and input signal. Therefore, any dynamic response obtained from (50) for K satisfying (52) and considering a variable $G(n)$, such that $G_{max} > G(n) > G_{min}$, will also be exponentially asymptotically stable.

4.6 DESIGN PROCEDURE AND EXAMPLE

The specifications for the proposed BCM flyback converter are presented in Table 4.II. The output voltage and magnetizing current ripples in the proposed design example will be exaggerated in order to improve the visualization and facilitate the plot of the trajectories. In addition, a low ripple case will be illustrated. The step-by-step design process is given next assuming that $\alpha/\beta = 1$.

4.6.A Transformer Turns Ratio

The turns ratio n is calculated by dividing the transformer rated primary and secondary voltages. The latest produces a duty cycle about 50% at rated conditions since $v_{inn} \approx V_{on,AVE}$ (see T_{ONn} and T_{OFFn} from (44)). Then,

$$n = N_p / N_s = v_{in} / v_o = 1/4. \tag{54}$$

4.6.B Output Capacitance

The frequency f_{sw} depends on the load conditions in BCM operation. However, a desired f_{sw} can be selected for rated conditions. By de-normalizing and solving (14) for Δi_{mn}, the following expression for Δi_m is obtained:

$$\Delta i_m = \frac{v_{in} \Delta v_o \overline{C}_o}{i_o \overline{L}_m}. \tag{55}$$

By substituting (55) into (45) and solving for $\overline{C}_o$, the output capacitance needed to operate with a voltage ripple Δv_o and a switching frequency f_{sw} when the output current is i_o is obtained as follows:

$$\overline{C}_o = \frac{i_o}{2 f_{sw} \Delta v_o} \approx 10 \mu F. \tag{56}$$

4.6.C Magnetizing Inductance

By de-normalizing (14) and solving for $\overline{L}_m$, the following expression based on the design specifications is derived:

$$\overline{L}_m = \left(v_{in} \Delta v_o \overline{C}_o \right) \Big/ \left(i_o \Delta i_m \right) \approx 45 \mu H. \tag{57}$$

There is a trade-off between Δi_{mn} and L_m since a lower Δi_{mn} implies a higher at the expense of increasing the transformer cost. However, a higher Δi_{mn} increases the rating of the semiconductor devices.

4.6.D Reference Impedance

The reference impedance Z_o is obtained from the previously calculated parameters by using (54), (56) and (57):

$$Z_o = (1/n)\sqrt{\overline{L}_m / \overline{C}_o} = 8.35\Omega. \tag{58}$$

4.6.E Start-Up Current

$I_{st\text{-}up}$ is obtained by substituting the calculated $\overline{C}_o$ and $\overline{L}_m$ parameters into (31):

$$I_{st-up} = V_r\sqrt{\overline{C}_o / \overline{L}_m} \approx 11.3\,\mathrm{A}. \tag{59}$$

4.6.F Steady-State Peak Magnetizing Current

The peak current during rated steady-state conditions $I_{m,max}$ is obtained from (43) as follows:

$$I_{m,max} = \left(4 i_o v_{in} V_r\right) \Big/ \left(i_o^2\,\overline{L}_m / \overline{C}_o + v_{in}^2\right) \approx 7.75\,\mathrm{A}. \tag{60}$$

4.6.G Transistor Current and Voltage Ratings

The transistor current rating $I_{Q,max}$ must be higher than $I_{st\text{-}up}$ if the start-up current is not limited. If it is desired to limit the transistor current to a lower value I_{max}, it should be greater than the steady-state value; that is:

$$I_{st-up} > I_{max} > I_{m,max}. \tag{61}$$

The transistor voltage rating $V_{Q,max}$, without considering the voltage spikes related to transformer leakage inductance is given by:

$$V_{Q,max} > v_{in} + v_o n. \tag{62}$$

Therefore, in practice, $V_{Q,max}$ will depend on the type of the snubber circuit used and the transformer leakage inductance [35].

4.6.H Diode Current and Voltage Ratings

The current and voltage ratings of the diode d can be obtained from (61) and (62) referred to the secondary side. Then, the breakdown voltage of the diode $V_{d,max}$ should be higher than:

$$V_{d,max} > v_{in}/n + v_o. \tag{63}$$

In case that $I_{st\text{-}up}$ is limited to $I_{m,max}$, the diode current rating should be:

$$I_{st-up} n > I_{d,max} > I_{m,max} n. \tag{64}$$

4.7 SIMULATION RESULTS

Matlab/Simulink™ simulations for a flyback with electrical parameters from Table 4.II and nominal components from Table 4.III are presented under different α/β conditions starting with the BCM NSS control scheme in Fig. 4.6. Initially, ideal conditions (α/β = 1) are considered. During the start-up, v_o and i_o are zero, so the expected start-up voltage V_x and current $I_{st\text{-}up}$ are calculated from (33) and (31) as:

$$V_x = \sqrt{I_{max} \frac{\overline{L}_m}{\overline{C}_o} \frac{\beta}{\alpha} \left(I_{max} - \frac{2.i_o}{n} \right)} - V_d = 20.95\,\text{V},$$

$$I_{st-up} = V_{TP} \sqrt{\overline{C}_o / \overline{L}_m} = 11.5\,\text{A}.$$

From the simulation results shown in Fig. 4.19, $I_{st\text{-}up}$ = 11.54 A and V_x = 21.08 V, representing errors of 0.35% and 0.62%, respectively. Thus, there is good agreement between simulation and

theoretical results. Moreover, the controller is able to react to an output current step change from 0.28 A to 0.48 A in only one switching cycle.

Next, a flyback with parameter uncertainties $\alpha/\beta = 4$, which could be the case where $\overline{C}_o = C_o/4$ and $\overline{L}_m = L_m$, is simulated. From (33) and (31), the expected start-up parameters should be $I_{st\text{-}up} =$ 5.75 A and $V_x = 8.79$ V. Simulation results are presented in Fig. 4.20(a) where $I_{st\text{-}up} = 5.85$ A and $V_x = 9.06$ V, representing errors of 1.7% and 3.07%, respectively. In this case, the errors are caused by the quantization of the signals, as decreasing the sampling time reduces the error. Moreover, the controller due to the parameter uncertainties will not reach the target voltage and has poor voltage regulation as the output current changes.

TABLE 4. III EXPERIMENTAL PROTOTYPE CHARACTERISTICS

Parameter	Value
Transformer T	Coilcraft® NA5919-AL, $L_m = 45.8$ µH, $n = 1/4$, $I_{sat} = 13.6$ A @ $L_m = 38.5$ µH
Transistor Q	Vishay® IRFP140PBF $V_{dss} = 100$ V, $I_D = 31$ A @ 25 °C
Diode D	Vishay® VS-8TQ100PBF $V_R = 100$ V, $I_D = 8$ A, $V_F = 0.58$ V
Output Capacitor C_o	10.52 µF Film

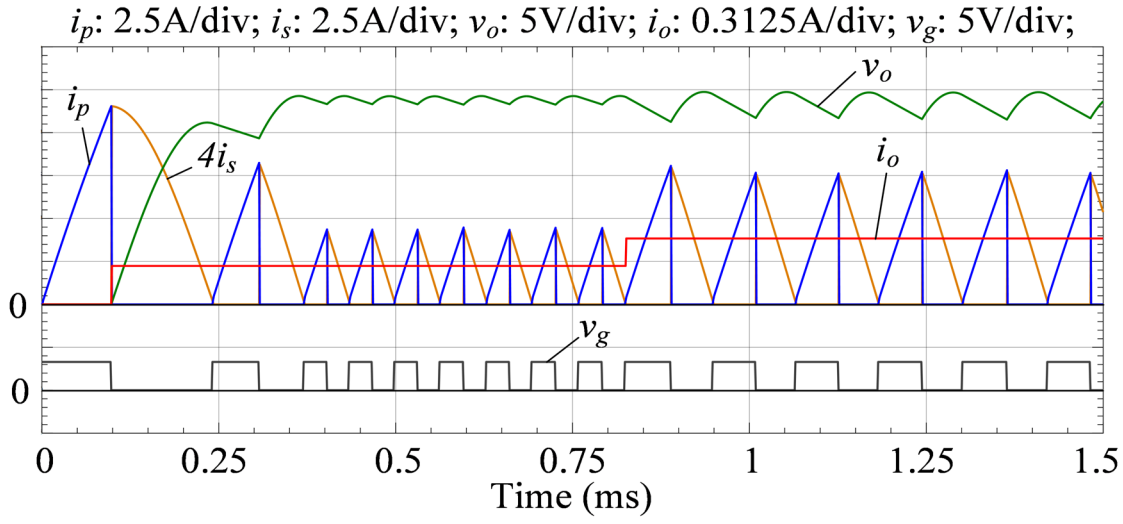

Fig. 4. 19. Simulation results of the BCM NSS control law (a) under ideal conditions.

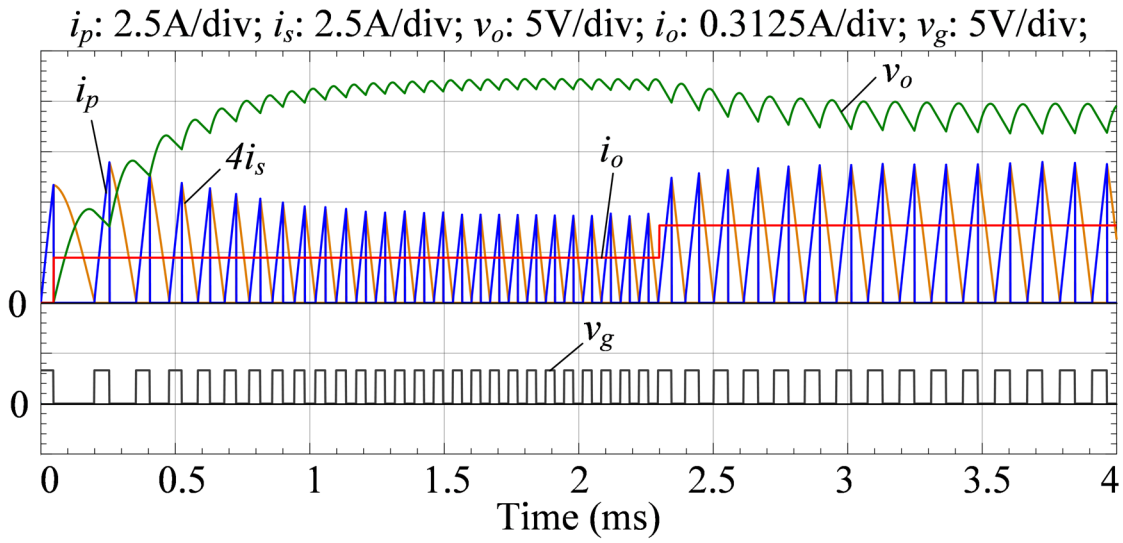

(a)

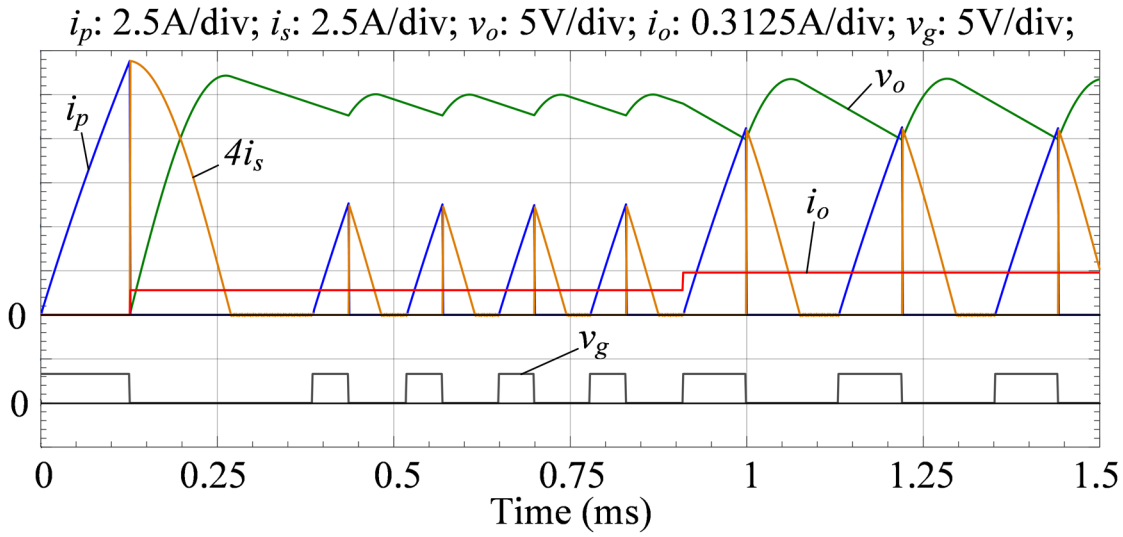

(b)

Fig. 4. 20. Simulation results of the BCM NSS control law (a) when $\alpha/\beta = 4$, and (b) when $\alpha/\beta = 0.64$.

Next, a case where $\alpha/\beta = 0.64$ is considered. That case could occur if for example $\overline{C}_o = C_o/0.64$ and $\overline{L}_m = L_m$. The calculated start-up parameters are $I_{st\text{-}up} = 14.38$ A and $V_x = 26.99$ V while the parameters from the simulation results in Fig. 4.20(b) are 14.41 A and 27.04 V, which represent errors of 0.21% and 0.18%, respectively. In this case, the controller due to the parameter uncertainties is operating in DCM instead of BCM. When the load increases, the time where the diode current is zero also increases.

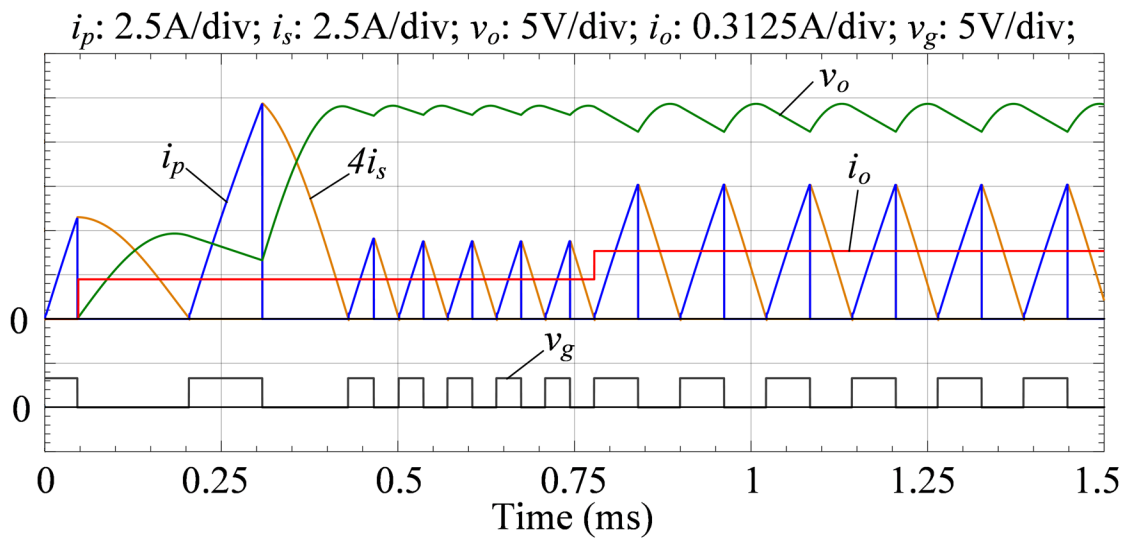

(a)

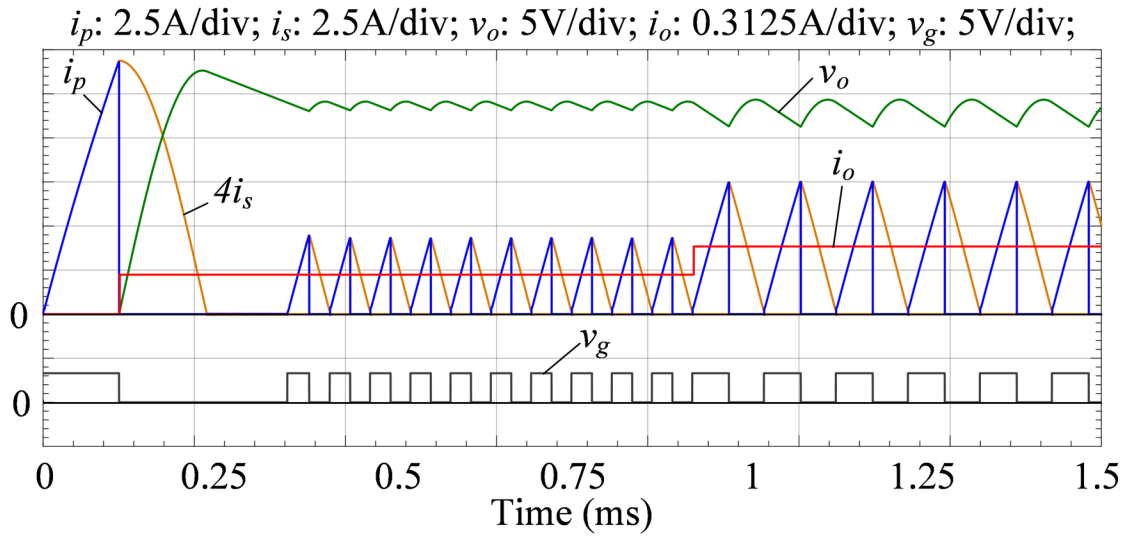

(b)

Fig. 4. 21. Simulation results of the adaptive BCM NSS control law when (a) $\alpha/\beta = 4$, and (b) $\alpha/\beta = 0.64$.

Then, the novel adaptive BCM NSS controller was simulated to show its effectiveness against parameter uncertainties. First, the adaptive controller is simulated for the case when $\alpha/\beta = 4$, and the results are shown in Fig. 4.21(a). In this case, the controller estimated $\alpha/\beta = 3.982$, which represents an error of 0.45%. Due to this estimation, the controller is able to track properly the reference voltage and is able to react to disturbance in the output current in one switching cycle.

Finally, the adaptive controller was simulated for the case when α/β = 0.64, and the simulation results are illustrated in Fig. 4.21(b). In this case, the controller estimated α/β = 0.6401, which represents an error of 0.016%. Due to this estimation, the controller is able to operate in BCM instead of DCM.

4.8 EXPERIMENTAL VERIFICATION

A flyback converter with the specifications of Table 4.II and the components of Table 4.III was built and tested. The output capacitor C_o was specifically designed in this first experiment with academic purposes to lead to a large output voltage ripple, so the figures can show clearly the behavior of the system. Later in this section, other results are included after replacing this capacitor by a larger one leading to a lower output voltage ripple to show a more realistic and practical application. The traditional and novel adaptive BCM NSS control laws were implemented using the TMS320F28335 DSP from Texas Instruments®. First, the BCM NSS control law was verified under ideal conditions and with parameter variations. Then, the adaptive control law was executed under similar conditions as those in the previous tests and a detailed comparison was performed. Fig. 4.22(a) presents the transient response of the BCM NSS control law shown in Fig. 4.6 under ideal conditions. The primary and secondary transformer currents, i_p and i_s; the output voltage and current i_o and v_o, as well as the DSP gate signal v_g are shown in the same figure. At start-up i_o and v_o are zero, Q turns ON until σ_{OFF} is reached when $I_{st\text{-}up}$ is 12.25 A which is slightly higher than the 11.52 A value calculated by replacing on (15) the converter parameters of Table 4. III. This is due to the processing time delay introduced by the DSP while computing the control structure. Once Q is OFF, i_o increases to its steady-state value (~ 0.28 A) and the voltage V_x when i_s reaches zero is 22.68 V while the calculated value using (33) is 22.95 V. These demonstrate the accuracy of the

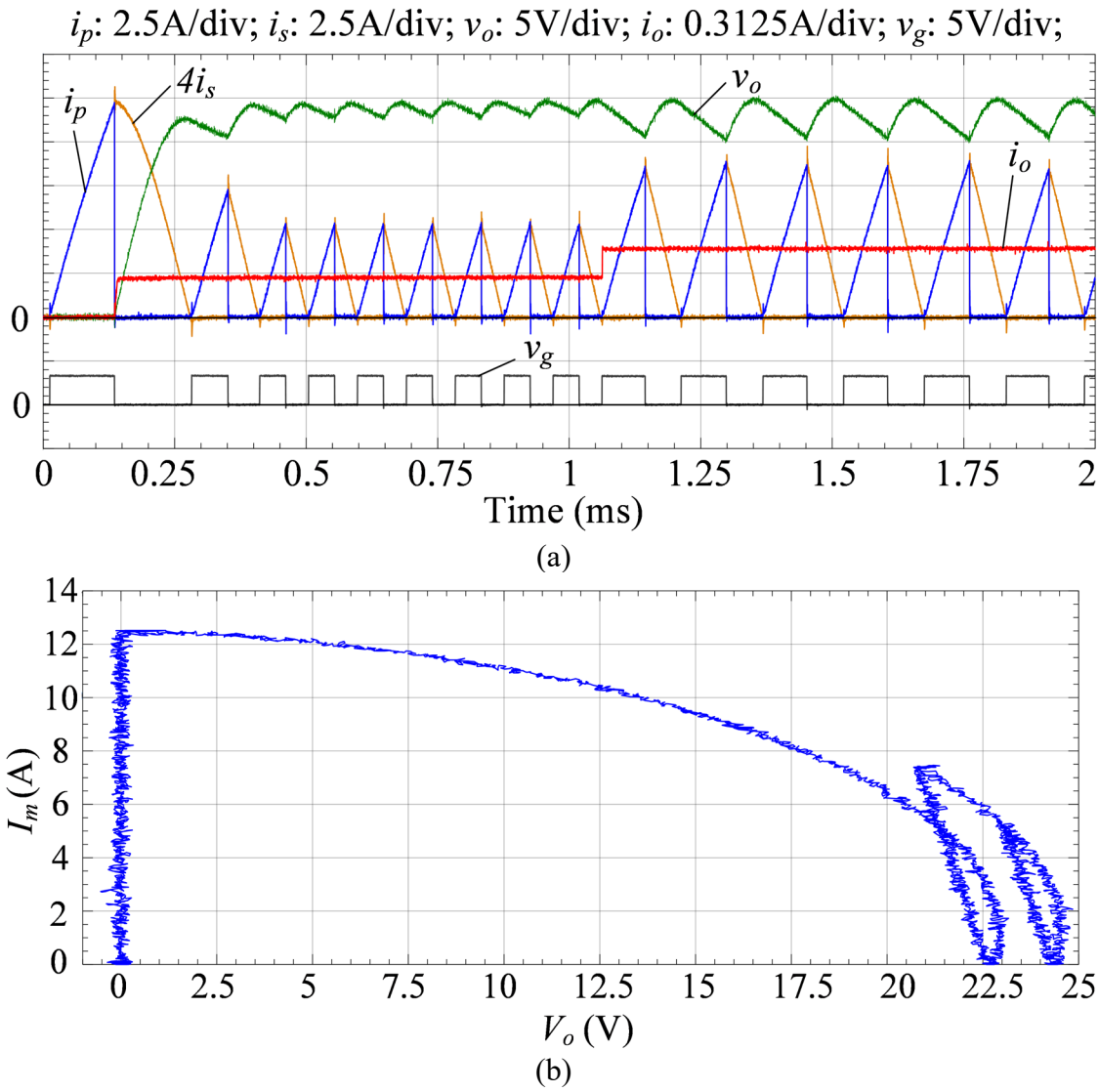

Fig. 4. 22. (a) Transient response, and (b) state-plane trajectory for the BCM NSS control law under ideal conditions.

derived trajectories and equations. During the next switching cycle, v_o will reach to the target point $V_{TP} = 24$ V and steady-state conditions as appreciated in Fig. 4.22 (a). At the tenth switching cycle, there is a sudden load increase of about 100% of its initial value. The controller was able to reach the target point in only a switching cycle since the load disturbance occurred while Q was ON, so σ_{OFF} was recalculated before turning OFF the switch. If the disturbance were produced during the OFF period, it would take two switching cycles to reach the target point. The state-plane trajectories

are given in Fig. 4.22(b) illustrating the similarity with the theoretical waveforms shown in Fig. 4.7. Fig. 4.23(a) displays the transient response of the BCM NSS control law when $\alpha/\beta > 1$. This particular case was implemented by changing the reference impedance to $Z_r = 2\overline{Z}_o$ during the normalization process in the DSP code, which is equivalent to have $\alpha/\beta = 4$ and $\overline{L}_m/\overline{C}_o = 17.42$ if $n = 4$.

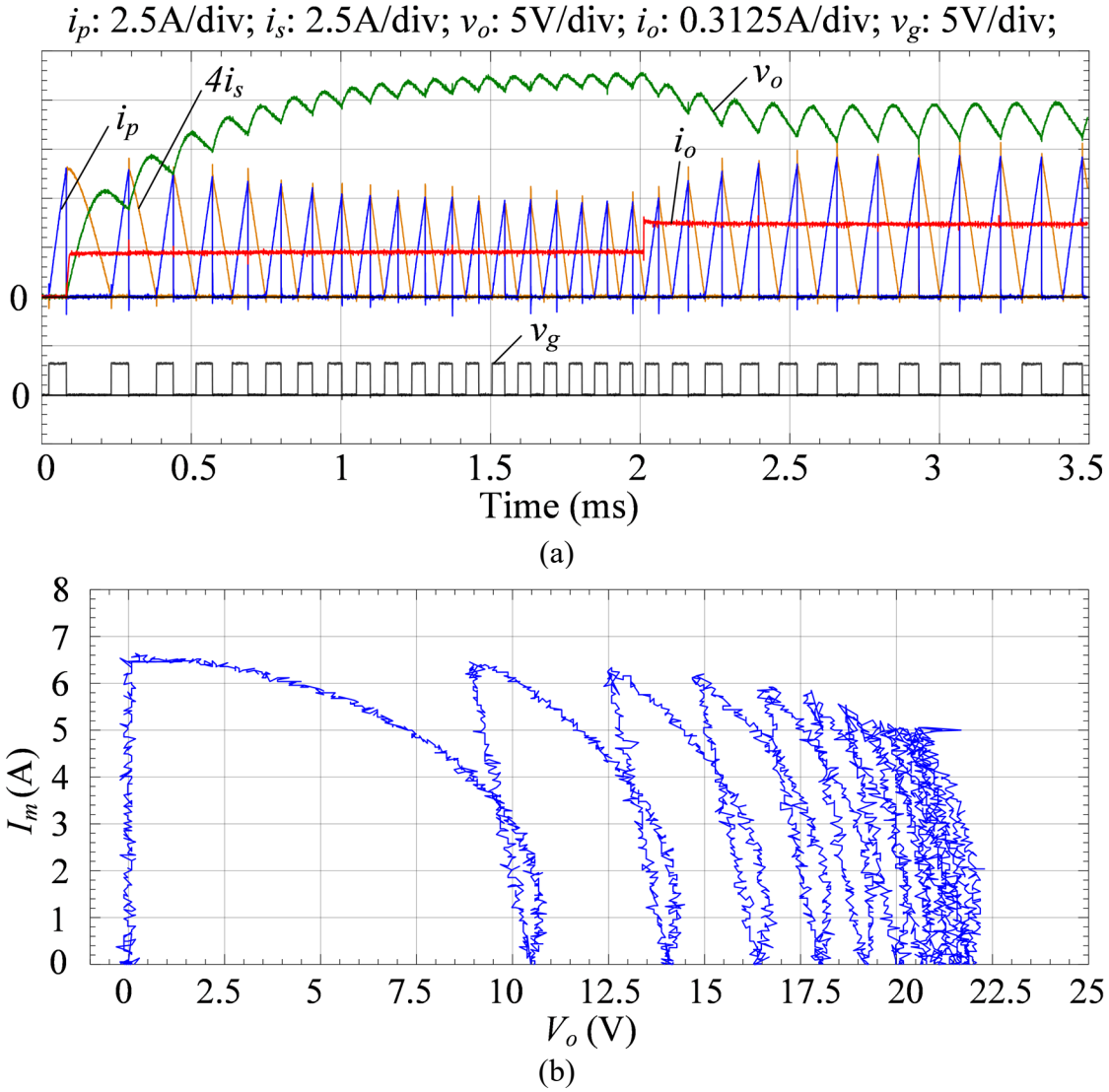

Fig. 4. 23. (a) Transient response, and (b) state-plane trajectory for the BCM NSS control law when $\alpha/\beta = 4$.

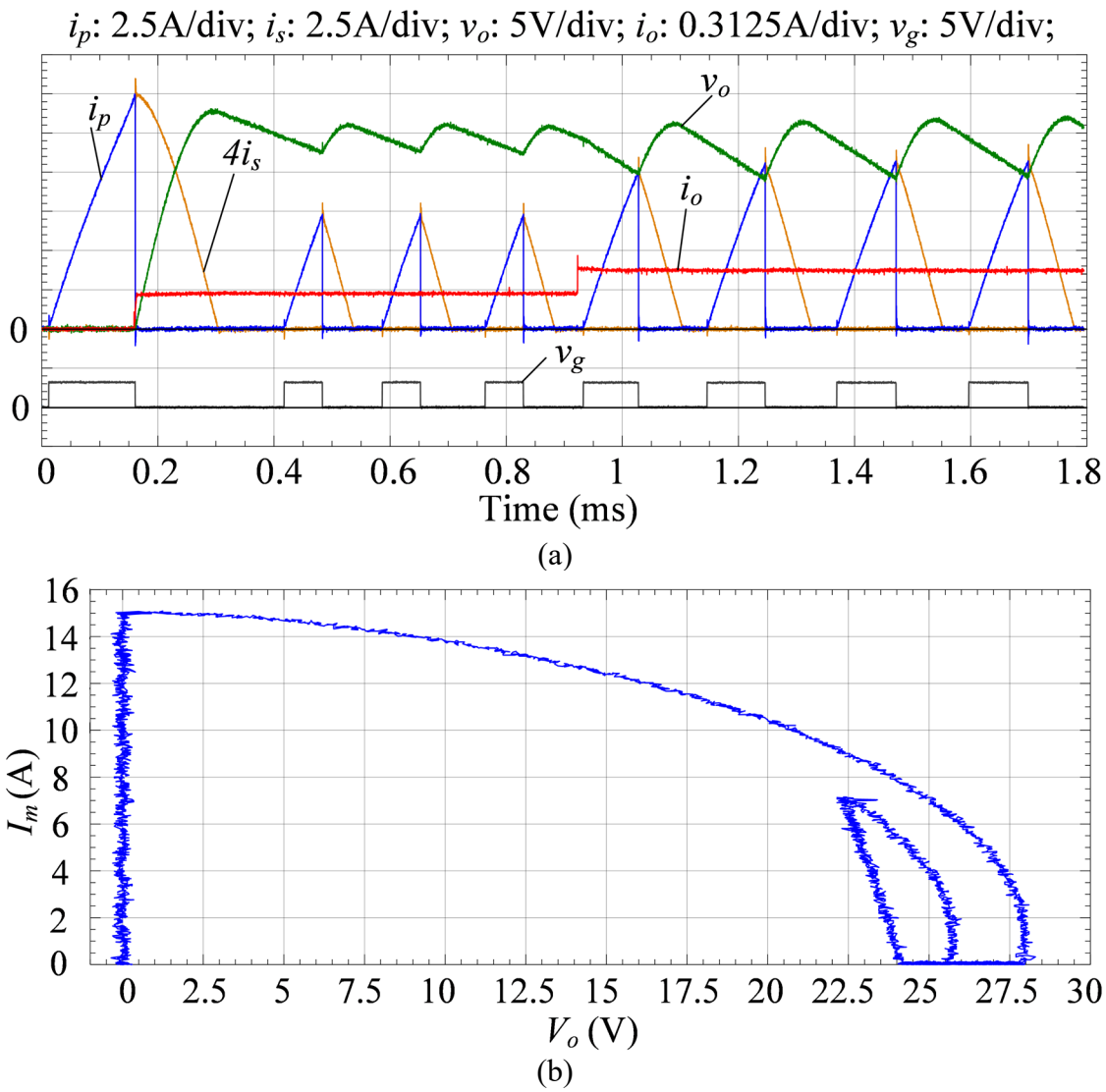

Fig. 4. 24(a) Transient response, and (b) state-plane trajectory for the BCM NSS control law when $\alpha/\beta = 0.64$.

From Fig. 4.23(a), the control performance worsens in comparison to the ideal case. At start-up conditions, it takes several cycles to reach the target point as shown in the state-plane trajectories presented in Fig. 4.23(b). $I_{st\text{-}up}$ is calculated by replacing $\alpha/\beta = 1$ into (15) as 5.75 A while the measured $I_{st\text{-}up}$ is 6.5 A. The measured start-up voltage V_x was 11 V while the calculated value using (26) when $\alpha/\beta = 4$ is 10.19 V. When a sudden load increase occurs, the target point will be lower than that one for the initial output current as noted in Fig. 4.11 which makes the output voltage dependable on the loading conditions.

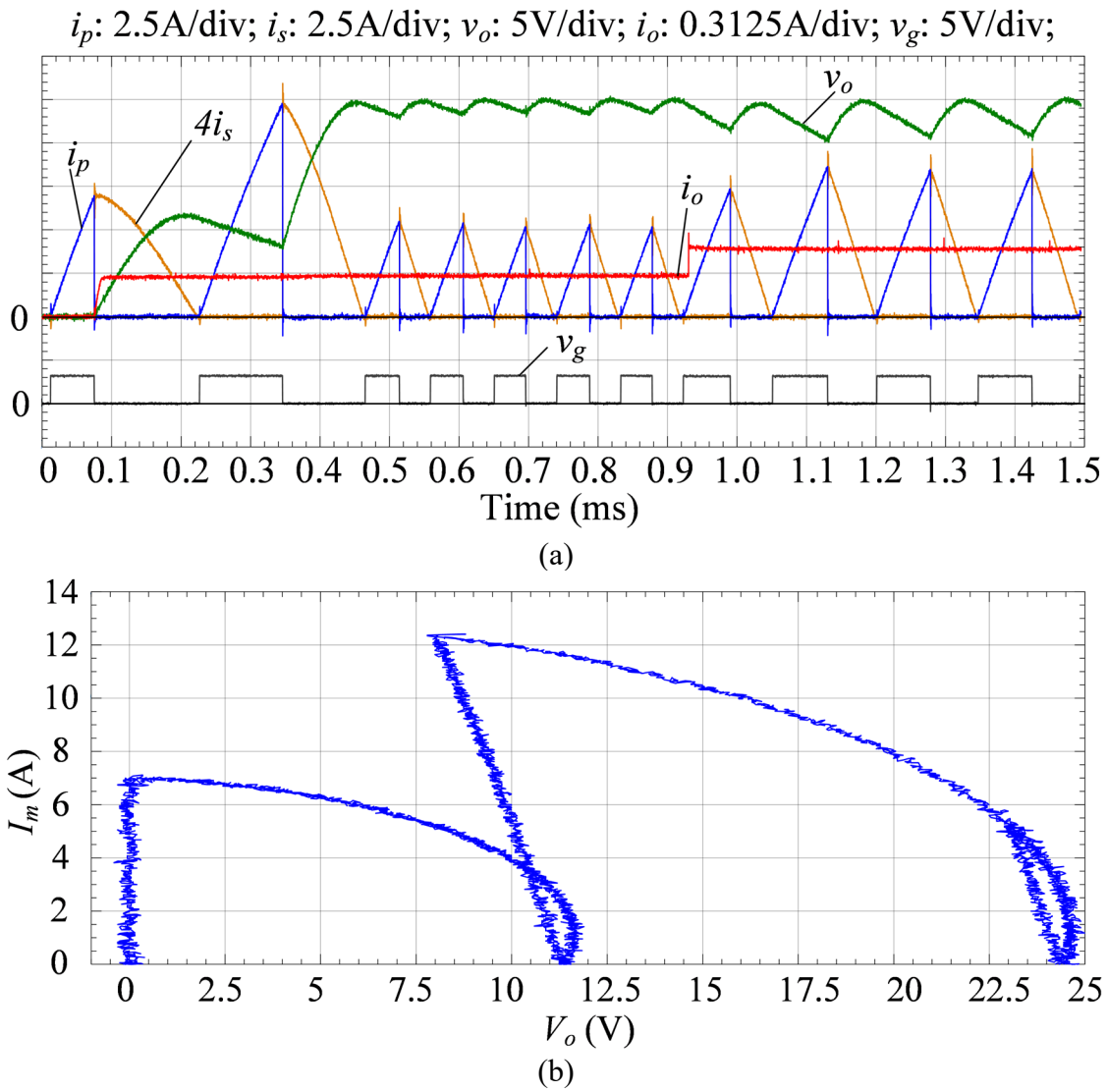

Fig. 4. 25 (a) Transient response, and (b) state-plane trajectory of the adaptive BCM NSS control law when $\alpha/\beta = 4$.

TABLE 4. IV SUMMARY RESULTS FOR THE BCM NSS CONTROL LAW

	Measured		Calculated		Error %	
	$I_{st\text{-}up}$	V_x	$I_{st\text{-}up}$	V_x	$I_{st\text{-}up}$	V_x
$\alpha/\beta = 1$	12.2 A	22.9V	11.5 A	23.3 V	4	1.04
$\alpha/\beta = 4$	6.5 A	11 V	5.7 A	10.2 V	11	7.36
$\alpha/\beta = 0.64$	15 A	28 V	14.4 A	28.1 V	4.1	0.21

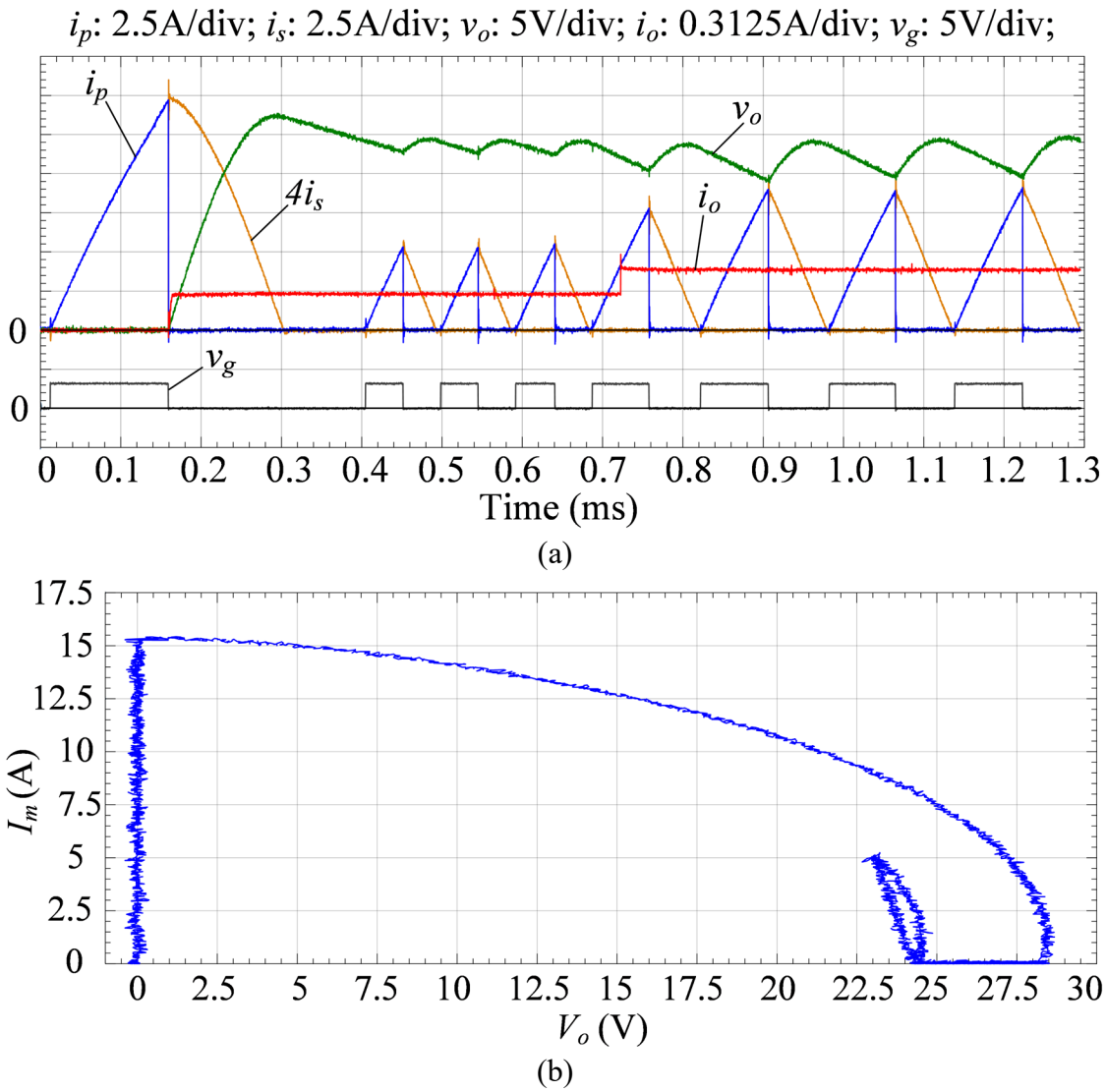

Fig. 4. 26. Transient response, and (b) state-plane trajectory of the adaptive BCM NSS control law when $\alpha/\beta = 0.64$.

Fig. 4.24(a) presents the transient response of the BCM control law when $\alpha/\beta < 1$ which it is obtained by modifying the reference impedance $Z_r = 0.8\overline{Z}_o$ on the DSP code which compares to have $\alpha/\beta = 0.64$ and $\overline{L}_m/\overline{C}_o = 2.7870$. $I_{st\text{-}up}$ is measured as 15 A while the calculated value from (15) was 14.38 A. The measured start-up voltage V_x is 28 V while the calculated value from (26) when $\alpha/\beta = 0.64$ is 28.06 V. When $\alpha/\beta < 1$, L_m is overcharged. Therefore, the output overvoltage produces DCM operation since the control law does not allow Q to turn ON again until $v_o \le V_{TP}$.

The measured state-plane trajectories are shown in Fig. 4.24(b). The main results from the BCM NSS control law are summarized in Table 4. IV.

Fig. 4.25 presents the transient response and the state-plane trajectories when $\alpha/\beta = 4$ and the novel adaptive BCM NSS control law of Fig. 4.18 is implemented. From the start-up conditions, the converter is able to reach the target point in only two switching cycles as in the ideal case. Under a sudden load change, the converter is also able to reach V_{TP} in a single switching cycle. The start-up current $I_{st\text{-}up}$ is measured as 6.95 A which is higher than the value obtained using the non-adaptive BCM NSS control law since the computation time is higher in the adaptive case. The start-up voltage V_x is measured as 12.1 V, so the first estimation of α/β using (26) is 4.093 which represents a 2.325% error. The transient and the state-plane waveforms for the case where $\alpha/\beta = 0.64$ using the proposed adaptive controller are shown in Fig. 4.26. As in the previous case, the converter is able to reach the target point from start-up conditions in only two switching cycles but the flyback operates during the first switching cycle in DCM due to an initial output overvoltage. Using the measured start-up current and voltage $I_{st\text{-}up} = 14.75$ A and $V_x = 28$ V, the first estimation of $\alpha/\beta = 0.6685$ based on (33) which means a 4.45% of error. During steady-state operation when the sudden load change occurs, the adaptive BCM NSS controller is able to reach the target point in one a single switching cycle as it occurs in the ideal case. The main results obtained from adaptive controller to make its first approximation to α/β are shown in Table 4. V.

To illustrate a more realistic design where a low output voltage ripple is desired, Fig. 4.27 shows the experimental results for a case where C_o is increased to 61.28 μF while keeping L_m as before. By replacing the converter parameters on (31), $I_{st\text{-}up} = 27.76$ A which is much higher than the value calculated in (59) for the parameters of Table 4.I. For designs with low ripple and high output voltage, $I_{st\text{-}up}$ may become many times greater than the steady-state magnetizing peak

TABLE 4. V

SUMMARY RESULTS FOR THE ADAPTIVE BCM NSS CONTROL LAW

	Measured		Calculated	Error %
	$I_{st\text{-}up}$	V_x	$(\alpha/\beta)_0$	$(\alpha/\beta)_0$
$\alpha/\beta = 1$	6.95 A	12.1 V	4.093	2.32
$\alpha/\beta = 0.64$	14.7 A	28 V	0.668	4.45

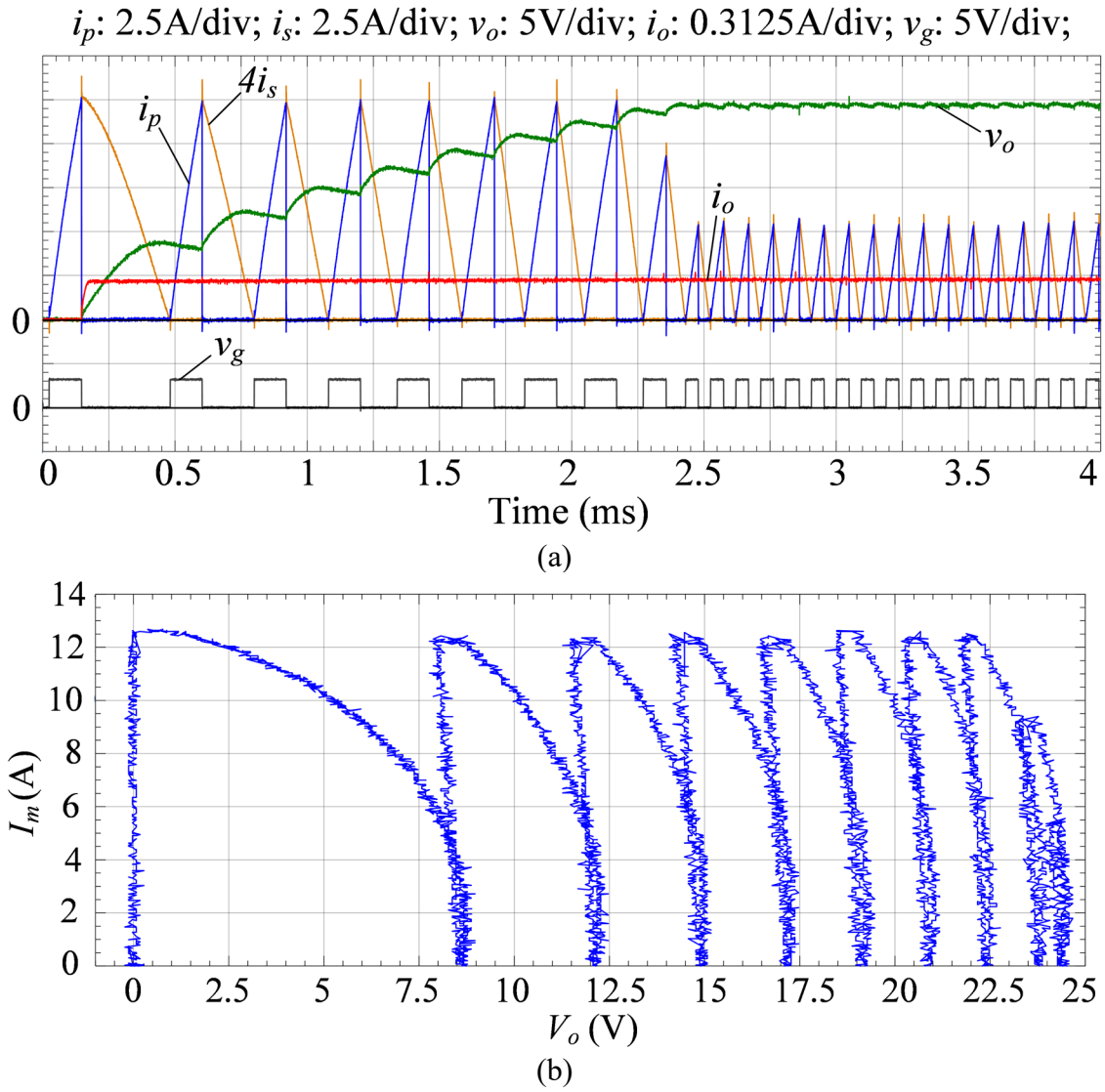

Fig. 4. 27(a) Transient response, and (b) state-plane trajectory for the adaptive BCM NSS control law when the $I_{st\text{-}up}$ is limited to 12 A.

current. Therefore, it is necessary in those cases to limit the start-up current using (61). In the particular case of Fig. 4.27, I_{max} = 12 A was selected since the steady-state peak magnetizing

current $I_{m,max}$ is 8 A from (60) when the load is at its maximum level. From Fig. 4.27, the ripple has decreased considerably with respect to previous experiments. A photograph of the experimental setup is provided in Fig. 4.28.

4.8.A Comparison with a Linear PI Controller

To compare the new adaptive NSS controller with a standard linear controller under nominal and uncertain parameters, a linear controller was designed following the basic ideas from references [8] and [9]. The performances of the linear controller and of the novel NSS controller are analyzed from experimental results where L_m and C_o are uncertain.

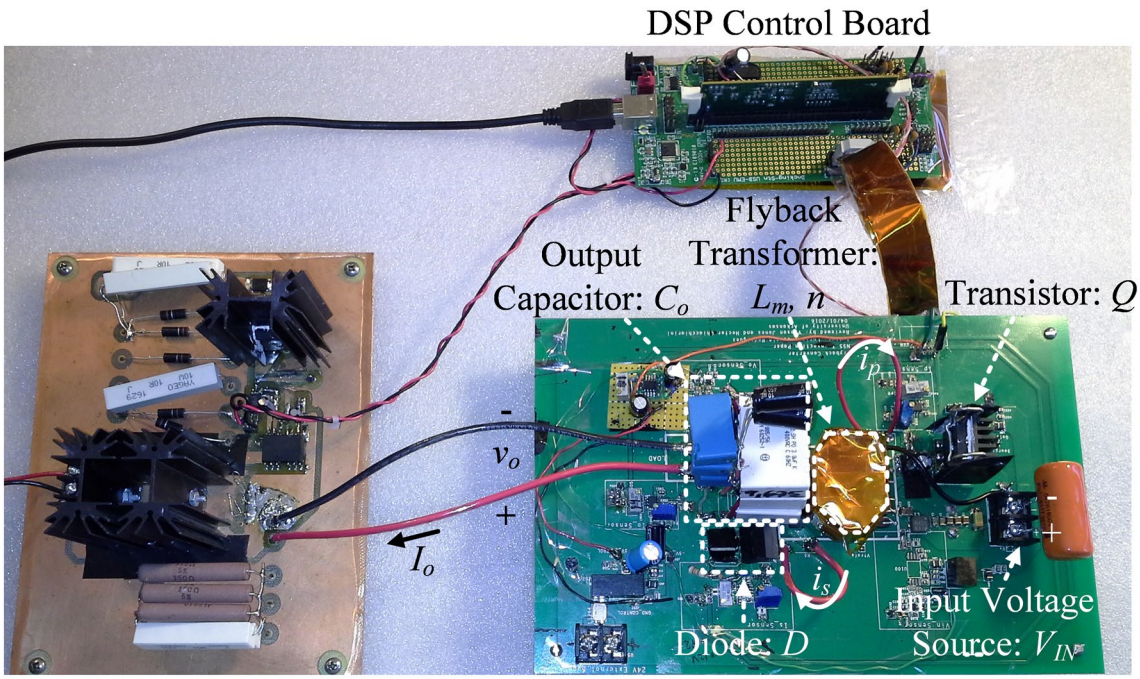

Fig. 4. 28. Photograph of the experiment setup (Photo by author).

TABLE 4. VI EXPERIMENTAL PROTOTYPE PARAMETERS FOR COMPARISON WITH A LINEAR COMPENSATOR

Parameter	Value
N_p/N_s	1/4
L_m	45.8 µH
C_o	20.52 µF (film)

References [8], [9] present a linear control approach for a flyback converter operating in critical conduction mode with a resistive load. In those papers, the model of the converter is obtained by calculating the average current through the diode and then linearizing the expression of the output voltage around a desired operating point. Then, the linear compensator is designed.

Based on those references, an extension is made to the case of a flyback converter operating with a constant-current load. The necessary calculations to estimate the performance of the linear controller for the nominal plant and parameter uncertainties are presented in the Appendix including the step-by-step design procedure. Below, experimental results are presented. A summary of parameters of the nominal plant is presented in Table 4.VI. The output capacitor is selected for the application to have high output voltage ripple, so the figures can show clearly the waveform characteristics.

A digital approximation to the designed continuous-time PI controller was implemented in a DSP using a high sampling rate of 200 kHz for testing purposes. The implemented controller had two main purposes: 1) to produce BCM operation by measuring constantly the diode current, turning ON the transistor when the current reaches zero, and later turning OFF the transistor when the magnetizing current reaches the desired value $I_{m,pk}$; 2) to measure the value of the output voltage and the reference voltage, evaluate the error signal and feed it to the PI compensator to evaluate the necessary $I_{m,pk}$ value which adjusts the output voltage.

Three designs were made: The first one considering the plant with nominal parameters and the latter considering variations of the nominal values. The experimental tests were made all on the nominal plant where the implemented linear PI controller is designed on the basis of different perturbed plant parameters. Each case is compared with the corresponding adaptive NSS design. It is important to mention that the magnetizing current is limited to 12 A in all cases to avoid the

saturation of the magnetic core (when the magnetizing current reaches 13.6 A, the value of the magnetizing inductance diminishes to 75% of the nominal value).

4.8.A.(1) First Case: Nominal Design

A linear PI controller was designed for ω_n = 4681 s-1, ξ = 0.856, leading to K_i = 7280, K_p = 2.5. Fig. 4.29(a) shows the performance of the experimental setup. Note the nonlinear effects of

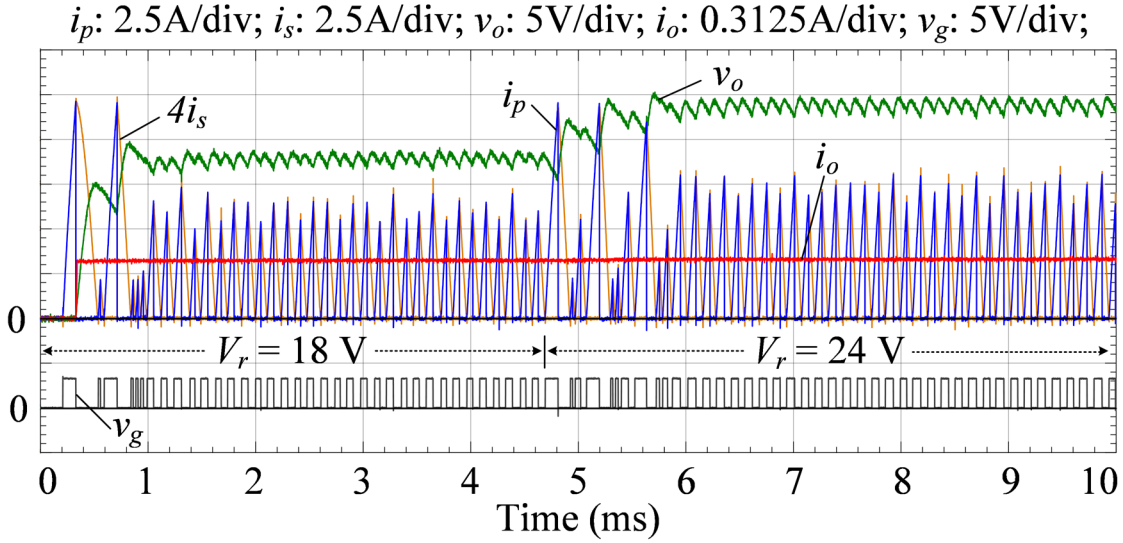

(a)

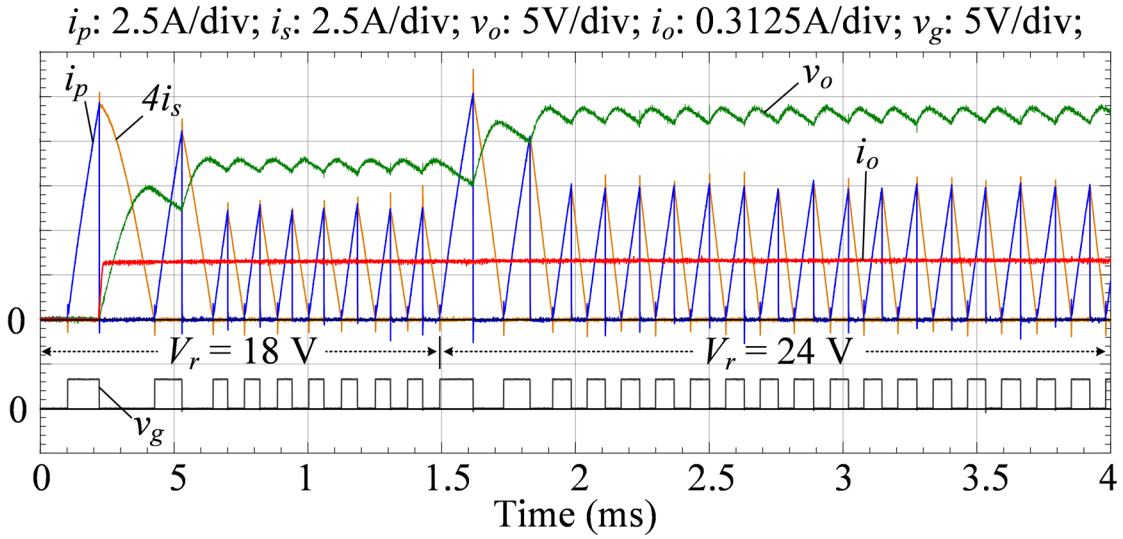

(b)

Fig. 4. 29. Closed-loop response for a design with nominal plant parameters when $I_{st\text{-}up}$ is limited to 12 A for (a) a PI controller, and (b) the novel adaptive NSS controller.

the saturation of the magnetizing current during startup as well as when applying a step change in the voltage reference at 4.693 ms from 18 V to 24 V. The PI controller demands approximately 1.3 ms to reach the new steady-state condition performing 11 switching actions, while the novel adaptive NSS for the same conditions (Fig. 4.29(b)) responds to the step change at 1.493 ms in approximately 0.4 ms performing two switching actions due to the limitation of the magnetizing

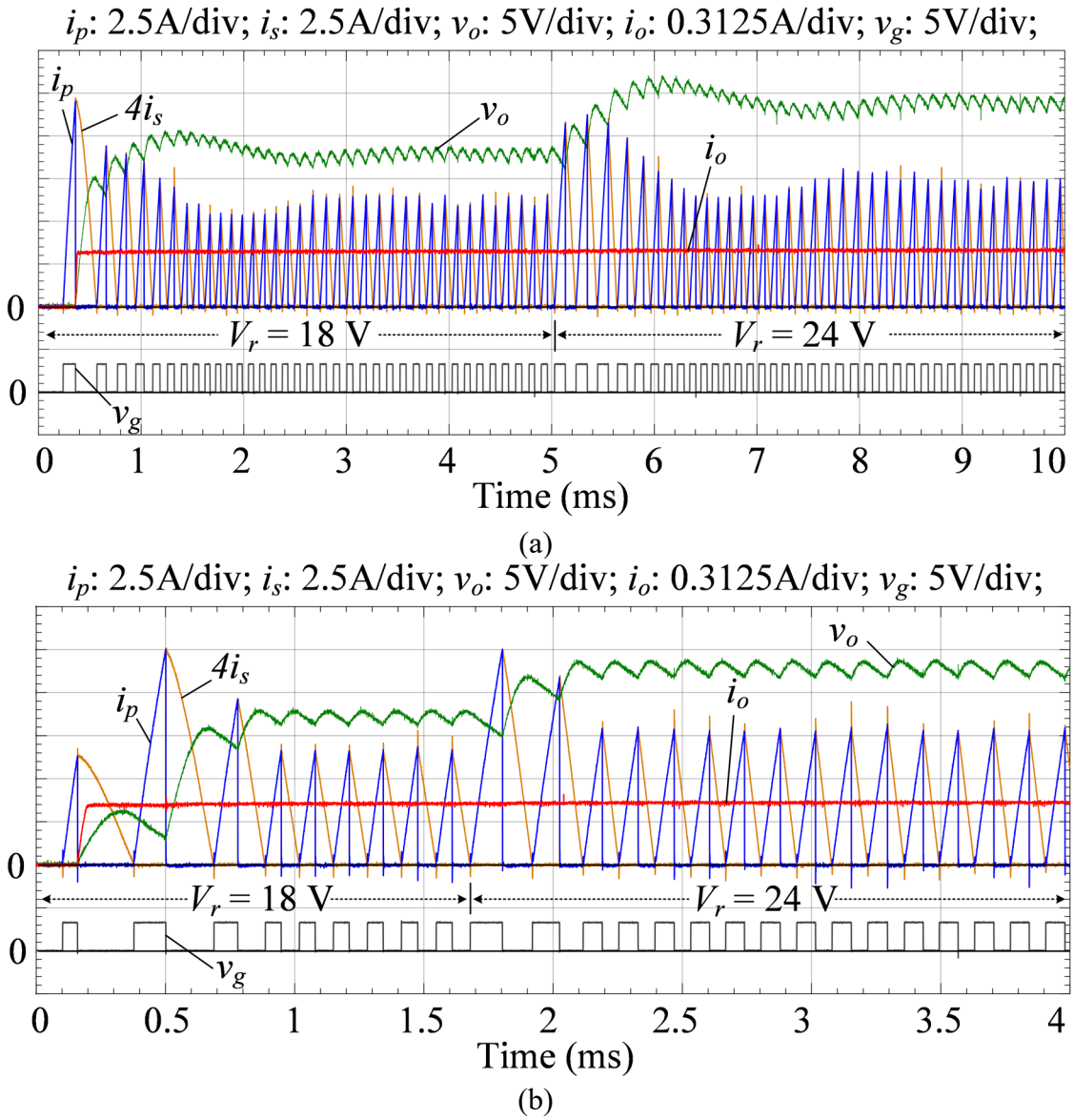

Fig. 4. 30. Closed-loop response for a design with uncertain plant parameters (α/β=4) when $I_{st\text{-}up}$ is limited to 12 A for (a) a PI controller, and (b) the novel adaptive NSS controller.

current. If the magnetizing current was not limited and the core would not saturate, it would need just one switching cycle to reach the target output voltage.

4.8.A.(2) Second Case: Design Based on Uncertain Parameters (α/β=4)

In this experiment, the plant remains the same, but the design of the PI controller is made on the basis of uncertain plant parameters, considering C_o = 5.13 μF. A linear PI controller was designed for ω_n = 4682.7 s^{-1}, ξ = 0.8387, leading to K_i = 1821.6, K_p = 0.4878. Fig. 4.30(a) shows that the performance of the experimental setup is more oscillatory than the previous case due to the parametric variations and demands more than 3 ms (i.e., more than 22 switching actions) to reach a steady-state condition for a sudden change on the voltage reference V_r from 18 V to 24 V occurring at 5.03 ms. As predicted by (A25), since $\beta < 1$, the response will be slower than in the ideal case. This case must be compared with Fig. 4.30(b) where the novel adaptive NSS controller is used and, despite the parametric error, the closed-loop response to the step change at 1.68 ms is very similar to the one obtained with the nominal design (Fig. 4.29(b)).

4.8.A.(3) Third case: design based on uncertain parameters (α/β=0.64)

The plant remains the same, but the design of the PI controller is made based on uncertain plant parameters, considering C_o = 32.06 μF. A linear PI controller was designed for ω_n = 4683.2 s^{-1}, ξ = 0.8385, leading to K_i = 11387.2, K_p = 3.9131. Fig. 4.31(a) shows the performance of the experimental setup. A rather unstable operation occurs during the first interval before the application of a step change in the output voltage reference from 18 V to 24 V at time 3.952 ms. The output voltage waveform is noticeable worse than the obtained with the nominal design (Fig. 4. 29(a)). The PI controller is reaching the new target point in about 1.3 ms after 13 switching actions. This case must be compared with Fig. 4.31(b) where the novel adaptive NSS controller

shows almost the same response to the step change at 1.494 ms as for the nominal case despite the parametric variations, reaching a steady-state condition in two switching actions.

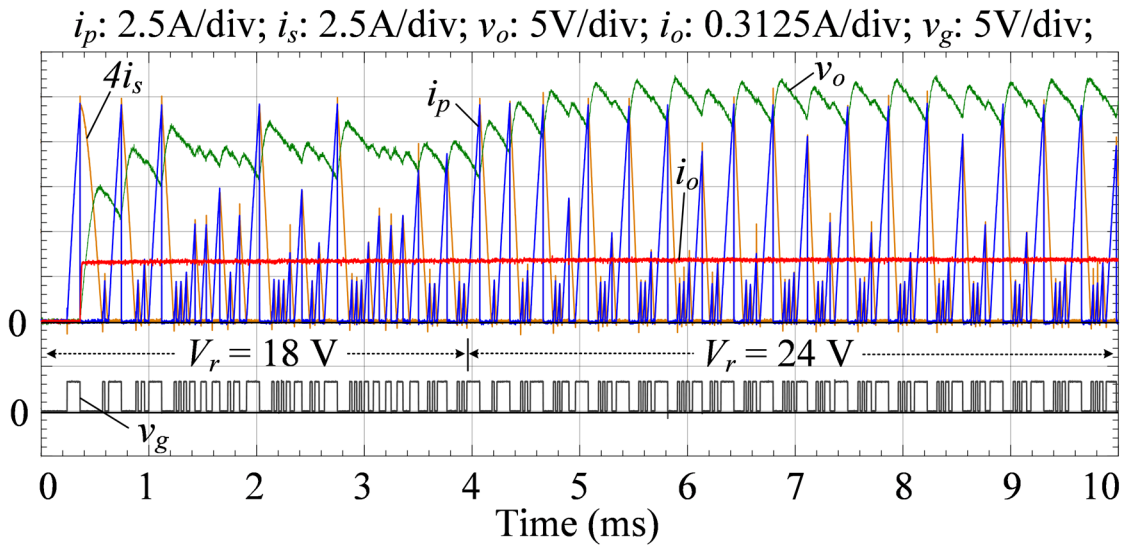

(a)

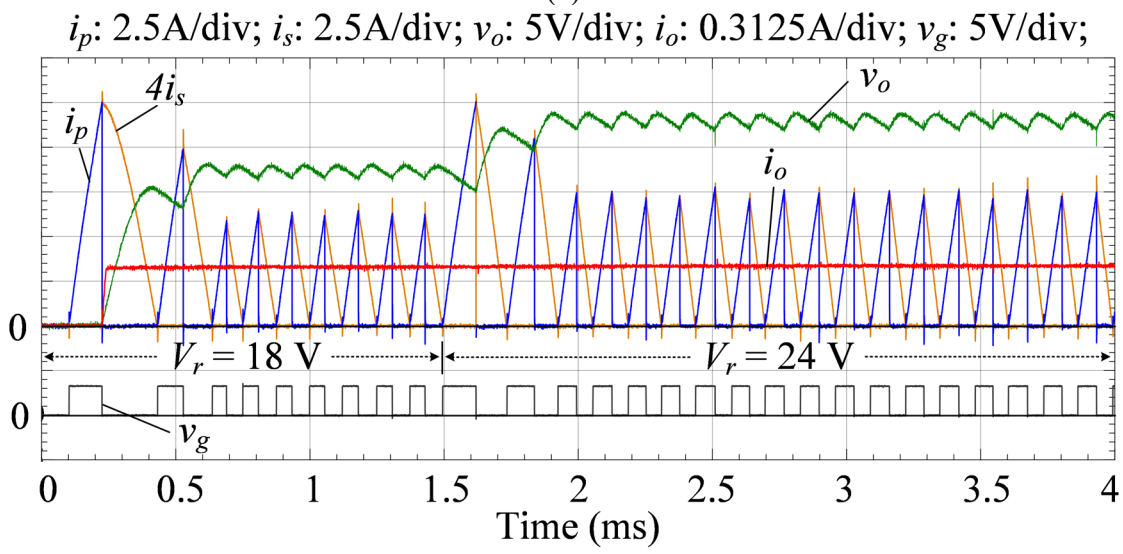

(b)

Fig. 4. 31. Closed-loop response with uncertain plant parameters ($\alpha/\beta = 0.64$) when $I_{st\text{-}up}$ is limited to 12 A using (a) a PI controller, and (b) the novel adaptive NSS controller.

4.9 CONCLUSION

The natural switching surfaces for a flyback converter with parameter uncertainties operating in the boundary conduction mode were obtained from the normalized converter differential equations. The derived nonlinear boundary control law brings the converter to the target point in a single switching cycle if the load does not change when the transistor Q is OFF during transient conditions. During start-up conditions where the load changes from zero to its rated value when the transistor is OFF, the worst-case scenario will be approaching the target point in only two switching cycles. During steady-state conditions, the controller will compensate for a sudden load change within only a single switching cycle.

The experimental results showed that for the nominal system ($\alpha/\beta = 1$, no parametric variations), the closed-loop response had no overshoot, zero steady-state error and excellent response to sudden load changes. When parameter uncertainties were present ($\alpha/\beta \neq 1$), the performance of the typical NSS control degraded considerably due to the dependence of the normalized control trajectories to the converter parameters. To improve the system performance, an adaptive control scheme was implemented predicting the variation on the converter parameters by using the precisely derived converter natural trajectories. The controller made its first estimation of the parameter variations during the start-up with a precision measured to be higher than 95%. Then, small adjustments were made cycle-by-cycle to adapt the control trajectories by measuring the error of the output voltage with respect to the target point producing a control response similar to the ideal case even under extreme parameter variations.

4.10 REFERENCES

[1] M. Kazimierczuk, “Pulse-width Modulated DC–DC Power Converters”, First Edition, John Wiley & Sons, ISBN: 978-0-470-69465-7, 2008.

[2] Q. Wu and Z. Zhu, "An Adaptive High-Precision OCP Control Scheme for Flyback AC/DC Converters," *in IEEE Transactions on Power Electronics*, vol. 32, no. 12, pp. 8969-8973, Dec. 2017.

[3] C. Zhao, J. Zhang and X. Wu, "An Improved Variable On-Time Control Strategy for a CRM Flyback PFC Converter," *in IEEE Transactions on Power Electronic*s, vol. 32, no. 2, pp. 915-919, Feb. 2017.

[4] T. Yan, J. Xu, F. Zhang, J. Sha and Z. Dong, "Variable-On-Time-Controlled Critical-Conduction-Mode Flyback PFC Converter," *in IEEE Transactions on Industrial Electronic*s, vol. 61, no. 11, pp. 6091-6099, Nov. 2014.

[5] S. B. Kjaer, J. K. Pedersen and F. Blaabjerg, "A review of single-phase grid-connected inverters for photovoltaic modules," *in IEEE Transactions on Industry Applications*, vol. 41, no. 5, pp. 1292-1306, Sept.-Oct. 2005.

[6] A. C. Kyritsis, E. C. Tatakis and N. P. Papanikolaou, "Optimum Design of the Current-Source Flyback Inverter for Decentralized Grid-Connected Photovoltaic Systems," *in IEEE Transactions on Energy Conversion*, vol. 23, no. 1, pp. 281-293, March 2008.

[7] L. A. Garcia Rodriguez and J. C. Balda, "A comparison of isolated DC-DC converters for microinverter applications," *2013 Twenty-Eighth Annual IEEE Applied Power Electronics Conference and Exposition (APEC)*, Long Beach, CA, USA, 2013, pp. 2084-2091.

[8] G. Spiazzi, D. Tagliavia and S. Spampinato, "DC-DC flyback converters in the critical conduction mode: a re-examination," Conference Record of the *2000 IEEE Industry Applications Conference. Thirty-Fifth IAS Annual Meeting and World Conference on Industrial Applications of Electrical Energy (Cat. No.00CH37129)*, Rome, 2000, pp. 2426-2432 vol.4.

[9] B. T. Irving, Y. Panov and M. M. Jovanovic, "Small-signal model of variable-frequency flyback converter," *Applied Power Electronics Conference and Exposition, 2003. APEC '03. Eighteenth Annual IEEE*, Miami Beach, FL, USA, 2003, pp. 977-982 vol.2.

[10] T. T. Song and H. S. h. Chung, "Boundary Control of Boost Converters Using State-Energy Plane," *in IEEE Transactions on Power Electronics*, vol. 23, no. 2, pp. 551-563, March 2008.

[11] J. M. Galvez, M. Ordonez, F. Luchino and J. E. Quaicoe, "Improvements in Boundary Control of Boost Converters Using the Natural Switching Surface," *in IEEE Transactions on Power Electronics*, vol. 26, no. 11, pp. 3367-3376, Nov. 2011.

[12] P. T. Krein, Nonlinear Phenomena in Power Electronics: Attractors, Bifurcation, Chaos, and Nonlinear Control. New York: IEEE Press, 2001, ch. 8.

[13] R. Munzert and P. T. Krein, "Issues in boundary control [of power convertors]," PESC Record. *27th Annual IEEE Power Electronics Specialists Conference*, Baveno, 1996, pp. 810-816 vol.1.

[14] M. Greuel, R. Muyshondt and P. T. Krein, "Design approaches to boundary controllers," PESC97. Record *28th Annual IEEE Power Electronics Specialists Conference. Formerly Power Conditioning Specialists Conference 1970-71. Power Processing and Electronic Specialists Conference 1972*, St. Louis, MO, 1997, pp. 672-678 vol.1.

[15] R. A. DeCarlo, S. H. Zak and G. P. Matthews, "Variable structure control of nonlinear multivariable systems: a tutorial," *in Proceedings of the IEEE*, vol. 76, no. 3, pp. 212-232, Mar 1988.

[16] V. I. Utkin, "Sliding mode control design principles and applications to electric drives," *in IEEE Transactions on Industrial Electronics*, vol. 40, no. 1, pp. 23-36, Feb 1993.

[17] C. N. Onwuchekwa and A. Kwasinski, "Analysis of Boundary Control for Buck Converters With Instantaneous Constant-Power Loads," *in IEEE Transactions on Power Electronics*, vol. 25, no. 8, pp. 2018-2032, Aug. 2010.

[18] K. K. S. Leung and H. S. H. Chung, "Derivation of a second-order switching surface in the boundary control of buck converters," *in IEEE Power Electronics Letters*, vol. 2, no. 2, pp. 63-67, June 2004.

[19] J. Y. C. Chiu, K. K. S. Leung and H. S. H. Chung, "High-Order Switching Surface in Boundary Control of Inverters," *in IEEE Transactions on Power Electronics*, vol. 22, no. 5, pp. 1753-1765, Sept. 2007.

[20] K. K. S. Leung and H. S. h. Chung, "A Comparative Study of Boundary Control With First- and Second-Order Switching Surfaces for Buck Converters Operating in DCM," *in IEEE Transactions on Power Electronics*, vol. 22, no. 4, pp. 1196-1209, July 2007.

[21] W. T. Yan, C. N. M. Ho, H. S. H. Chung and K. T. K. Au, "Fixed-Frequency Boundary Control of Buck Converter With Second-Order Switching Surface," *in IEEE Transactions on Power Electronics*, vol. 24, no. 9, pp. 2193-2201, Sept. 2009.

[22] P. K. W. Chan, H. Shu-Hung Chung and S. Y. Hui, "A Generalized Theory of Boundary Control for a Single-Phase Multilevel Inverter Using Second-Order Switching Surface," *in IEEE Transactions on Power Electronics*, vol. 24, no. 10, pp. 2298-2313, Oct. 2009.

[23] Y. He, H. S. H. Chung, C. N. M. Ho and W. Wu, "Use of Boundary Control With Second-Order Switching Surface to Reduce the System Order for Deadbeat Controller in Grid-

Connected Inverter," *in IEEE Transactions on Power Electronics*, vol. 31, no. 3, pp. 2638-2653, March 2016.

[24] Y. He, H. S. h. Chung, C. N. M. Ho and W. Wu, "Direct Current Tracking Using Boundary Control With Second-Order Switching Surface for Three-Phase Three-Wire Grid-Connected Inverter," *in IEEE Transactions on Power Electronics*, vol. 32, no. 7, pp. 5723-5740, July 2017.

[25] T. Messikh, N. Rahim and M. Saad, "Boundary control of dual-output boost converter using state-energy plane," *in IET Power Electronics*, vol. 7, no. 9, pp. 2310-2321, September 2014.

[26] S. Chen, Y. M. Lai, S. C. Tan and C. K. Tse, "Boundary Control With Ripple-Derived Switching Surface for DC–AC Inverters," *in IEEE Transactions on Power Electronics*, vol. 24, no. 12, pp. 2873-2885, Dec. 2009.

[27] M. Ordonez, M. T. Iqbal and J. E. Quaicoe, "Selection of a curved switching surface for buck converters," *in IEEE Transactions on Power Electronics*, vol. 21, no. 4, pp. 1148-1153, July 2006.

[28] M. Ordonez, J. E. Quaicoe and M. T. Iqbal, "Advanced Boundary Control of Inverters Using the Natural Switching Surface: Normalized Geometrical Derivation," *in IEEE Transactions on Power Electronics*, vol. 23, no. 6, pp. 2915-2930, Nov. 2008.

[29] J. M. Galvez and M. Ordonez, "High Performance Boundary Control of Boost-Derived PFCs: Natural Switching Surface Derivation and Properties," *in IEEE Transactions on Power Electronics*, vol. 27, no. 8, pp. 3807-3816, Aug. 2012.

[30] J. M. Galvez, M. Ordonez, T. T. Nguyen and F. Luchino, "Boundary control of buck-boost converters: normalized trajectories and the Natural Switching Surface," *2012 IEEE Energy Conversion Congress and Exposition (ECCE)*, Raleigh, NC, 2012, pp. 358-363.

[31] G. G. Oggier, M. Ordonez, J. M. Galvez and F. Luchino, "Fast Transient Boundary Control and Steady-State Operation of the Dual Active Bridge Converter Using the Natural Switching Surface," *in IEEE Transactions on Power Electronics*, vol. 29, no. 2, pp. 946-957, Feb. 2014.

[32] G. G. Oggier and M. Ordonez, "Boundary Control of Full-Bridge ZVS: Natural Switching Surface for Transient and Steady-State Operation," *in IEEE Transactions on Industrial Electronics*, vol. 61, no. 2, pp. 969-979, Feb. 2014.

[33] L. A. Garcia-Rodriguez, E. Williams, J. C. Balda, J. Gonzalez-Llorente and H. Chiacchiarini, "Control of a flyback converter operating in BCM using the natural switching surface," *2015 IEEE 6th International Symposium on Power Electronics for Distributed Generation Systems (PEDG)*, Aachen, 2015, pp. 1-8.

[34] L. A. G. Rodriguez, H. Chiacchiarini and J. C. Balda, "Control of a flyback converter with parametric uncertainties operating in BCM Using the natural switching surface," *2016 IEEE Biennial Congress of Argentina (ARGENCON)*, Buenos Aires, Argentina, 2016, pp. 1-7.

[35] E. O. Lindstrom, L. A. Garcia-Rodriguez, A. R. Oliva and J. C. Balda, "Designing an optimum non-dissipative LC snubber for step-up flyback converters in DCM," *2017 IEEE 8th Latin American Symposium on Circuits & Systems (LASCAS)*, Bariloche, Argentina, 2017, pp. 1-4.

4.11 APPENDICES

4.11.A Linear Controller for BCM Operation

The average current I_d through the diode in the secondary side of the transformer can be calculated from Fig. 4.32 as:

$$I_d = \frac{I_{m,pk}.n.(1-D)}{2} = \frac{v_{in}}{L_m}.D.T_{sw}.n.\frac{(1-D)}{2}, \tag{A1}$$

where D is the duty cycle which is calculated by analyzing the steady-state voltage waveform across the magnetizing inductance in BCM as:

$$D = n.(V_o + V_d)/(v_{in} + n.(V_o + V_d)), \tag{A2}$$

where V_d is the voltage drop across the diode.

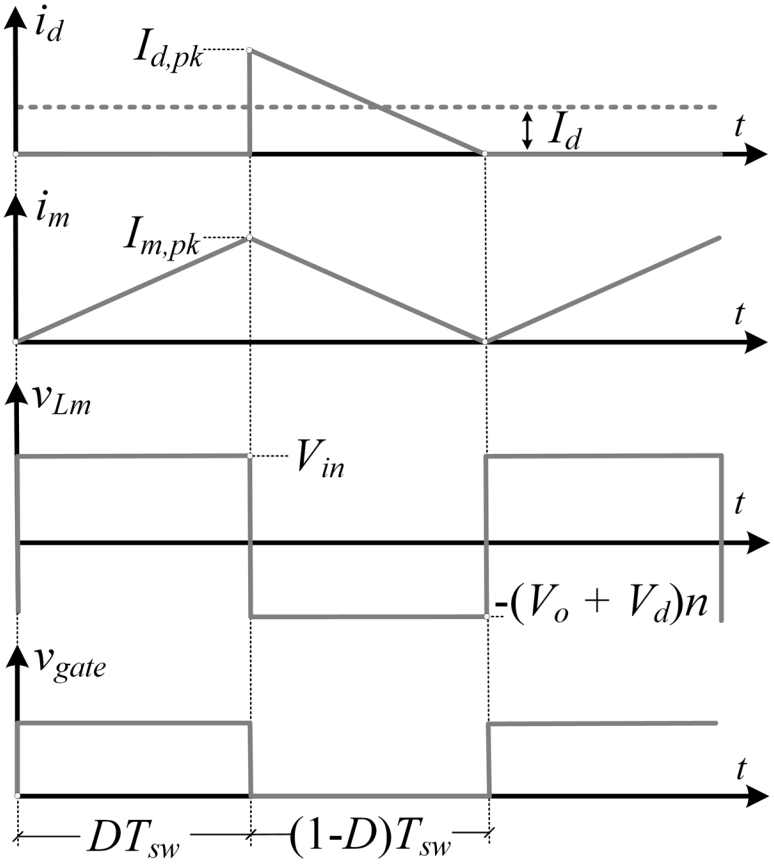

Fig. 4. 32. Main waveforms for a flyback converter operating in BCM.

From (A1), I_d depends on the magnetizing inductance peak current $I_{m,pk}$. Therefore, $I_{m,pk}$ is used as the control variable to set the required average diode current [8], [9]. By replacing (A2) into (A1), I_d can be expressed as follows:

$$I_d = \frac{I_{m,pk}}{2} n \frac{v_{in}}{v_{in} + n\left(v_o + V_d\right)}. \tag{A3}$$

From (A3), I_d is a nonlinear function which depends on v_{in}, v_o and $I_{m,pk}$. Linearizing (A3) around an operating point, $\hat{I}_d$ can be expressed by:

$$\hat{I}_d = K_{in}\hat{V}_{in} + K_m\hat{I}_{m,pk} + K_o\hat{V}_o. \tag{A4}$$

Where K_{in}, K_m and K_o are calculated by:

$$K_{in} = \frac{\partial I_d}{\partial V_{in}} = \frac{I_{m,pk} n^2 \left(V_o + V_d\right)}{2\left(V_{in} + n\left(V_o + V_d\right)\right)^2}, \tag{A5}$$

$$K_m = \frac{\partial I_d}{\partial I_{m,pk}} = \frac{n.V_{in}}{2\left(V_{in} + n\left(V_o + V_d\right)\right)}, \tag{A6}$$

$$K_o = \frac{\partial I_d}{\partial V_o} = -\frac{n^2 V_{in} I_{m,pk}}{2\left(V_{in} + n\left(V_o + V_d\right)\right)^2}. \tag{A7}$$

From the simplified flyback converter model shown in Fig. 4.33, the diode current in the Laplace *s*-domain can be expressed as follows:

$$\hat{\imath}_d(s) = \hat{\imath}_o(s) + s\bar{C}_o\hat{v}_o(s). \tag{A8}$$

By combining (A4) and (A8) the following expression is obtained:

$$K_{in}\hat{V}_{in} + K_m\hat{I}_{m,pk} + K_o\hat{v}_o = \hat{\imath}_o(s) + s\bar{C}_o\hat{v}_o(s). \tag{A9}$$

To analyze the effect of $I_{m,pk}$ on $\hat{v}_o$, $\hat{V}_{in}$ and $\hat{\imath}_o$ are assumed to be zero in (A9). Then, the following transfer function is determined:

$$G(s) = \frac{v_o(s)}{I_{m,pk}(s)} = \frac{K_m/\bar{C}_o}{s - K_o/\bar{C}_o}. \tag{A10}$$

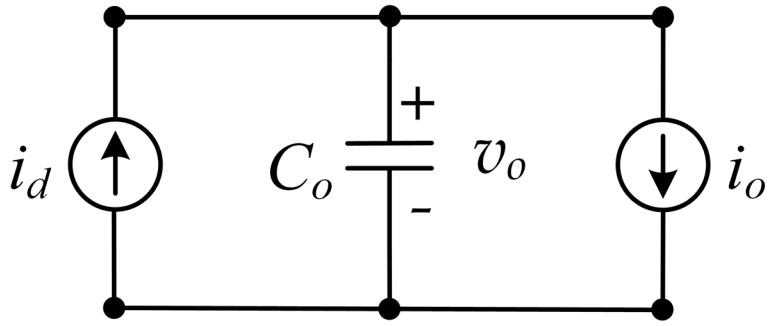

Fig. 4. 33. Simplified averaged model of the flyback converter operating in BCM.

From (A7), K_o is negative so (A10) is a stable transfer function. As (A10) is based on an averaged model of the discontinuous diode current, it represents the averaged dynamics of the output voltage variations as a function of the variations of $I_{m,pk}$. Therefore, the model is valid for a frequency range whose upper limit is lower than the switching frequency of the flyback converter.

To evaluate the switching frequency, the ON and OFF time periods can be calculated from Fig. 4.32 as:

$$\overline{T}_{ON} = \frac{I_{m,pk}\overline{L}_m}{V_{in}}, \tag{A11}$$

$$\overline{T}_{OFF} = \frac{I_{m,pk}\overline{L}_m}{n\left(V_o + V_d\right)}. \tag{A12}$$

Then, the nominal switching frequency is calculated by:

$$\overline{f}_{sw} = \frac{V_{in}.\left(V_o + V_d\right)}{I_{m,pk}.\overline{L}_m.\left(V_o + V_d + V_{in}/n\right)} = \frac{V_{in}.D}{I_{m,pk}.\overline{L}_m}. \tag{A13}$$

Similarly, it can be done for the actual switching frequency:

$$f_{sw} = \frac{V_{in}.\left(V_o + V_d\right)}{I_{m,pk}.L_m.\left(V_o + V_d + V_{in}/n\right)} = \frac{V_{in}.D}{I_{m,pk}.L_m}. \tag{A14}$$

From the ratio between (A13) and (A14), the following relationship between f_{sw} and $\overline{f}_{sw}$ is obtained:

$$\frac{f_{sw}}{\overline{f}_{sw}} = \frac{\overline{L}_m}{L_m} = \alpha. \tag{A15}$$

So, changes on the magnetizing inductance will produce switching frequency f_{sw} variations. The reference peak magnetizing current $I_{m,pk}$ used in the controller defines the steady-state output current level.

If a digital controller were to be designed to regulate the average output voltage of the plant (A10) by adjusting $I_{m,pk}$, it should use a sampling rate lower than the switching rate of the converter since the plant used for the design is an averaged model of the system. So, the minimum practical value of the switching frequency (A14), which occurs when V_{in} and D are minimum and L_m and $I_{m,pk}$ are maximum, would fix an upper limit to the closed-loop system bandwidth.

But, the following closed-loop transfer function is obtained if a continuous-time PI compensator is used to regulate the output voltage:

$$\frac{v_o(s)}{v_r(s)} = \frac{\left(\overline{K}_p.s + \overline{K}_i\right)K_m/\overline{C}_o}{s^2 + s\left(\overline{K}_p K_m - K_o\right)/\overline{C}_o + K_m\overline{K}_i/\overline{C}_o}, \tag{A16}$$

where K_p and K_i are the proportional and integral gains of the PI controller.

If voltage V_r is pre-filtered as seen in Fig. 4.34, the zero in (A16) introduced by the compensator can be eliminated:

$$\frac{v_o(s)}{v_r(s)} = \frac{\frac{\overline{K}_i}{\overline{K}_p}}{s + \frac{\overline{K}_i}{\overline{K}_p}} \frac{\left(\overline{K}_p s + \overline{K}_i\right)\frac{K_m}{\overline{C}_o}}{s^2 + s\frac{\left(\overline{K}_p K_m - K_o\right)}{\overline{C}_o} + \frac{K_m}{\overline{C}_o}\overline{K}_i} = \frac{\overline{\omega}_n^2}{s^2 + 2\xi\overline{\omega}_n s + \overline{\omega}_n^2}. \tag{A17}$$

To guarantee that the model of (A10) is valid, the closed-loop dynamics should be selected to have its natural frequency at least ten times slower than the nominal operating switching frequency calculated from (A13). Therefore, the following identity should be established:

$$\overline{\omega}_n = \sqrt{\frac{K_m \overline{K}_i}{\overline{C}_o}} < \frac{1}{10}\overline{\omega}_{fsw} = \frac{1}{10} 2\pi \overline{f}_{sw}. \tag{A18}$$

Then, K_i can be obtained as:

$$\overline{K}_i < \left(\frac{1}{10} 2\pi \overline{f}_{sw}\right)^2 \frac{\overline{C}_o}{K_m}. \tag{A19}$$

The proportional gain $\overline{K}_p$ can be designed by selecting the adequate damping ratio ξ for the closed-loop transfer function for the selected resonance frequency $\overline{\omega}_n = \sqrt{K_m \overline{K}_i / \overline{C}_o}$:

$$\overline{K}_p = \frac{2\overline{\xi}\overline{\omega}_n \overline{C}_o + K_o}{K_m}. \tag{A20}$$

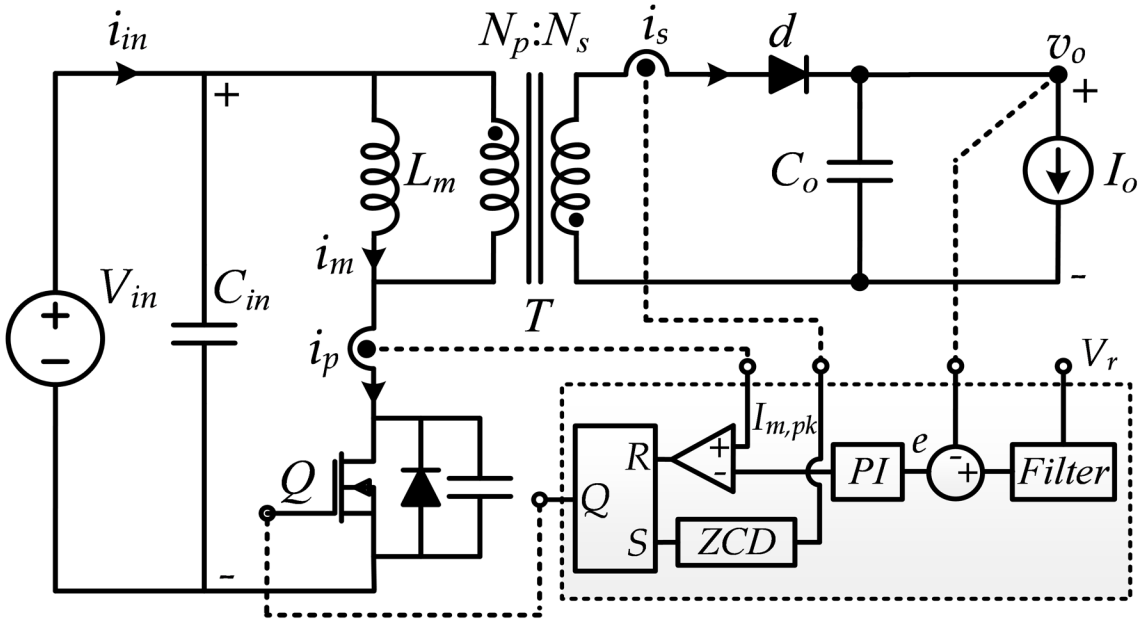

Fig. 4. 34. Standard control strategy using a PI compensator [34] [35].

If a PI compensator with nominal $\overline{K}_i$ and $\overline{K}_p$ is used to control a flyback converter with actual parameters C_o and L_m, the closed-loop transfer function pre-filtering V_r can be derived as follows:

$$\frac{v_o}{v_r} = \frac{\dfrac{\overline{K}_i}{\overline{K}_p}}{s + \dfrac{\overline{K}_i}{\overline{K}_p}} \frac{\dfrac{\left(\overline{K}_p s + \overline{K}_i\right)}{C_o} K_m}{s^2 + s\dfrac{\left(\overline{K}_p K_m - K_o\right)}{C_o} + \dfrac{K_m \overline{K}_i}{C_o}}. \tag{A21}$$

Therefore, the actual second-order parameters ξ and ω_n are given by:

$$2\xi\omega_n = \frac{\overline{K}_p K_m}{C_o} - \frac{K_o}{C_o}, \tag{A22}$$

$$\omega_n^2 = \frac{K_m \overline{K}_i}{C_o}. \tag{A23}$$

By substituting $\overline{K}_i$ and $\overline{K}_p$ by the maximum allowable value obtained from (A19) and (A20) into (A22) and (A23), the following relationships between the nominal and actual second-order time response parameters are obtained:

$$\xi = \overline{\xi}\sqrt{\beta}, \tag{A24}$$

$$\omega_n = \overline{\omega}_n\sqrt{\beta}, \tag{A25}$$

where β is the ratio between the nominal output capacitance $\overline{C}_o$ and the actual value C_o. Therefore, the parameter β will change the dynamic response of the controller. This continuous PI controller is implemented digitally by discretizing its dynamics at a high sampling rate of 200 kHz.

4.11.B Author Biographies

Luciano Andres Garcia Rodriguez (S'12) received the B.S. degree in electronics engineering from the Universidad Nacional del Sur (UNS), Bahía Blanca, Argentina. He is currently pursuing the Ph.D. degree in electrical engineering at the University of Arkansas, Fayetteville, AR, USA; where he has been working as a research and teaching assistant. His current research interests include novel topologies for power electronics converters, high-frequency and high-power transformer design, and novel non-linear adaptive control schemes.

Héctor Gerardo Chiacchiarini was born in Villa Regina, Argentina, in 1964. He received the B.Sc. degree in electronics engineering and the Ph.D. degree in control systems, from the Universidad Nacional del Sur, Bahía Blanca, Argentina, in 1990 and 1996, respectively. In 2001, he was a visiting Scholar at the ETH Zurich, Switzerland, and, in 2004, at the University of Arkansas, USA. He is currently a Professor with the Departamento de Ingeniería Eléctrica y de Computadoras, Universidad Nacional del Sur, Bahía Blanca, Argentina, teaching power electronics and industrial robotics. He is also a Researcher in CONICET, since 1999, with the Instituto de Investigaciones en Ingeniería Eléctrica "Alfredo Desages" (UNS-CONICET). He has coauthored more than 110 works published in journals, book chapters and conferences. He has participated in more than 30 research projects being director of thirteen of them. His main research interests include power electronics, robotics, mechatronics, motor drives, control systems, and applications in energy storage and power management.

David Carballo Rojas (S'14) was born in Santiago, Panama, in 1993. He received his B.S. in Electrical Engineering from the University of Arkansas (Fayetteville, U.S.A) in 2016, where he is currently pursuing the M.S. degree with the Department of Electrical Engineering under the supervision of Dr. J. C. Balda. His current research interests include power electronics, stability of grid connected power electronics and power quality.

Juan Carlos Balda (M'78–SM'94) received the B.Sc. degree in electrical engineering from the Universidad Nacional del Sur, Bahía Blanca, Argentina, in 1979, and the Ph.D. degree in electrical engineering from the University of Natal, Durban, South Africa, in 1986. He was a Researcher and a part-time Lecturer at the University of Natal until 1987. He was a Visiting Assistant Professor at Clemson University, Clemson, SC, USA, for two years. He has been with the University of Arkansas, Fayetteville, AR, USA, since 1989, where he is currently a University Professor, a Department Head, and an Associate Director of Applications with the National Center for Reliable Electric Power Transmission and a Campus Director with the NSF IUCRC Grid-Connected Advanced Power Electronic Systems. His current research interests include power electronics, electric power distribution systems, motor drives, and electric power quality. Dr. Balda is a member of the honor society Eta Kappa Nu. He is also the Vice-Chair of the IEEE Power Electronics Society (PELS) TC5 Committee and a Faculty Advisor of the local chapter of the IEEE PELS.

4.11.C Paper Permissions

UNIVERSITY OF
ARKANSAS
College of Engineering

Department of Electrical Engineering

1 University Avenue, 3217 Bell Engineering Center, Fayetteville, AR 72701, (479) 575-3005, (479) 575-7967 (fax)

November 6, 2019

To whom it may concern,

This letter is to verify that Mr. Luciano Andrés Garcia Rodriguez, ID 010593736, is the first author and did at least 51% of the work for the paper titled "Control of a Flyback Converter Operating in BCM Using the Natural Switching Surface".

Kind Regards,

Dr. Juan Carlos Balda

University Professor, Department Head and Major Advisor to Mr. Luciano Andrés Garcia Rodriguez

CHAPTER 5

Adaptive Boundary Control Using Natural Switching Surfaces for Flyback Converters Operating in the Boundary Conduction Mode with Reduced Number of Sensors

L. A. Garcia Rodriguez, H. G. Chiacchiarini, and J. C. Balda, "Adaptive Boundary Control Using Natural Switching Surfaces for Flyback Converters Operating in the Boundary Conduction Mode with Parameter Uncertainties," to be submitted to *IEEE Transactions on Power Electronics*.

5.1 ABSTRACT

Boundary control using the natural switching surfaces (NSS) has been extensively studied for multiple converter topologies with nominal parameters, showing an improved performance in the control of nonlinear systems. However, the NSS performance considerably deteriorates when the real parameters of the converter are different from the ones used in the design process. Therefore, an adaptive NSS control strategy has been proposed elsewhere to compensate for the parameter uncertainties of the converter in a minimum number of switching actions. This paper presents the derivation of an adaptive sensorless boundary control using the NSS for a flyback converter. The proposed approach eliminates the use of all sensors in the secondary side of the transformer, while stills estimating the converter parameters and keeping a very completive performance. The analytical derivation of the proposed adaptive sensorless switching surfaces is presented with simulation results showing adequate performance under different situations.

5.2 INTRODUCTION

Flyback converters are widely used in low power applications [1] as seen in computers and TV sets, AC/DC converters for battery chargers and LED loads [2]–[4], photovoltaic microinverters [5], [6] and others due to low part count, low cost, electrical isolation, and wide voltage ratio among many other benefits. High frequency operation of flyback converters is broadly done in the boundary conduction mode (BCM) due to zero-current turn-ON of the switching device and zero-current turn-OFF of the diode [7]. Also, conduction losses and current stresses and voltage ripple are kept lower in comparison with operation in the discontinuous conduction mode (DCM) [3], [8]. Other relevant advantages are related to less electromagnetic interference (EMI) and lower power losses respect to operation in continuous conduction mode (CCM) [9]–[10].

A detailed study of a flyback converter operating in BCM under natural switching surfaces (NSS) was done in [11] considering also parametric uncertainties. There, an adaptive control strategy was presented, including experimental results and simulations. The proposed control law provided a very precise estimation of the parameter variations in only the first switching action while continuously adapting the control switching surfaces before a new switching action occurs. Therefore, the converter reached the steady-state operation in a single switching action for sudden load changes even under extreme converter parameter variations. Although, a drawback of the proposed strategy is the need of fully measuring all electrical variables for feedback: output voltage and current, primary and secondary currents. Three of the four measured variables require a voltage insulation which increases the system cost and complexity.

Sensorless alternatives for closed loop control of flyback converters are readily available in the literature, but actually there are not many results for flyback converters operating in BCM mode under natural surface control. Other authors have worked on control schemes which are sensorless,

or need a reduced number of sensors, either for flyback converters or other topologies. For example, an estimator is constructed in [12] for the output current of a boost converter that can be operated either in BCM, quasiresonant mode (QRM), or discontinuous conduction mode (DCM). The estimator needs the knowledge of the input and output voltage, and the duration of the ON-interval. In [13] is presented the inner current control of a flyback converter operating in BCM, where the duration of the freewheeling and conduction phase can be readily determined just by measuring the output voltage, without current measurement. Other authors [14] proposed the incorporation of a tertiary winding in the flyback transformer, used to estimate the magnetizing current, thus eliminating the current sensor. This solution requires a more complex transformer.

But up to these author's knowledge, no previous reports exist in the literature for adaptive NSS BCM control of flyback converters with reduced number of sensors.

This paper presents an alternative to reduce the number of sensors in the adaptive NSS BCM control scheme presented in [11], estimating the output current while preserving the adaptation capacity and original performance. This is a novel result. The proposed control law can provide a very precise estimation of the parameter variations and the output current in only two switching actions, and then continuously adapt the control switching surfaces before a new switching action occurs. Therefore, the converter can reach the steady-state operation in two single switching actions for sudden load changes even under extreme converter parameter variations and constant output load current. The analytical derivation of the proposed adaptive sensorless switching surfaces is presented together with simulations and experimental results showing adequate performance under different tests, including comparisons with the standard sensored strategy.

This paper is organized as follows. The basic theory is exposed in-Section 5.3. Then, the proposed strategy without sensing any variable at the secondary side of the transformer is presented in

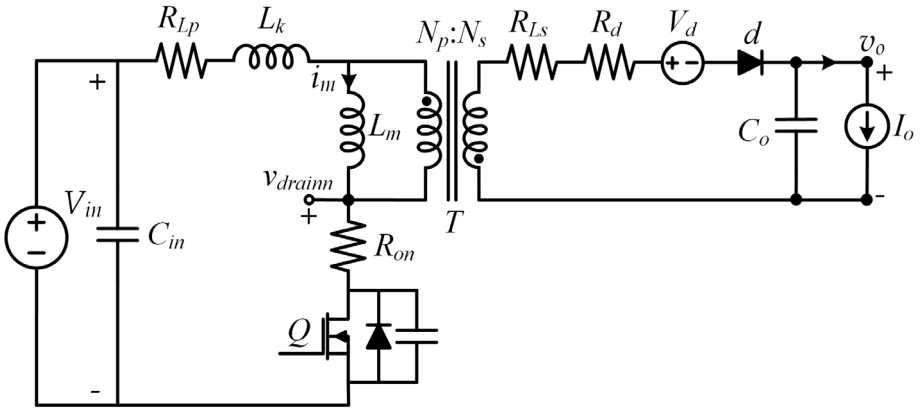

Fig. 5. 1. Flyback converter with constant load current.

Section 5.4. Simulations are included in Section 5.5, while experimental results are in Section 5.6. Finally, Section 5.7 presents the conclusions.

5.3 BASIC DESCRIPTION AND PROBLEM FORMULATION

A detailed description of the topology, circuit analysis and definition of the natural switching surfaces is presented in [11] where also an adaptive BCM control strategy is shown, analyzed and tested experimentally. The control strategy presented there does need the measurement of four signals: output voltage and current, and primary and secondary currents of the transformer. As measurements add complexity to the hardware implementation, it is worth studying sensor-less alternatives. This work presents a strategy where no signals at the transformer secondary side are measured, while preserving the performance characteristics and adaptive behavior of the original proposal [11].

The first part of this section extracts from [11] some basic information for completeness. The reader should consult it for further details. Fig. 5.1 shows the circuit of a flyback converter with a constant current load I_o which is considered the worst-case scenario in terms of stability [15]. Also,

these parasitic elements are included: R_{LP}: primary-side winding resistance, R_{ON}: switch ON resistance, $R_P = R_{LP} + R_{ON}$: total primary resistance, L_k: transformer leakage inductance, L_m: transformer magnetizing inductance, R_d: diode ON resistance, R_{LS}: secondary-side winding resistance, $R_S = R_d + R_{LS}$: total secondary resistance, V_d: diode forward voltage drop, and N_p/N_s: transformer turns ratio.

A detailed analysis included in [11] shows that flyback circuits with typical parasitic components can be analyzed under ideal conditions (no parasitic components) without giving rise to relevant errors in the calculation of system trajectories. So, a simplified version of a flyback converter will be used, just considering a transistor Q, a diode d, a flyback transformer T with magnetizing inductance L_m, as well as input and output capacitors, C_{in} and C_o. The magnetizing inductance and output capacitance determine the dynamic behavior of the flyback converter [7]. A general solution for the dynamic flyback behavior is obtained after a normalization of the main variables, which allows a scale change of the differential equations [16]. Due to the transformer, it is necessary to relate the system parameters to one side. In this case the secondary side is chosen.

The normalization process requires the definition of nominal voltage, nominal impedance and nominal frequency as reference values. The nominal reference output voltage is defined as $V_r = v_o$. The characteristic nominal reference impedance Z_r is defined considering the combined nominal magnetizing inductance referred to the secondary side and the nominal output capacitor: $\overline{Z_o} = \left(N_s / N_p\right)\sqrt{\overline{L}_m / \overline{C}_o}$. The reference frequency f_r is defined as the natural frequency $\overline{f_o} = \left(N_p / N_s\right) / \left(2\pi\sqrt{\overline{L}_m.\overline{C}_o}\right)$.

The normalizing equations of the voltage, current and time variables as well as their derivatives for the secondary variables are as follows:

$$v_n = \frac{v}{V_r}, \qquad dv_n = \frac{dv}{V_r}, \tag{1}$$

$$i_n = i\frac{Z_r}{V_r}, \qquad di_n = di\frac{Z_r}{V_r}, \tag{2}$$

$$t_n = t.f_r, \qquad dt_n = dt.f_r, \tag{3}$$

where the standard voltage, current and time variables of the secondary side are v, i, and t, and v_n, i_n, and t_n are their normalized versions. To normalize primary variables, the normalizing equations must be reflected back to the primary side as follows:

$$v_n = \frac{v}{V_r}\frac{N_s}{N_p}, \qquad i_n = i\frac{Z_r}{V_r}\frac{N_p}{N_s}, \tag{4}$$

$$dv_n = dv\frac{N_s}{V_r N_p}, \qquad di_n = di\frac{Z_r}{V_r}\frac{N_p}{N_s}. \tag{5}$$

The nominal parameters used for the normalization process, $\overline{C}_o$, $\overline{L}_m$ may differ from the actual converter parameters L_m and C_o.

The two possible states of the transistor Q determine two natural behaviors for the circuit which depend on the generic initial conditions, input voltage and output current. The normalized OFF- and ON-state general natural trajectories evolve on the plane i_{mn} vs. v_{on}. Signal i_{mn} is equivalent to the normalized primary current i_{pn} when Q = ON, and to the normalized secondary current i_{sn} when Q = OFF.

5.3.A OFF-State Trajectory

During the OFF-state of transistor Q, the energy stored in the transformer during the ON-state is transferred to the load through diode d. The primary equivalent voltage, applied to the magnetizing inductance, is the output voltage multiplied by the transformer turns ratio.

The locus of the OFF-state trajectory is the solution of:

$$\lambda_{OFF} := v_{on}^2 \frac{\alpha}{\beta} + \left(i_{mn} - i_{on}\right)^2 - A^2 - B^2 = 0, \tag{6}$$

where $\alpha = \overline{L}_m / L_m$, $\beta = \overline{C}_o / C_o$, $A = i_{mn}\left(0^-\right) - i_{on}$ and $B = \frac{1}{2\pi\sqrt{\alpha\beta}} \frac{di_{mn}\left(0^-\right)}{dt_n}$.

5.3.B ON-State Trajectory

When transistor *Q* is ON, the magnetizing inductance is connected to the input voltage source and the diode in the secondary side is reverse biased. The natural trajectory is given by:

$$\lambda_{ON} := i_{mn} + \frac{\alpha}{\beta} \frac{v_{inn}}{i_{on}} v_{on} - H = 0, \tag{7}$$

where the constant *H* depends on the initial conditions selected for starting the ON-trajectory.

The loci λ_{OFF} and λ_{ON} are the natural trajectories of the system when the switch is OFF and ON, respectively. The switching times of *Q* determine the initial conditions for each locus. By properly selecting the ON-and OFF-switching times, the NSS can be selected to lead the converter to the target operating condition.

5.3.C Selection of the Target Point for Operation in BCM

To maintain the converter operating in BCM for all loading conditions, the initial conditions of λ_{ON} and λ_{OFF} in (6) and (7) should be selected for the natural trajectories to contain a specific target operating point. BCM operation requires that the target normalized magnetizing current be zero. The target voltage V_{TPn} for the normalized output voltage is selected in order to have the desired output RMS voltage equal to the reference voltage V_r. The normalized BCM ON-state trajectory noted as σ_{ON} is given by:

$$\sigma_{ON} := i_{mn} + \frac{\alpha}{\beta}\frac{v_{INn}}{i_{on}} v_{on} - \frac{\alpha}{\beta}\frac{v_{INn}}{i_{on}} V_{TPn} = 0. \quad (8)$$

The complete normalized BCM OFF-state trajectory σ_{OFF} is defined as follows:

$$\sigma_{OFF} := \frac{\alpha}{\beta} v_{on}^2 + \left(i_{mn} - i_{on}\right)^2 - \frac{\alpha}{\beta} V_{TPn}^2 - i_{on}^2 = 0, \quad (9)$$

where v_{on} and i_{on} are the normalized output voltage and current, i_{mn} is the normalized magnetizing current, and α/β collects the estimated parameter variations.

5.3.D BCM Control Law

The goal of the control law is to force the converter to move to and stay on the identified NSS trajectories for each state of transistor Q and the above conditions. Basically, the control law decides between two options: either Q should be turned ON or OFF, based on the current state of transistor Q and the relative location of the current operating point with respect to the NSS trajectories.

The control law in BCM mode is detailed in [11] and briefly explained below for completeness. While Q is ON, the converter state moves up the i_{mn} vs. v_{on} plane. If the converter is currently operating below σ_{OFF}, Q is kept ON if $v_{on} \leq V_{TPn}$ while the converter continues to move up the plane until σ_{OFF} is reached. Then, Q is turned OFF. If the converter were operating anywhere above σ_{OFF}, Q should be turned OFF.

Since the objective is to operate in BCM, once Q has been switched OFF, it is not allowed to switch back ON until i_{mn} = 0 p.u. and $v_{on} \leq V_{TPn}$, where the ON-state trajectory starts again.

In resume, the control law is defined based on the previously calculated BCM trajectories as:

- If Q = OFF, i_{mn} = 0 and v_{on} <= 1 then Q = ON
- If Q = ON and σ_{OFF} >= 0 then Q = OFF

As seen from the definition of σ_{OFF}, its evaluation requires the knowledge of v_{on}, i_{on} and α/β. The following section shows how to estimate those variables from measurements done on the primary side, and the estimated parameter α/β is obtained from an adaptive algorithm.

5.4 ESTIMATION OF ISOLATED MEASUREMENTS AND PARAMETER UNCERTAINTIES

Avoiding insolated measurements is critical when it is desired to increase the reliability and reduce the complexity and cost of a system. In the case of a flyback converter, the output voltage v_o, output current i_o, and transformer secondary current i_s are the insulated measurements that many control approaches use to perform correctly. In the proposed novel solution, the drain voltage v_{drainn} is used to estimate all the needed insulated measurements for the boundary control using the natural switching surfaces of the converter. Therefore, the shape of the v_{drainn} signal must be maintained free of any distortion. Auxiliary snubber circuits may happen to be necessary for this, as shown later. This section explains in detail how the estimation of the required variables is done. Finally, the proposed control diagram is presented in Fig. 5.2.

5.4.A Approach to estimate v_{on}

By measuring v_{drainn}, the output voltage can be indirectly obtained during the OFF-time when $i_{sn} > 0$ since $v_{drainn} = v_{inn} + v_{on}$ if Q = OFF and $i_{sn} \neq 0$. Therefore, $v_{on}^{*} = v_{drainn} - v_{inn}$ is an estimation of v_{on} during Q = OFF.

Since $v_{drainn} = 0$ when Q is ON, v_{on} cannot be estimated directly from the instantaneous v_{drainn} measurement. However, since dv_{on}/di_{mn} is constant during the ON-period (due to (7), as can also be seen in Fig. 5.3(a) below), the following expression derived from (7) is obtained to estimate v_{on} when Q is ON:

$$v_{on}^{*} = v_{drainn,0} - V_{inn} - \frac{i_{pm} i_{on}^{*}}{V_{inn}} \frac{\beta}{\alpha} > 0, \tag{10}$$

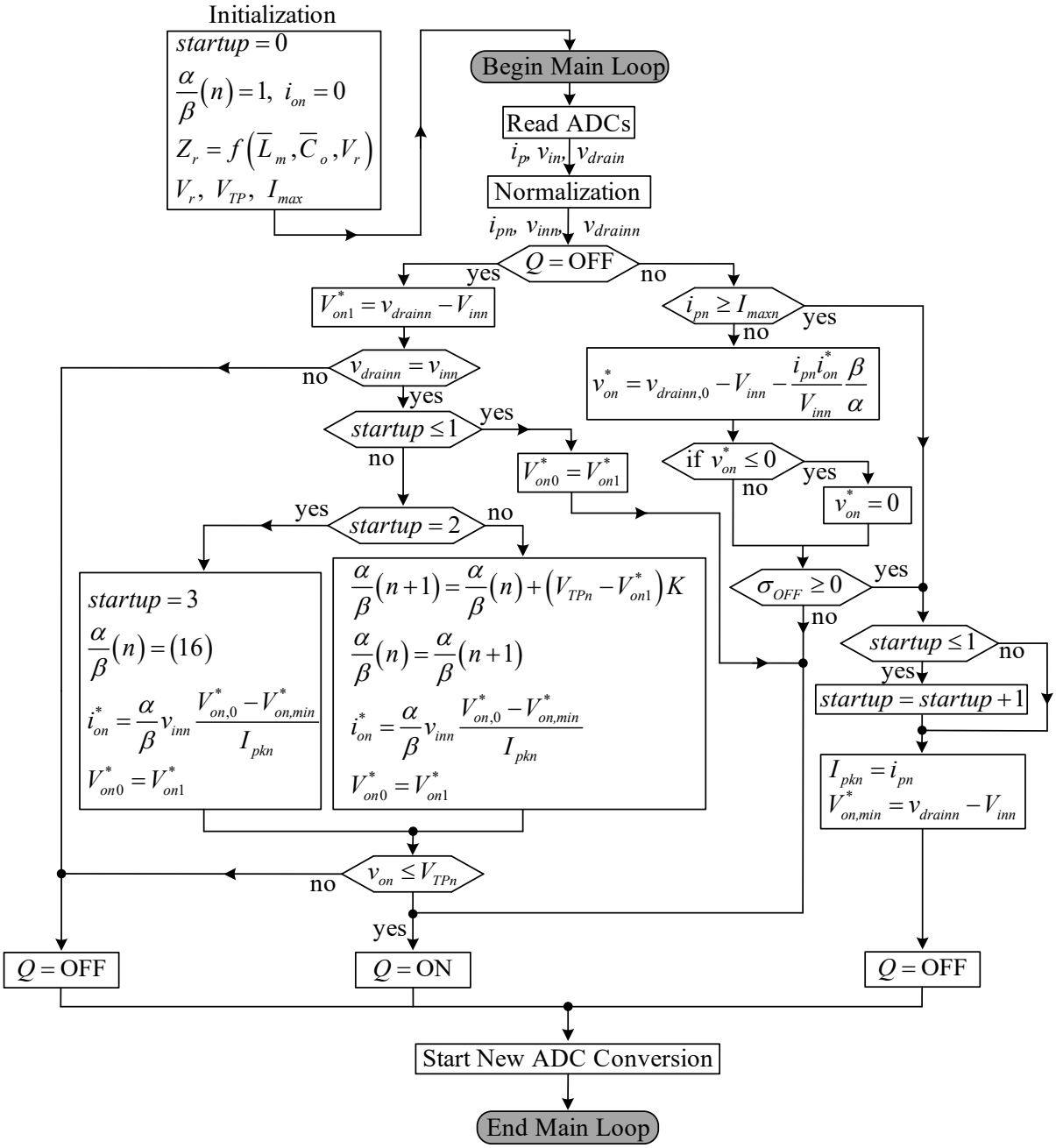

Fig. 5. 2. Flow diagram of the sensorless adaptive BCM NSS control law.

where $v_{drainn,0}$ is the value of v_{drainn} before Q turns ON, and i_{on}^* is the estimated value of the output current whose derivation is shown later. It is worth noticing that only positive values for v_{on}^* are valid from (3).

5.4.A Approach to estimate i_{on}

During the ON-time, the normalized differential equations representing current and voltage dynamics, are [11]:

$$2\pi \frac{\overline{L}_m}{L_m} v_{inn} = \frac{di_{mn}}{dt_n}, \tag{11}$$

$$-2\pi \frac{\overline{C}_o}{C_o} i_{on} = \frac{dv_{on}}{dt_n}. \tag{12}$$

Since i_{on} and v_{inn} are considered to remain constant over a switching period, from (3) and (4), the derivative of i_{mn} and v_{on} respect to time is constant, as can be seen in any of the simulations and experiments in [11]. Dividing these two normalized equations, i_{on}^* can be expressed as:

$$i_{on}^* = -\frac{\alpha}{\beta} v_{inn} \frac{dv_{on}^*}{d_{imn}}. \tag{13}$$

An approximation for $\frac{dv_{on}^*}{d_{imn}}$ can be easily obtained upon considering that it is rather constant during the entire ON-period, as can be seen in Fig. 5.3. Therefore, $\frac{dv_{on}^*}{d_{imn}} \cong \frac{V_{on,0}-V_{on,min}}{I_{pkn}}$. The normalized peak primary current I_{pkn} is directly obtained from the measuring. The voltage values are obtained as follows: The voltage $V_{on,0}$ when $I_{mn} = 0$ is obtained by measuring v_{drainn} at the beginning of the ON-period and subtracting V_{inn}. Similarly, the voltage $V_{on,min}$ when $I_{mn} = I_{pkn}$ is obtained by measuring v_{drainn} at the end of the ON-period and subtracting V_{INn}. The estimation of i_{on} is performed after the end of each OFF-period, once α/β is updated, as:

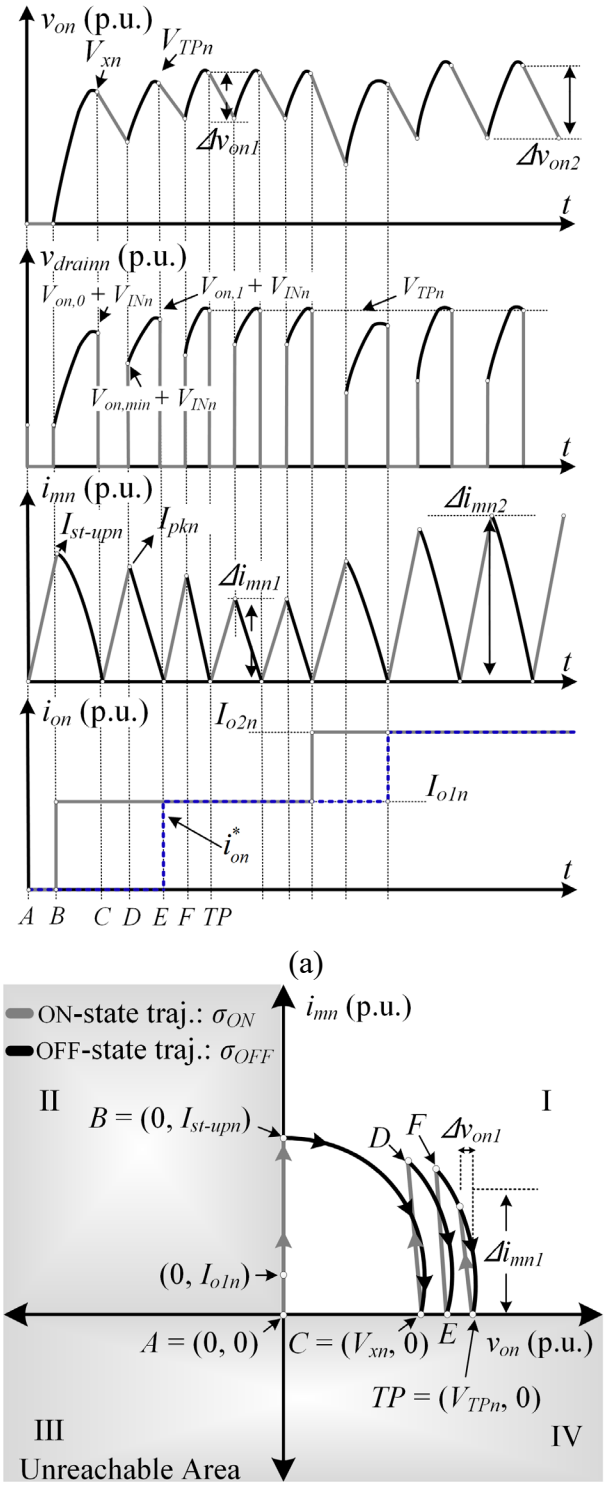

Fig. 5. 3(a) Normalized output voltage v_{on}, drain source voltage v_{drainn}, magnetizing inductance current i_{mn}, and real and estimated output currents i_{on} and i^*_{on}. (b) NSS trajectories for the proposed sensorless flyback converter operating in BCM when $\alpha/\beta = 1$.

$$i_{on}^{*} = \frac{\alpha}{\beta} v_{inn} \frac{V_{on,0} - V_{on,min}}{I_{pkn}} = \frac{\alpha}{\beta} v_{inn} \frac{V_{drainn,0} - V_{drainn,min}}{I_{pkn}}. \quad (14)$$

As soon as the switch Q is OFF, the energy stored in the transformer magnetizing inductance creates a current in the secondary winding, turning ON the diode d and thus charging the output capacitor. The phenomenon creates also a transient response which produces undesired oscillations in the current and voltage waveforms due to the existence of parasitic elements such as the drain-source capacitance and the transformer leakage inductance. The parasitic oscillations will perturb the measurement of v_{drainn} unless they are adequately damped. Since, v_{drainn} is usually a noisy signal, designing a snubber circuit correctly is fundamental to preserve the shape of the v_{drainn} waverform. The design process is shown in the Appendix 5.9.A.

5.4.B Approach to estimate α/β

The first estimation of α/β is implemented at the end of the second switching action after start-up conditions, and an adaptation is performed cycle by cycle as will be shown below.

During the first switching cycle in start-up conditions, no estimation for α/β is performed because the initial estimation of i_{on} will be wrong if the load is connected to the output of the flyback converter, and that affects the estimation of α/β. Therefore, during the first switching cycle $i_{on}^{*} = 0$ and $\alpha/\beta = 1$.

In the second switching cycle, once Q turns OFF, the flyback converter evolves on its actual OFF-trajectory, as described in (6), with initial conditions $(i_{mn}, v_{on}) = (I_{pkn}, V_{on,min})$. By replacing the point where the i_{mn} axis is intersected $(i_{mn}, v_{on}) = (0, V_{on,1})$, the following expression for α/β is obtained:

$$\frac{\alpha}{\beta} = \frac{I_{pkn}\left(I_{pkn} - 2i_{on}^{*}\right)}{V_{on,1}^{2} - V_{on,\min}^{2}}. \quad (15)$$

By replacing (6) in (15) and solving for α/β, an expression that only depends on measured parameters is found as:

$$\frac{\alpha}{\beta}=\frac{I_{pkn}^2}{V_{on,1}^2-V_{on,min}^2+2V_{inn}\left(V_{on,0}-V_{on,min}\right)}. \tag{16}$$

Equation (16) provides the first estimation for α/β. Then, i_{on}^* is calculated from (14) at the end of the switching period.

Later, as presented in [11], the ratio α/β can be adapted following a recursive procedure

$$\frac{\alpha}{\beta}(n+1)=\frac{\alpha}{\beta}(n)+K\left(V_{TPn}-V_{on}^*(n)\right), \tag{17}$$

where the constant K is a real number selected by the designer, $\alpha/\beta(n)$ and V_{on}^* are the actual values of the parameter ratio and measured target point voltage to obtain the future value $\alpha/\beta(n+1)$. A brief description and justification of the adaptation algorithm is presented in the mentioned reference. This adaptive adjustment is designed by proper selection of constant K so to provide a smooth and extremely slow variation of the parameters, which in real life change mainly due to aging of the components.

5.4.C Approach to estimate $i_{sn} = 0$

Ideally, when $i_{sn} = 0$, the diode d turns OFF and $v_{drainn} = V_{inn}$. However, v_{drainn} will oscillate around V_{inn} due to the presence of the parasitic components. A circuit that detects the oscillation in v_{drainn} (the moment when $i_{sn} = 0$) is shown in the Appendix 5.9.B.

5.4.D Start-up and steady-state characteristics

The normalized trajectories and main waveforms for the sensorless flyback converter operating in BCM are shown in Fig. 5.3. At startup conditions (point A, Fig. 5.3(b)), i_{mn}, v_{on}, and i_{on} are zero. When Q turns ON, i_{mn} starts rising while v_{on} remains at zero. At point B, σ_{ON} intersects σ_{OFF} and Q

turns OFF. If the load is connected, since σ_{OFF} was calculated with i_{on} equals zero, intersection of the OFF-trajectory with the v_{on} axis (point C) will be at a point lower than the target point. At this point no estimation of i_{on} and α/β is performed because from (6) i_{on}^{*} is zero which will generate errors in the calculation of α/β. However, the value of v_{on} is estimated from v_{drainn} ($v_{on,0}^{*}$ is saved). Then, Q turns ON until σ_{OFF} is intersected (point D) and I_{pkn} and $v_{on,min}^{*}$ are saved. Q turns back OFF until i_{mn} equals zero (point E). Since σ_{OFF} was calculated with i_{on} equals zero, the intersection of the OFF-trajectory is produced at a voltage lower than the target one V_{TPn}. At point E, after v_{on} is estimated as $v_{on,1}^{*}$, α/β and i_{on}^{*} are calculated for the first time from (6) and (16), and Q turns back ON.

Q turns OFF when σ_{OFF} is intersected at point F, and new values for I_{pkn} and $v_{on,min}^{*}$ are obtained. Since this time σ_{OFF} was calculated with the estimation of i_{on}, the intersection with the v_{on} axis will be at the voltage target point V_{TPn} and steady-state conditions are reached. Then, at the end of each switching period, a new calculation of i_{on} is performed, and α/β is adapted cycle by cycle based on the error to the target point. During steady-state conditions, in case of a sudden load change, i_{on} can be estimated in a single switching action if the load is kept stable during a switching period.

5.5 SIMULATION RESULTS

Simulations using Matlab/Simulink™ for a flyback converter with electrical parameters from Table 5.I and nominal components from Table 5.II are presented under different α/β conditions using the proposed sensorless BCM NSS control scheme shown in Fig. 5.2. To consider a realistic situation, the sampling frequency of the analog signals is selected to be 200 kHz.-First, a case with ideal conditions ($\alpha/\beta = 1$) is analyzed and presented in Fig. 5.4. After the start-up, at the end first switching cycle there is no calculation of i_{on}, and α/β remains equal to one. The first estimations

TABLE 5. I
FLYBACK CONVERTER PARAMETERS

Parameter	*Value*
v_o	24 V
v_{in}	6 V
i_o	0.5 A

TABLE 5. II
EXPERIMENTAL PROTOTYPE CHARACTERISTICS

Parameter	*Value*
Transformer T	Coilcraft® NA5919-AL L_m = 45.8 µH, n = 4, I_{sat} = 13.6 A @ L_m = 38.5 µH
Transistor Q	Vishay® IRFP140PBF V_{dss} = 100 V, I_D = 31 A @ 25 °C
Diode D	Vishay® VS-8TQ100PBF V_R = 100 V, I_D = 8 A, V_F = 0.58 V
Output Capacitor C_o	10.52 µF Film

of α/β and i_{on} are performed using (6) and (16) at the end of the second switching cycle. The estimation of i_{on} has an error of 1.57% and the one of α/β and error of 1.45%. At approximately 0.7 ms, just before Q turns ON, a sudden load increment of 71.42% is applied to the converter, and in a single switching period, the current is estimated with an error of only 1.58 %. At 1.25 ms the load decreases to 37.5% of its current value, creating a discontinuous conduction mode operation (DCM). The latter is because σ_{OFF} was calculated for a much higher current which made the inductor to overcharge, producing an output overvoltage, so Q was not allowed be turned back ON until $v_{on} \leq V_{TPn}$. Once the current is stable for a switching period, the estimation of i_{on} is satisfactory with an error of only 1.55%. Then, the converter returns to BCM.

A case when α/β = 4 is shown in Fig. 5.5. Like the case when α/β = 1, during the first two cycles i_{on}^{*} = 0 and α/β = 1. At the end of the second switching period, the first calculation of i_{on} is

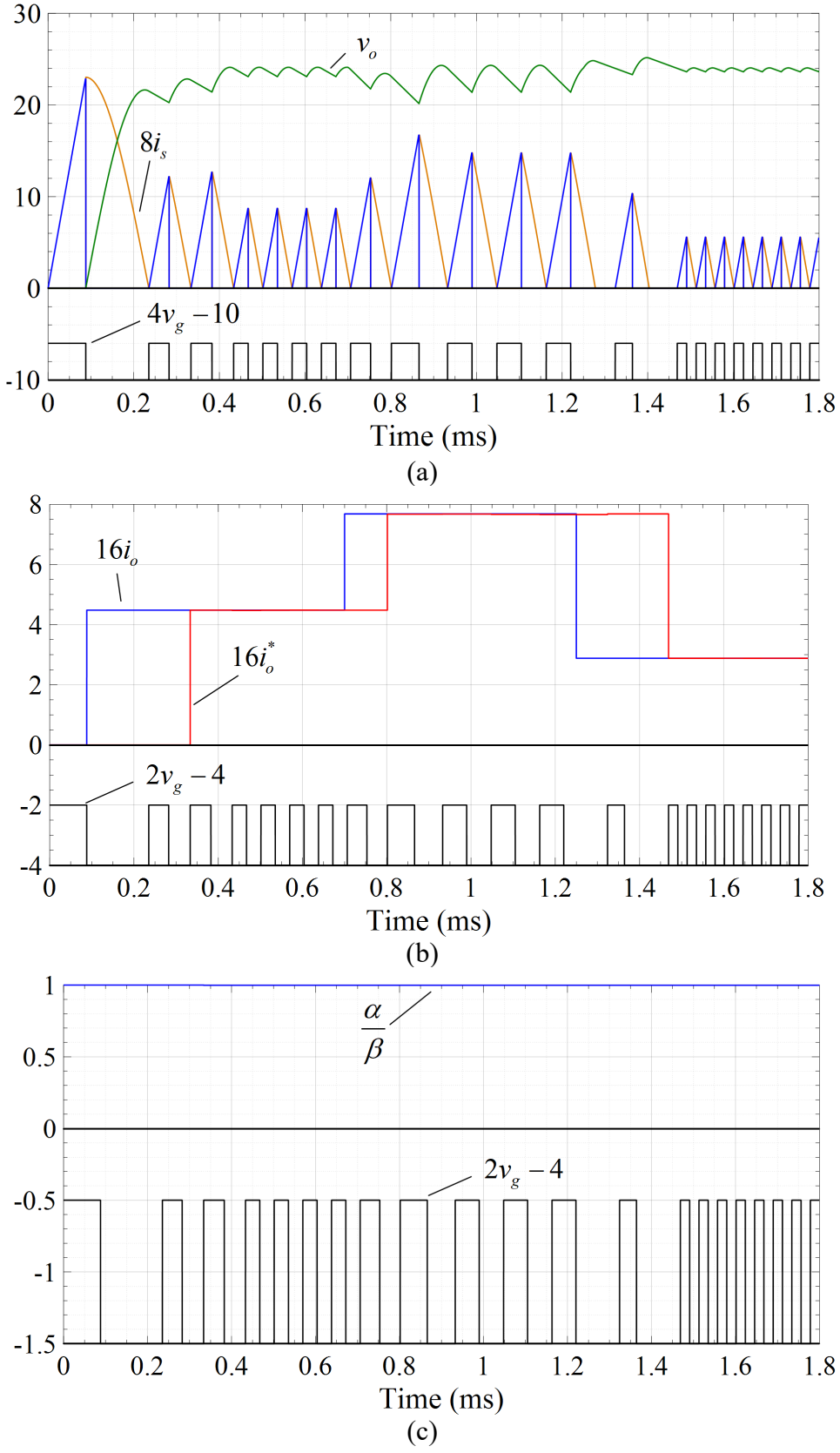

Fig. 5. 4. Simulation results of BCM NSS control law under ideal conditions.

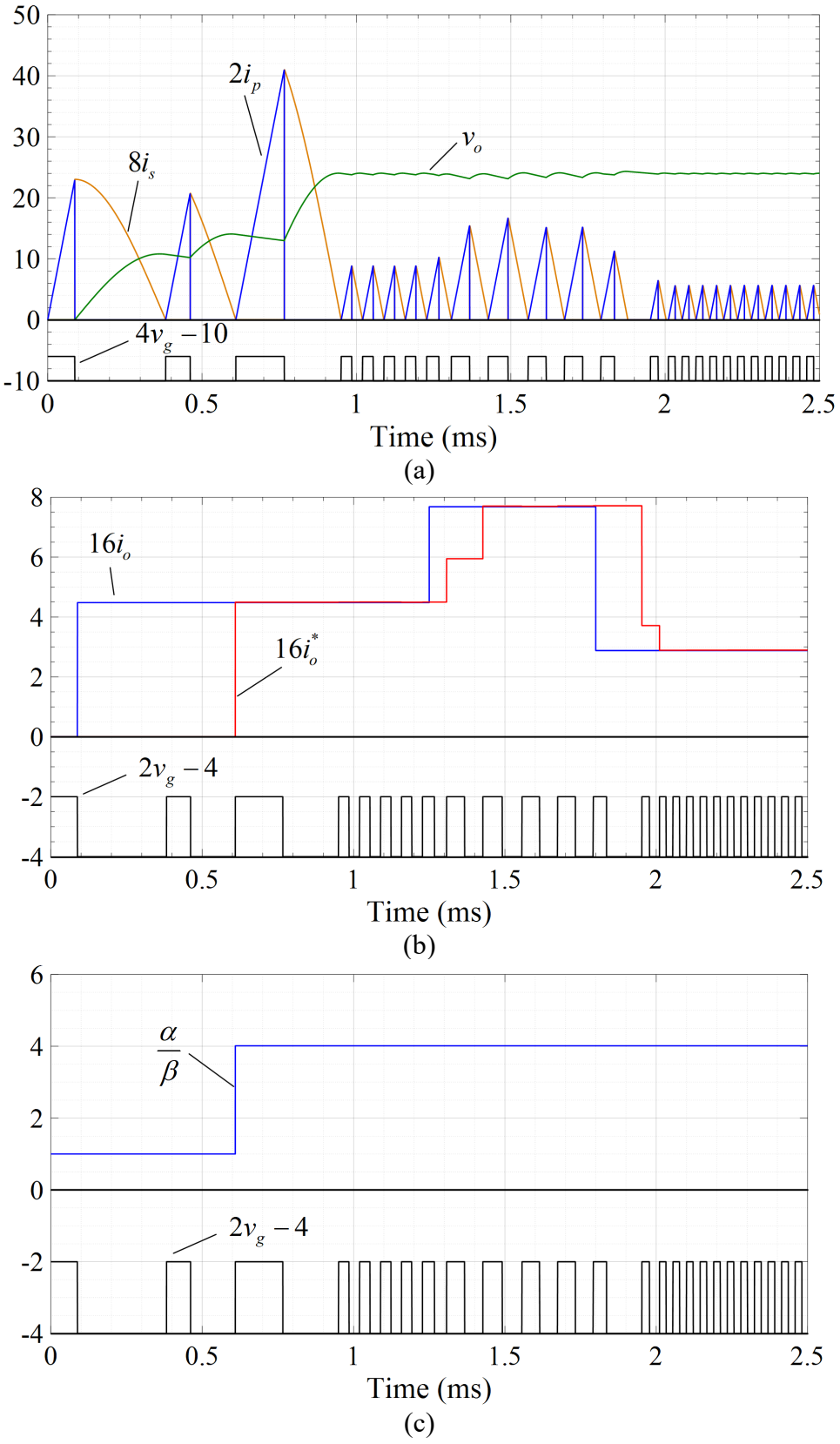

Fig. 5. 5. Simulation results of BCM NSS control law under $\alpha/\beta = 4$.

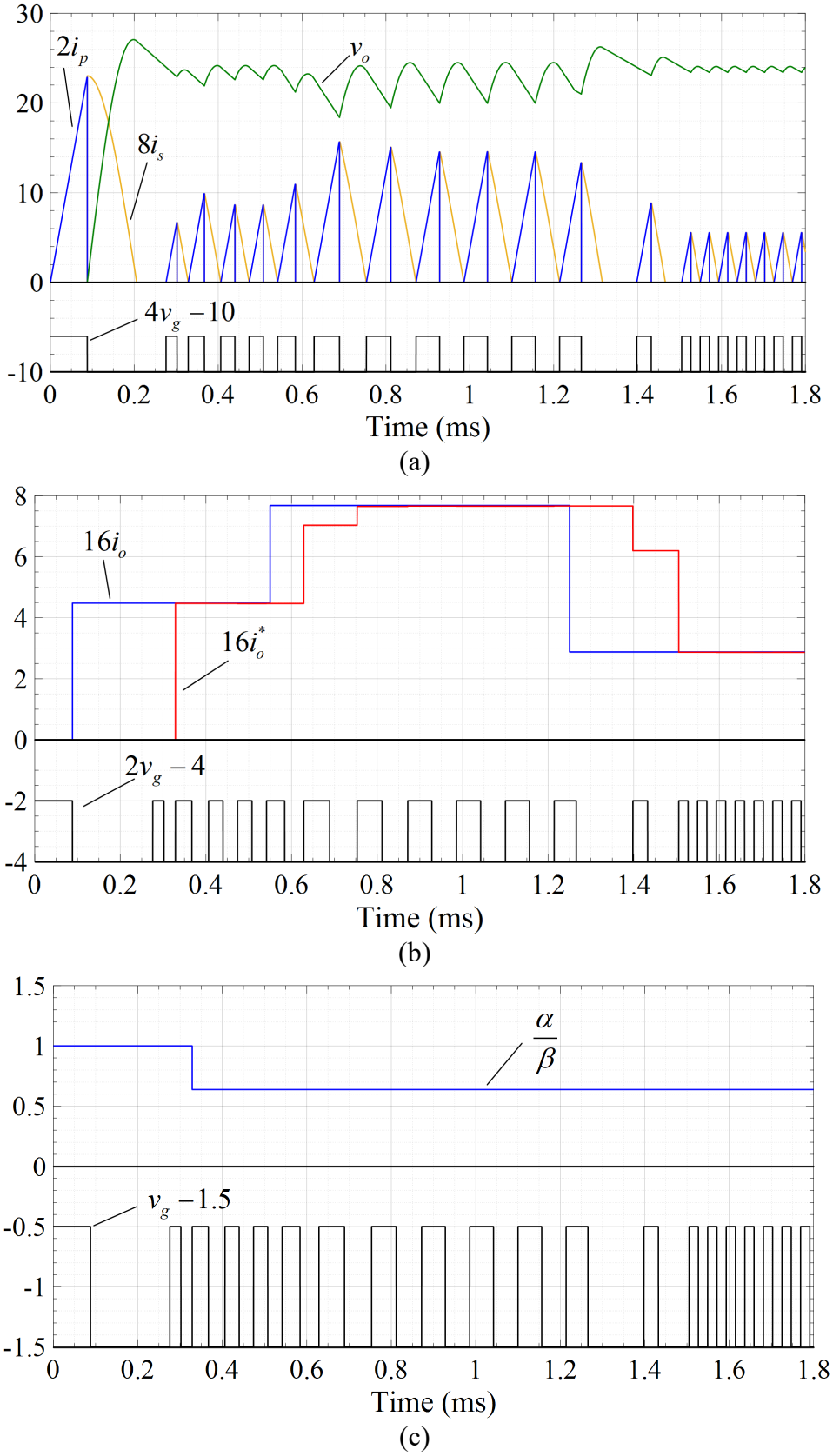

Fig. 5. 6. Simulation results of BCM NSS control law under $\alpha/\beta = 0.64$.

performed as seen in Fig. 5.5(b) with an error of only 0.96%. At the same time, the first estimation of α/β is completed with an error of 0.82% (see Fig. 5.5(c)). When the load increases from 0.28 A to 0.48 A, i_{on} is estimated with an error of 0.94%. When the load decreases from 0.48 A to 0.18 A, the first estimation of i_{on} is 0.1817 A which represents a 0.94% of error.

The last case is when $\alpha/\beta = 0.64$ as shown in Fig. 5.6. The first estimation of i_{on} has an error of 9.07% while the first estimation of α/β has an error of 8.95%. When i_{on} increases from 0.28 A to 0.48 A, i_{on}^{*} equals 0.52 A which represents a 9.06% of error. Lastly, when i_{on} decreases from 0.48 A to 0.18 A, i_{on}^{*} equals 0.1963 A which represents a 9.05% of error.

5.6 CONCLUSIONS

A novel sensorless control approarch for a flyback converter operating in the boundary conduction mode using the natural switching surfaces with parameter uncertainties was proposed in this paper. All the isolated measurements used in the conventional adaptive control approach were estimated by measuring the variables at the primary side of the transformer. Therefore, the required number of sensors not only got reduced but also isolated measurements were not required.

The proposed sensorless approach was able to indirectly measure and estimate the output voltage v_o, the output current i_o, the moment when the secondary currents i_s becomes zero, and the converter parameter variations α/β. After startup conditions, the controller was able to estimate i_o and α/β in only two switching cycles with a minimum error for different operating conditions. During steady-state conditions, the controller was able estimate a sudden load change in a single switching cycle if the load is kept constant during an entire switching period.

5.7 ACKNOWLEDGEMENT

The authors are grateful to University of Arkansas, Universidad Nacional del Sur, and CONICET for the support of this research work.

5.8 REFERENCES

[1] M. Kazimierczuk, “Pulse-width Modulated DC–DC Power Converters”, First Edition, John Wiley & Sons, ISBN: 978-0-470-69465-7, 2008.

[2] Q. Wu and Z. Zhu, “An Adaptive High-Precision OCP Control Scheme for Flyback AC/DC Converters," *in IEEE Transactions on Power Electronics*, vol. 32, no. 12, pp. 8969-8973, Dec. 2017.

[3] C. Zhao, J. Zhang and X. Wu, “An Improved Variable On-Time Control Strategy for a CRM Flyback PFC Converter,” in *IEEE Transactions on Power Electronics*, vol. 32, no. 2, pp. 915-919, Feb. 2017.

[4] T. Yan, J. Xu, F. Zhang, J. Sha and Z. Dong, “Variable-On-Time-Controlled Critical-Conduction-Mode Flyback PFC Converter,” in *IEEE Transactions on Industrial Electronics*, vol. 61, no. 11, pp. 6091-6099, Nov. 2014.

[5] S. B. Kjaer, J. K. Pedersen and F. Blaabjerg, “A review of single-phase grid-connected inverters for photovoltaic modules,” in *IEEE Transactions on Industry Applications*, vol. 41, no. 5, pp. 1292-1306, Sept.-Oct. 2005.

[6] A. C. Kyritsis, E. C. Tatakis and N. P. Papanikolaou, “Optimum Design of the Current-Source Flyback Inverter for Decentralized Grid-Connected Photovoltaic Systems,” in *IEEE Transactions on Energy Conversion*, vol. 23, no. 1, pp. 281-293, March 2008.

[7] L. A. Garcia-Rodriguez, E. Williams, J. C. Balda, J. Gonzalez-Llorente and H. Chiacchiarini, "Control of a flyback converter operating in BCM using the natural switching surface," *2015 IEEE 6th International Symposium on Power Electronics for Distributed Generation Systems (PEDG)*, Aachen, 2015, pp. 1-8.

[8] L. A. Garcia Rodriguez and J. C. Balda, “A comparison of isolated DC-DC converters for microinverter applications,” *2013 Twenty-Eighth Annual IEEE Applied Power Electronics Conference and Exposition (APEC)*, Long Beach, CA, USA, 2013, pp. 2084-2091.

[9] G. Spiazzi, D. Tagliavia and S. Spampinato, “DC-DC flyback converters in the critical conduction mode: a re-examination,” Conference Record of the *2000 IEEE Industry Applications Conference. Thirty-Fifth IAS Annual Meeting and World Conference on Industrial Applications of Electrical Energy (Cat. No.00CH37129)*, Rome, 2000, pp. 2426-2432 vol.4.

[10] B. T. Irving, Y. Panov and M. M. Jovanovic, “Small-signal model of variable-frequency flyback converter,” *Applied Power Electronics Conference and Exposition, 2003. APEC '03. Eighteenth Annual IEEE*, Miami Beach, FL, USA, 2003, pp. 977-982 vol.2.

[11] L. A. Garcia Rodriguez, H. G. Chiacchiarini, D. Carballo Rojas and J. C. Balda, “Adaptive Boundary Control Using Natural Switching Surfaces for Flyback Converters Operating in the Boundary Conduction Mode with Parameter Uncertainties,” in *IEEE Transactions on Power Electronics*, vol. 34, no. 8, pp. 8118-8137, Aug. 2019.

[12] Gab-Su Seo, Jong-Won Shin, Bo-Hyung Cho, and Kyu-Chan Lee, “Digitally Controlled Current Sensorless Photovoltaic Micro-Converter for DC Distribution”, *IEEE Transactions on Industrial Informatics*, vol. 10, no. 1, pp. 117-126, Feb. 2014.

[13] Thorben Hoffstadt, Jürgen Maas, “Sensorless BCM control for a bidirectional flyback-converter”, IECON 2016 - *42nd Annual Conference of the IEEE Industrial Electronics Society*, Florence, Italy 23-26 Oct. 2016.

[14] Radin Za’im, Jafferi Jamaludin, and Nasrudin Abd, “Photovoltaic Flyback Microinverter With Tertiary Winding Current Sensing Rahim”, *IEEE Transactions on Power Electronics*, vol. 34, no. 8, pp. 7588 – 7602, Aug. 2019.

[15] J. M. Galvez, M. Ordonez, F. Luchino and J. E. Quaicoe, "Improvements in Boundary Control of Boost Converters Using the Natural Switching Surface," in *IEEE Transactions on Power Electronics*, vol. 26, no. 11, pp. 3367-3376, Nov. 2011.

[16] M. Ordonez, M. T. Iqbal and J. E. Quaicoe, "Selection of a curved switching surface for buck converters," in *IEEE Transactions on Power Electronics*, vol. 21, no. 4, pp. 1148-1153, July 2006.

5.9 APPENDICES

5.9.A Snubber Design for Flyback Converters: When the V_{ds} Waveform Matters

5.9.A.(1) Drain-source waveform calculation

Fig. 5.7 and Fig. 5.8 show the schematic circuit of a flyback converter with parasitic components before and after the switch Q is opened. Before transistor Q turns OFF, the current flowing through the primary winding of the transformer i_p is equal to the magnetizing current i_m and has a peak magnitude of I_{mpk} (Fig. 5.7).

If Q turns OFF and immediately the diode d turns ON, i_m flows to the secondary side and charges the output capacitor while the energy stored in the leakage inductance L_k will make L_k to resonate with the transistor output capacitance C_{ds} (Fig. 5.8).

The time response of $v_{drain}(t)$ during the natural oscillation driven by the opening of switch Q is obtained by circuit analysis. Analyzing the transformer primary side, the circuit equations expressed in Laplace Transform are:

$$\frac{V_{in}}{s} - I_p(s)\left(R_{Lp} + R_{on}\right) - L_k\left(sI_p(s) - i_p\left(0^-\right)\right) - V_p(s) - V_{drain}(s) = 0, \tag{18}$$

$$I_p(s) = C_{ds}\left(sV_{ds}(s) - v_{drain}\left(0^-\right)\right). \tag{19}$$

By replacing (19) in (18), and the initial conditions $i_p(0^-) = I_{mpk}$ and $v_{drain}(0^-) = 0$, the following equation is obtained:

$$\frac{V_{in}}{s} - \left(s^2 L_k C_{ds} + sC_{ds}\left(R_{Lp} + R_{on}\right) + 1\right)V_{drain}(s) + L_k I_{mpk} - V_p(s) = 0. \tag{20}$$

By considering that the output voltage v_o is constant during the ON-OFF transition time,

$$V_p(s) = -\frac{n\left(V_o + V_d + I_o\left(R_{Ls} + R_d\right)\right)}{s}. \tag{21}$$

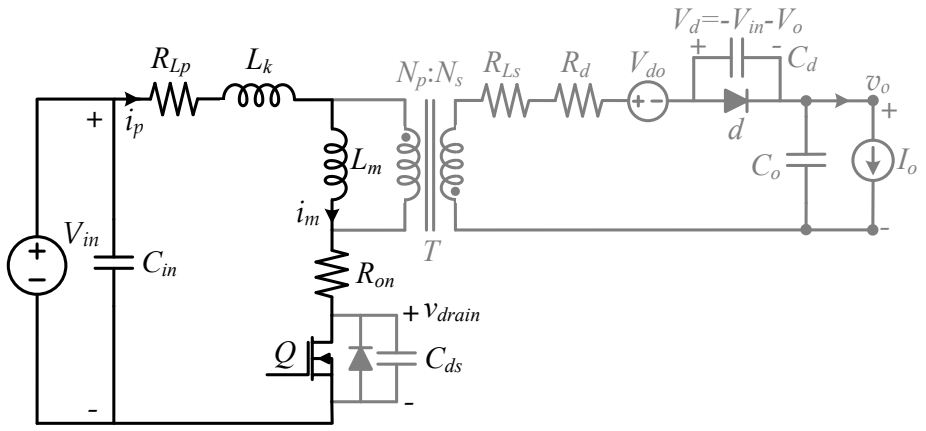

Fig. 5. 7. Flyback equivalent circuit during the ON-time.

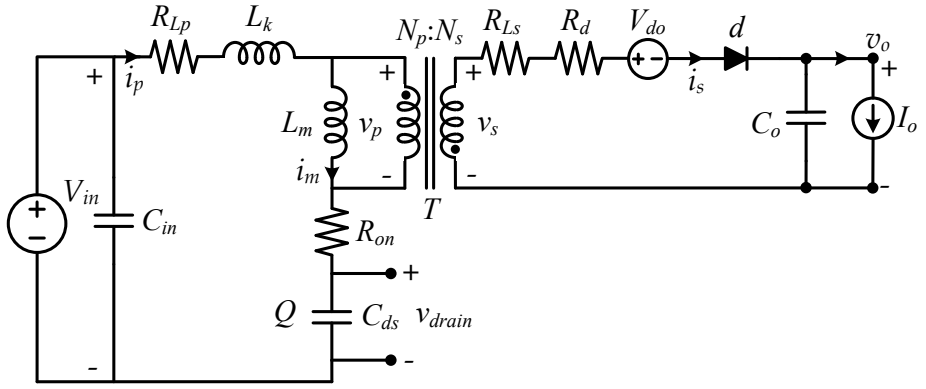

Fig. 5. 8 Flyback equivalent circuit in the transition between ON- and OFF-times.

By replacing (21) in (20), and solving for $V_{drain}(s)$, the following is obtained:

$$v_{drain}(s) = I_{mpk} L_k \frac{\dfrac{1}{L_k C_{ds}}}{s^2 + s\dfrac{R_{Lp}+R_{on}}{L_k} + \dfrac{1}{L_k C_{ds}}} + \frac{\dfrac{V_{in} + n\left(V_o + V_d + I_o\left(R_{Ls}+R_d\right)\right)}{L_k C_{ds}}}{s\left(s^2 + s\dfrac{R_{Lp}+R_{on}}{L_k} + \dfrac{1}{L_k C_{ds}}\right)}. \qquad (22)$$

Then, defining $\omega_{no} = \dfrac{1}{\sqrt{L_k C_{ds}}}$ and $\xi_o = \dfrac{R_{Lp}+R_{on}}{2}\sqrt{\dfrac{C_{ds}}{L_k}}$, and considering that $\xi_o < 1$, $v_{drain}(t)$ is expressed as:

$$v_{drain}(t)=\left(V_{in}+n\left(V_o+V_d+I_o\left(R_{Ls}+R_d\right)\right)\right)+I_{mpk}L_k\frac{\omega_{no}e^{-\xi_o\omega_{no}t}}{\sqrt{1-\xi_o^2}}\sin\left(\omega_{no}\sqrt{1-\xi_o^2}t\right)$$
$$-\left(V_{in}+n\left(V_o+V_d+I_o\left(R_{Ls}+R_d\right)\right)\right)\frac{e^{-\xi_o\omega_{no}t}}{\sqrt{1-\xi_o^2}}\sin\left(\omega_{no}\sqrt{1-\xi_o^2}t+\tan^{-1}\left(\frac{\sqrt{1-\xi_o^2}}{\xi_o}\right)\right). \quad (23)$$

As for an arbitrary phase shift and for generic values of a, b, x, y, it is true that

$$a\sin(x)+b\sin(x+y)=c\sin(x+z), \quad (24)$$

$$c=\sqrt{a^2+b^2+2ab\cos(y)}, \quad (25)$$

$$z=\tan^{-1}\left(\frac{b\sin(y)}{a+b\cos(y)}\right). \quad (26)$$

Then, $v_{drain}(t)$ from (23) can be expressed as:

$$v_{drain}(t)=\left(V_{in}+n\left(V_o+V_d+I_o\left(R_{Ls}+R_d\right)\right)\right)+\overbrace{I_{mpk}L_k\frac{\omega_{no}e^{-\xi_o\omega_{no}t}}{\sqrt{1-\xi_o^2}}}^{a}\sin\left(\overbrace{\omega_{no}\sqrt{1-\xi_o^2}t}^{x}\right)$$
$$\overbrace{-\left(V_{in}+n\left(V_o+V_d+I_o\left(R_{Ls}+R_d\right)\right)\right)\frac{e^{-\xi_o\omega_{no}t}}{\sqrt{1-\xi_o^2}}}^{b}\sin\left(\overbrace{\omega_{no}\sqrt{1-\xi_o^2}t}^{x}+\overbrace{\tan^{-1}\left(\frac{\sqrt{1-\xi_o^2}}{\xi_o}\right)}^{y}\right). \quad (27)$$

The parameter c can be expressed as a function of the converter component values by replacing (23) and (24) in (25),

$$c^2=\left(I_{mpk}L_k\frac{\omega_{no}e^{-\xi_o\omega_{no}t}}{\sqrt{1-\xi_o^2}}\right)^2+\left(\left(V_{in}+n\left(V_o+V_d+I_o\left(R_{Ls}+R_d\right)\right)\right)\frac{e^{-\xi_o\omega_{no}t}}{\sqrt{1-\xi_o^2}}\right)^2$$
$$-2\left(I_{mpk}L_k\frac{\omega_{no}e^{-\xi_o\omega_{no}t}}{\sqrt{1-\xi_o^2}}\right)\left(\left(V_{in}+n\left(V_o+V_d+I_o\left(R_{Ls}+R_d\right)\right)\right)\frac{e^{-\xi_o\omega_{no}t}}{\sqrt{1-\xi_o^2}}\right)\cos\left(\tan^{-1}\left(\frac{\sqrt{1-\xi_o^2}}{\xi_o}\right)\right). \quad (28)$$

Similarly, z from (26) can expressed as function of the converter parameters as follows:

$$\tan(z)=\frac{-\left(V_{in}+n\left(V_o+V_d+I_o\left(R_{Ls}+R_d\right)\right)\right)\frac{e^{-\xi_o\omega_{no}t}}{\sqrt{1-\xi_o^2}}\sin\left(\tan^{-1}\left(\frac{\sqrt{1-\xi_o^2}}{\xi_o}\right)\right)}{I_{mpk}L_k\frac{\omega_{no}e^{-\xi_o\omega_{no}t}}{\sqrt{1-\xi_o^2}}-\left(V_{in}+n\left(V_o+V_d+I_o\left(R_{Ls}+R_d\right)\right)\right)\frac{e^{-\xi_o\omega_{no}t}}{\sqrt{1-\xi_o^2}}\cos\left(\tan^{-1}\left(\frac{\sqrt{1-\xi_o^2}}{\xi_o}\right)\right)} \quad (29)$$

By applying to (29) the following trigonometric identities, the following expression of z is found in (32):

$$\sin\left(\tan^{-1}(x)\right)=\frac{x}{\sqrt{1+x^2}}, \quad (30)$$

$$\cos\left(\tan^{-1}(x)\right)=\frac{1}{\sqrt{1+x^2}}. \quad (31)$$

$$\tan(z)=\frac{-\left(V_{in}+n\left(V_o+V_d+I_o\left(R_{Ls}+R_d\right)\right)\right)e^{-\xi_o\omega_{no}t}}{I_{mpk}L_k\frac{\omega_{no}e^{-\xi_o\omega_{no}t}}{\sqrt{1-\xi_o^2}}-\left(V_{in}+n\left(V_o+V_d+I_o\left(R_{Ls}+R_d\right)\right)\right)\frac{\xi_o e^{-\xi_o\omega_{no}t}}{\sqrt{1-\xi_o^2}}}. \quad (32)$$

Then $v_{drain}(t)$ can be expressed as function of the converter parameters as:

$$v_{drain}(t)=\left(V_{in}+n\left(V_o+V_d+I_o\left(R_{Ls}+R_d\right)\right)\right)+c\sin\left(\omega_{no}\sqrt{1-\xi_o^2}t+z\right). \quad (33)$$

Then, the upper and lower exponential decay limits of (27) can be found as:

$$v_{drain\_up}(t)=\left(V_{in}+n\left(V_o+V_d+I_o\left(R_{Ls}+R_d\right)\right)\right)+c, \quad (34)$$

$$v_{drain\_down}(t)=\left(V_{in}+n\left(V_o+V_d+I_o\left(R_{Ls}+R_d\right)\right)\right)-c. \quad (35)$$

Fig. 5.9 presents the drain to source voltage waveform $v_{drain}(t)$ using the parameters of Table 5.III (light gray) and considering no parasitic elements (dark gray). For the particular case of Table 5.III, the real $v_{drain}(t)$ signal has a peak value about 20 times greater than the ideal one. The oscillation frequency of the $v_{drain}(t)$ corresponds to approximately 8.275 MHz.

TABLE 5. III

EXPERIMENTAL PROTOTYPE CHARACTERISTICS

Parameter	*Value*
n	1/4
F_{sw}	20 kHz
I_{pk}	2.5 A
I_o	0.16 A
V_o	24 V
V_{in}	6 V
V_d	0.7 V
R_s	0.1 Ω
R_{1p}	0.05 Ω
R_{1s}	0.5 Ω
R_d	0.5 Ω
R_{on}	0.05 Ω
L_k	1.85 µH
L_m	45 µH
C_{ds}	200 pF

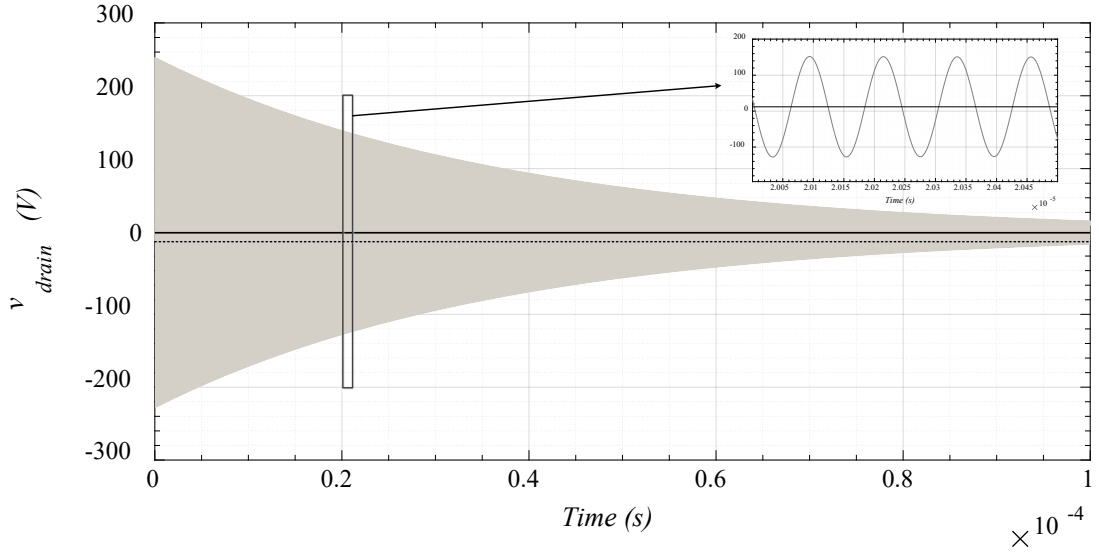

Fig. 5. 9. Drain source voltage V_{drain} as function of time using (27) for a flyback converter with the parameters of Table 5.III.

5.9.A.(2) Snubber Design

As seen from previous section, $v_{drain}(t)$ is a voltage signal that oscillates at a frequency $f = \omega_n/2\pi$, and whose peak could be multiple times higher than the same signal without parasitic elements. In the proposed control law, the signal $v_{drain}(t)$ is used to measure indirectly the output voltage v_o, to estimate the output current i_o, and to detect when the secondary side current i_s becomes zero. Therefore, $v_{drain}(t)$ should be kept as close as possible to the ideal case. Since, it is impossible to reduce up to zero the leakage inductance of the transformer and the output capacitance of the transistor, a snubber circuit should be added to the flyback converter to reduce the peak magnitude of $v_{drain}(t)$ and the oscillation frequency, as shown in Fig. 5.10.

Before turning Q OFF, the diode d was OFF, and the primary side current i_p was creating the magnetizing and leakage fluxes through the magnetizing L_m and leakage inductances L_k. When Q turns OFF, by assuming that d_s and d turns ON at the same time, the magnetizing flux creates the secondary current i_s while the leakage flux defines the current i_p according to the following equations (already transformed to the Laplace domain):

$$\frac{V_{in}}{s} - I_p(s)R_{Lp} - L_k\left(sI_p(s) - i_p\left(0^-\right)\right) - V_p(s) - V_{drain}(s) - C_{ds}R_{on}\left(sV_{drain}(s) - v_{drain}\left(0^-\right)\right) = 0, \quad (36)$$

$$I_p(s) = I_{Rs}(s) + I_{Cs}(s) + C_{ds}\left(sV_{drain}(s) - v_{drain}\left(0^-\right)\right), \quad (37)$$

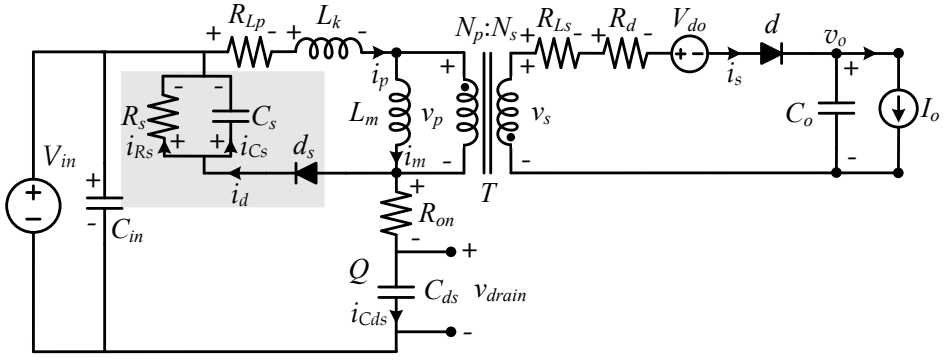

Fig. 5. 10. Flyback schematic circuit with a passive snubber.

$$I_{Rs}(s) = -\frac{V_{in}}{sR_s} + \frac{V_{drain}(s)}{R_s} + C_{ds}\frac{R_{on}}{R_s}\left(sV_{drain}(s) - v_{drain}\left(0^-\right)\right), \tag{38}$$

$$I_{Cs}(s) = C_s\left(sV_{Cs}(s) - v_{Cs}\left(0^-\right)\right), \tag{39}$$

$$V_{Cs}(s) = -\frac{V_{in}}{s} + V_{drain}(s) + C_{ds}R_{on}\left(sV_{drain}(s) - v_{drain}\left(0^-\right)\right), \tag{40}$$

$$V_p(s) = -n\frac{V_o + V_d + I_o\left(R_{Ls} + R_d\right)}{s}. \tag{41}$$

By replacing the initial conditions $v_{drain}(0^-) = 0$ V, $v_{Cs}(0^-) = 0$ V, and $i_p(0\text{-}) = I_{mpk}$ in (36) to (41), neglecting the transistor ON resistance R_{on} because of being significatively smaller than the usual snubber resistance R_s, and solving for $V_{drain}(s)$, the following equation is found:

$$V_{drainn}(s) = \frac{sV_{in} + \frac{V_{in}R_{Lp}}{L_k} + \frac{I_{mpk}}{C_s} + \frac{V_{in}}{C_sR_s} + \frac{V_{in} + V_{in}R_{Lp}/R_s + n(V_o + V_d + I_o(R_{Ls} + R_d))}{sL_kC_s}}{\frac{C_{ds} + C_s}{C_s}\left(s^2 + s\left(\frac{R_{Lp}}{L_k} + \frac{1/R_s}{C_{ds} + C_s}\right) + \frac{1 + R_{Lp}/R_s}{L_k\left(C_{ds} + C_s\right)}\right)}. \tag{42}$$

The steady-state value of $v_{drain}(t)$: = $V_{drain,ss}$ can be found by applying the final value theorem to (42):

$$V_{drain,ss} = \lim_{t\to\infty} v_{drain}(t) = \lim_{s\to 0} sV_{drain}(s) = \frac{V_{in} + V_{in}R_{Lp}/R_s + n\left(V_o + V_d + I_o\left(R_{Ls} + R_d\right)\right)}{\frac{1 + R_{Lp}/R_s}{C_sL_k}}. \tag{43}$$

Back to the time domain by Laplace anti-transforming (42), the following expression for $v_{drain}(t)$ is obtained:

$$v_{drain}(t) = -\frac{C_s V_{in}}{C_s + C_{ds}} \frac{e^{-\xi\omega_n t}}{\sqrt{1-\xi^2}} \sin\left(\omega_n \sqrt{1-\xi^2}\, t - \tan^{-1}\left(\frac{\sqrt{1-\xi^2}}{\xi}\right)\right)$$
$$+ \frac{R_s C_s V_{in} R_{Lp} + L_k\left(R_s I_{mpk} + V_{in}\right)}{R_s + R_{Lp}} \frac{\omega_n e^{-\xi\omega_n t}}{\sqrt{1-\xi^2}} \sin\left(\omega_n \sqrt{1-\xi^2}\, t\right) \tag{44}$$
$$+ \left(V_{in} + \frac{R_s n\left(V_o + V_d + I_o\left(R_{Ls} + R_d\right)\right)}{R_s + R_{Lp}}\right)\left(1 - \frac{e^{-\xi\omega_n t}}{\sqrt{1-\xi^2}} \sin\left(\omega_n \sqrt{1-\xi^2}\, t + \tan^{-1}\left(\frac{\sqrt{1-\xi^2}}{\xi}\right)\right)\right).$$

Where ω_n and ξ are calculated as:

$$\omega_n = \sqrt{\frac{R_s + R_{Lp}}{R_s\left(C_s + C_{ds}\right) L_k}}. \tag{45}$$

$$\xi = \frac{R_s R_{Lp}\left(C_s + C_{ds}\right) + L_k}{2\sqrt{R_s L_k\left(C_s + C_{ds}\right)\left(R_s + R_{Lp}\right)}}. \tag{46}$$

Since $R_s >> R_{Lp}$ and $C_s >> C_{ds}$, ω_n, ξ, and $v_{drain}(t)$ can be approximated as:

$$\omega_n \simeq \sqrt{\frac{1}{C_s L_k}}, \tag{47}$$

$$\xi = \frac{R_s R_{Lp} C_s + L_k}{2R_s\sqrt{L_k C_s}}. \tag{48}$$

$$v_{drain}(t) = -\frac{V_{in} e^{-\xi\omega_n t}}{\sqrt{1-\xi^2}} \sin\left(\omega_n \sqrt{1-\xi^2}\, t - \tan^{-1}\left(\frac{\sqrt{1-\xi^2}}{\xi}\right)\right)$$
$$+ \left(C_s V_{in} R_{Lp} + I_{mpk} L_k + \frac{V_{in} L_k}{R_s}\right) \frac{\omega_n e^{-\xi\omega_n t}}{\sqrt{1-\xi^2}} \sin\left(\omega_n \sqrt{1-\xi^2}\, t\right) \tag{49}$$
$$+ \left(V_{in} + n\left(V_o + V_d + I_o\left(R_{Ls} + R_d\right)\right)\right)\left(1 - \frac{e^{-\xi\omega_n t}}{\sqrt{1-\xi^2}} \sin\left(\omega_n \sqrt{1-\xi^2}\, t + \tan^{-1}\left(\frac{\sqrt{1-\xi^2}}{\xi}\right)\right)\right).$$

The oscillation frequency f_n ($\omega_n = 2\pi f_n$) should be chosen to be much higher than the converter switching frequency f_{sw}, so it does not affect the shape of the $v_{drain}(t)$ waveform. Also, the damping parameter ξ is selected to be closed to 1 to minimize oscillations. When $\xi \approx 1$, but not greater than

1, the small angle approximation for the trigonometric functions in (35) can be applied, so $v_{drain}(t)$ can be expressed as:

$$v_{drain}(t) \simeq -V_{in}\left(\omega_n t - \frac{1}{\xi}\right)e^{-\xi\omega_n t} + \left(C_s V_{in} R_{Lp} + L_k\left(I_{mpk} + \frac{V_{in}}{R_s}\right)\right)\omega_n^2 t e^{-\xi\omega_n t} + \left(V_{in} + n\left(V_o + V_d + I_o\left(R_{Ls} + R_d\right)\right)\right)\left(1 - e^{-\xi\omega_n t}\left(\omega_n t + \frac{1}{\xi}\right)\right). \tag{50}$$

From (47) and (48), the snubber components R_s and C_s can be expressed as function of the second order response parameters ω_n and ξ, and the flyback converter parasitic components L_k and R_{Lp} as:

$$C_s = \frac{1}{L_k \omega_n^2}, \tag{51}$$

$$R_s = \frac{\left(L_k \omega_n\right)^2}{2\xi L_k \omega_n - R_{Lp}}. \tag{52}$$

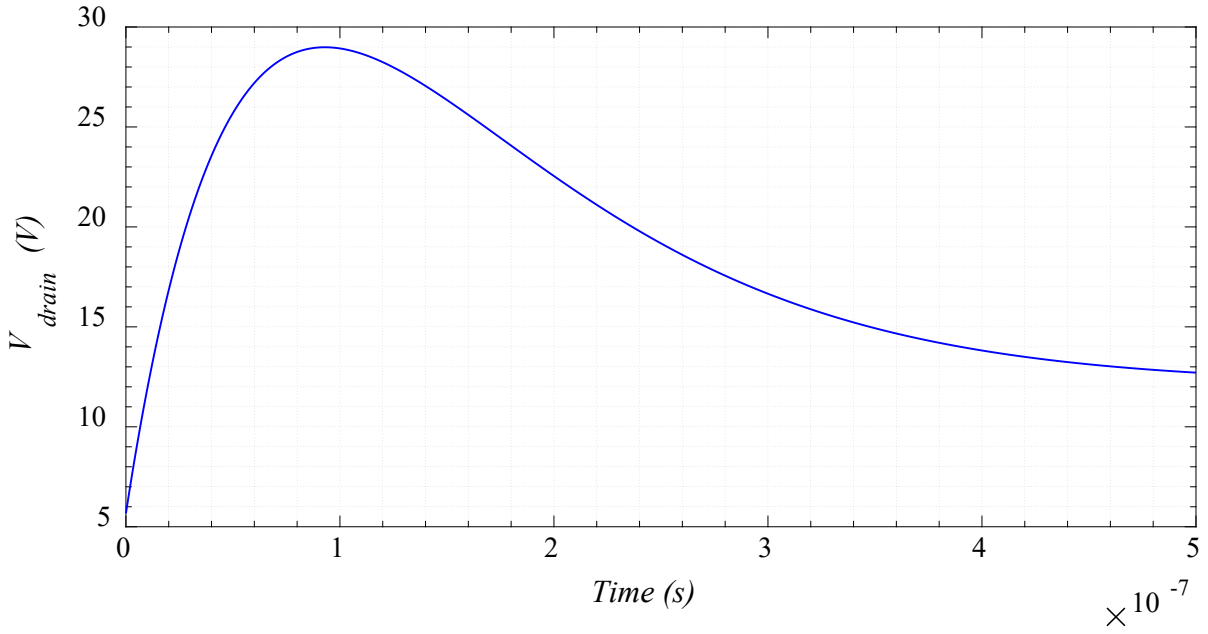

Fig. 5. 11. V_{drain} as function of time after connecting an RCD snubber with C_s = 3.42 nF and R_s = 11.75 Ω.

By using the parameters of Table 5.III, and considering that $\xi \approx 1$ and $f_n = 100 f_{sw}$, the Snubber components can be calculated from (51) and (52) as: C_s = 3.42 nF and R_s = 11.75 Ω. Fig. 5.11 presents a plot of $v_{drain}(t)$ from (50) using the flyback converter parameters from Table 5.III and the Snubber parameters just calculated. The peak value $v_{drain}(t)$ is multiple times higher than the steady-state value $V_{drain,ss.}$

By replacing (51) and (52) in (50), $v_{drain}(t)$ can be expressed as function of ξ, ω_n and the converter parameters:

$$v_{drain}(t) \simeq \left(I_{mpk} L_k \omega_n^2 + 2V_{in}\omega_n(\xi - 1)\right) t e^{-\xi\omega_n t} + V_{in} + n\left(V_o + V_d + I_o\left(R_{Ls} + R_d\right)\right)\left(1 - e^{-\xi\omega_n t}\frac{e^{-\xi\omega_n t} + 1}{\xi}\right). \tag{53}$$

The time at the peak of $v_{drain}(t)$ can be found by first calculating the time derivative of $v_{drain}(t)$, then equating it to zero, and last solving for t. The peak time is found as:

$$t_{pk} = \frac{I_{mpk} L_k \omega_n + 2V_{in}(\xi - 1)}{\left(-n\left(V_o + V_d + I_o\left(R_{Ls} + R_d\right)\right) + I_{mpk} L_k \omega_n + 2V_{in}(\xi - 1)\right)\xi\omega_n}. \tag{54}$$

Since the denominator of t_{pk} from (54) should be greater than zero for it to be valid, the minimum value for ω_n can be obtained as:

$$\omega_{n,min} = \frac{n\left(V_o + V_d + I_o\left(R_{Ls} + R_d\right)\right) - 2V_{in}(\xi - 1)}{I_{mpk} L_k}. \tag{55}$$

By evaluating $v_{drain}(t)$ at the peak time t_{pk}, $v_{drain,pk}$ can be found as a function of ξ and ω_n. Since the maximum value of ω_n occurs when no snubber is connected, $\omega_{n,max} = \omega_{no}$. Fig. 5.12 presents a plot of $V_{drain,pk}/V_{drain,ss}$ as function of ω_n for ξ ranging from 0.9 to 1. For example, if it is desired a drain to source peak voltage 4 times larger than its steady-state value, the snubber components R_s and C_s should be selected from (51) and (52) so ω_n is in the range from 0.41 and 0.46 times ω_{no} depending on the selected value of ξ.

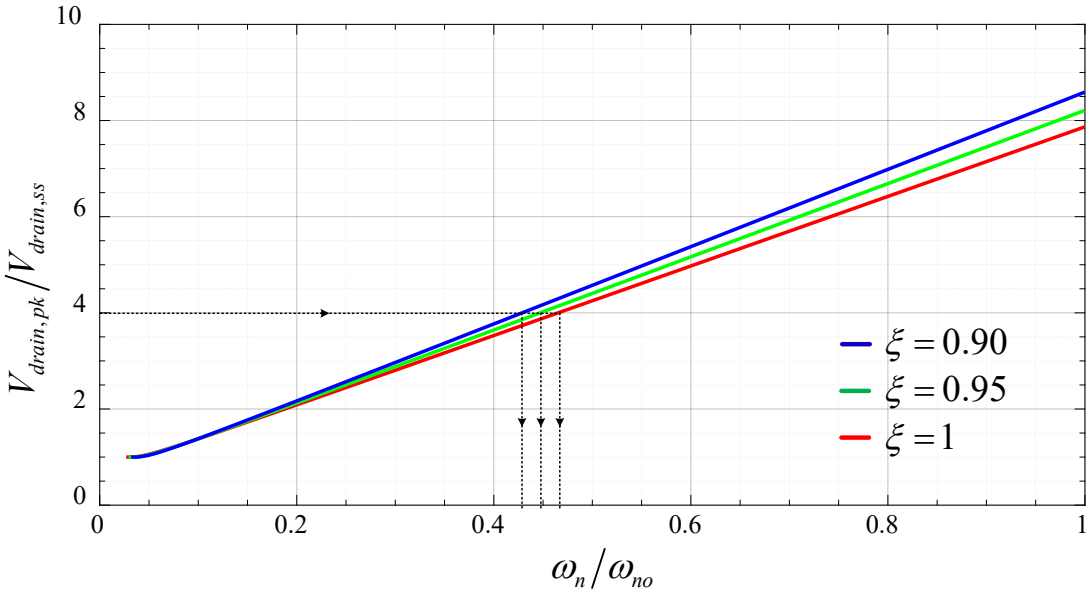

Fig. 5. 12. Peak drain source voltage divided by the steady state value of v_{ds} as function of ω_n/ω_n.

5.9.B Detecting the time when $i_{sn} = 0$

A circuit that detects the oscillation in $v_{drain}(t)$, which determines the moment when $i_{sn} = 0$, is shown in Fig. 5.13(a). The op-amp circuit at the left side is a derivator which consists of two resistors R_1 and R_2 and a capacitor C_1 which Laplace domain transfer function can be obtained as:

$$\frac{V_{der}}{V_{drain}} = -\frac{R_2 C_2 s}{1 + R_1 C_1 s}. \tag{56}$$

The resistor R_1 and the capacitor C_1 introduce a pole that limits the derivative effect for higher frequencies to prevent noise amplification and to improve stability. When $i_s = 0$ A, V_{drain} drops and starts oscillating around V_{in}. Therefore, the derivative of V_{drain} is negative, so the output V_{der} is positive. The second op-amp stage is a comparator which output will be read by the digital controller.

Fig. 5.13(b) presents the experimental waveforms of the proposed circuit to detect when $i_s = 0$ A from the drain voltage signal. As seen from the Fig. 5.13(b) when Q is OFF and the current i_s is greater than zero, V_{ds} is positive and can be used to estimate V_o if the snubber circuit was designed correctly. As soon as $i_s = 0$, the proposed circuit detects the slope of V_{ds}, so a signal $I_{s,zero}$ is generated and read by the controller, so Q can get turned ON and BCM operation is obtained.

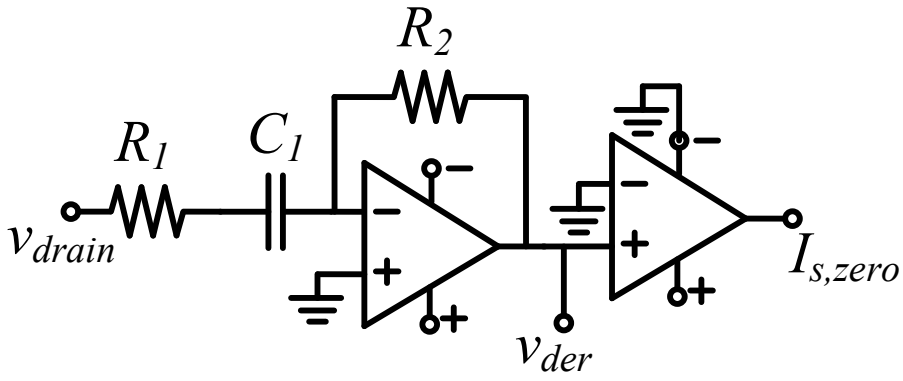

(a)

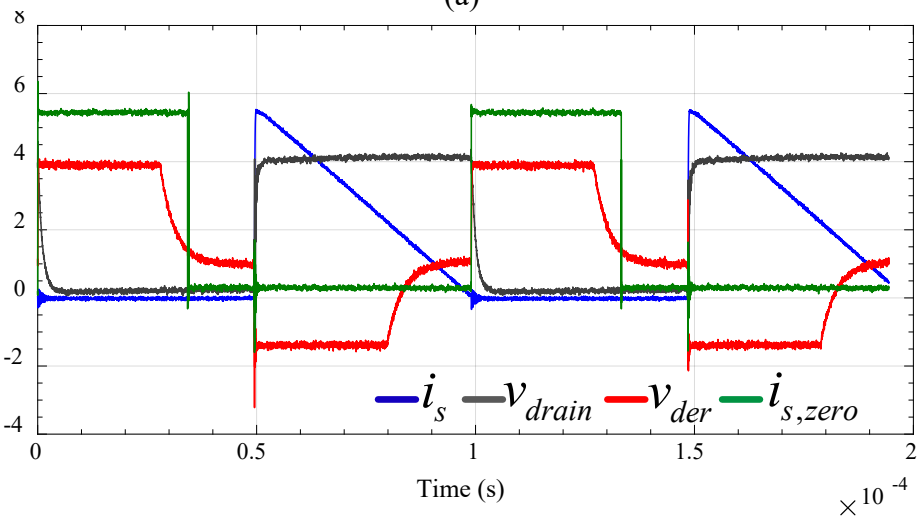

(b)

Fig. 5.13. (a) Circuit to detect from V_{ds} when $i_s = 0$, and (b) experimental waveforms of the proposed circuit.

CHAPTER 6

Conclusions and Future Work

This chapter summarizes the novel contributions and conclusions presented in each chapter of this dissertation. Also, some recommendations for future work are proposed by the author.

6.1 CHAPTER 2 CONCLUSIONS [1]

6.1.A Derivation of the Natural Switching Surfaces for a flyback converter operating under BCM

The normalized switching trajectories for a flyback converter were obtained from the differential equations for boundary and continuous conduction mode of operation by carefully selecting the target operating point. The proposed control law using the derived trajectories was tested in simulations and in an experimental prototype. As anticipated, the obtained transient response had no voltage overshoot, zero steady-state error, and an adequate response to sudden load changes.

6.1.B Comparison of different start-up methods to avoid over currents

A large magnetizing current peak during a transient could occur depending on the values of the converter parameters since the proposed control law made the converter reach a target point in only one switching action. Such a transient current could destroy the converter components if the control law would not be modified correctly. Therefore, several modifications of the control law were successfully implemented under start-up conditions which showed excellent performance.

6.2 CHAPTER 3 CONCLUSIONS [2]

6.2.A Derivation of the Natural Switching Surfaces considering parameter uncertainties

The shape of the system trajectories of a flyback converter depends on two main parameters, the output capacitance C_o and the magnetizing inductance L_m. If there are uncertainties in those parameters, the slope of the ON-trajectory changes, and the OFF trajectory becomes an ellipse instead of a circle affecting notably the control performance. In order to overcome that issue, the Natural Switching Surfaces for a flyback converter were obtained considering parameter uncertainties. A new parameter named "α/β" was first introduced which, if estimated correctly, can compensate the trajectories for uncertainties in the parameters.

Simulations showed that for the nominal system, the closed-loop response has no overshoot, zero steady-state error and an adequate response to sudden load changes. For the case of parameter uncertainties, the performance of the closed-loop system controlled with the nominal controller degraded. An adaptive scheme was successfully proposed to improve system performance by adjusting the parameter α/β at the end of each switching cycle, after analyzing the locus of the true OFF trajectory.

6.3 CHAPTER 4 CONCLUSIONS [3]

6.3.A Analysis of influence of parasitic elements in the system trajectories

A flyback converter was analysed with parasitic elements such as winding resistance, transformer leakage inductance, diode forward voltage drop, diode resistance, and transistor resistance. The load lines for the ideal flyback and the flyback with parasitic elements were derived and compared. The actual and the ideal load lines were alike when the duty cycle was within the $0 < D < 0.8$ range; therefore, it was concluded that the flyback converter could be analysed under ideal conditions (no parasitic components) without producing relevant errors.

6.3.B Start-up and steady-state characteristic when parameter are uncertain

Each start-up and steady-state parameter of the flyback converter was derived analytically as function of α/β. For example, the start-up current $I_{st\text{-}up}$, the start-up output voltage V_x, the output voltage ripple Δv_{on}, the target point V_{TP} and the switching frequency f_{sw} among others were plotted as function of α/β to determine the influence of the variation in the converter parameters [3].

6.3.C Experimental validation of the Natural Switching Surfaces considering parameter uncertainties

The natural switching surfaces for a flyback converter with parameter uncertainties operating in the boundary conduction mode were obtained from the normalized converter differential equations. The derived nonlinear boundary control law brought the converter to the target point in a single switching cycle if the load did not change when the transistor Q was OFF during transient conditions. During start-up conditions where the load changes from zero to its rated value when the transistor is OFF, the worst-case scenario will be approaching the target point in only two switching cycles. During steady-state conditions, the controller would compensate for a sudden load change within only a single switching cycle [2], [3].

The experimental results showed that for the nominal system ($\alpha/\beta = 1$, no parametric variations), the closed-loop response had no overshoot, zero steady-state error and excellent response to sudden load changes. When parameter uncertainties were present ($\alpha/\beta \neq 1$), the performance of the typical NSS control degraded considerably due to the dependence of the normalized control trajectories to the converter parameters. An adaptive control scheme predicting the variation of the converter parameters by using the precisely derived converter natural trajectories was implemented to improve the system performance. The controller made its first estimation of the parameter variations during the start-up with a precision measured to be higher

than 95%. Then, small adjustments were made cycle-by-cycle to adapt the control trajectories by measuring the error of the output voltage with respect to the target point producing a control response like that one in the ideal case, even under extreme parameter variations.

6.3.D Comparisson with a linear compensator

A linear proportional integral PI compensator was implemented in a DSP with the sample ADC sampling frequency than the NSS controller with the purpose to produce BCM operation by measuring the diode current and the output voltage. The performances of the linear and the NSS controller were compared for the cases with ideal parameters and with parameter uncertainties, respectively.

For the case with ideal parameters, a voltage reference change from 18 V to 24 V was implemented. The PI controller demanded approximately 1.3 ms to reach the new steady-state condition performing 11 switching actions, while the novel adaptive NSS for the same conditions responded to the step change (at 1.493 ms) in approximately 0.4 ms performing two switching actions due to the limitation of the limit in the magnetizing current. If the magnetizing current was not limited and the core would not saturate, it would just need one switching cycle to reach the target output voltage.

For the case when $\alpha/\beta > 1$ ($\alpha/\beta = 4$), the performance of the PI controller became oscillatory and slower demanding more than 3 ms (after 22 switching actions) to reach the steady-state condition for a sudden load change on the voltage reference from 18 V to 24 V. In the case of the NSS adaptive control, the performance was like that one for the ideal case.

When $\alpha/\beta < 1$ ($\alpha/\beta = 0.64$), the system controlled by the PI controller became rather unstable reaching the target point in about 1.3 ms (after 13 switching actions) while the novel NSS control presented almost the same response as that one for the ideal case.

6.4 CHAPTER 5 CONCLUSIONS

6.4.A Sensorless Natural Switching Surface control considering parameter uncertainties

A novel sensorless control scheme was proposed to estimate all the needed variables that are located at the secondary side or the flyback transformer. Therefore, isolated sensors are not used in this control unlike the conventional approach which requires sensing output voltage, output current, and transformer secondary current.

By sensing the transistor drain voltage, the transformer primary current, and the flyback converter input voltage, precise estimations for the isolated variables were obtained. Also, the converter parametric uncertainties were estimated in only two switching cycles from a start-up condition.

Simulation results considering a realistic sampling frequency of 200 kHz showed that the greatest errors for the first estimations of the output current and the converter parameter uncertainties were less than 9%. In those tests, extreme parameter variations and sudden load increase or decrease were considered and in all cases the performance of the control was adequate.

6.5 RECOMMENDATIONS FOR FUTURE WORK

There are multiple research areas in which the material of this dissertation could be applied and extended. Some examples are proposed below.

6.5.A Implementation of the proposed controllers in a integrated circuit (IC)

One of the main drawbacks of the proposed controller is the need of high processing and sampling speeds in order to obtain a satisfactory performance. The proposed first step is moving from a Digital Signal Processor (DSP) to a Field Programable Gate Array (FPGA) implementation. Once the FPGA control is working satisfactorily, an integrated circuit (IC) could be fabricated.

6.5.B Converter operation at high-temperature conditions

Operating at high temperatures could be one suitable application for the proposed controller if an integrated circuit is fabricated on a Silicon Carbide (SiC) wafer. No optocouplers are needed since no isolated measurements are required which increases the reliability of the system. Also, in case flyback converter components degrade with the temperature, the controller should be able to adapt performing always as in ideal conditions as shown in the dissertation.

6.5.C Detecting when components age

If the ideal components of a flyback converter are known and it is detected a certain change in the uncertainty parameter α/β, a fault signal could be generated to advice about the converter aging or a possible failure. More in depth research could be done to determine what range of α/β is an indicator of a possible failure. That information could be used to implement preventive maintenance to sensible equipment.

6.5.D Self-tuning IC controllers

A control IC solution could be proposed as one that does not require any configuration, compensation or adjustment. Simply as that, a single chip could be used for any flyback converter without need to add external circuits or compensation networks.

6.5.E Extending the proposed controller to other topologies

Another research area could be implementing the adaptive Natural Switching Surface (NSS) control to other converters. Starting with the buck and boost converters and following with more complicated ones like the dual-active bridge.

6.6 REFERENCES

[1] L. A. Garcia-Rodriguez, E. Williams, J. C. Balda, J. Gonzalez-Llorente and H. Chiacchiarini, "Control of a flyback converter operating in BCM using the natural switching surface," *2015 IEEE 6th International Symposium on Power Electronics for Distributed Generation Systems (PEDG)*, Aachen, 2015, pp. 1-8.

[2] L. A. G. Rodriguez, H. Chiacchiarini and J. C. Balda, "Control of a flyback converter with parametric uncertainties operating in BCM Using the natural switching surface," *2016 IEEE Biennial Congress of Argentina (ARGENCON)*, Buenos Aires, Argentina, 2016, pp. 1-7.

[3] L. A. Garcia Rodriguez, H. G. Chiacchiarini, D. Carballo Rojas and J. C. Balda, ”Adaptive Boundary Control Using Natural Switching Surfaces for Flyback Converters Operating in the Boundary Conduction Mode with Parameter Uncertainties,” in *IEEE Transactions on Power Electronics*, vol. 34, no. 8, pp. 8118-8137, Aug. 2019.